12-2015

Effects of Magnetically Induced Micro-mixing on Nanofiltration Performance

Guanghui Song
University of Arkansas, Fayetteville

Effects of Magnetically Induced Micro-mixing on Nanofiltration Performance

A dissertation submitted in partial fulfillment
of the requirements for the degree of
Doctor of Philosphy in Chemical Engineering

by

Guanghui Song
Xiamen University
Bachelor of Science in Chemical and Pharmaceutical Engineering, 2008
New Jersey Institute of Technology
Master of Science in Chemical Engineering, 2011

December 2015
University of Arkansas

This thesis is approved for recommendation to the Graduate Council.

_____
Dr. Xianghong Qian
Advisor

_____
Dr. Ranil Wickramasinghe
Co-advisor

_____
Dr. Paul Millett
Committee Member

_____
Dr. Jamie Hestekin
Committee Member

_____
Dr. Mathias Ulbricht
Committee Member

Abstract

Nanofiltration (NF) is a relatively new membrane separation process mainly used for removing low molecular weight species from aqueous and non-aqueous solutions. NF membranes suffer from concentration polarization leading to membrane fouling thus compromised membrane performance. Magnetically responsive nanofiltration (NF) membranes functionalized with superparamagnetic nanoparticles (SPNs) attached to the chain ends of grafted polymer nanolayers have been shown to be effective in breaking concentration polarization at the membrane-liquid interface under an appropriate external oscillating magnetic field. Under an oscillating magnetic field, the movement of the polymer chains acts as micro-mixer leading to the suppression of concentration polarization and improved filtration performance. NF270 is one of the most commonly used NF membranes for removing low molecular weight species and di- and trivalent ions from the feed solutions. In this dissertation, the effects of grafted polymer chain length and chain density on NF performance were investigated. Feed solutions containing salts (NaCl, $CaCl_2$, $MgSO_4$, 10mM pH=7 sodium phosphate buffer and $(CH_3)_3N{\cdot}HCl$) at varied concentrations as well as model oily wastewater were used to investigate the performance of these magnetic responsive membranes as anti-fouling self-cleaning membranes. Several commonly used mathematical models for describing NF processes have been adopted to quantify the solvent and solute transport of the functionalized membranes and the effects of micro-mixing on the performance of these NF membranes. Our results demonstrate that there is a significant improvement in both flux and rejection in the presence of an external oscillating magnetic field compared to results without an external field. Moreover, the improvement becomes more evident as the chain length and chain density of

grafted polymer increases. An increase in membrane selectivity due to decreased concentration polarization for the functionalized membranes in the presence of an external field has been analyzed using several models. Besides the inorganic and organic salt feed solutions, our functionalized magnetically responsive nanofiltration membranes exhibit anti-fouling capacity towards model oily waste water.

Acknowledgements

First, I would like to thank my advisor, Dr. Xianghong Qian, for her experienced guidance, help and encouragement that keeps me running on the right path towards my goals of study and research. My gratitude also goes out to my committee members, Dr. Ranil Wickramasinghe, Dr. Jamie Hestekin, Dr. Paul Millett and Dr. Mathias Ulbricht along with other professors in the Ralph E. Martin Department of Chemical Engineering and the University of Arkansas for their advice and help along the way. Also, I need to thank all my research group members for their help.

Second, I would like to acknowledge the financial support from National Science Foundation (NSF) CBET 0630200 and CBET 1066505. Moreover, my gratitude goes out to the Membrane Research Group in the Department of Chemical Engineering of the University of Arkansas for granting me such great chance to perform my favorite research that is related to one of the hottest fields in chemical engineering—membrane separation, and all of their supports. In addition, I need to thank the Arkansas Nano & Bio Materials Characterization facility for doing XPS, Mr. Zizhao Liu in my group for doing AFM for me, Mr. Anh Vu in my group for doing AFM and testing zeta potential for me, and the Quality Writing Center of the University of Arkansas for their guide and help during the composition of my thesis.

Last, I need to thank my parents in China, and all my friends for their support and encouragement. My gratitude needs to go to the members in the Grace Chinese Christian Church of NWA and the Mission Blvd Baptist Church, for their spiritual support along my way that made me stand even enjoy all my difficulties.

Table of Contents

1. Introduction and Background

1.1 Membrane Separation

Nowadays, the global shortage of water and energy becomes significant. At the same time, the economic development is calling for more and more water and energy. Separation processes are critically involved during every stage of water purification and energy production. Membrane based separation processes have several advantages over traditional separation processes such as distillation and extraction. Membrane-based processes are generally more economical, safer, cleaner, and more energy-saving, easier to operate and environmentally friendlier. High separation factor under mild operational conditions can be achieved. Finally, membrane processes often have unmatched operational flexibility and can be widely used in industry.[1]

Membrane separation has been widely used for wastewater treatment, water recycle and reuse in chemical industry. Feed and permeate are the two phases separated by the selective membrane materials in between. Selective transportation of species from the feed to the permeate side is often driven by pressure or electrochemical potential. The feed typically contains a mixture of products and other species whereas the permeate generally contains only the desired product. The mechanism of membrane separation is shown in Figure 1.1.[1, 2]

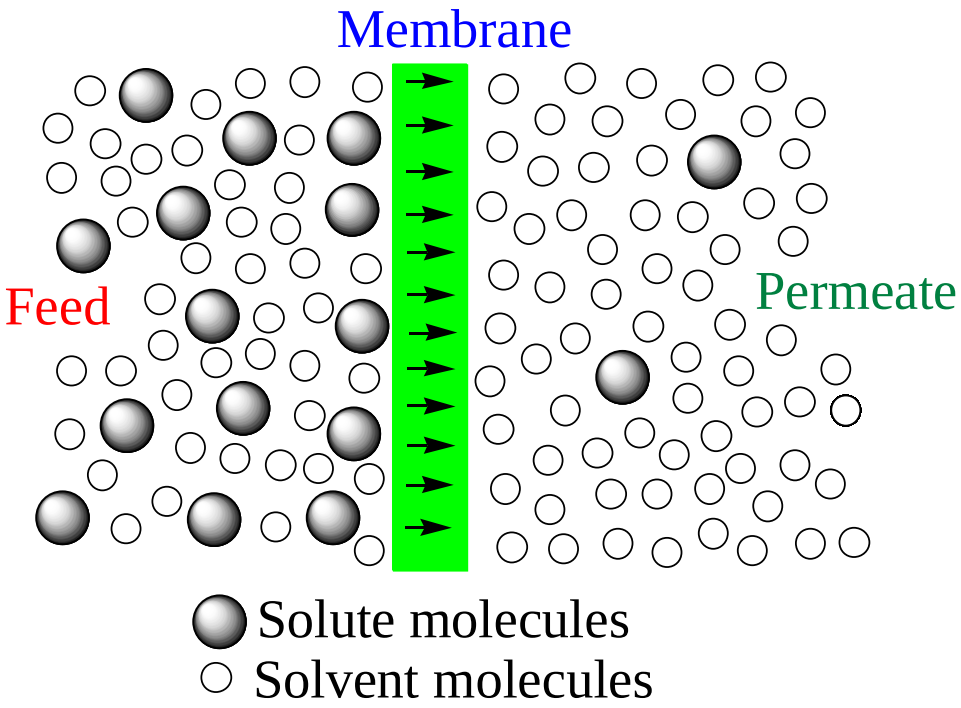

Figure 1.1 Principle of membrane separation. Here the solute particles are to be retained by the membrane, and the solvent molecules are selectively transported through the membrane.[2]

The membrane barrier layer selectively permits certain types of molecules in the feed to permeate through the membrane and rejects other molecules in the feed, thus increasing the concentrations of the rejected species in the feed and permeable species in the permeate to achieve separation. The driving forces for the separation include differences in pressure, temperature, concentration, electrical potential or pH across the membrane, both physical and chemical. Industrial application of membrane technology often involves synthetic ceramic or polymeric membranes. The membranes ideally need to have uniform thickness and very narrow pore size distribution for the porous membranes.[1, 2]

1.2 Stimuli-responsive Membranes

Stimuli-responsive membranes are membranes that can respond to stimuli around them, such as pH, pressure, temperature, concentration, light and electromagnetic field. Magnetically

responsive membranes are membranes that respond to a magnetic field exerted on them.[3] Compared to the conventional membranes, they often have improved performances. For example, we have developed the anti-fouling magnetically responsive micro-mixing NF membranes for improved separations.[4] Responsive membranes often have innovative functions that are tunable by varying the external stimuli. Himstedt *et al.* and Du *et al.* have reported their work on application of the pH and temperature responsive membranes to improve separation efficiency.[5, 6] So far, the most widely used stimuli are pH and temperature, in some cases also salt ions.[6]

In most cases, these responsive membranes are fabricated by grafting responsive functional groups onto commercially available membranes. These membranes will then respond to the stimuli exerted.[4, 7, 8]

1.3 Nanofiltration and Its Problems

Nanofiltration is a relatively new pressure-driven membrane separation technology with diameter and molecular weight cutoff (MWCO) between those of ultrafiltration (UF) and reverse osmosis (RO). The schematics for the function and the range of cutoff dimension are shown in Figure 1.2. The typical MWCO is in the range of 100~2000g/mol.[9, 10]

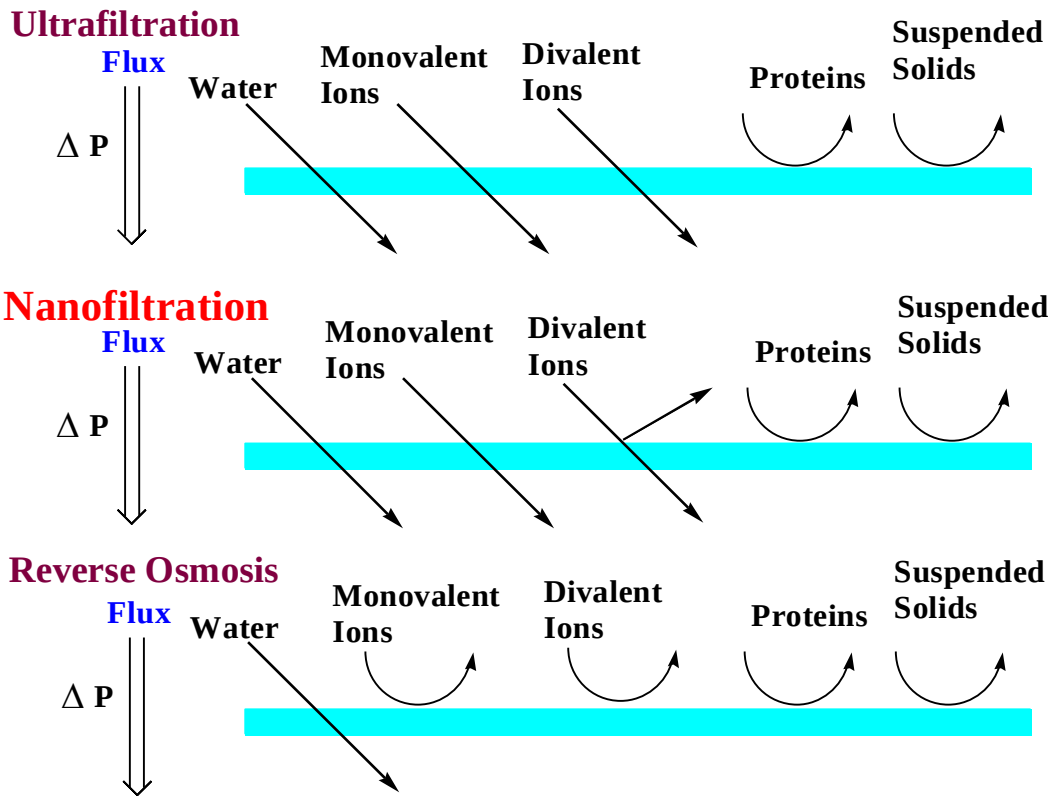

Figure 1.2 Schematics of separation properties of NF membranes compared to UF and RO membranes.[11] The membranes are represented in turquoise color.

As a pressure-driven membrane separation process with a holdup diameter between UF and RO, NF membranes are mainly used for the removal of low molecular weight species dissolved in water, and tri- and some divalent ions from water. While UF processes have been used to separate macromolecules and colloidal particles and RO processes are often used in water desalination, applications of NF membranes include partial desalination of brackish water, partial softening of ground water and removal of micro-pollutants and small organic molecules during water treatment processes. NF is often more economical for water purification compared to RO. NF is also more efficient for water treatment compared to UF.[9, 12]

Although NF has much broader applications compared to most other membrane

separation processes, NF processes also suffer from membrane fouling and concentration polarization, both of which cause a significant decrease in productivity and rejection. Fouling and concentration polarization begin soon after filtration process starts. Also, for NF membranes fouling is mainly caused by concentration polarization from the feed. The mechanisms for NF membrane fouling are schematically shown in Figure 1.3, and the principle of concentration polarization is shown in Figure 1.4.[13, 14]

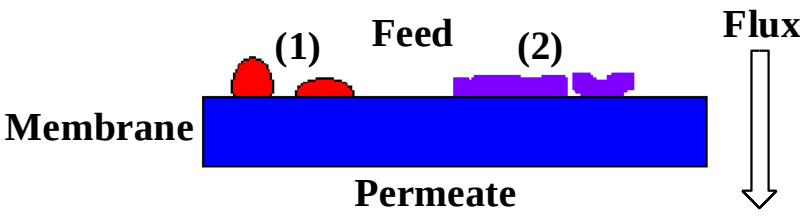

Figure 1.3 Mechanisms of nonporous NF membrane fouling:
(1) Deposition of big and soft particles onto the surface;
(2) Precipitation and adsorption of solute molecules onto the surface.[13, 15]

Membrane fouling refers to processes resulting in loss of performance of a membrane due to deposition of suspended or dissolved substances on its external surfaces, at its pore openings, or within its pores.[16] It is also described as irreversible flux decline. Most fouling are irreversible, and can only be removed by chemical cleaning. When chemical cleaning had to be used, additional environmental problems would be caused, and many chemicals used for cleaning may potentially damage the membrane layers irreversibly.

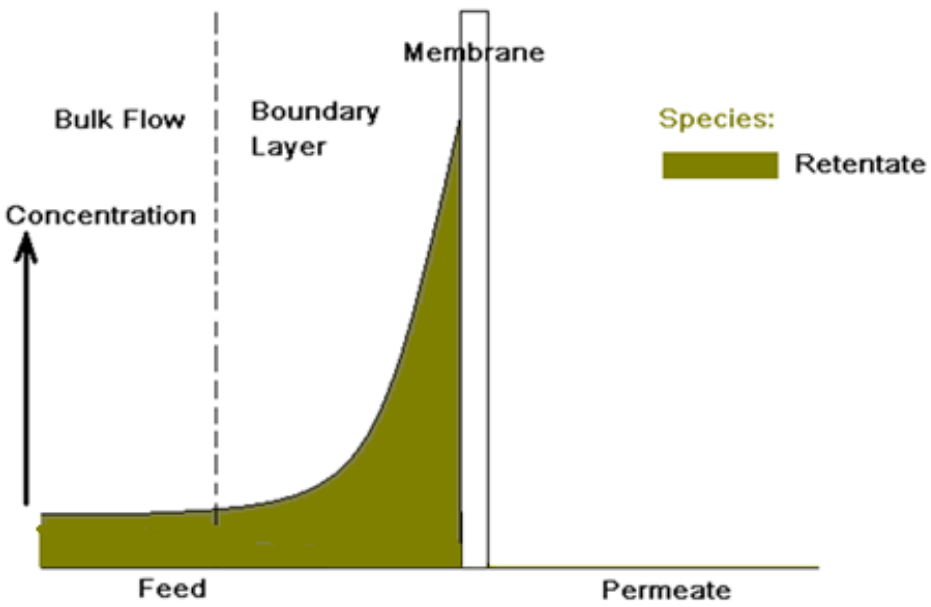

Figure 1.4 Principle of concentration polarization.[17]

As from Figure 1.4, during filtration operation, the membrane concentrates the impermeable solutes against the membrane wall, building up a gradient towards the upstream membrane surface. In such a case, the permeate flux decreases as a higher trans membrane pressure difference is needed to surmount the increasing osmotic pressure to maintain a constant flux. Furthermore, as the rejected species continuously accumulate above the membrane surface on the feed side, the concentrations of the rejected species increases reaching or exceeding their limits of solubility. In such situation, the rejected species precipitate or crystallize immediately onto the membrane, leading to membrane fouling.[13, 17] For non-porous NF membranes that mainly reject small organic molecules and di- or trivalent ions, their fouling mainly occurs on the surface and is mainly caused by concentration polarization. This work thus aims at investigating the effect of magnetically activated micro-mixing on concentration polarization of NF membranes.

The following methods against concentration polarization and membrane fouling are reported in recent year's literature:[2, 11]

1) Producing mixing during operation, such as stirring, back pulsing and cross-flow velocity.
2) Optimization of membrane module design, such as increasing roughness of the membrane surface, or adding some spacers in close touch with the membrane surface. This helps to generate turbulent flow to increase mixing on membrane surface.
3) Pretreatment of the feeding solution, such as changing temperature, pH, concentration or adding some other species into the feed.
4) Anti-fouling surface modification of the membrane.[18]

However, these methods have their own corresponding drawbacks:[1, 2]

1) It consumes a huge amount of energy to induce mixing during operation. Also, this only affects the bulk flow, but concentration polarization mainly occurs within the boundary layer close to the membrane surface.[1]
2) Increasing the roughness of membrane surface or adding spacers in close touch with membrane surface would actually greatly reduce the active area on membrane surface. Moreover, in this case, the foulants are possible to accumulate in some "dead-zone" on membrane surface to aggravate partial fouling.[1]
3) Feed pretreatment changes the physical and chemical properties of the feed, even damaging some of its functions. Moreover, some extreme conditions such as high temperature or high acidity and basicity would always cause damages to the membrane. Also, a significant amount of money and time is often required to pretreat the feed, or to remove the molecules added during pretreatment.[1, 2, 11]

4) Anti-fouling surface modification is effective to prevent fouling in some cases, but this cannot suppress concentration polarization. Also, for non-porous NF membranes that are mainly used for removing salts and small organic molecules from water, most fouling is actually caused by concentration polarization.[19]

1.4 Magnetically Responsive Micro-mixing Self-cleaning NF Membranes, and Their Functionalization

With the expectation to overcome the drawbacks of NF processes to make them more cost-effective, the magnetically responsive micro-mixing self-cleaning NF membranes are developed via surface modification.[7] The membrane modification procedure consists of two steps. First, linear hydrophilic polymer chains are grafted onto the polyamide separation layer via surface-initiated atom transfer radical polymerization (SI-ATRP). Then, superparamagnetic nanoparticles (SPNs) are attached to the polymer chain ends. After membrane functionalization, an oscillating magnetic field with certain frequency is exerted to the membrane with the magnetic field direction being parallel to the functionalized surface layer.[7, 20] The oscillating magnetic field induces a force onto the SPNs to make them move with the same frequency as the external oscillating magnetic field.[4] The movement of tethered SPNs leads to the movement of polymer chains, inducing micro-mixing above the membrane-liquid interface to minimize concentration polarization.[3, 7, 20]

In order to guarantee effective micro-mixing, grafted polymer chains with uniform length and density on membrane surfaces is necessary, and the SPNs only attach to the ends of the grafted polymer chains. In the presence of an external magnetic field, all polymer chains

are linear. The polymer chains will move flexibly but synchronically in water, with the same frequency as the external field, with minimum entangling onto each other and without showing individual movements.

The NF270 membrane is among the most successfully commercialized NF membranes with myriad applications. It has been successfully applied to water purification through removal of small organic contaminants, and partial softening of surface and ground water. Other advantages of NF membranes lie in their relatively low operating pressure required and often high permeate flux generated.[21] Besides industrial applications, there are active areas of research for further performance improvement and for developing solvent resistant NF membranes. Here we also chose NF membranes for this dissertation research to further understand and develop magnetically activated NF membranes. The physical structure of an NF270-400 membrane layer can be described by Figure 1.5.[21]

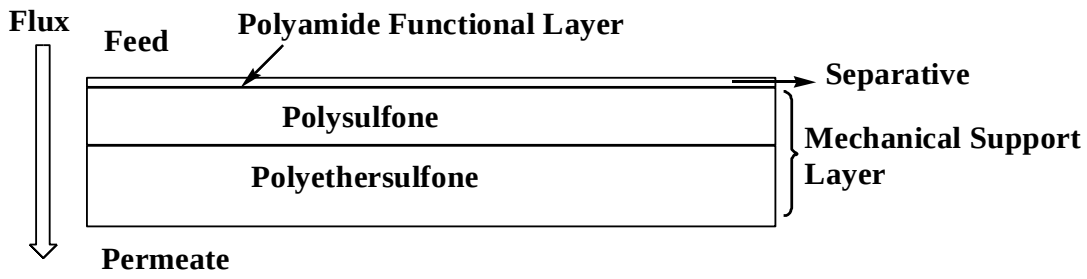

Figure 1.5 Physical structure of a nonporous NF270-400 NF membrane.[21]

The NF270 membrane is composed of three different layers: a polyamide layer on the feed side, a polysulfone layer in the middle and a polyethersulfone layer on the permeate side. The polyamide layer is the functional layer that performs separation, and the other two layers work together to serve as a mechanical support layer. Here the focus is on the functional layer.[21]

Characterizations of the modified membranes are necessary in order to achieve desired

membrane properties. These methods include contact angle measurement, ATR-FTIR, AFM and deionized water fluxes. Based on the flux and rejection data of salt solutions for the base membrane and modified membranes in the presence and absence of an external magnetic field, the effects of magnetically activated micro-mixing can be determined and quantified.[3, 7]

1.4.1 Detailed Membrane Functionalization Process

Surface modification to graft linear polymer chains has been established earlier using surface-initiated atom transfer radical polymerization (SI-ATRP) reaction to grow hydrophilic 2-hydroxyethyl methacrylate poly (HEMA) chains onto the membrane surface.[20, 28] Subsequently, the Fe_3O_4 nanoparticles are immobilized to the ends of grafted poly (HEMA) chains. After functionalization, an oscillating magnetic field that reverses direction periodically was applied to the membrane surface. The external magnetic field exerts a force on the SPNs in the direction of magnetic field, enabling the nanoparticles and the polymer chains to move together in the presence of the switching magnetic field direction. Resulting from the movement of hydrophilic polymeric chains within the alternating magnetic field, it generates a micro-mixing effect within the boundary layer above the feed side membrane surface.[7] The micro-mixing disrupts concentration polarization and improves the membrane performance, resulting in less frequent cleaning hence leading to longer life time for the membranes. The detailed functionalization procedure to the NF270 NF membranes is shown in Figure 1.6.[7]

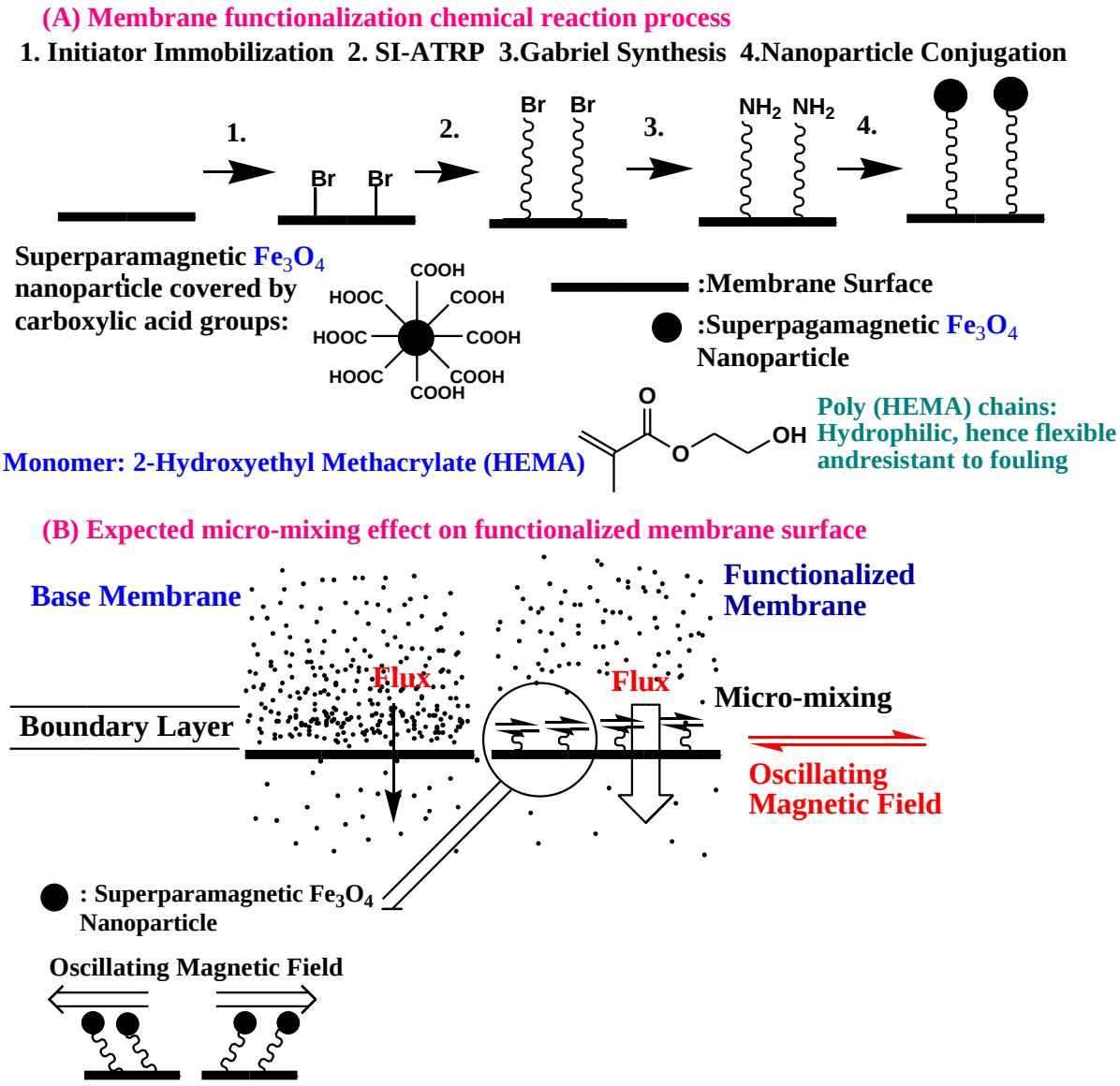

Figure 1.6 Magnetically responsive functionalization for NF270 membranes.[3, 7, 20]

1.4.2 The Choice of Superparamagnetic Fe_3O_4 Nanoparticles

Superparamagnetic Fe_3O_4 nanoparticles are immobilized to the ends of grafted poly (HEMA) chains on NF membrane surface. The differences in microstructures between such nanoparticles and the conventional ferromagnetic particles are shown in Figure 1.7.[29]

The diameter of SPM Fe_3O_4 nanoparticles is smaller than that of ferromagnetic particles, and below the critical diameter of multiple magnetic domains. All such nanoparticles hence

only have a single magnetic domain, and are much lighter in weight than ferromagnetic particles. Flip of the magnetic field within each SPM nanoparticle is easy and quick due to extremely low energy barrier.[30] As a result, when an external magnetic field is exerted to the nanoparticles, the magnetic field within each nanoparticle would immediately flip to same as the external field. Then, when the external field switches its direction, the magnetic field within each nanoparticle would flip to same as the switched external field instantaneously. As soon as the magnetic field within each nanoparticle becomes same as the external field, the nanoparticles would be immediately exerted a strong force towards the generator of the magnetic field.[20]

Therefore, such nanoparticles are energy-efficient, and will instantaneously respond to the external magnetic field.[30] As a result, these nanoparticles and the polymer chains chemically bonded to them can move back and force almost in the same frequency with the external oscillating magnetic field. Micro-mixing of the fluid at the membrane surface-liquid interface can be generated.[7, 20]

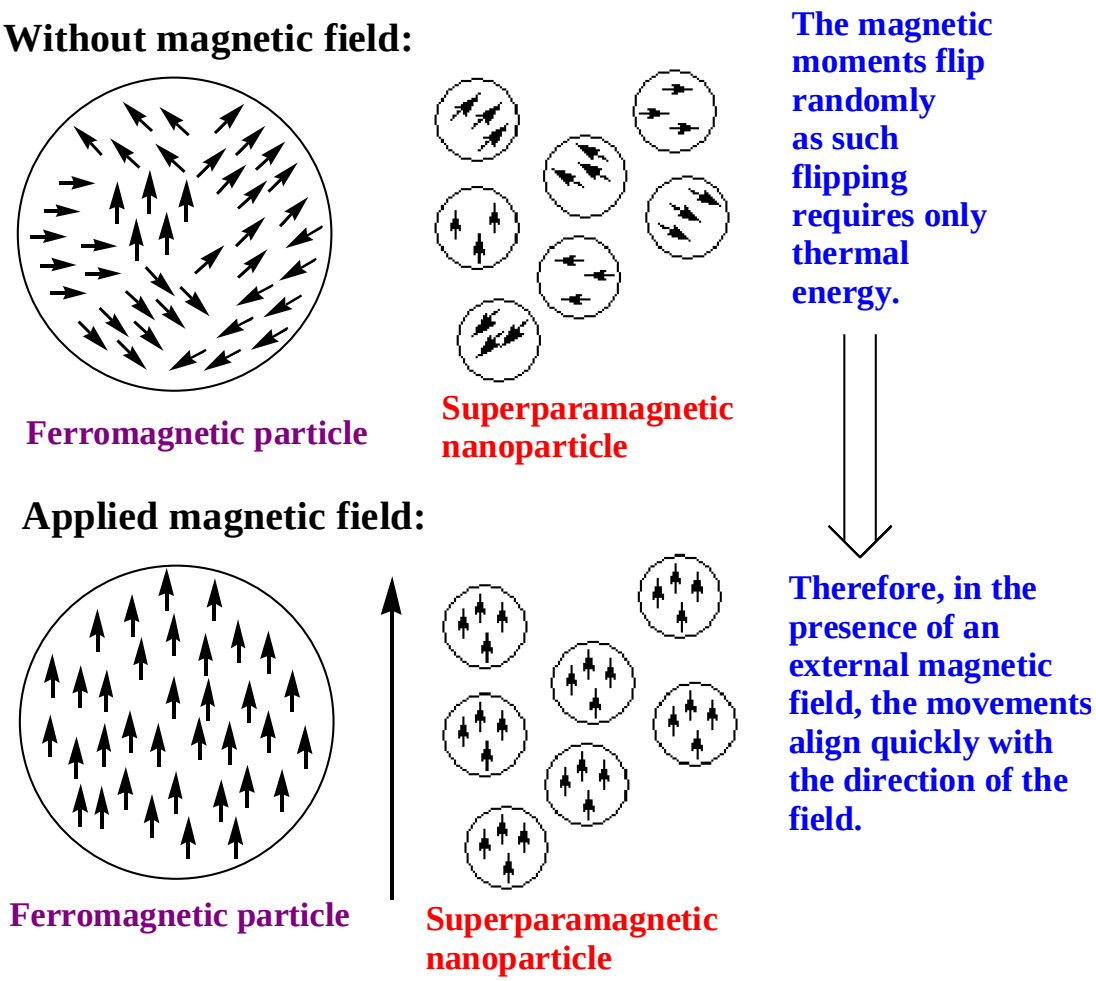

Figure 1.7 Superparamagnetic Fe_3O_4 nanoparticles and ferromagnetic particles: the differences in their microstructures.[31]

1.5 Transport Modeling for the NF processes

During the past few decades, quite a few mathematical models have already been developed for the evaluation of NF membrane performances and solvent and solute transport across the membranes. However, several of such mathematical models are already widely used.[22, 23] For solvent transport, the Spirgler-Kedem Katchalsky model based on the Hagen-Poiseuille-type relationship has been widely adopted.[24] For solute transport, the most widely used model is the Nernst-Plank equation, and the Film Theory has been widely used for describing and quantifying concentration polarization.[25] Later on, researchers such as Chaabane[26] and Xiao[27] improved the precision of NF process modeling based on the

combination of Nernst-Plank equation, Spirgler-Kedem Katchalsky model and the Film Theory. These models are widely used for the prediction of membrane performances with different feed compositions. But in this project, the experimental results will be fitted into these models to determine the effect of membrane functionalization and the external oscillating magnetic field on transport properties.[22]

1.6 Hypothesis and Research Objective

Magnetically responsive micro-mixing membranes have been primarily studied by Himstedt *et al.* in recent years.[7, 20, 32] They've tested the flux and salt rejection of 500 ppm $CaCl_2$ and 2000 ppm $MgSO_4$ salt solutions for both base and functionalized NF270 membranes, in the presence and absence of an external alternating field. At the same time, Himstedt *et al*. have studied different poly(HEMA) chain density and chain length. [20] Variations among the flux and salt rejection data with the two different salt solutions for both base and functionalized NF270 have been shown.[7] Then, for the functionalized NF270 membranes with different polymer chain length and density, the flux and salt rejection for both 500 ppm $CaCl_2$ and 2000 ppm $MgSO_4$ salt solutions have shown evident improvement with an external field. Improvements of both permeate flux and salt rejection were demonstrated in the presence of an external field, but the degree of improvement seems to depend on the length and density of polymer chains.[20]

1.6.1 Hypothesis

Concentration polarization at the membrane-liquid interface can be significantly reduced by induced mixing via the movement of the polymer chains grafted on the membrane

surface. The movement of the polymer chains is caused by the interaction between the magnetic nanoparticles attached to the chain ends of the polymer and an external oscillating magnetic field. Both the length and density of polymer chains could affect the effectiveness of concentration polarization reduction by micro-mixing. Moreover, the magnetically activated micro-mixing affects the transport of different salt ions differently. The micro-mixing effect depends on the degrees of hydration of the ions, which in turn are determined by the ionic charges and sizes.[7, 20]

1.6.2 Research Objectives

As SI-ATRP is a controlled polymerization process, the polymer chain length and density can be controlled and varied independently. From prior work, it's evident both the polymer chain length and density have evident effect on the performances of the functionalized NF membranes.[20] Therefore, the combined effects of the length and density of the polymer chains under an alternating magnetic field is investigated in this work. Moreover, feed solutions containing monovalent, divalent and trivalent salt ions with various concentrations are used to systematically investigate the effects of micro-mixing on concentration polarization and transport of salt ions. Indeed, the type and concentration of salt ions will significantly affect concentration polarization at the membrane-liquid interface. The correlations between the transport coefficients and the physical and chemical properties of functionalized membranes have also been investigated based on the experimental results obtained. Finally, the anti-fouling properties for our novel magnetically activated NF membranes has been investigated by using model oily waste water system.

Mathematical modeling helps to understand the transport processes of the membranes,

and predict membrane performances. For mathematical description of the NF processes, some models have already been developed and are found to agree well with experimental results.[22, 33] Most researchers make use of these membrane transport models to predict membrane quality and performances in order to design a process, or theoretically study some processes by adjusting the constants and variables in the models.[34] However, some of the most widely used mathematical models for NF processes should be applied to correlate the experimental results under varied conditions, and theoretically explain the effects of membrane functionalization and the alternating magnetic field to base and functionalized NF270 membrane performances.[22, 24] Based on the correlation of the fluxes and the corresponding rejections as variables, the constants in the models that describe the characteristics and transport properties of the membranes can be obtained. By analyzing the values of these constants and the trends of their variations, the transport process across different NF membranes under various feed compositions and magnetic field operation conditions can be better understood.[26, 35]

References

1. Ho, W. S. W.; Sirkar, K. K., Membrane Handbook. Springler: 1992.

2. **Mulder, M.**, ***Basic Principle of Membrane Technology***. 2 ed.; **Enschede: Kluwer Academic Publishers**: **Netherlands**, 1996.

3. Himstedt, H. H.; Marshall, K. M.; Wickramasinghe, S. R., pH-responsive nanofiltration membranes by surface modification. *Journal of Membrane Science* **2011,** *366* (1-2), 373-381.

4. Wandera, D.; Wickramasinghe, S. R.; Husson, S. M., Stimuli-responsive membranes. *Journal of Membrane Science* **2010,** *357* (1-2), 6-35.

5. Himstedt, H. H.; Du, H. B.; Marshall, K. M.; Wickramasinghe, S. R.; Qian, X. H., pH Responsive Nanofiltration Membranes for Sugar Separations. *Industrial & Engineering Chemistry Research* **2013,** *52* (26), 9259-9269.

6. Du, H.; Wickramasinghe, R.; Qian, X., Effects of Salt on the Lower Critical Solution Temperature of Poly (N-Isopropylacrylamide). *Journal of Physical Chemistry B* **2010,** *114* (49), 16594-16604.

7. Himstedt, H. H.; Yang, Q.; Dasi, L. P.; Qian, X.; Wickramasinghe, S. R.; Ulbricht, M., Magnetically Activated Micromixers for Separation Membranes. *Langmuir* **2011,** *27* (9), 5574-5581.

8. Bhattacharyya, D.; Schafer, T.; Wickramasinghe, S. R.; Daunert, S., *Responsive Membranes and Materials*. WILEY: 2013.

9. Fane, A. G. F. I. S. D. W. G., *Nanofiltration: Principles and Applications*. Elsevier Advanced Technology: Australia, 2004.

10. Al-Zoubi, H.; Omar, W., Rejection of salt mixtures from high saline by nanofiltration membranes. *Korean Journal of Chemical Engineering* **2009,** *26* (3), 799-805; Gupta, V. K. *Experimental and theoretical studies in reverse osmosis and nanofiltration*. University of Cincinnati, Cincinnati, 2003.

11. **Schäfer, A. I.**; Fane, A. G.; Waite, T. D., ***Nanofiltration, Principles and Applications***. Elsevier Advanced Technology: New York, 2005.

12. Hilal, N.; Al-Zoubi, H.; Mohammad, A. W.; Darwish, N. A., Nanofiltration of highly concentrated salt solutions up to seawater salinity. *Desalination* **2005,** *184* (1-3), 315-326; Wang, R.; Li, Y.; Wang, J.; You, G.; Cai, C.; Chen, B. H., Modeling the permeate flux and rejection of nanofiltration membrane separation with high concentration uncharged aqueous solutions. *Desalination* **2012,** *299*, 44-49.

13. Violleau, D.; Essis-Tome, H.; Habarou, H.; Croue, J. P.; Pontie, M., Fouling studies of a polyamide nanofiltration membrane by selected natural organic matter: an analytical approach. *Desalination* **2005,** *173* (3), 223-238.

14. Sachs, J. N.; Petrache, H. I.; Zuckerman, D. M.; Woolf, T. B., Molecular dynamics simulations of ionic concentration gradients across model bilayers. *Journal of Chemical Physics* **2003,** *118* (4), 1957-1969.

15. Li, Q. L.; Elimelech, M., Organic fouling and chemical cleaning of nanofiltration membranes: Measurements and mechanisms. *Environmental Science & Technology* **2004,** *38* (17), 4683-4693.

16. Boussu, K.; Kindts, C.; Vandecasteele, C.; Van der Bruggen, B., Surfactant fouling of nanofiltration membranes: Measurements and mechanisms. *Chemphyschem* **2007,** *8* (12), 1836-1845.

17. Deon, S.; Dutournie, P.; Fievet, P.; Limousy, L.; Bourseau, P., Concentration polarization phenomenon during the nanofiltration of multi-ionic solutions: Influence of the filtrated solution and operating conditions. *Water Research* **2013,** *47* (7), 2260-2272.

18. Lalia, B. S.; Kochkodan, V.; Hashaikeh, R.; Hilal, N., A review on membrane fabrication: Structure, properties and performance relationship. *Desalination* **2013,** *326*, 77-95; Roy, S.; Ntim, S. A.; Mitra, S.; Sirkar, K. K., Facile fabrication of superior nanofiltration membranes from interfacially polymerized CNT-polymer composites. *Journal of Membrane Science* **2011,** *375* (1-2), 81-87.

19. Zuo, G.; Wang, R., Novel membrane surface modification to enhance anti-oil fouling property for membrane distillation application. *Journal of Membrane Science* **2013,** *447*, 26-35.

20. Yang, Q.; Himstedt, H. H.; Ulbricht, M.; Qian, X.; Wickramasinghe, S. R., Designing magnetic field responsive nanofiltration membranes. *Journal of Membrane Science* **2013,** *430*, 70-78.

21. Cot, S. N. D. A. D. K. D., *Intrinsic properties and performances of NF270 and XLE membranes for water purification*. *Water Science&Technology: Water Supply* **2011,** *11* (2), 186-193.

22. Bowen, W. R.; Welfoot, J. S., Modeling the performance of membrane nanofiltration - critical assessment and model development. *Chemical Engineering Science* **2002,** *57* (7), 1121-1137.

23. Mmbaga, J.; Hayes, R. E.; Pikus, W.; Afacan, A.; Bressler, D. C., NUMERICAL MODELING AND CHARACTERIZATION OF NANOFILTRATION MEMBRANES FOR THE SEPARATION OF CARBOHYDRATE MIXTURES. *Canadian Journal of Chemical*

Engineering **2011,** *89* (2), 314-324.

24. Welfoot, J. S., Predictive modeling of nanofiltration: membrane specification and process optimisation. Bowen, W. R., Ed. Desalination: 2002.

25. Zydney, A. L., Stagnant film model for concentration polarization in membrane systems. *Journal of Membrane Science* **1997,** *130* (1-2), 275-281.

26. Chaabane, T.; Taha, S.; Ahmed, M. T.; Maachi, R.; Dorange, G., Coupled model of film theory and the Nernst-Planck equation in nanofiltration. *Desalination* **2007,** *206* (1-3), 424-432.

27. Xiao, H.; Hefei, Z.; Ruijin, Y.; Wenbing, Z.; Wei, Z., Coupled model of extended Nernst-Planck equation and film theory in nanofiltration for xylo-oligosaccharide syrup. *Journal of Food Engineering* **2010,** *100* (2), 302-9.

28. Robinson, K. L.; Khan, M. A.; Banez, M. V. D.; Wang, X. S.; Armes, S. P., Controlled polymerization of 2-hydroxyethyl methacrylate by ATRP at ambient temperature. *Macromolecules* **2001,** *34* (10), 3155-3158; Magenau, A. J. D.; Kwak, Y.; Schroeder, K.; Matyjaszewski, K., Highly Active Bipyridine-Based Ligands for Atom Transfer Radical Polymerization. *Acs Macro Letters* **2012,** *1* (4), 508-512.

29. Alishiri, T.; Oskooei, H. A.; Heravi, M. M., Fe3O4 Nanoparticles as an Efficient and Magnetically Recoverable Catalyst for the Synthesis of alpha,beta-Unsaturated Heterocyclic and Cyclic Ketones under Solvent-Free Conditions. *Synthetic Communications* **2013,** *43* (24), 3357-3362; Cheng, C.-J.; Bai, X.-X.; Fan, W.-Q.; Wu, H.-M.; Shen, L.; Huang, Q.-H.; Tu, Y.-M., Synthesis of a photoactive gemini surfactant and its use in AGET ATRP miniemulsion polymerisation and UV curing. *Chemical Papers* **2014,** *68* (1), 136-144.

30. Demas, V.; Lowery, T. J., Magnetic resonance for in vitro medical diagnostics: superparamagnetic nanoparticle-based magnetic relaxation switches. *New Journal of Physics* **2011,** *13*.

31. Zengin, A.; Yildirim, E.; Tamer, U.; Caykara, T., Molecularly imprinted superparamagnetic iron oxide nanoparticles for rapid enrichment and separation of cholesterol. *The Analyst* **2013,** *138* (23), 7238-45; Gao, J.; Ran, X.; Shi, C.; Cheng, H.; Cheng, T.; Su, Y., One-step solvothermal synthesis of highly water-soluble, negatively charged superparamagnetic Fe3O4 colloidal nanocrystal clusters. *Nanoscale* **2013,** *5* (15), 7026-7033.

32. Himstedt, H. H.; Yang, Q.; Qian, X.; Wickramasinghe, S. R.; Ulbricht, M., Toward remote-controlled valve functions via magnetically responsive capillary pore membranes. *Journal of Membrane Science* **2012,** *423*, 257-266.

33. Bowen, W. R.; Welfoot, J. S., Predictive modeling of nanofiltration: membrane specification and process optimisation. *Desalination* **2002,** *147* (1-3), 197-203.

34. Coronell, O.; Mi, B.; Marinas, B. J.; Cahill, D. G., Modeling the Effect of Charge Density in the Active Layers of Reverse Osmosis and Nanofiltration Membranes on the Rejection of Arsenic(III) and Potassium Iodide. *Environmental Science & Technology* **2013,** *47* (1), 420-428; Kelewou, H.; Lhassani, A.; Merzouki, M.; Drogui, P.; Sellamuthu, B., Salts retention by nanofiltration membranes: Physicochemical and hydrodynamic approaches and modeling. *Desalination* **2011,** *277* (1-3), 106-112.

35. Murthy, Z. V. P.; Gupta, S. K., Estimation of mass transfer coefficient using a combined nonlinear membrane transport and film theory model. *Desalination* **1997,** *109* (1), 39-49.

2. Magnetically Responsive Self-Cleaning Micro-Mixing Nanofiltration Membranes

2.1 Introduction

Development of economical, efficient and durable water purification processes is called for in recent years to address global water shortage. Membrane separation processes have already demonstrated successful commercialization out of their significant advantage in seawater desalination and removal of organic and inorganic compounds from wastewater and drinking water. As discussed in Chapter 1, the cutoff size of NF membranes is somewhere between those of UF and RO membranes. Whereas UF processes are mainly used for the removal of organic compounds and RO processes are used largely for the complete desalination to obtain deionized water, NF processes are mostly applied for the removal of the divalent or trivalent ions and small organic compounds from water. NF is more economical compared to RO for water purification and achieves more complete water purification compared to UF. Besides water purification, NF has various other industrial applications as listed in Table 2.1.

Table 2.1 Applications of nanofiltration in industry.[1, 2]

Industry	**Application of NF processes**
Fine chemistry and pharmaceuticals	• Non-thermal solvent recovery and management • Room temperature solvent exchange
Oil and petroleum industry	• Removal of tar components in feed • Purification of gas condensates
Bulk chemistry	• Product polishing • Continuous recovery of homogeneous catalysts

However, NF processes suffer from concentration polarization leading to membrane fouling and compromised performance. As the membrane operation process continues, more and more rejected species would accumulate within the membrane surface boundary layer to cause concentration polarization. Concentration polarization induces precipitation, deposition and

adsorption of the undissolved species onto membrane surface which causes membrane fouling. Recent studies[3] only involve direct physical or chemical modifications to the membrane surface to mitigate fouling. After surface modification with fouling resistant materials, the strong adhesive forces between the membrane surface and the foulants are reduced. However, low surface adhesion does not reduce concentration polarization with rejected species accumulating at the membrane boundary layer. This still leads to compromised membrane performance with declined flux and rejection. Besides substantial flux decline due to concentration polarization, the rejected species would precipitate and cause membrane fouling when their concentrations exceed their solubility. For the nonporous NF membranes used for removing dissolved small organic molecules and tri- or divalent salts in water, it has been demonstrated that most fouling is actually caused by concentration polarization.[4] Our magnetically responsive micro-mixing membranes, when subject to an appropriate alternating magnetic field, will self-clean by breaking concentration polarization. Micro-mixing is generated by the movement of the polymer chains grafted on the membrane surface under an external magnetic field. The schematic of the design is shown in Figure 2.1.[5]

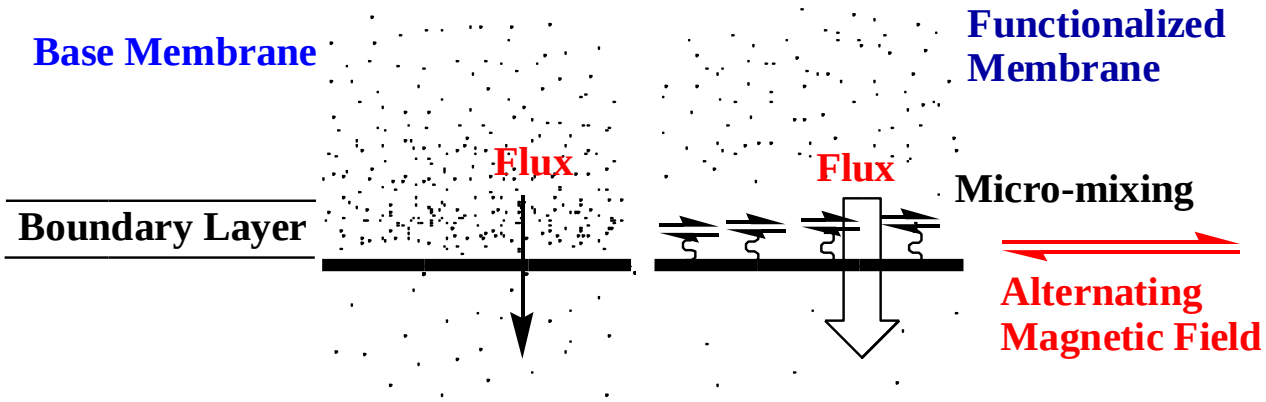

Figure 2.1 Magnetically responsive functionalization to NF270 membrane to break concentration polarization and prevent membrane fouling.[5, 6]

2.2 Experimental Section

2.2.1 Materials

NF270 composite polyamide nanofiltration membranes are thin film flat-sheet membranes provided by Dow Chemical (Edina, MN, USA). All membrane samples were cut from such NF270 membrane sheets, and into small circular membrane discs with a diameter of 44.5 mm.

Carboxylic acid functionalized superparamagnetic nanoparticles (SPNs) conjugated to the polymer chain ends were directly purchased from Ocean Nanotech (Springdale, AR). The Fe_3O_4 nanoparticles have a core diameter of 15 nm and 5 nm coating layer of oleic acid ($CH_3(CH_2)_7CH=CH(CH_2)_7COOH$). According to the manufacturer, the approximate number of carboxylic acid groups on the surface of each nanoparticle is around 120. The estimated density

$$\frac{N}{A} = \frac{120}{4\pi(25/2)^2} = 0.0611/nm^2 \qquad (2.1)$$

where N is the number of carboxylic acid group and A is the surface area of the individual nanoparticle.

The deionized water came from Siemens/ELGA Purelab Ultra deionizer and SCMK2 filters, Siemens Water Technologies (Warrendale, PA). The details about all the chemicals used during the membrane functionalization process and membrane performance tests are listed in APPENDIX A6.

2.2.2 Membrane Functionalization Process

Information about chemical reactions involved in NF270 membrane functionalization can be found in Appendix A1. Membrane functionalization requires the grafting of uniform polymer chains on membrane surface, followed by the attachment of SPNs to the polymer chain ends. The grafting of polymer chains consists of initiator immobilization onto the membrane surface

followed by atom transfer radical polymerization (ATRP) to grow polymer chains. ATRP is a well-controlled polymerization reaction with polymer molecular weight increases linearly with the reaction time and results in a low polydispersity.[7] In order to attach the nanoparticles to the polymer chain ends, a Gabriel synthesis step was used to convert the bromide group at the chain end to an amine group. The last step involves the conjugation of amine group with a carboxylic acid group on the nanoparticle. The grafting degree of the functionalized membrane is calculated using Equation 2.2.[8]

$$GD = \frac{M - M_o}{S} \qquad (2.2)$$

where

GD is the grafting degree in $\mu g/cm^2$;

M and M_o are the weight of the membrane after and before ATRP reaction and S is the membrane surface area.

2.2.3 Membrane Surface Characterization

Contact angle, ATR-FTIR and XPS measurements were conducted to the NF270 base membranes and the functionalized membranes with a range of grafting degrees. FESEM (Field Emission Scanning Electron Microscopy) and AFM (Atomic Force Microscopy) were also performed to confirm the successful functionalization and nanoparticle conjugation.[9, 10]

Contact Angle

DI water contact angles were measured for the base NF270 membrane, and functionalized membranes with varying chain length and chain density. The water contact angle provides information on the relative hydrophilicity and roughness of the membrane surface.[11, 12] The measurements were carried out using OCA 15EC from Future Digital Scientific Corporation

(Garden City, NY).

Attenuated Total Reflectance Fourier Transform Infrared Spectroscopy (ATR-FTIR)

ATR-FTIR measurements were conducted for the base and functionalized NF270 membranes under various grafting conditions. The spectra contains chemical information of the membrane.[11] Spectroscopic measurements were measured using SHIMADZU spectrophotometer.

X-ray Photoelectron Spectroscopy (XPS)

XPS provides elemental and chemical information of membranes during various modification steps. In particular, the appearance of the Fe peak is a clear indication of successful nanoparticle conjugation.[5, 6]

XPS spectroscopy was obtained with Physical Electronics (PHI) Versaprobe XPS workstation (Chanhassen, MN).

FESEM (Field Emission Scanning Electron Microscopy)

FESEM images the membrane surface at the micro-scale.[5, 6, 10, 13] FESEM used for this study was a FEI/Philips Sirion 12 Field Emission SEM (Hillsboro, OR, USA). Membrane samples were coated by a 10 nm gold layer before analysis.

Atomic Force Microscopy (AFM)

AFM is an alternative to FESEM in obtaining micro- or even nanoscale images of the membrane surfaces.[10] Unlike other micro-scale imaging methods, AFM can be conducted in-situ. Moreover, AFM can generally provide higher resolution compared to FESEM.[9, 10, 14] BRUKER (Camarillo, CA) AFM was used for this study.

2.2.4 Membrane Performance Tests

In order to investigate the effects of micro-mixing on concentration polarization of salt solution during NF processes, transport properties of salt solutions with varying concentration

and salt type were systematically investigated. Similar to our previous work,[5, 6] membrane performance tests including flux and salt rejection measurements were conducted. This was done in a dead-end operation mode with a 50 mL Amicon 8050 membrane cell purchased from Millipore (Billerica, MA). In order to compare the effects of membrane functionalization in the presence and absence of an external field, the filtration experiments were conducted without stirring. Salt rejections were determined using a conductivity meter.[5] The detailed procedures for membrane flux and salt rejection tests were described in Appendix A2 and Appendix A3, respectively. The information on pre-conditioning the base and functionalized NF270 membranes before filtration experiments is included in Appendix A4. Information about the solenoids and the external magnetic field is described in Appendix A5.

2.3 Results and Discussion

2.3.1 Grafting Degrees

ATRP is a controlled polymerization process with polymer chain length growing almost proportionally to the reaction time and low poly-dispersity. The grafted polymer chain density can be controlled by varying initiator anchoring time and/or initiator concentration. According to prior work by Yang *et al.*,[5] the grafting degree with 6 h of initiator anchoring time is almost twice as that of 2 h initiator anchoring time for samples with 4 hours of ATRP. The same procedure and reaction condition as those in earlier studies were adopted.[7]

Figure 2.2 shows the grafting degree versus reaction time for high density (HD) and low density (LD) polymer chains. As mentioned before, grafting degree is generally found to be linearly depending on ATRP time. Earlier studies show that membrane samples with 1 to 4 h ATRP time generate pronounced micro-mixing effects.[8, 15] As a result, membranes with 1-4 hours

of ATRP times with 2 and 6 hours of initiator anchoring times were investigated.

As shown in Figure 2.2, grafting degrees at both high and low chain densities are linearly dependent on the ATRP reaction time. The grafting degree increases faster for the HD polymer chains than for the LD chains. Membrane samples are designated with either HD or LD and the ATRP reaction time. For example, LD1h represents membrane sample grafted with low density poly (HEMA) with 1 hour of ATRP reaction time.

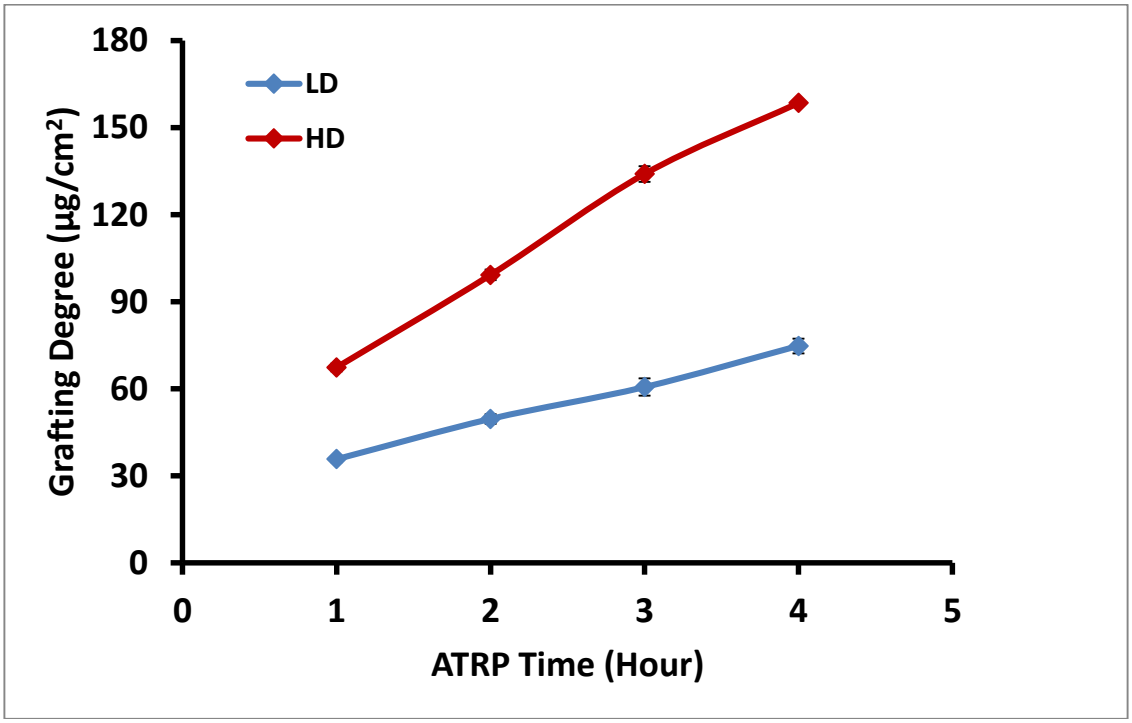

Figure 2.2 Grafting degrees as a function of ATRP time for low (LD) and high (HD) polymer chain densities with 2 or 6 hours of initiator immobilization time.

2.3.2 Contact Angle Measurement

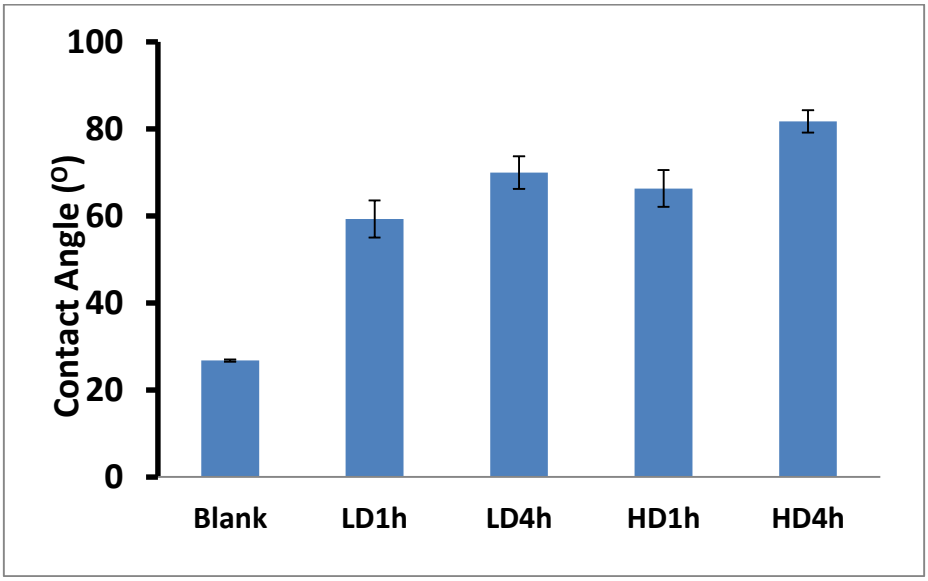

Figure 2.3 Contact angles for the base and functionalized membranes at various conditions. The estimated errors are based on three different measurements at three different locations for each membrane sample. The blank sample is the base NF270 membrane.

DI water contact angle measurements plotted in Figure 2.3 reveal the relative hydrophilicity of the membrane surfaces after nanoparticle conjugation, and with different ATRP modification conditions.[12] Before measurement, the base membrane was immersed in DI water for 24 hours and subsequently vacuum-dried overnight.

The contact angle increased after poly (HEMA) chains grafting on membrane surface followed by SPN conjugation to the polymer chain ends. Largely due to the increased polymer coverage, contact angle increases with increases in polymer chain length for both the HD and LD grafting. For the same ATRP time thus possibly similar polymer chain length, membranes with higher density polymer chains show slightly larger contact angle.[12] This is due to the higher polymer coverage for the high density grafting. In addition, for the membranes grafted with high density polymer chains, the density of nanoparticles should be relatively higher compared to the membranes grafted with low density polymer chains even though not all polymer chain ends are

attached by a superparamagnetic nanoparticle. As the nanoparticles are more hydrophobic than the polyamide barrier layer and the poly (HEMA) gel layer, it is expected that DI water contact angle is higher for samples with the same ATRP reaction time but increased chain density.

2.3.3 ATR-FTIR Spectroscopy

The ATR-FTIR spectroscopy of the base and functionalized NF270 membranes with the lowest and highest grafting degrees for both the low and high polymer chain density is shown in Figure 2.4.

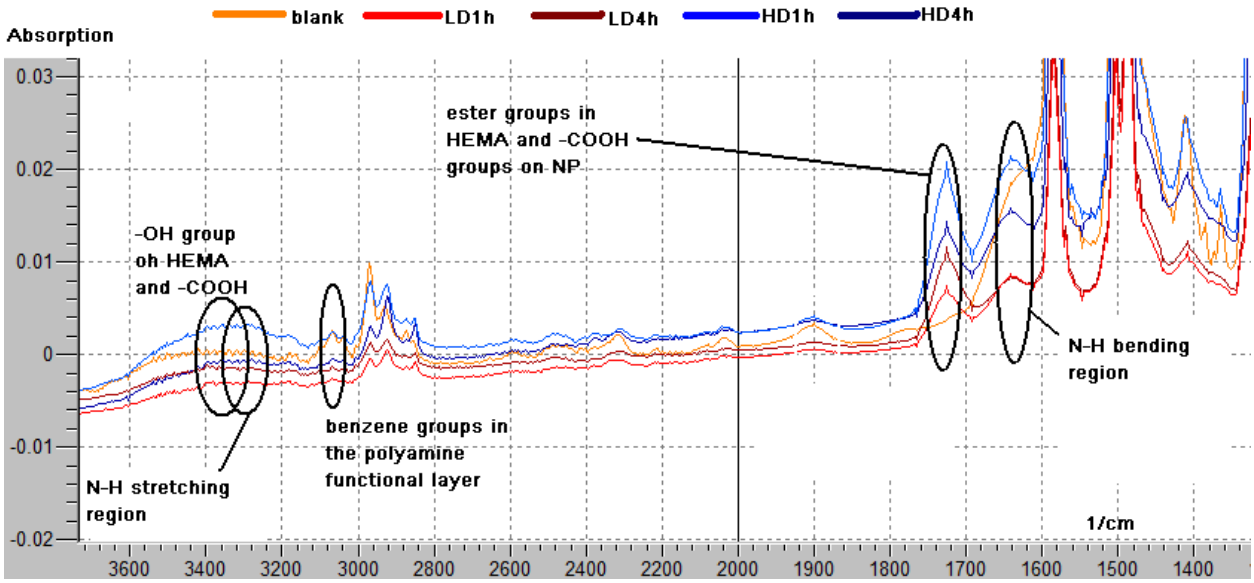

Figure 2.4 ATR-FTIR of the NF270 membrane substrates grafted with poly (HEMA) at various polymer chain density and chain length after nanoparticle conjugation. The blank sample is the base NF270 membrane.

As shown in Figure 2.4, the 3450~3300 cm^{-1} region in ATR-FTIR spectroscopy is due to O-H stretching. The peak increases after functionalization particularly for the HD1h modification condition due to the increased number of -COOH groups on the membranes conjugated with nanoparticles functionalized with carboxylic acid groups.

The peaks at 3350~3250 cm^{-1} region are due to N-H stretching from the primary and

secondary amines. The peaks increase for the HD1h modification condition after functionalization, indicating increased number of the N-H bonds in the surface region. Other modification conditions appear to have reduced intensities in this region.

The peaks around 1650~1580 cm^{-1} are due to N-H bending from primary amine. The peaks in this region are observed to increase after surface functionalization for HD1h. All three regions at 1650~1580 cm^{-1}, 3350~3250 cm^{-1} and 3450~3300 cm^{-1} show increased intensity for the HD1h sample. This is due to the fact that HD1h functionalized membrane should have the largest density of the functional groups including –COOH, -NH and $–NH_2$ groups. The HD4h membrane sample will have relatively lower numbers of these functional groups due to radical terminations as well as buried polymer chain ends within longer chains.

The peaks just above 3000 cm^{-1} come from C=C or benzene. These peaks come from the polyamide barrier layer of the NF270 base membranes. After functionalization, the peaks are somewhat reduced, indicating the effects of surface modification.

The peaks located at 1760~1700 cm^{-1} region come from the C=O group of the ester bond. The peak appears after functionalization with poly (HEMA) grafting and the subsequent nanoparticle conjugation.[5, 6, 11, 12]

2.3.4 XPS Spectroscopy of Nanoparticle Conjugated Membranes

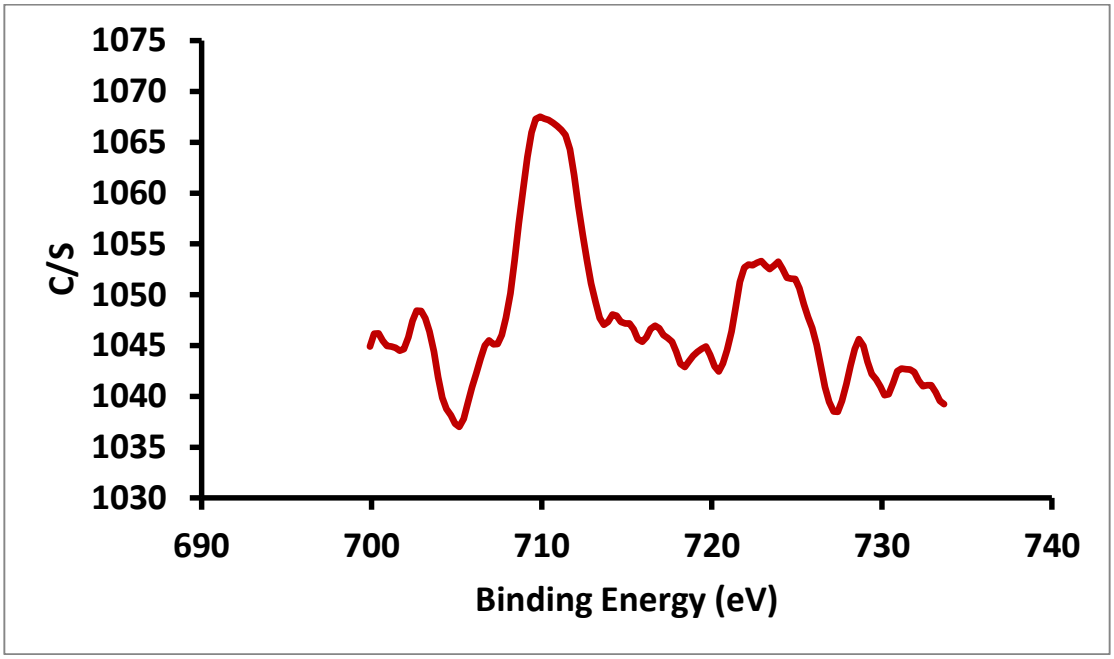

Figure 2.5 XPS spectroscopy in the Fe region for the nanoparticle functionalized NF270 membrane.

XPS spectroscopy of the functionalized membrane samples in Fe region is shown in Figure 2.5. The two peaks located at around 708 and 723 eV belong to Fe $2p_{3/2}$ and Fe $2p_{1/2}$ in the Fe_3O_4.[16] According to earlier studies, the binding energies of Fe $2p_{3/2}$ and Fe $2p_{1/2}$ for Fe in Fe_3O_4 should be located at 710 and 725 eV, respectively.[17] The 2 eV decrease of the binding energy for both peaks are possibly due to the charging effect. Moreover, the intensity of Fe $2p_{1/2}$ peak is higher than the Fe $2p_{3/2}$ peak but narrower in width in agreement with previous results.[17] This indicates the successful attachment of Fe_3O_4 superparamagnetic nanoparticles onto the membrane surface.[6]

2.3.5 AFM Imaging of Functionalized Membranes

Figure 2.6 shows the AFM images of a functionalized polyamide membrane with high polymer chain density and 2 h of ATRP time. It is evident that the nanoparticles are successfully attached onto the membrane surface and are evenly distributed. It is clear that the diameters of all

the nanoparticles on the membrane surface are close to 25 nm, the same as the size provided by the supplier, Ocean Nanotech.[9, 14] Moreover, these AFM images provide useful information on the relative density of the polymer chains grafted on the membrane substrate and show that membrane functionalization is successful. Most importantly, these AFM images show that no nanoparticle aggregation is present on the functionalized membranes and that they are attached at the polymer chain ends as no buried nanoparticles are seen. This is significant as nanoparticles are prone to aggregate which could prevent the movement of the particles in the presence of an external field.

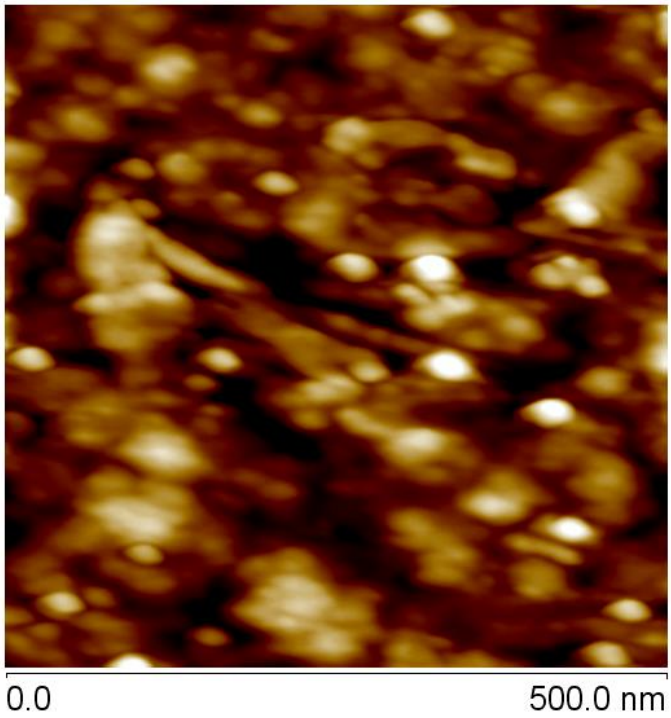

(a) 500 nm scale.

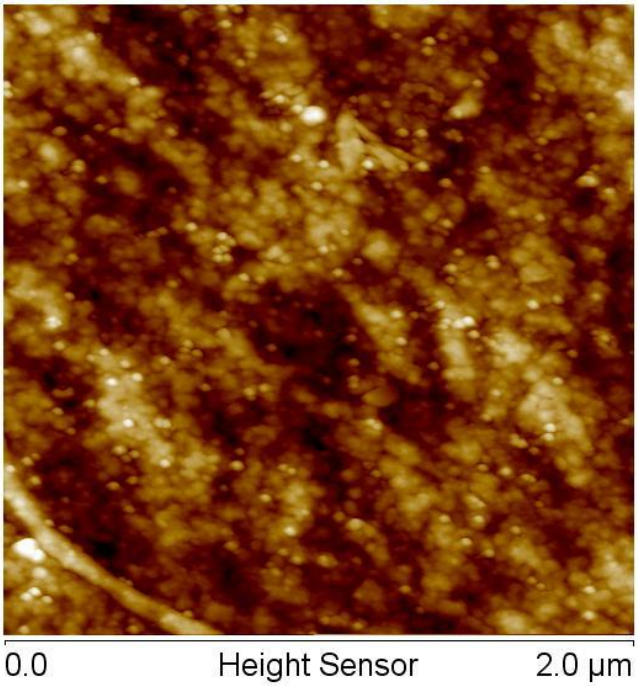

(b) 2 µm scale.

Figure 2.6 AFM images of HD2h sample with conjugated nanoparticles at high (500 nm) and low (2 µm) resolutions.

2.3.6 Membrane Performances for the Functionalized Membranes

According to the most recent literature on nanofiltration for water purification,[18, 19] monovalent and divalent salt ions have significantly different transport properties across the same NF membrane. We will investigate the transport properties of the commonly used model monovalent and divalent salts of NaCl and $MgSO_4$. In addition, $CaCl_2$, $MgCl_2$ and trivalent Na_3PO_4 salt solutions were also investigated here in order to understand the effects of charge on the transport properties. The salt concentrations investigated start from 500 ppm to 1000, 2000, 4000 and 6000 ppm.[5, 6] All measurements were performed at room temperature and under constant pressure of 45 psig using an Amicon cell with 50 ml maximum volume. The permeate was accumulated, and weighted after every 3 minutes.

The previous work[5, 6] show that an oscillating magnetic field of 20 Hz demonstrated the best performance for NF270 membranes compared to other field conditions. Therefore, for all the results under external field listed in this dissertation, 20 Hz magnetic field was used throughout unless stated otherwise. The duration for all the performance measurements was kept at 33 minutes. The flux reported for performance improvement study is the average flux during the last 12 minutes of each 33-minute testing. This period was used since the flux tends to stabilize during this time period compared to the first 21 minutes. Also, in order to guarantee consistency, salt rejection was based on the conductivity of all the permeate collected at around 2.6~3.0 g. Performances of base and functionalized NF270 membranes for 2000, 4000 and 6000 ppm NaCl and $MgSO_4$ salt solutions are given in Table 2.1 and Table 2.2, respectively. Table 2.1 shows the flux and rejection data for functionalized LD1h and HD1h membranes at three NaCl concentrations. Table 2.2 shows the transport data for functionalized LD1h and LD4h membranes at three $MgSO_4$ salt concentrations.

Table 2.2 Flux and rejection for filtration of NaCl solutions using LD1h and HD1h membranes with and without 20 Hz oscillating magnetic field.

	Magnetic field	**Membrane**	**2000 ppm**	**4000 ppm**	**6000 ppm**
Flux $L/(m^2*h)$	Under 20 Hz magnetic field	Base	21.7±0.2	19.7±0.2	18.0±0.4
		LD1h	13.8±0.1	13.6±0.1	13.4±0.1
		HD1h	11.6±0.1	11.4±0.2	11.2±0.2
	No magnetic field	Base	21.4±0.2	19.3±0.1	17.8±0.2
		LD1h	12.7±0.1	12.4±0.1	12.1±0.2
		HD1h	10.4±0.1	10.1±0.2	9.8±0.2
Rejection %	Under 20 Hz magnetic field	Base	4.7±0.1	3.6±0.1	2.8±0.2
		LD1h	12.2±0.1	10.7±0.1	8.6±0.2
		HD1h	21.2±0.2	18.8±0.3	16.1±0.2
	No magnetic field	Base	4.6±0.1	3.5±0.1	2.8±0.1
		LD1h	10.8±0.2	9.1±0.2	7.2±0.1
		HD1h	17.8±0.1	15.7±0.2	13.1±0.1

Table 2.3 Flux and rejection for filtration of $MgSO_4$ solutions using LD1h and LD4h membranes with and without 20 Hz oscillating magnetic field.

	Magnetic field	**Membrane**	**2000 ppm**	**4000 ppm**	**6000 ppm**
Flux $L/(m^2*h)$	Under 20 Hz magnetic field	Base	8.3±0.1	7.8±0.2	7.3±0.2
		LD1h	7.3±0.1	7.0±0.1	6.7±0.1
		LD4h	5.4±0.1	5.0±0.1	4.6±0.1
	No magnetic field	Base	8.2±0.1	7.7±0.2	7.3±0.1
		LD1h	6.7±0.2	6.3±0.1	5.9±0.2
		LD4h	3.8±0.1	3.4±0.1	3.0±0.1
Rejection %	Under 20 Hz magnetic field	Base	30.4±0.5	28.5±0.3	26.6±0.3
		LD1h	74.1±0.1	73.7±0.2	73.0±0.2
		LD4h	76.9±0.2	76.6±0.3	75.5±0.2
	No magnetic field	Base	30.4±0.1	28.3±0.2	26.5±0.1
		LD1h	70.0±0.1	68.3±0.2	67.0±0.1
		LD4h	70.9±0.2	70.2±0.2	68.6±0.2

Both Table 2.1 and 2.2 show that flux decreases after surface modification due to increased membrane resistance to the permeate flow after grafting poly (HEMA) layer. The rejection also improves after functionalization. The decreases in flux and the increases in rejection both depend on salt type and salt concentration as well as on the surface modification condition. For each functionalized membrane, presence of an external 20 Hz oscillating magnetic field affects the transport properties substantially. It can be seen that both flux and salt rejection increase in the presence of an external field compared to the data without field. In addition, flux and rejection improvements are salt type and salt rejection dependent. Meanwhile, the flux and rejection for the base membranes do not seem to be affected much by the external magnetic field.[5, 6]

For all the functionalized membranes, it seems that the improvement in flux and rejection increases with the increase of the feed concentration for both NaCl and $MgSO_4$. At a higher bulk feed concentration, concentration polarization is severer due to the larger concentration gradient. The micro-mixing effect induced by the movement of the nanoparticle functionalized polymer chains in the presence of an oscillating field helps break down the concentration polarization. Thus the effects are more evident for higher concentration feed solutions. More quantitative analysis and detailed discussions on this topic will be presented in Chapter 3.

2.3.7 Flux Results for Functionalized Membranes with $CaCl_2$ Feed Solutions

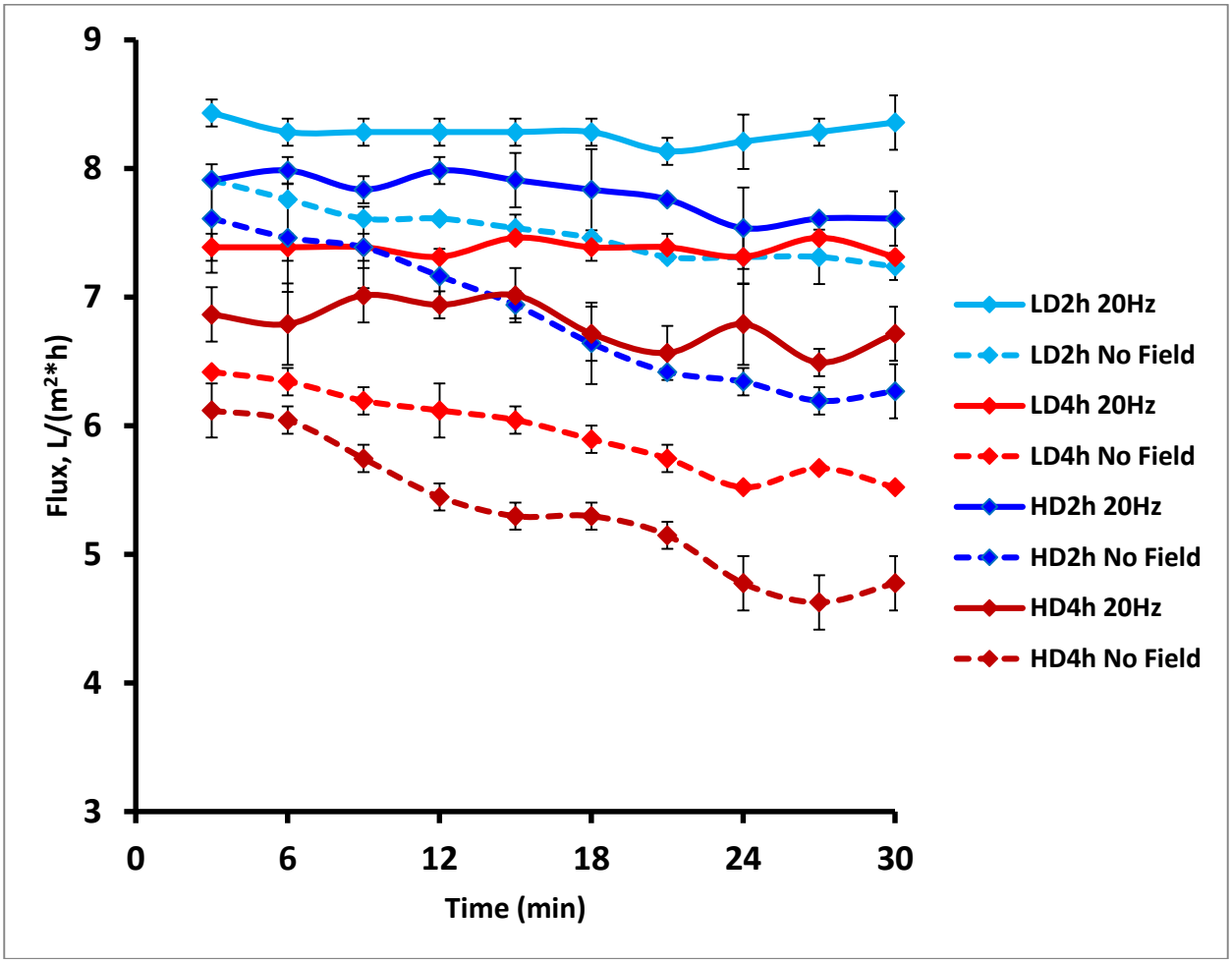

Figure 2.7 The effect of magnetic field on flux for functionalized LD2h, LD4h, HD2h and HD4h membranes with 6000 ppm $CaCl_2$ feed solutions.

Figure 2.7 shows the flux measurement over time for functionalized LD2h, LD4h, HD2h and HD4h membranes using the 6000 ppm $CaCl_2$ feed solution. The solid lines represent the fluxes in the presence of 20 Hz magnetic field. It can be seen that they remain more or less the same during the entire measurement. The dashed lines represent the fluxes without an external magnetic field. It can be seen that they decrease continuously during the entire testing period. Moreover, it appears that fluxes are higher in the presence of an external field than those without the field for the same functionalized membrane. Clearly, an external magnetic field reduces

concentration polarization thus improves the transport properties. In the absence of an external field, the fluxes decrease continuously over time due to the accumulation of rejected salt ions at the membrane-liquid boundary layer. However, when an oscillating magnetic field is exerted at the membrane-liquid intrface parallel to the membrane surface, the superparamagnetic nanoparticles attached to the chain ends experience an oscillating magnetic force proportional to the gradient of the external magnetic field and the magnetic moment of the superparamagnetic nanoparticle. The movement of the nanoparticles causes the polymer chains to move back and force at the same frequency as the external field. Movements of the polymer chains generate micro-mixing effect within the boundary layer, decreasing the concentration of rejected salt ions on membrane surface and reducing the salt concentration difference across the membrane. Therefore, for the same feed, flux is higher when the field is present. The micro-mixing effect due to the movement of the grafted polymer chains also improves rejection.

To note, for all the results listed in this dissertation, "improvement" and "percentage improvement" concern flux and rejection for the same functionalized NF270 membrane with the same feed solution in the presence of an external field compared to those in the absence of the field.

2.3.8 Flux and Rejection Improvements for LD Membranes with $MgSO_4$ Feed Solutions

Figures 2.8 and 2.9 show the flux and rejection percentage improvements for the LD1h, LD2h, LD3h and LD4h functionalized membranes with various concentrations of $MgSO_4$ feed solutions. The corresponding grafting degrees for ATRP 1-4 hours are 35.8, 49.6, 60.6 and 74.8 $\mu g/cm^2$, respectively. It's evident that percentage improvements of both flux and rejection tend to increase with the increases of grafting degree as well as feed salt concentration. Concentration

polarization is severer under higher feed solute concentrations due to a higher concentration gradient. In the presence of oscillating magnetic field, the micro-mixing generated by the movements of polymer chains on the functionalized NF membranes effectively breaks concentration polarization within the boundary layer thus improves the membrane's flux and rejection. The effects therefore are stronger for the higher salt concentration feed solutions. Moreover, with the same polymer chain density, longer polymer chains tend to generate stronger micro-mixing in the presence of an external 20 Hz oscillating magnetic field. As a result, the effect of magnetic field on flux improvement increases with the increase of grafting degree. This is in agreement with the earlier results.[5]

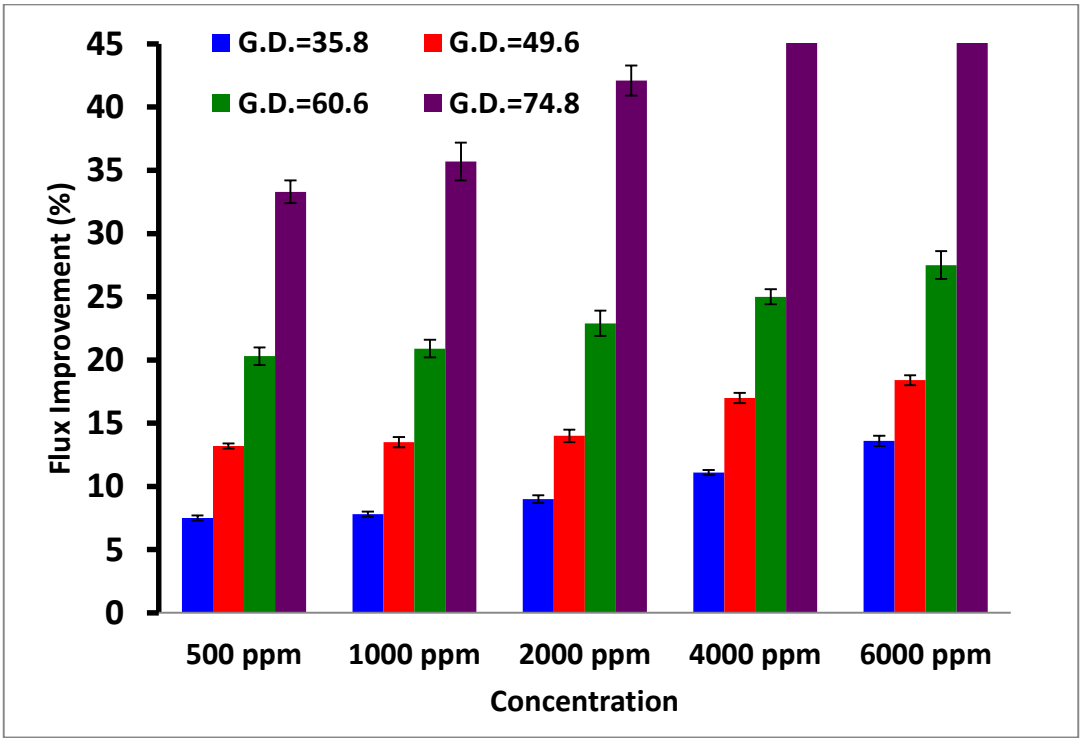

Figure 2.8 Percentage flux improvement for LD1h, Ld2h, Ld3h and LD4h membranes with different concentrations of $MgSO_4$ feed solutions in the presence of a 20 Hz magnetic field, with G.D. representing the grafting degree.

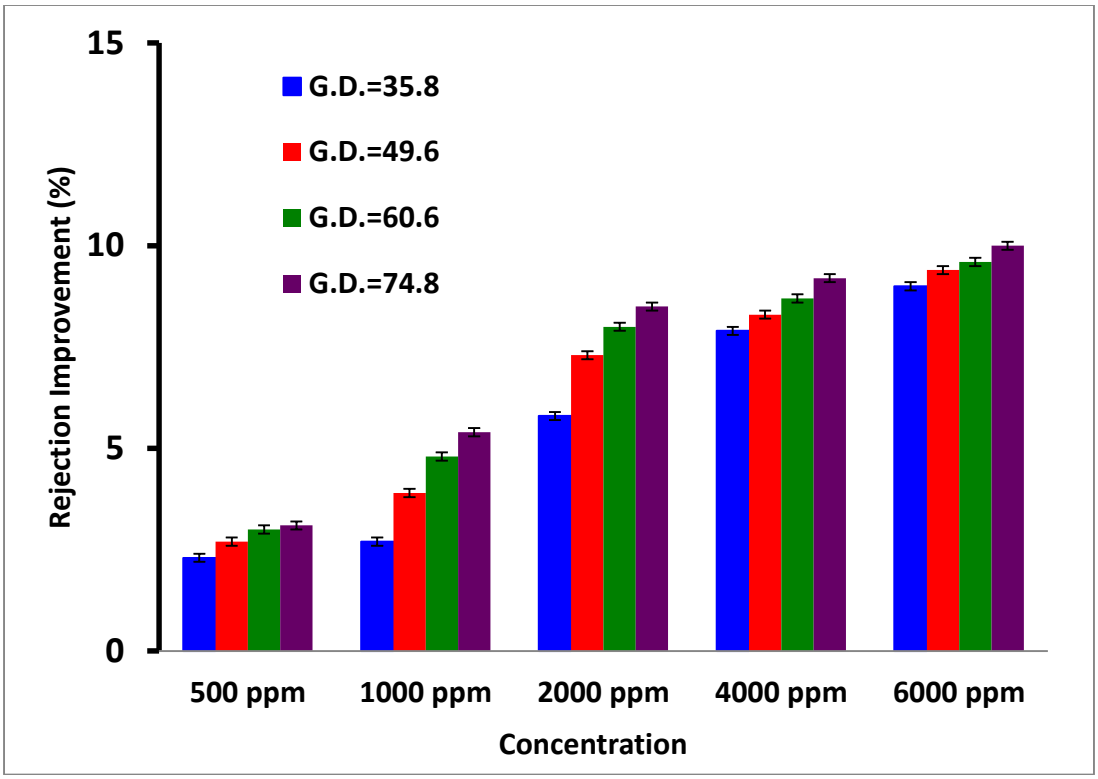

Figure 2.9 Percentage salt rejection improvement for LD1h, LD2h, LD3h and LD4h membranes with various concentrations of $MgSO_4$ feed solutions in the presence of 20 Hz magnetic field, with G.D. representing the grafting degree.

2.3.9 Performance of Functionalized LD and HD Membranes with $CaCl_2$ Feed Solutions

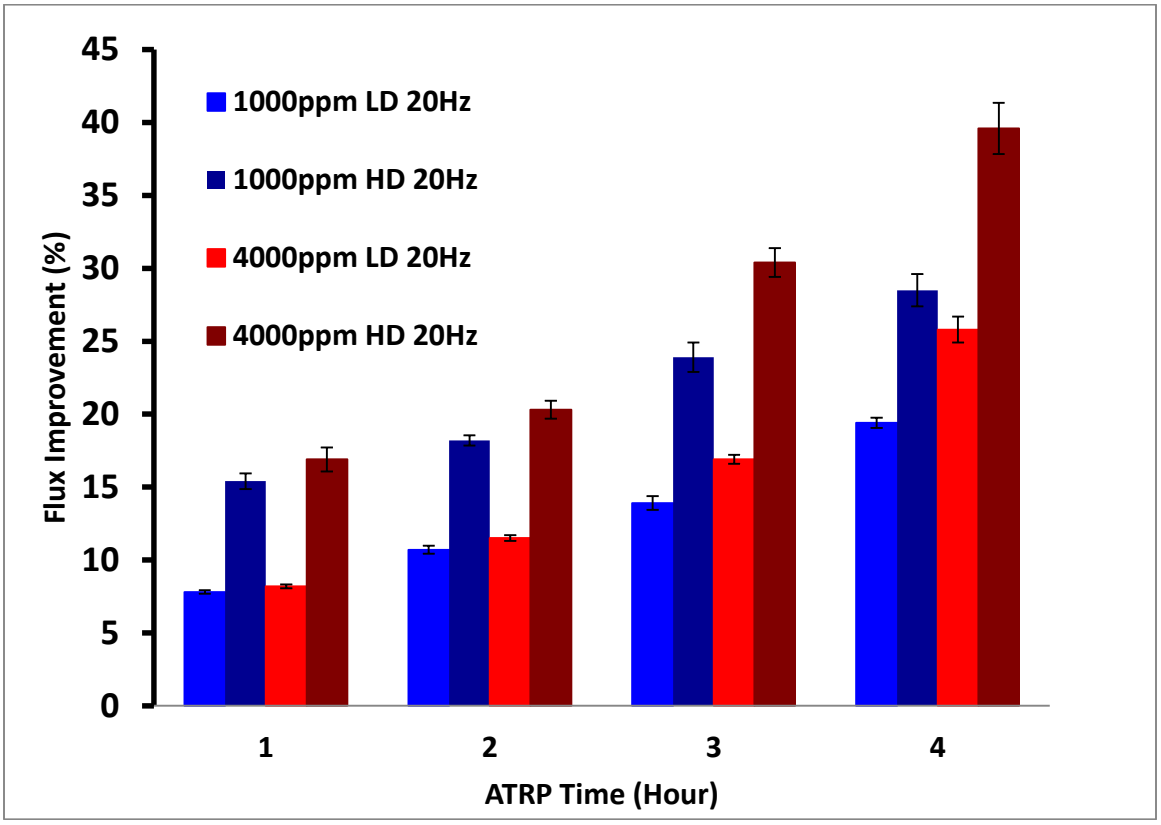

Figure 2.10 Flux improvement vs. ATRP time for functionalized LD and HD membranes with 1000 ppm and 4000 ppm $CaCl_2$ feed solutions.

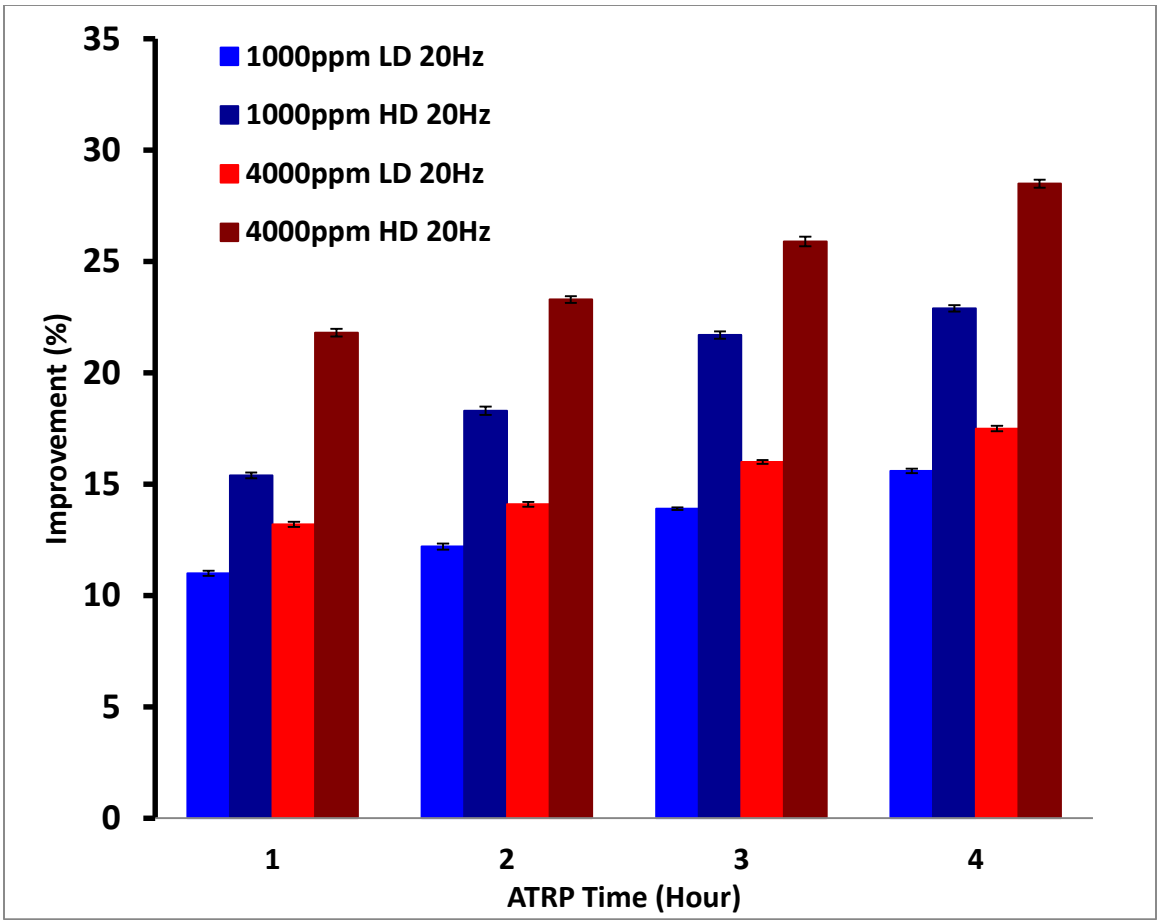

Figure 2.11 Percentage improvements in rejections for functionalized HD and LD membranes with 1000 ppm and 4000 ppm $CaCl_2$ feed solutions.

Figures 2.10 and 2.11 show the percentage improvement in flux and rejection for $CaCl_2$ salt feed solutions at 1000 and 4000 ppm concentrations with HD and LD functionalized membranes at various chain lengths (ATRP time). These results are consistent with previous conclusions that increasing chain length or chain density would improve the percentage improvements of both flux and rejection of functionalized membranes.[5] Moreover, the percentage improvement is more significant at higher feeding salt concentrations when concentration polarization is more severe.[6, 20]

The differences in percentage improvement for different functionalized membranes in the presence of an oscillating magnetic field for $MgSO_4$ and $CaCl_2$ salt feed solutions can be

explained by the different micro-mixing effects under varied chain length and density. Generally, longer polymer chains and higher polymer chain density induces stronger micro-mixing effects leading to the more effective suppression of concentration polarization.

However, further increase in polymer chain length or chain density may not improve the performance any longer. The increase in grafting degree might actually weaken the effect of magnetic field due to chain entanglement during chain movements.[5] Moreover, longer polymer chains will encounter higher resistance during movement in the liquid solution. Higher polymer chain density would increase the chance of radical termination during the slow polymerization process.[6, 7] In addition, higher polymer chain density would increase the chance of conjugating multiple polymer chains to the same nanoparticle, increasing the resistance of polymer movement. Due to the presence of a denser and thicker layer of poly (HEMA) on membrane surface, excessive increase in polymer chain length or density also increases membrane layer resistance to permeate flow. Therefore, the following discussion focuses on the performances of LD functionalized membranes.

2.3.10 Performance of LD Functionalized NF270 Membranes

Percentage improvements in flux and rejection for the functionalized LD membranes using feed solutions with different salts at 2000 ppm concentration are shown in Figure 2.12 and Figure 2.13, respectively. The feed salt solutions investigated include NaCl, $CaCl_2$, $MgCl_2$, $MgSO_4$ and Na_3PO_4 involving salt ions with different valences.[5, 6, 21]

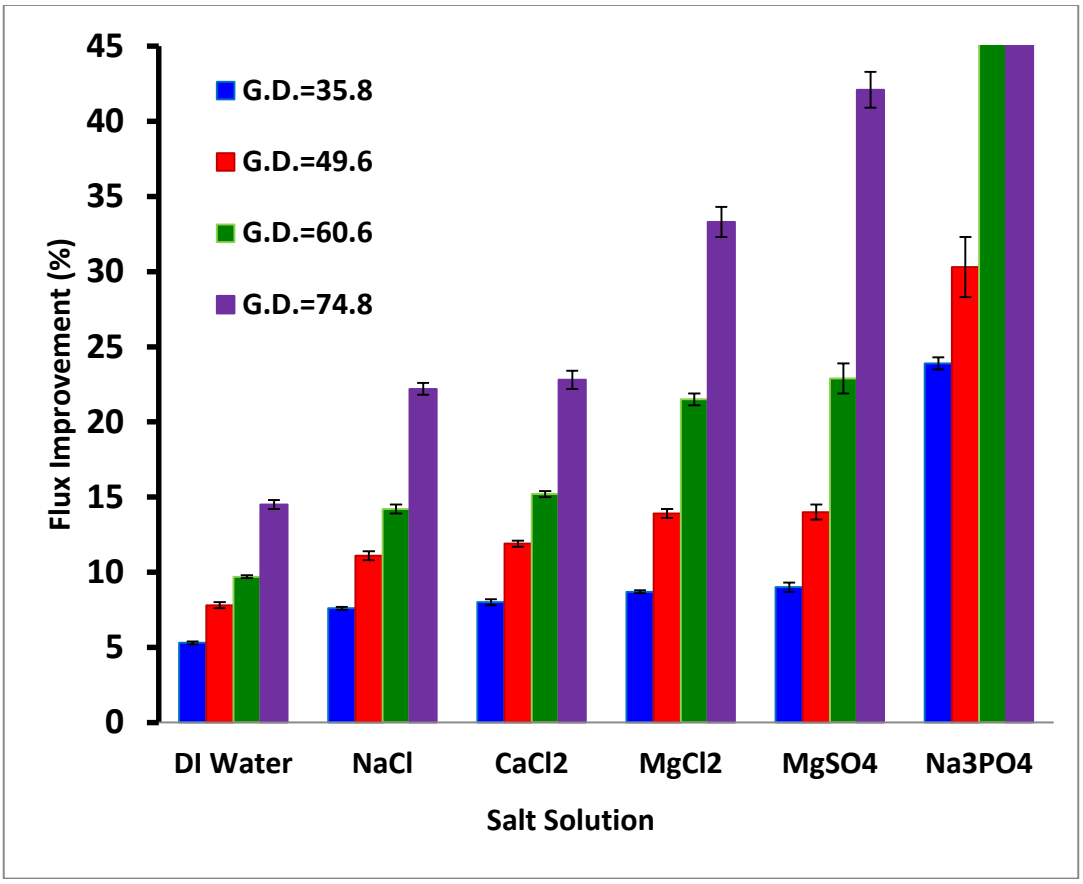

Figure 2.12 Percentage improvement in flux for various 2000 ppm feed solutions as a function of grafting degree in the presence of 20 Hz magnetic field, with G.D. representing the grafting degree.

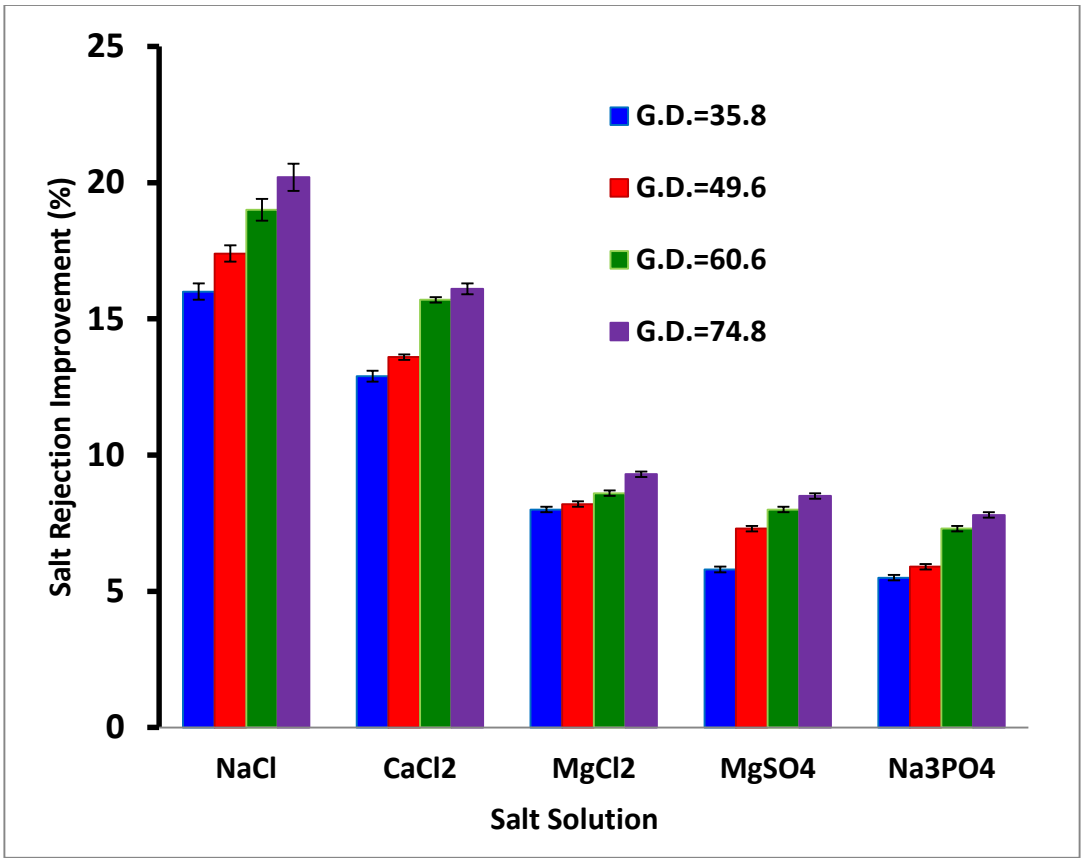

Figure 2.13 Percentage improvement in salt rejection for 2000 ppm feed solutions in the presence of 20 Hz magnetic field, with G.D. representing the grafting degree.

For LD functionalized membranes, percentage improvement in flux and rejection for the same salt solution increases with increasing grafting degree (grafted polymer chain length). From the mono-valent to the tri-valent salt feed solutions, percentage improvement in flux increases as valence increases whereas the percentage improvement in salt rejection decreases as valence increases. As is known, NF is mainly used for the removal of trivalent and some divalent ions from water.[2, 22] As a result, micro-mixing within the membrane's boundary layer mainly increases rejection for the mono- and divalent salt ions that are generally easy to go through the membrane. This is due to the reduced concentration polarization at the boundary layer resulting from the micro-mixing effects. However, for salt with both cations and anions divalent or salt containing one trivalent ion, rejection is already high without mixing. Reducing concentration

polarization under the effect of micro-mixing only improves salt rejection slightly. The opposite is true for flux. For mono- or divalent salt solutions, the flux improvement is slight as flux is relatively high. However, for salt with cations and anions both being divalent ions or salt containing one trivalent ion, flux improvements are significant reaching over 60% for the trivalent Na_3PO_4. It is also clear that flux percentage improvement increases for the same salt feed solution as grafting degree increases, with the effect stronger for high valent salt solutions. On the other hand, the effects of grafting degree on salt rejection percentage improvement are very slight for the same feed salt solution.[19, 20, 23]

As shown in Figure 2.12, DI water flux improvement within the magnetic field also increases with increasing grafting degree. This is due to the fact that grafted polymer chains with attached SPNs change their conformations under an external magnetic field. For NF membranes, surface modification mostly occurs on the membrane surface, leading to the decreased flux. The alignment and stretching of polymer chains by applying an external magnetic field leads to the reduced resistance for water permeation. Decreases in membrane layer resistance are more evident after the alignment and stretching of longer polymer chains on the membranes with higher grafting degree.

2.4 Conclusions

Our results show that polymer chains were successfully grafted on membrane surfaces with polymer grafting degree increasing linearly with ATRP time. Superparamagnetic nanoparticles were also successfully attached onto the ends of grafted poly (HEMA) polymer chains. Magnetically responsive functionalization of NF membrane is effective in breaking concentration polarization by generating micro-mixing effect within the membrane's upstream

side concentration boundary layer. Micro-mixing increases both the flux and rejection therefore the overall performance of the NF membranes. Membrane performance improvement under an external magnetic field always increases with the increase of grafted polymer chain length or density. This is because with increases in either the chain density or chain length, a stronger micro-mixing effect would be generated within the boundary layer to more effectively minimize concentration polarization. Moreover, for the studied salt solutions with concentrations in the 500-6000 ppm range, performance improvements always become more evident at higher salt concentration and after longer periods of performance testing.[24]

References

1. **Schäfer, A. I.**; Fane, A. G.; Waite, T. D., ***Nanofiltration, Principles and Applications***. Elsevier Advanced Technology: New York, 2005.

2. Fane, A. G. F. I. S. D. W. G., *Nanofiltration: Principles and Applications*. Elsevier Advanced Technology: Australia, 2004.

3. Zuo, G.; Wang, R., Novel membrane surface modification to enhance anti-oil fouling property for membrane distillation application. *Journal of Membrane Science* **2013,** *447*, 26-35; Zhao, L.; Chang, P. C. Y.; Yen, C.; Ho, W. S. W., High-flux and fouling-resistant membranes for brackish water desalination. *Journal of Membrane Science* **2013,** *425*, 1-10; Abu Seman, M. N.; Johnson, D.; Al-Malek, S.; Hilal, N., Surface modification of nanofiltration membrane for reduction of membrane fouling. *Desalination and Water Treatment* **2009,** *10* (1-3), 298-305.

4. Listiarini, K.; Chun, W.; Sun, D. D.; Leckie, J. O., Fouling mechanism and resistance analyses of systems containing sodium alginate, calcium, alum and their combination in dead-end fouling of nanofiltration membranes. *Journal of Membrane Science* **2009,** *344* (1-2), 244-251.

5. Yang, Q.; Himstedt, H. H.; Ulbricht, M.; Qian, X.; Wickramasinghe, S. R., Designing magnetic field responsive nanofiltration membranes. *Journal of Membrane Science* **2013,** *430*, 70-78.

6. Himstedt, H. H.; Yang, Q.; Dasi, L. P.; Qian, X.; Wickramasinghe, S. R.; Ulbricht, M., Magnetically Activated Micromixers for Separation Membranes. *Langmuir* **2011,** *27* (9), 5574-5581.

7. Robinson, K. L.; Khan, M. A.; Banez, M. V. D.; Wang, X. S.; Armes, S. P., Controlled polymerization of 2-hydroxyethyl methacrylate by ATRP at ambient temperature. *Macromolecules* **2001,** *34* (10), 3155-3158.

8. Yang, Q.; Ulbricht, M., Cylindrical Membrane Pores with Well-Defined Grafted Linear and Comblike Glycopolymer Layers for Lectin Binding. *Macromolecules* **2011,** *44* (6), 1303-1310.

9. Stawikowska, J.; Livingston, A. G., Assessment of atomic force microscopy for characterisation of nanofiltration membranes. *Journal of Membrane Science* **2013,** *425*, 58-70.

10. Russell, P.; Batchelor, D.; Thornton, J., Scanning Electron Microscopy (SEM) and Atomic Force Microscopy (AFM): Complementary techniques for high resolution surface investigations. *Surface Modification Technologies XV* **2002**, 109-118.

11. Wandera, D.; Wickramasinghe, S. R.; Husson, S. M., Stimuli-responsive membranes. *Journal of Membrane Science* **2010,** *357* (1-2), 6-35.

12. Himstedt, H. H.; Marshall, K. M.; Wickramasinghe, S. R., pH-responsive nanofiltration membranes by surface modification. *Journal of Membrane Science* **2011,** *366* (1-2), 373-381.

13. James, B. J.; Jing, Y.; Chen, M. D., Membrane fouling during filtration of milk - a microstructural study. *Journal of Food Engineering* **2003,** *60* (4), 431-437.

14. Hilal, N.; Al-Zoubi, H.; Darwish, N. A.; Mohammad, A. W., Characterisation of nanofiltration membranes using atomic force microscopy. *Desalination* **2005,** *177* (1-3), 187-199.

15. Friebe, A.; Ulbricht, M., Controlled pore functionalization of poly(ethylene terephthalate) track-etched membranes via surface-initiated atom transfer radical polymerization. *Langmuir* **2007,** *23* (20), 10316-10322.

16. Magenau, A. J. D.; Kwak, Y.; Schroeder, K.; Matyjaszewski, K., Highly Active Bipyridine-Based Ligands for Atom Transfer Radical Polymerization. *Acs Macro Letters* **2012,** *1* (4), 508-512.

17. Gao, J.; Ran, X.; Shi, C.; Cheng, H.; Cheng, T.; Su, Y., One-step solvothermal synthesis of highly water-soluble, negatively charged superparamagnetic Fe3O4 colloidal nanocrystal clusters. *Nanoscale* **2013,** *5* (15), 7026-7033.

18. Luo, J.; Wan, Y., Effects of pH and salt on nanofiltration—a critical review. *Journal of Membrane Science* **2013,** *438* (1), 18–28; Haochen, Z.; Ghoufi, A.; Szymczyk, A.; Balannec, B.; Morineau, D., Computation of the Hindrance Factor for the Diffusion for Nanoconfined Ions: Molecular Dynamics Simulations Versus Continuum-based Models. *Molecular Physics* **2012,** *110* (11-12), 1107-1114; Richards, L. A.; Richards, B. S.; Corry, B.; Schaefer, A. I., Experimental Energy Barriers to Anions Transporting through Nanofiltration Membranes. *Environmental Science & Technology* **2013,** *47* (4), 1968-1976; Lefebvre, X.; Palmeri, J.; David, P., Nanofiltration theory: An analytic approach for single salts. *Journal of Physical Chemistry B* **2004,** *108* (43), 16811-16824.

19. Tansel, B.; Sager, J.; Rector, T.; Garland, J.; Strayer, R. F.; Levine, L.; Roberts, M.; Hummerick, M.; Bauer, J., Significance of hydrated radius and hydration shells on ionic permeability during nanofiltration in dead end and cross flow modes. *Separation and Purification Technology* **2006,** *51* (1), 40-47.

20. Deon, S.; Dutournie, P.; Fievet, P.; Limousy, L.; Bourseau, P., Concentration polarization phenomenon during the nanofiltration of multi-ionic solutions: Influence of the filtrated solution and operating conditions. *Water Research* **2013,** *47* (7), 2260-2272.

21. Hussain, A. A.; Abashar, M. E. E.; Al-Mutaz, I. S., Influence of ion size on the prediction of nanofiltration membrane systems. *Desalination* **2007,** *214* (1-3), 150-166.

22. Mulder, M., *Basic Principle of Membrane Technology*. Kluwer Academic Publishers: Enschede, Netherlands, 1996.

23. Richards, L. A.; Schafer, A. I.; Richards, B. S.; Corry, B., The Importance of Dehydration in Determining Ion Transport in Narrow Pores. *Small* **2012,** *8* (11), 1701-1709.

24. Yaroshchuk, A.; Martinez-Llado, X.; Llenas, L.; Rovira, M.; de Pablo, J.; Flores, J.; Rubio,

P., Mechanisms of transfer of ionic solutes through composite polymer nano-filtration membranes in view of their high sulfate/chloride selectivities. *Desalination and Water Treatment* **2009,** *6* (1-3), 48-53.

3. The Effect of Magnetic Field on Concentration Polarization and Transport Properties for the Magnetically Activated Nanofiltration Processes

3.1 Introduction

Nanofiltration (NF) is a widely adopted membrane-based water purification process that is driven by pressure difference across the membrane. NF is a relatively new water purification technology that is more economical than reverse osmosis (RO) and that achieves more complete water purification than ultrafiltration (UF). With both size and molecular weight cutoff between those of RO and UF, NF membranes are capable of achieving selective separation of different ions. Currently NF membranes are mainly used for the removal of small and low molecular weight organic molecules and di- or trivalent ions from water. The most common applications of NF membranes include softening or partial desalination of water, purification of groundwater by removal of pesticides or other organic pollutants.[1, 2] Other industrial applications of NF processes include sugar concentration, organic solvent recovery and water reuse.

Membrane fouling refers to the loss of productivity due to adsorption, precipitation or accumulation of the particulate or other organic or inorganic matter onto the membrane surface or into the pores of the membrane barrier layer. Membrane fouling leads to the loss of flux and rejection. Similar to RO and UF membranes, NF membranes also suffer from fouling after some periods of usage. Since NF membranes are non-porous and mainly used for the removal of ions and small molecules dissolved in water, the main cause of NF membrane fouling is concentration polarization. Concentration polarization refers to the reversible accumulation of the rejected species within the thin layer immediately above the upstream membrane surface,

forming a concentration boundary layer with a concentration gradient that increases towards the membrane surface. Flux decreases continuously due to increased osmotic pressure difference across the membrane when operated under constant pressure. The rejected species would precipitate and adsorb onto the membrane surface, leading to membrane fouling when the concentration immediately above the upstream membrane surface exceeds the solubility of the rejected species.[3-5]

In recent years, there have been extensive investigations and publications on developing anti-fouling NF membranes. These methods often include chemical modification of membrane structure, or inducing turbulence in the membrane-liquid interface. Surface modification reduces the affinity of the foulant to the membrane surface whereas turbulence improves mixing of the solutes between the concentration polarization boundary layer and the bulk feed. However, chemical modification does not suppress concentration polarization since the rejected species still accumulate continuously at the boundary layer.[3] Moreover, introducing stirring generally affects only the bulk feed above the concentration polarization layer. In order to mitigate concentration polarization and fouling for the NF membranes, magnetically responsive micro-mixing self-cleaning NF membranes have been developed in our group.[6] The procedures for developing these magnetically activated membranes include grafting hydrophilic polymerized 2-hydroxyethyl methacrylate (poly (HEMA)) chains onto the upstream membrane surface followed by conjugating superparamagnetic nanoparticles (SPNs) to the ends of grafted polymer chains. Applying an external oscillating magnetic field exerts oscillating magnetic force to the SPNs, causing the polymer chains to move laterally and generating localized mixing at the membrane-liquid interface. Such micro-mixing effect

suppresses concentration polarization.[7]

NF270 is one of the widely commercialized NF membranes in industry, and one of the most frequently used NF membranes for investigations. Similar to most polymeric NF membranes, NF270 is a thin film composite (TFC) membrane which consists of a polyamide barrier layer that selectively permits ions and molecules to cross the membrane, and two polysulfone mechanical support layers beneath the barrier layer.[8] Chapter 2 investigates the flux and rejection improvement in the presence of an oscillating magnetic field for the functionalized NF270 membranes with varying polymer chain length and chain density using different concentrations of mono-, di- and trivalent feed salt solutions. The filtration experiments were conducted under a constant operation pressure of 45 psig and in the presence or absence of a 20 Hz magnetic field. All filtrations were performed in a dead-end mode without stirring. Compared to tangential flow filtration, dead end filtration is easier to operate and requires less operation volume. In order to investigate the effects of an external magnetic field on concentration polarization, all the tests were done without stirring.[7] From the results in Chapter 2, membrane performances and their percentage improvements in the presence of an oscillating 20 Hz magnetic field demonstrate systematic trends for functionalized membranes with varying polymer chain length and chain density for the same feed salt solution, as well as for a specific modification condition with feed solutions of different salt ions at various concentrations.

Built upon earlier works from our group,[6, 7, 9] the objective of this part of the dissertation is to quantify and understand solvent and solute transport across these magnetically activated NF membranes. Modeling the transport of solvent and solute through these functionalized

membranes will enable us to better understand these transport processes occurring within the membrane barrier layers as well as within the concentration boundary layer above the membrane surface. Developing quantitative models will be helpful to predict the membrane performances under various operation conditions. For quantitative description of the NF processes, several models have already been developed and are found to agree well with experimental outcomes.[10] In recent years, many researchers have adopted these models to predict the physical and chemical properties of NF membranes, and to optimize the membrane separation processes. By adjusting the physical parameters in these models, membrane performance can be determined. Some other researchers also relied on these models to theoretically investigate separation and transport processes based on their experimental outcomes.[11, 12] In this work, several commonly used mathematical models for NF and RO processes are adopted to correlate the parameters based on the experimentally measured membrane performances. This could help us obtain more insights into the effects of an oscillating magnetic field on the performances of both the base and functionalized NF270 membranes with different polymer chain length and chain density when tested with different feed salt solutions.[13]

Two different transport mechanisms coexist within the NF membranes. They are the convective transport as in the porous UF membranes and the diffusive transport as in the non-porous RO membranes. In the solution diffusion imperfection model (SDIM),[14] one assumes that the transport through NF membrane occurs both convectively through the pores and diffusively through the membrane layer outside the pores. There are only detailed theoretical descriptions of this model in the literature since the values of most coefficients are still

unattainable using current experimental methods.[11, 14] Therefore, direct fitting of SDIM equation using the experimentally measured fluxes and rejections is not possible at this time.

The dynamical characteristics of the ions in solutions are described by the Stokes Einstein (S-E) Equation. Since anions and cations need to move together to maintain charge neutrality, the S-E Equation should be used to correlate the dynamical properties of the salt as a whole with those of its ions. The Hagen-Poiseuille model (HPM) was originally used to describe the UF processes assuming uniform pore diameter. The non-porous NF membranes are generally considered tight UF membranes with large free volumes in the barrier layer, especially for the loose thin film composite NF270 membranes.[8] Therefore, researchers frequently made use of the HPM to get information about the physical properties of the NF membrane's barrier layer.[15, 16] Based on the dynamical properties of the salt and the physical properties of the membrane, the retention coefficient of a certain membrane to a certain salt could be calculated by an appropriate steric hindrance model.[16, 17]

The Spiegler-Kedem Katchalsky model (SKKM) has been widely used to describe solute and solvent transport across NF membranes. By considering the membrane as a 'black box', this irreversible thermodynamic model was developed without knowledge of the exact mechanisms of solute and solvent transport across the membrane that are based on the complex morphological details of the membrane layer.[18-23] Moreover, the SKKM assumes the transport of solvent and the transport of solute are not coupled with each other. Along with the SKKM, more recently, researchers frequently adopted the Extended Nernst-Planck equation (ENP) to theoretically describe ion and molecule transport within NF membrane layers. Based on the ENP, transport of ions across the layers of NF membranes is composed of convection, diffusion

and electromigration.[19, 22-25] It's worthwhile to integrate SKKM and ENP to model the NF processes. However, both SKKM and ENP do not contain any coefficient that could reflect transport within the concentration polarization layer, and researchers making use of ENP always assume complete elimination of concentration polarization under fast stirring or high enough tangential flow rate.[18]

The main goal of this research is to investigate concentration polarization under various membrane functionalization and feed conditions. Based on the theoretical work by Zydney in 1997,[26] the film theory model (FTM) has been commonly used to quantify concentration polarization and describe transport within the concentration polarization layer during NF and RO processes.[24, 26-29] Since the presence of concentration polarization significantly affects the transport of solvent and solute, FTM was used in combination with several other models to describe salt transport across the NF membranes taking into account concentration polarization.[24, 28, 29] Nagy *et al*. developed a predictive model by considering the coupled effects of concentration polarization and transport via the membrane layer. The predicted results are almost the same as those observed experimentally.[30] More recently, Fang *et al*. also showed improved modeling results for NF membrane performance by combining ENP and FTM models.[23] Therefore, integration of FTM with SKKM and ENP models has been adopted in the current work.[24, 28, 31, 32]

Most previous studies used cross flow to model the NF processes. The experimentally observed flux and retention were correlated with the physical properties of the membrane layer and the dynamical properties of solutes. These models have been applied to quantify the solvent and solute transport across the NF membranes.[24, 28, 29] Hence these models could also be used

for analyzing concentration polarization and cross-membrane transport for the dead end filtration mode in this work. The cross membrane pressure was kept at constant 45 psig throughout the investigation. Based on the correlation between the experimentally observed fluxes and rejections, concentration polarization could be quantified. Moreover, mass transfer coefficients and other transport parameters could also be obtained. Most importantly, through the analysis of concentration polarization and salt transport in the presence or absence of a magnetic field for the same feed salt and concentration, the effect of oscillating magnetic field on concentration polarization and ion transport properties could be better quantified and understood.[28, 29]

Based on the flux and salt rejection of the functionalized membranes in the presence and absence of oscillating magnetic field as shown in the previous chapter, it is evident that increasing polymer chain length or chain density would produce more effective micro-mixing effect at the membrane-solution boundary layer. However, it also leads to a greater sacrifice of permeate flux. In addition, further increase in polymer grafting degree could cause one nanoparticle conjugating to multiple polymer chains and chain entanglements resulting in substantial reduction in polymer chain mobility. The results shown in Chapter 2 demonstrate that flux and rejection exhibit systematic trends with regard to polymer chain length for the LD functionalized membranes. The longer the grafted polymer chain length is, the lower the flux becomes and the higher the rejection is. The improvement in flux and rejection in the presence of an external oscillating field also demonstrates systematic trends. The longer the polymer chain, the higher the improvement in both flux and rejection due to the more effective micro-mixing effects produced by the longer polymer chains. Moreover, the improvement in the

transport properties in the presence of a magnetic field is also shown to be dependent on the feed solution type and concentration. The higher the feed concentration is, the more effective the polymer chain is in breaking down concentration polarization to lead to better performance improvements for both flux and rejection. The lower valence salt ions show better improvement in rejection whereas higher valence ions show larger improvement in flux in the presence of an oscillating field. In order to quantitatively investigate the effects of micro-mixers on concentration polarization using the integrated FTM, SKKM and ENP models, transport properties of LD1h, LD2h, LD3h and LD4h functionalized membranes were used. The feed solutions investigated include 2000, 4000 and 6000 ppm NaCl, $CaCl_2$ and $MgSO_4$ salt solutions. The improvement in both flux and rejection was correlated with the concentration polarization in the presence and absence of 20 Hz magnetic field. The results from the base NF270 membranes with the corresponding feed salt solutions were also investigated and modeled for comparisons.

Nomenclature

A_k: effective porosity of the NF membrane

C_b: bulk feed solute concentration, mol L^{-1}

C_m: maximum concentration of solute at membrane surface, mol L^{-1}

C_m/C_b: concentration polarization modulus

$(C_m-C_b)/\delta$: average concentration gradient within the concentration polarization layer, mol L^{-1} m^{-1}

C_p: solute concentration in the permeate, mol L^{-1}

c_i: concentration of ion i in the ENP, mol L^{-1} or kmol m^{-3}

$D_{i,b}$: bulk diffusivity coefficient of species i, m^2 s^{-1}

$D_{i,p}$: pore diffusion coefficient of species i, m^2 s^{-1}

F: Faraday constant, equals to 96487 C mol^{-1}

J_v: volumetric flux of solvent across the membrane, m s^{-1}

J_s: overall salt transport rate across the membrane layer, mol m^{-2} s^{-1}

j_i: ionic flux of ion i based on pore area in the ENP, mol m^{-2} s^{-1}

$K_{H,c}$: hindrance factor for the convection in the ENP, dimensionless,

$K_{H,c}=(1+2\lambda-\lambda^2)(1+0.054\lambda-0.988\lambda^2+0.44\lambda^3)$ for $0<\lambda<0.8$ and

$K_{H,c}=(1+2\lambda-\lambda^2)(-6.830+19.348\lambda-12.518\lambda^2)$ for $0.8<\lambda<1$

$K_{H,d}$: hindrance factor for diffusion, dimensionless, $K_{H,d}=1-2.3\lambda+1.154\lambda^2+0.224\lambda^3$ for $0<\lambda<0.8$ and $K_{H,d}=-0.105+0.318\lambda-0.213\lambda^2$

k: mass transfer coefficient of solute within the concentration boundary layer, m s^{-1}

k_B: Boltzmann constant, equals to 1.381e-23 J K^{-1}

k_m: membrane diffusive mass transfer coefficient, m s^{-1}

L_p: hydraulic permeability, equals to pure water permeability, $m^3\ N^{-1}\ s^{-1}$

l: effective membrane thickness, can be considered equal to the effective thickness of NF270's polyamide functional layer, m

n: Van Hoff coefficient, which is the number of individual particles that a compound generates after dissolving in water, such that it's 3 for $MgCl_2$, 4 for Na_3PO_4, 2 for NaCl and 1 for glucose

n_p: average number of pores per m^2 of membrane surface

ΔP: pressure of operation, equals to the pressure exerted by the pressurized gas cylinder or the pump, $N\ m^{-2}$

ΔP_e: effective operation pressure, $N\ m^{-2}$

Pe_l: Peclet number within the concentration boundary layer, dimensionless

Pe_m: Peclet number within the NF membrane's barrier layer, dimensionless

R: intrinsic rejection, $R=1-C_p/C_m$

R_g: universal gas constant, R_g=8314.46 L Pa K^{-1} mol^{-1} or 8.314 m^3 Pa K^{-1} mol^{-1}

R_o: observed rejection, and $R_o=1-C_p/C_b$

r_i: Stokes Einstein radius of the ions and salts, m

$r_{m,p}$: effective pore radius, m

T: absolute temperature, K

x: axial position within the pore, m

z_i: valence of ion i

Greek letters

Ψ: potential within the pore used in the ENP, V

μ: water viscosity within the pore, N s m^{-2}

μ_o: bulk viscosity of water, equals to 8.91E-4 N s m^{-2} under T=298.15 K, and $\mu/\mu_o=1+18d/r_{m,p}-9(d/r_{m,p})^2$,[30] where d=0.28 nm for water

δ: concentration polarization boundary layer thickness, m

β: concentration polarization factor, $\beta=(C_m-C_p)/(C_b-C_p)$, dimensionless

λ: ratio of the Stokes Einstein radius of salt i (r_i) to the effective pore size within NF membrane layer ($r_{m,p}$)

σ: Staverman reflection coefficient, ranged between 0 and 1, dimensionless

π_i: osmotic pressure of salt i, kPa or kN m^{-2}

$\Delta\pi$: osmotic pressure difference across the membrane, N m^{-2}

$\Delta\pi_{eff}$: effective osmotic pressure difference across the membrane, $\Delta\pi_{eff}=\varphi\cdot\Delta\pi$, N m^{-2}

$\sigma\cdot\Delta\pi$: defined as the critical pressure that the trans-membrane pressure difference has to overcome to get permeate flux, N m^{-2}

φ: osmotic coefficient, dimensionless

3.2 Review of Theoretical Models

In this section, the theories and analytical methods to correlate experimentally observed fluxes and rejections are discussed. Several commonly used mathematical models used in literature to analyze concentration polarization and ion transport under different conditions are reviewed. They were subsequently applied to evaluate the effects of membrane functionalization and external oscillating magnetic field on the transport properties.[31]

3.2.1 Spiegler-Kedem Katchalsky Model (SKKM)

The SKKM is a widely used irreversible thermodynamics model for solvent transport across NF membranes.[33] The SKKM was originally used for evaluating RO processes based on non-equilibrium thermodynamics equations. By considering both NF and RO membrane layers as a "black box", SKKM allows to model the transport properties without the detailed knowledge of the structural properties and transport mechanisms inside the membrane layer.[18-23, 33] The SKKM model for NF processes is based on the Hagen-Poiseuille model (HPM).[19, 30, 34] HPM and SKKM are based on the correlation of permeate flux (J_v), effective operation pressure (ΔP_e) and the membrane's hydraulic permeability L_p described by Equation 3.1.[12, 16]

$$J_v = L_p \Delta P_e \qquad (3.1)$$

The HPM was originally used for hindered transport across porous UF or MF membranes. The strict application of HPM requires uniform pore size. However, HPM has been used widely for UF and MF processes. Based on the assumption of a homogeneous NF membrane layer full of theoretically long and narrow cylindrical pores,[35] the HPM has been frequently used for NF processes. The HPM is given by Equation 3.2.[10, 19, 34, 36-38]

$$J_v = \frac{A_k r_{m,p}^2}{8\mu} \frac{\Delta P_e}{l} = L_p \Delta P_e \qquad (3.2)$$

where A_k is the NF membrane's effective porosity and is equal to $A_k = \pi n_p r_{m,p}^2$

Assuming a homogeneous membrane layer, n_p is the number of theoretical pores within each unit area of membrane surface. The effective radius of the theoretical pore across the membrane layer is $r_{m,p}$.

The μ in Equation 3.2 is the solution viscosity within the theoretical NF membrane pores. The water viscosity within the confined pores of NF membranes is enhanced due to the restricted structural orientation of water molecules close to the pore wall. According to Bowen and Julian,[10] Nagy *et al*.[30] and Bandini and Vezzani:[39]

$$\frac{\mu}{\mu_o} = 1 + 18\frac{d}{r_{m,p}} - 9\left(\frac{d}{r_{m,p}}\right)^2$$

Where μ_o is the bulk water viscosity outside the membrane layer, $r_{m,p}$ is the effective pore size and d=0.28 nm for water.

The SKKM is given by Equation 3.3.[18-23, 34, 38, 40]

$$J_v = L_p(\Delta P - \sigma\Delta\pi_{eff}) = L_p\Delta P_e \qquad (3.3)$$

Osmotic pressure calculation on each side of the membrane was primarily based on the Van't Hoff equation incorporating osmotic coefficient φ:[38, 41-43]

$$\pi_i = n\varphi c_i R_g T \qquad (3.4)$$

The value of osmotic coefficient is solute and concentration dependent. However, based on the osmotic coefficient data in the literature and the observed C_b and C_p and the estimated C_m values, the osmotic pressure coefficient on the permeate side is extremely close to that on the feed side during each of our filtration test.[41-44] Hence the effective osmotic pressure difference across the membrane can be calculated with Equation 3.5.

$$\Delta\pi_{eff} = n\varphi R_g T(C_m - C_p) = \varphi\Delta\pi \qquad (3.5)$$

where

$\Delta\pi$: osmotic pressure difference, N m^{-2};

C_m: salt concentration immediately above the upstream membrane surface, mol l^{-1};

C_p: permeate solute concentration, mol L^{-1} and

$$C_p=C_b(1-R_o) \qquad (3.6)$$

where C_b is salt concentration in the bulk feed, R_o is the experimentally observed salt rejection.

The value of osmotic coefficient φ in this work equals the average of those under the concentrations of C_p and C_b. Based on the effective osmotic pressure difference at constant T=298.15 K, C_m can be calculated by Equation 3.7.

$$C_m = \frac{\Delta\pi_{eff}}{n\varphi R_g T} + C_p = \frac{\Delta\pi_{eff}}{n\varphi R_g T} + C_b(1-R_o) \qquad (3.7)$$

Based on the value of C_m, the intrinsic rejection can be obtained with Equation 3.8.

$$R=1-C_p/C_m \qquad (3.8)$$

The Staverman reflection coefficient σ is a parameter that directly indicates the selectivity of a certain membrane towards a certain ion or molecule. The value of σ ranges from 0 to 1. For a membrane completely rejects solute species, σ=1. For a membrane that allows solute species to go through completely, σ=0.[37, 45] According to Kelewou *et al*.[12] and Sherma and Chellam,[25] the intrinsic rejection of a salt by a NF membrane approaches σ under a large value of J_v. Since the membranes were defined as a selective barrier, membrane separation relies on the different reflection coefficients of different species in the feed stream. Similar to the original consideration of membranes as sieves, the reflection coefficient was originally based on steric hindrance of the membrane. However, besides steric hindrance, transport of salts across charged polyamide TFC NF membranes is affected by membrane surface charge

and charge distribution in the membranes.[46] Earlier studies showed that surface charge for poly (HEMA) functionalized NF270 membranes is negligible.[47] Moreover, strong charge screening effects arising from concentration polarization leading to the relatively high salt concentration concentration at the membrane-liquid interface weakens the electrostatic interaction between the salt ions and membrane surface charge.[28, 48] Hence we neglect the surface charges for both the functionalized and base NF270 membranes here.

Often considered as loose RO or dense UF membranes, NF membranes possess large percentage of free volumes in the barrier layer. The uniform pore sizes in NF membranes considered here are more hypothetical.[49] Cylindrical pores across the membrane barrier layer are assumed during the quantitative description of NF processes here.[21, 50] The reflection coefficients of each salt to both the base and functionalized NF270 membranes are calculated with the steric hindrance pore (SHP) model described by Equation 3.9.[38, 39]

$$\sigma=1-(1-\lambda)^2(1+2\lambda-\lambda^2)(1+0.054\lambda-0.988\,\lambda^2+0.441\lambda^3) \text{ for } 0<\lambda<0.8$$

$$\sigma=1-(1-\lambda)^2(1+2\lambda-\lambda^2)(-6.830+19.348\lambda-12.518\lambda^2) \text{ for } 0.8<\lambda<1 \qquad (3.9)$$

r_i is the ion's Stokes-Einstein (S-E) radii determined by the Stokes Einstein equation given by Equation 3.10.[51]

$$D_{i,b}=\frac{k_BT}{6\pi\mu r_i} \qquad (3.10)$$

For the low salt concentrations investigated here, there is no study on effects of magnetic field to the viscosity of water or S-E radii. As a result, we assume ion's diffusivity is unaffected by an external magnetic field.[52] At the same time, diffusivity coefficient of the salt ($D_{i,b}$) molecule as a whole can be calculated by correlating those of the cation and anion using Equation 3.11.[51, 53]

$$D_{i,b} = \frac{(|z_1| + |z_2|) D_1 D_2}{|z_1| D_1 + |z_2| D_2} \qquad (3.11)$$

where

$D_{i,b}$: bulk diffusivity of the salt, $m^2\ s^{-1}$;

z_i: valence of the ions, dimensionless;

D_i: bulk diffusivity of the ions, $m^2\ s^{-1}$;

The suffixes 1 and 2 represent the cation and anion, respectively.

According to Equation 3.10, $D_{i,b} \propto \frac{1}{r_i}$ at constant temperature, pressure and solvent viscosity.

The Stokes, Born and Pauling radii have all been used during the modeling of ion transport across NF membranes.[54, 55] However, only the Stokes radius correlates with the dynamic ionic transport across the NF membranes. Combining Equations 3.10 and 3.11, the S-E radius of a salt r_{12} can be obtained by correlating those of the cation and anion:

$$\frac{1}{r_{12}} = \frac{(|z_1| + |z_2|)/r_1 r_2}{|z_1|/r_1 + |z_2|/r_2} \Rightarrow r_{12} = \frac{|z_1|/r_1 + |z_2|/r_2}{(|z_1| + |z_2|)/r_1 r_2} = \frac{|z_1| r_2 + |z_2| r_1}{|z_1| + |z_2|} \qquad (3.12)$$

Based on the ratio of the salt's S-E radius to the membrane's effective pore radius, the reflection coefficient is determined using the SHP model given by Equation 3.9. However, Equation 3.9 is only applicable for the salt species with S-E radii smaller than the effective membrane pore radius.

3.2.2 Film Theory Model (FTM) for Quantifying Concentration Polarization

During nanofiltration, water molecules could go through the membrane but salt ions are partially rejected. The rejected salt ions accumulate at the membrane boundary layer forming a concentration gradient from the bulk to the upstream membrane surface, as shown

in Figure 3.1.[3] The FTM to quantify concentration polarization is given by Equation 3.13.[24, 29]

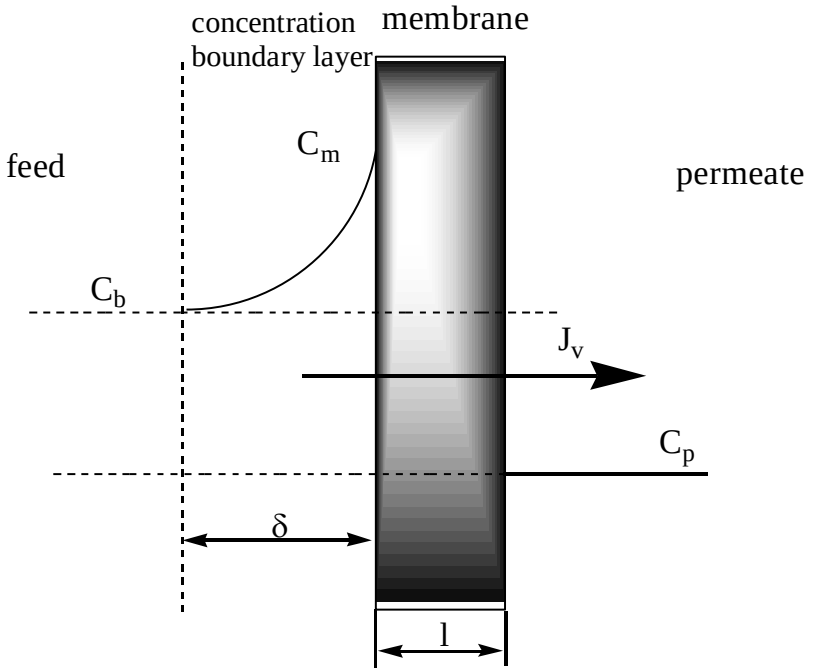

Figure 3.1 Concentration profile within the concentration polarization layer.[26]

$$\ln\frac{C_m - C_p}{C_b - C_p} = \frac{J_v\delta}{D_{i,b}} = \frac{J_v}{k} \qquad (3.13)$$

In Equation 3.13, k is the solute mass transfer coefficient within the concentration boundary layer, δ is the concentration boundary layer thickness and $k=D_{i,b}/\delta$. During concentration polarization, accumulation of rejected ions tends to increase the thickness of concentration boundary layer, while rejected ions with higher bulk diffusivity are easier to diffuse back into the bulk feed from the membrane surface. Therefore, for the same salt, k is proportional to the bulk diffusivity of salt and inversely proportional to the thickness of concentration boundary layer.[24] The order of magnitude for k is generally the same as J_v.[23] While the value of k indicates the intensity of mixing above the membrane surface,[56] k is also affected by cross-membrane solute transport.

Based on the film theory, the concentration polarization modulus C_m/C_b and the concentration polarization factor $\beta=(C_m-C_p)/(C_b-C_p)$ have been widely used for quantifying

concentration polarization in recent literature on RO, NF and UF processes.[4, 5, 26] They were also used here to investigate the effects of membrane functionalization and micro-mixing on concentration polarization. Since the objective is to quantitatively investigate concentration polarization and salt transport under various conditions, FTM together with other models are used to quantify concentration polarization during the non-stirred dead end NF processes here.[24, 27-29]

3.2.3 Extended Nernst-Planck Equation (ENP)

The Extended Nernst-Plank Equation (ENP) has been widely used to phenomenologically describe ion transport within the layer of NF membranes. ENP is given by Equation 3.14: [19, 39, 57-59]

$$j_i = -D_{i,p}\frac{dc_i}{dx} - \frac{z_i c_i D_{i,p}}{R_g T} F \frac{d\Psi}{dx} + (1-\sigma)c_i J_v \qquad (3.14)$$

ENP is one of the most widely used mechanistic models for predicting and describing NF performances.[19, 22-25] ENP takes into account particle size and membrane structure to describe the transport of particles across the membranes.[25] Equation 3.14 is generally applicable only for the low-pressure NF processes.[10, 34, 60] Equation 3.14 assumes the theoretical pore size in NF membrane is significantly smaller than the membrane barrier layer thickness. ENP assumes ideal solution both in the bulk feed and in the membrane pores within a homogeneous NF membrane barrier layer. In addition, ENP assumes all of the ions within the membrane layer are mobile, with J_v defined by the Hagen-Poiseuille model and σ determined by the ratio of r_s to $r_{m,p}$. Therefore, ion transport across the NF membrane layer consists of diffusion due to concentration gradient, electromigration due to the presence of an

electromagnetic gradient and convective flow due to pressure difference across the membrane.[19, 22-25, 38, 58, 61]

However, the ENP described in Equation 3.21 does not necessarily follow charge neutrality principle in the feed and permeate. According to earlier work, the surface charge of functionalized membranes covered by poly (HEMA) is negligible around a neutral pH.[47] The surface charge for the base NF270 membrane is also insignificant due to the screening effects caused by concentration polarization.[28] Therefore, the following charge neutrality conditions should be taken into account:

$$\sum_i z_i c_i = 0 \quad \text{and} \quad \sum_i z_i j_i = 0$$

Reducing the ENP to Equation 3.15, which is also called the Kedem-Speigler equation, by neglecting the electromigration effect.[24, 25, 28, 39, 57]

$$j_i = -D_{i,p} \frac{dc_i}{dx} + (1-\sigma_i) c_i J_v \qquad (3.15)$$

3.2.4 Integrated Model of SKKM, FTM and ENP (ISFE)

As described earlier, ENP only considers ion transport within the membrane barrier layer in the absence of concentration polarization. SKKM treats the membrane barrier layer as a "black box". Therefore, the integration of all three SKKM, ENP and FTM models (ISFE) will be more suitable to quantitatively describe salt ions and water transport during NF processes in the presence of concentration polarization.[62] According to Lee *et al.*[18] and Chaabane *et al.*[28], integrated Equation 3.16 has been frequently used to improve the accuracy of NF modeling. By coupling the concentration boundary layer and the NF membrane's barrier layer using ISFE, Chaabane *et al.*[28] and Murthy *et al.*[31, 32] have obtained solute mass transfer coefficients

considerably close to experimentally observed.[24, 28]

$$\frac{R_o}{1-R_o} = \left(\frac{\sigma}{1-\sigma}\right)[1 - \exp(-Pe_m)] \cdot exp\left(-\frac{J_v\delta}{D_{i,b}}\right) \qquad (3.16)$$

where the concentration boundary layer thickness δ equals to:

$$\delta = -\frac{D_{i,b}}{J_v} \cdot ln\left[\frac{\frac{R_o}{1-R_o}\cdot\frac{1-\sigma}{\sigma}}{1-exp(-Pe_m)}\right] \qquad (3.17)$$

Although Equation 3.16 was originally used for uncharged solutes or membranes, other researchers have extended its application to salt ions[63] transport through charged membranes.[31, 32, 64] Equation 3.16 does not require complex derivations and calculations in which many experimentally unavailable variables and coefficients are needed.[32] Considering salt cation and anion as one particle to ensure charge neutrality, salt transport across the NF membranes is dominated by both diffusion and convection.[27] Peclet number has been widely used to investigate transport during the NF processes.[4, 18, 30] The Peclet number for the membrane (Pe_m) given by Equation 3.18 quantifies the ratio of convective to diffusive solute transport rates within the NF membrane barrier layer.[4, 18]

$$Pe_m = ln\left[\frac{\sigma(1-R)}{\sigma-R}\right] \qquad (3.18)$$

The Peclet number for the solution (Pe_l) quantifies the ratio of convective to diffusive solute transport rates within the concentration boundary layer and is given by Equation 3.19.

$$Pe_l = J_v/k \qquad (3.19)$$

Solute transport in both the membrane layer and the concentration boundary layer are dominated by diffusive or convective transport depending whether the Peclet number is smaller or larger than 1, respectively.[4, 18]

3.2.5 Quantification of Total Cross-Membrane Solute Transport

Based on the work by Kedem and Spiegler,[20] Kelewou *et al.*[12], Lv *et al.*[65] and Nagy *et*

al.[30], total solute transport rate across the membrane layer in the presence of concentration polarization can be determined using the non-equilibrium thermodynamic Equation 3.20.[12, 19, 20, 30, 65, 66]

$$J_s = k_m(C_m - C_p) + (1-\sigma)J_v \frac{C_m - C_p}{\ln(\frac{C_m}{C_p})} \qquad (3.20)$$

Solute transport across the NF membranes includes diffusive and convective transport terms.[66] Convective transport is mainly influenced by the operation pressure and the hydrodynamic conditions.[12] Diffusive transport is mainly affected by solute concentration difference across the membrane layer and the interaction between solute particles and membrane layer. According to Nagy *et al*., the value of membrane diffusive mass transport coefficient (k_m) is based on both the dynamical and physical properties of salt and the physical properties of membrane layer.[30] Based on the hypothetical pores within a homogeneous NF membrane layer, k_m is calculated with Equation 3.21.[67]

$$k_m = \frac{D_{i,b}K_{H,d}A_k}{l(\mu/\mu_o)} \qquad (3.21)$$

3.2.6 Assumptions Made in the Current Study

In order to describe quantitatively the effects of magnetic field on concentration polarization and transport properties of salt permeation through the functionalized NF270 membranes, a number of assumptions have to be made in order to adopt the models described above for the current investigation. These assumptions are listed below.

- A fully developed concentration polarization layer leads to stabilized C_m and C_b.
- No precipitation or cake formation occurs above the upstream membrane surface.
- Uniform membrane layer structures with homogeneous barrier layer thickness and pore size distribution for the base and all functionalized membranes.

- Constant temperature at T=296.15 K during operation leads to constant water viscosity and solute diffusivity.[16, 68]
- The 33-minute dead end filtration NF processes operated with low initial feed salt concentration and low permeate flux leads to slight to medium concentration polarization. Therefore, both the diffusivity coefficient of salt and the viscosity of water within the entire concentration boundary layer are assumed to be the same as in the bulk feed.[26]
- The polysulphone mechanical support layers beneath the selective layer of NF270 membranes do not exert any resistance to water and salt transport. Therefore, salt concentration immediately below the barrier layer and within the entire mechanical support layer is assumed equal to C_p.
- Charge neutrality needs to be guaranteed within the bulk feed, the concentration boundary layer, the polyamide barrier layer and the permeate. Therefore, the cations and anions have to move together. Each single salt is considered to be a charge neutral component.[20]
- Surface modification reduces the effective pore size and increases the effective barrier layer thickness simultaneously due to the grafting of a poly (HEMA) nanolayer above the NF270 membrane's polyamide layer surface. Hypothetical pore density remains constant before and after membrane functionalization.

3.3 Experimental Procedures

The following chemical were purchased from Alfa Aesar (Ward Hill, MA): 2-hydroxyethyl methacrylate (HEMA), 97% purity, ethanol, trietnylamine (TEA), potassium phthalimide, hydrazine monohydrate, 1-ethyl-3-(3-dimethyl- aminopropyl) carbodiimide

(EDC) and magnesium chloride (all ACS grade). Calcium chloride was purchased from EMD Chemicals (Billerica, MA) in 96% purity. The following chemical were all ACS grade: boric anhydride, sodium chloride and magnesium sulfate purchased from Avantor (Center Valley, PA) Acetonitrile, methanol and hydrochloride acid were purchased from from EMD Chemicals (Billerica, MA), α-bromoisobutyrylbromide, aluminum oxide, 2, 2'-bipyridine (Bpy), copper (I) chloride, copper (II) chloride and N, N, N', N", N"- pentamethyl diethylenetriamine (PMDETA), were obtained from Aldrich (St. Louis, MO). 4-N', N'-dimethylamino-pyridine (DMAP) was obtained from Fluka (St Louis, MO). Copper (II) bromide and N-hydroxysuccinimide (NHS) was purchased from ACROS Organics (Thermo Fisher Scientific, NJ), and disodium phosphate was purchased from AMRESCO (Solon, OH). Monosodium phosphate was purchased from VWR (Radnor, PA) but produced by BDH Chemicals (Umm Ramool, Dubai, United Arab Empires). Superparamagntic nanoparticles (diameter, 15 nm) coated with a 5 nm polymer coating containing carboxylic groups were obtained from Ocean Nanotech (Springdale, AR). NF270 thin film composite polyamide nanofiltration membranes were provided by Dow Chemical (Edina, MN, USA). All DI water required was made with Siemens/ELGA Purelab Ultra deionizer using SCMK2 filters, Siemens Water Technologies (Warrendale, PA).

Magnetically responsive membrane functionalization included the grafting of polymer chains onto the membrane surface, and the subsequent attachment of SPM NPs at the polymer chain ends. Detailed procedure and reaction mechanisms are same as in the prior work by Himstedt *et al.*[7] During membrane functionalization, polymer chain density was controlled by the ATRP initiator immobilization time. The membranes functionalized with initiator

immobilization time 2 h and 6 h are designated as low density (LD) and high density (HD) membranes, respectively. The polymer chain length is controlled by the ATRP ATRP time varying from 1 to 4 hours. As a result, functionalized membranes are designated as LD1h, LD2h, LD3h, LD4h, HD1h, HD2h, HD3h and HD4h.[7]

All membrane performance tests were done using the Amicon 8050 filtration cell which has a total feed volume of 50mL and an operational membrane diameter of 44.5 mm. In order to investigate the micro-mixing effect on concentration polarization, dead end filtration mode without stirring was used for all tests. A constant operation pressure of ΔP=45 psig and a pH of about 7 were kept during all the tests. The procedures for flux and rejection measurement and the operation of oscillating magnetic field system were same as in the prior work by Himstedt *et al*.[6, 7]

The zeta potentials of the membranes were measured with a Delsa Nano HC particle analyzer manufactured by Beckman Coulter (Brea, CA).

The volume of feed salt solution was fixed at 50mL at the beginning of all the tests. The length of each membrane filtration experiment lasted 33 minutes. Fluxes used in the modeling were averaged during the last 12 minutes of the test. The observed salt rejections were determined by the conductivity measurement after collecting the first 2.6-3.7 g permeate. During the filtration experiments, fluxes appear to stabilize after 12-20th minute of run, which corresponds to about 2.6 g of permeate. The smallest amount of permeate should be collected to minimize concentration increase in the dead end filtration feed reservoir. In order to avoid any possible error in flux measurement, the accumulated permeate was weighted with 3 minute intervals. Since each membrane has different conditions, variation in permeate volume for

conductivity measurement was expected. Moreover, flux stabilizes just before conductivity measurement, making the observed flux and rejection generally agree with each other.

3.4 Phenomenological Modeling

According to AFM imaging of the cross sectional barrier layer in NF270 by Freger *et al.*, the thickness of hydrated polyamide barrier layer l is about 16.0 nm.[69] The bulk viscosity of water μ_o at room temperature is $8.91 \cdot 10^{-4}$ N s m^{-2}.[68] The constant operation pressure of ΔP=45 psig (310264.078 N/m^2) was kept during all the filtration experiments. For DI water flux tests, the osmotic pressure difference was neglected therefore the effective operation pressure (ΔP_e) was assumed equal to the pressure applied. An increased water viscosity within the pores was considered when applying the HPM model. The hydraulic permeability of the base NF270 membrane L_p is determined to be 2.75×10^{-11} m^3 N^{-1} s^{-1}. Based on earlier studies, the effective porosity A_k of base NF270 membrane is 0.21.[69] The effective pore radius $r_{m,p}$ of our base NF270 membrane was obtained using the HPM and equals to 0.36 nm. Pore density within the barrier layer of base NF270 membrane was subsequently obtained using Equation 3.2, and equals to $n_p=4.39 \times 10^{17}$ m^{-2}.

During our modeling, it was assumed that membrane functionalization makes pore narrower and barrier layer thicker, without changing the number of pores n_p. Further, our grafting degree results show linear growth for polymer chains over ATRP time. As a result, the increase in barrier layer thickness is assumed constant for each hour of ATRP reaction at the same chain density. The water viscosities in the pores are calculated bases on the barrier layer thickness and effective pore radius for each functionalized membrane. For a base NF membrane,

μ/μ_o is around 10. Based on our earlier studies,[70] the most possible increase rate of the effective barrier layer thickness during polymerization is 1.5 nm/h for LD functionalized membranes.[71] Subsequently, the effective pore radius of each functionalized membrane was obtained using Equation 3.2. The DI water flux, barrier layer thickness and effective pore radius for the base and functionalized membranes are listed in Table 3.1.

Table 3.1 DI water fluxes, barrier layer thicknesses and effective pore radius of the base and functionalized NF270 membranes.

Membrane	DI water flux at 45 psig ($L/(m^2 \cdot h)$)	Barrier layer thickness (nm)	Effective pore radius (nm)
Base	30.6	16.0	0.360
LD1h	19.3	17.5	0.344
LD2h	17.5	19.0	0.343
LD3h	15.8	20.5	0.341
LD4h	13.7	22.0	0.335

Table 3.2 lists the literature values of S-E radius and bulk diffusivity for the ions investigated.[51, 54] Table 3.3 lists the bulk diffusivity and S-E radius for NaCl, $CaCl_2$ and $MgSO_4$ salt obtained by Equations 3.11 and 3.12. Based on the ratio of S-E radius to effective membrane pore radius, the reflection coefficient of each salt to each membrane was obtained by Equation 3.9 and listed in Table 3.3 (a).[38, 54, 55, 72] Meanwhile, k_m values for each salt and membrane were obtained using Equation 3.21, and listed in Table 3.3 (b).[30]

Table 3.2 S-E radius and bulk diffusivity of each ion.

Cation	S-E radius (nm)	Bulk diffusivity ($m^2/s \cdot 10^9$)	Anion	S-E radius (nm)	Bulk diffusivity ($m^2/s \cdot 10^9$)
Na^+	0.184	1.33	Cl^-	0.121	2.03
Ca^{2+}	0.309	0.79	SO_4^{2-}	0.230	1.07
Mg^{2+}	0.341	0.72			

Table 3.3 (a) Physical properties of each salt.

Salt	Bulk diffusivity ($m^2/s \cdot 10^9$)	S-E radius (nm)	Reflection coefficient (σ)				
			Base	LD1h	LD2h	LD3h	LD4h
NaCl	1.61	0.153	0.5726	0.6066	0.6096	0.6146	0.6285
$CaCl_2$	1.33	0.184	0.7173	0.7518	0.7548	0.7598	0.7734
$MgSO_4$	0.86	0.290	0.9531	0.9714	0.9728	0.9752	0.9812

Table 3.3 (b) Membrane diffusive mass transfer coefficients.

Membrane	Diffusive mass transfer coefficient (k_m)		
	NaCl	$CaCl_2$	$MgSO_4$
Base	4.70E-04	2.43E-04	1.31E-05
LD1h	3.52E-04	1.73E-04	9.75E-06
LD2h	3.19E-04	1.56E-04	8.79E-06
LD3h	2.87E-04	1.39E-04	7.86E-06
LD4h	2.46E-04	1.16E-04	6.57E-06

Based on the flux and rejection from the base membrane by varying ΔP_e, R and $\Delta\pi$ were obtained using Equations 3.1-3.8. The osmotic coefficient was taken into consideration when calculating C_m based on $\Delta\pi_{eff}$ and C_p. Since all membrane performance tests were done under constant temperature between 24-25℃, the osmotic coefficients for each salt at different concentrations were primarily obtained from the literature and shown in Table 3.4 (a). Based on the φ value, C_m and $\Delta\pi$ were obtained using Equation 3.7 and 3.5, respectively.

Table 3.4 (a) Osmotic coefficients for each salt under different concentrations.

Salt	Molar concentration (2000 ppm)	φ	Molar concentration (4000 ppm)	φ	Molar concentration (6000 ppm)	φ
NaCl [41]	0.034 M	0.95	0.068 M	0.94	0.103 M	0.93
$CaCl_2$ [42]	0.018 M	0.93	0.036 M	0.91	0.054 M	0.89
$MgSO_4$ [43]	0.017 M	0.60	0.033 M	0.59	0.050 M	0.59

In order to guarantee the accuracy of our approach using a dead end filtration NF system, feed concentration increase during the course of 33 minute test was taken into account. The accumulated weight of permeate generated from the original 50 mL of feed at the time of permeate conductivity measurement is listed in Table 3.4 (b). During the determination of δ, k, Pe_m and Pe_l using the ISFE and the subsequent calculations of C_m/C_b, β and $(C_m-C_b)/\delta$, a modified feed concentration C_b' and a modified observed rejection R_o' had to replace the original C_b and R_o, respectively. The values of C_b' and R_o' are:

$$C_b' = C_b \frac{50}{50-m} \text{ and } R_o' = 1 - \frac{C_p}{C_b'}$$

where m is the weight in g of permeate at the permeate conductivity measurement.

Table 3.4 (b) Permeate amount (g) at the moment of permeate conductivity measurements. N.F. and 20 Hz refers to in the absence of an external magnetic field and in the presence of a 20 Hz magnetic field, respectively.

Salt	**NaCl**			**$CaCl_2$**			**$MgSO_4$**		
Concentration in ppm	**2000**	**4000**	**6000**	**2000**	**4000**	**6000**	**2000**	**4000**	**6000**
base N.F.	3.45	2.77	3.79	3.33	3.4	3.33	3.19	2.94	3.02
base 20 Hz	3.39	2.69	3.76	3.02	3.35	3.27	3.11	2.87	3.29
LD1h N.F.	2.78	2.61	2.75	3.11	3.06	2.95	2.88	2.97	2.94
LD1h 20 Hz	2.75	2.74	2.61	3.20	3.07	3.12	2.98	2.90	2.90
LD2h N.F.	2.95	3.36	2.65	2.91	2.82	3.10	2.86	3.04	2.92
LD2h 20 Hz	2.70	2.73	3.34	3.04	2.92	2.76	2.75	3.12	2.92
LD3h N.F.	3.33	3.20	2.63	2.69	3.11	2.91	2.93	2.94	2.81
LD3h 20 Hz	2.73	2.69	3.21	2.87	2.81	2.97	2.82	3.01	3.01
LD4h N.F.	3.12	2.97	3.34	2.91	2.81	2.97	2.77	2.94	2.83
LD4h 20 Hz	2.66	3.02	2.92	2.76	3.08	2.97	2.94	2.88	2.88

Zeta potential of our base NF270 membrane as a function of pH is shown in Figure 3.2. Surface charge of the base NF270 membrane is due to the protonation of polyamine end groups and the dissociation of carboxylic end groups on polyamide layer surface. Zeta potential

directly indicates the surface charge of NF membranes. Similar to most other researchers, zeta potential for our base NF270 membrane becomes more negative with the increases of pH. There is an isoelectric point around pH=2.8. At pH 7, base NF270 membranes are negatively charged with an absolute zeta potential of about -27 mV, which is normal for a commercial NF270[8] membrane.[42, 73] The ISFE described by Equation 3.17 is used for our modeling based on the assumption of electrical neutrality[74] for the Extended Nernst-Planck Equation.[28]

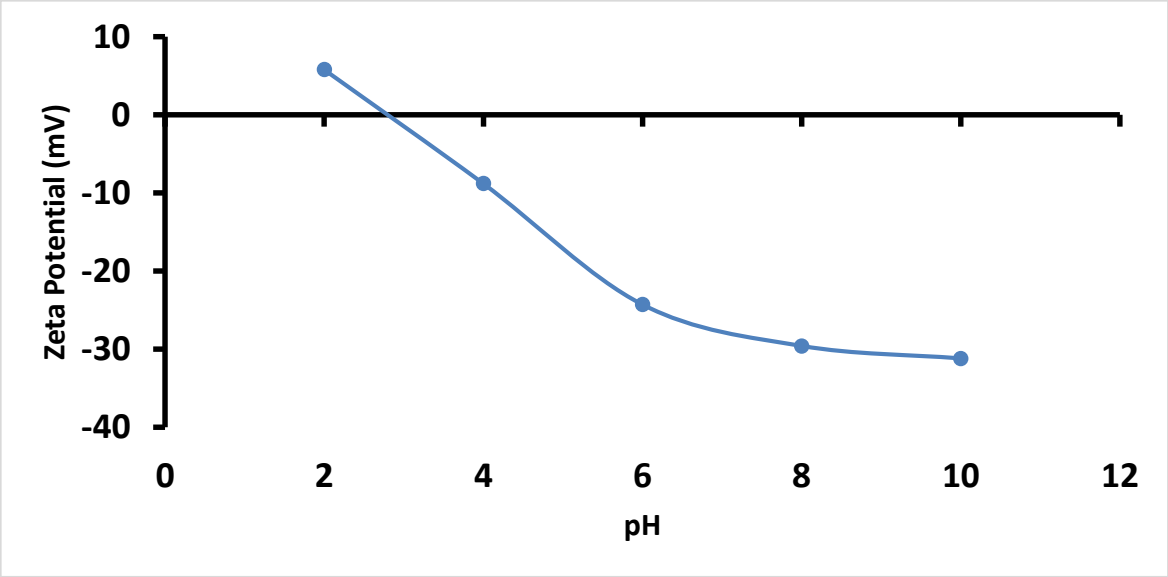

Figure 3.2 Zeta potential vs. pH for base NF270 membrane.

After obtaining R with Equation 3.8, Pe_m and δ were obtained using Equation 3.18 and 3.17, respectively. The value of Pe_l was subsequently obtained using Equation 3.19 based $k=D_{i,b}/\delta$. Finally, the total salt transport rate across the membrane layer was quantified using Equation 3.20. All the data related to membrane performance, concentration polarization and salt transport are listed in Tables 3.5-3.10. Instead of $\Delta\pi_{eff}$, the values of $\Delta\pi$ were used for evaluating the influence of membrane functionalization and magnetic field on cross-membrane osmotic pressure difference.

3.5 Results and Discussion

The main objective of quantitative analysis of functionalized NF micro-mixer membranes by correlating experimental transport data with the properties of membrane and feed solution is to test out hypothesis that micro-mixing at the membrane-liquid interface suppresses concentration polarization. More specifically, the following hypothesis are tested:

a) Movement of the grafted polymer chains generates micro-mixing at the membrane-liquid interface which minimizes concentration polarization during nanofiltration (NF) processes;
b) Concentration polarization is affected mainly by the type and feed concentration of the ionic species;
c) Polymer chain length and polymer chain density have a strong effect on concentration polarization and salt transport;
d) Concentration polarization and the effects of micro-mixing are strongly ion type and ion concentration dependent.

Performances of the base and functionalized NF270 membranes LD1h, LD2h, LD3h and LD4h were used for the analysis, including the flux and rejection of NaCl, $CaCl_2$ and $MgSO_4$ feed solutions at 2000, 4000 and 6000 ppm concentrations in the presence and absence of 20 Hz magnetic field. As expected, concentration polarization and salt transport depend on the type and concentration of salt, and polymer chain length during membrane functionalization.

Table 3.5 Membrane performances of NaCl salt solutions.

Conc. (ppm)		Mag. Field	σ	J_v (L $m^{-2}h^{-1}$)	R_o	ΔP_e (N m^{-2})	$\Delta\pi_{eff}$ (N m^{-2})	$\Delta\pi$ (N m^{-2})	Js (mol m^{-2} s^{-1})
2000	Base	No	0.5726	21.3	0.046	2.16E+05	1.65E+05	1.73E+05	1.66E-05
2000	Base	20 Hz	0.5726	21.7	0.047	2.20E+05	1.58E+05	1.66E+05	1.59E-05
2000	LD1h	No	0.6066	12.7	0.107	2.04E+05	1.75E+05	1.85E+05	1.32E-05
2000	LD1h	20 Hz	0.6066	13.8	0.125	2.22E+05	1.46E+05	1.54E+05	1.10E-05
2000	LD2h	No	0.6096	12.1	0.109	2.14E+05	1.58E+05	1.66E+05	1.07E-05
2000	LD2h	20 Hz	0.6096	13.5	0.126	2.39E+05	1.17E+05	1.23E+05	7.99E-06
2000	LD3h	No	0.6146	11.6	0.112	2.29E+05	1.33E+05	1.40E+05	8.15E-06
2000	LD3h	20 Hz	0.6146	13.3	0.133	2.62E+05	7.85E+04	8.26E+04	4.83E-06
2000	LD4h	No	0.6285	10.6	0.113	2.39E+05	1.13E+05	1.19E+05	5.94E-06
2000	LD4h	20 Hz	0.6285	13	0.136	2.94E+05	2.65E+04	2.79E+04	3.38E-06
4000	Base	No	0.5726	19.3	0.035	1.96E+05	2.00E+05	2.13E+05	2.04E-05
4000	Base	20 Hz	0.5726	19.7	0.036	2.00E+05	1.93E+05	2.05E+05	1.97E-05
4000	LD1h	No	0.6066	12.4	0.091	1.99E+05	1.83E+05	1.95E+05	1.40E-05
4000	LD1h	20 Hz	0.6066	13.6	0.107	2.18E+05	1.51E+05	1.61E+05	1.16E-05
4000	LD2h	No	0.6096	11.8	0.094	2.09E+05	1.66E+05	1.77E+05	1.15E-05
4000	LD2h	20 Hz	0.6096	13.3	0.111	2.35E+05	1.23E+05	1.31E+05	8.52E-06
4000	LD3h	No	0.6146	11.3	0.099	2.23E+05	1.43E+05	1.52E+05	8.87E-06
4000	LD3h	20 Hz	0.6146	13.1	0.118	2.58E+05	8.49E+04	9.03E+04	5.32E-06
4000	LD4h	No	0.6285	10.3	0.101	2.33E+05	1.24E+05	1.31E+05	6.60E-06
4000	LD4h	20 Hz	0.6285	12.8	0.122	2.89E+05	3.37E+04	3.59E+04	4.55E-06
6000	Base	No	0.5726	17.8	0.028	1.80E+05	2.27E+05	2.44E+05	2.34E-05
6000	Base	20 Hz	0.5726	18	0.028	1.82E+05	2.23E+05	2.40E+05	2.30E-05
6000	LD1h	No	0.6066	12.1	0.072	1.94E+05	1.91E+05	2.06E+05	1.48E-05
6000	LD1h	20 Hz	0.6066	13.4	0.086	2.15E+05	1.57E+05	1.69E+05	1.21E-05
6000	LD2h	No	0.6096	11.5	0.076	2.03E+05	1.75E+05	1.88E+05	1.23E-05
6000	LD2h	20 Hz	0.6096	13.1	0.091	2.32E+05	1.29E+05	1.38E+05	9.05E-06
6000	LD3h	No	0.6146	11	0.078	2.17E+05	1.52E+05	1.64E+05	9.60E-06
6000	LD3h	20 Hz	0.6146	12.9	0.093	2.54E+05	9.13E+04	9.82E+04	5.82E-06
6000	LD4h	No	0.6285	10	0.079	2.26E+05	1.34E+05	1.44E+05	7.28E-06
6000	LD4h	20 Hz	0.6285	12.6	0.095	2.85E+05	4.09E+04	4.40E+04	4.49E-06

Table 3.6 Concentration polarization and transport mode of NaCl.

Conc. (ppm)		Mag. Field	δ (m)	β	C_m/C_b	k ($m\ s^{-1}$)	R	$(C_m-C_b)/\delta$ ($mol\ L^{-1}m^{-1}$)	Pe_m	Pe_l
2000	Base	No	6.19E-04	8.51	1.84	2.60E-06	0.551	49.86	2.458	2.275
2000	Base	20 Hz	5.97E-04	8.17	1.80	2.70E-06	0.540	49.22	2.089	2.235
2000	LD1h	No	9.05E-04	6.56	1.87	1.78E-06	0.574	34.87	2.075	1.982
2000	LD1h	20 Hz	7.17E-04	4.95	1.68	2.24E-06	0.536	34.53	1.382	1.708
2000	LD2h	No	8.88E-04	5.70	1.76	1.81E-06	0.552	31.11	1.550	1.854
2000	LD2h	20 Hz	6.43E-04	3.97	1.51	2.50E-06	0.483	28.95	0.915	1.497
2000	LD3h	No	8.20E-04	4.50	1.60	1.96E-06	0.516	26.76	1.105	1.642
2000	LD3h	20 Hz	4.73E-04	2.55	1.28	3.40E-06	0.395	21.42	0.525	1.086
2000	LD4h	No	8.21E-04	3.90	1.49	1.96E-06	0.476	21.69	0.769	1.501
2000	LD4h	20 Hz	3.95E-04	2.06	1.19	4.07E-06	0.351	17.62	0.384	0.887
4000	Base	No	6.13E-04	6.70	1.50	2.63E-06	0.428	59.61	0.816	2.041
4000	Base	20 Hz	5.92E-04	6.52	1.48	2.72E-06	0.419	59.25	0.772	2.012
4000	LD1h	No	7.02E-04	3.93	1.41	2.29E-06	0.419	41.76	0.631	1.502
4000	LD1h	20 Hz	5.16E-04	2.88	1.29	3.12E-06	0.383	41.08	0.515	1.212
4000	LD2h	No	6.51E-04	3.14	1.33	2.47E-06	0.408	37.42	0.583	1.325
4000	LD2h	20 Hz	4.36E-04	2.28	1.20	3.69E-06	0.341	34.01	0.401	1.001
4000	LD3h	No	6.00E-04	2.67	1.26	2.68E-06	0.374	31.90	0.470	1.170
4000	LD3h	20 Hz	2.83E-04	1.52	1.09	5.69E-06	0.273	22.09	0.269	0.640
4000	LD4h	No	5.90E-04	2.36	1.21	2.73E-06	0.343	25.88	0.368	1.049
4000	LD4h	20 Hz	2.70E-04	1.42	1.07	5.96E-06	0.278	19.88	0.258	0.596
6000	Base	No	5.51E-04	4.35	1.34	2.92E-06	0.381	68.71	0.615	1.693
6000	Base	20 Hz	5.42E-04	4.31	1.33	2.97E-06	0.377	68.57	0.602	1.684
6000	LD1h	No	6.26E-04	3.10	1.26	2.57E-06	0.342	44.86	0.410	1.308
6000	LD1h	20 Hz	4.51E-04	2.35	1.18	3.57E-06	0.304	43.32	0.334	1.042
6000	LD2h	No	6.10E-04	2.80	1.23	2.64E-06	0.324	40.09	0.366	1.210
6000	LD2h	20 Hz	3.47E-04	1.67	1.10	4.63E-06	0.282	32.33	0.289	0.785
6000	LD3h	No	5.66E-04	2.41	1.18	2.85E-06	0.298	34.13	0.309	1.073
6000	LD3h	20 Hz	2.28E-04	1.19	1.03	7.07E-06	0.228	14.10	0.205	0.507
6000	LD4h	No	5.21E-04	1.88	1.12	3.09E-06	0.287	26.24	0.271	0.899
6000	LD4h	20 Hz	1.94E-04	1.10	1.01	8.29E-06	0.209	18.27	0.170	0.422

Table 3.7 Membrane performances of $CaCl_2$ salt solutions

Conc. (ppm)		Mag. Field	σ	J_v (L $m^{-2}h^{-1}$)	R_o	ΔP_e (N m^{-2})	$\Delta\pi_{eff}$ (N m^{-2})	$\Delta\pi$ (N m^{-2})	Js (mol m^{-2} s^{-1})
2000	Base	No	0.7173	13.8	0.119	1.40E+05	2.38E+05	2.55E+05	8.39E-06
2000	Base	20 Hz	0.7173	13.9	0.121	1.41E+05	2.36E+05	2.54E+05	8.34E-06
2000	LD1h	No	0.7518	8.8	0.256	1.41E+05	2.25E+05	2.42E+05	5.64E-06
2000	LD1h	20 Hz	0.7518	9.5	0.292	1.53E+05	2.10E+05	2.26E+05	5.27E-06
2000	LD2h	No	0.7548	8.1	0.27	1.43E+05	2.21E+05	2.38E+05	5.00E-06
2000	LD2h	20 Hz	0.7548	9	0.307	1.59E+05	2.00E+05	2.15E+05	4.52E-06
2000	LD3h	No	0.7598	7.5	0.278	1.48E+05	2.14E+05	2.30E+05	4.31E-06
2000	LD3h	20 Hz	0.7598	8.6	0.322	1.69E+05	1.85E+05	1.99E+05	3.74E-06
2000	LD4h	No	0.7734	6.7	0.286	1.51E+05	2.06E+05	2.21E+05	3.47E-06
2000	LD4h	20 Hz	0.7734	8.2	0.335	1.85E+05	1.62E+05	1.74E+05	2.73E-06
4000	Base	No	0.7173	12.3	0.105	1.25E+05	2.59E+05	2.84E+05	9.35E-06
4000	Base	20 Hz	0.7173	12.5	0.104	1.27E+05	2.56E+05	2.81E+05	9.25E-06
4000	LD1h	No	0.7518	8.5	0.245	1.36E+05	2.31E+05	2.54E+05	5.94E-06
4000	LD1h	20 Hz	0.7518	9.2	0.276	1.48E+05	2.16E+05	2.38E+05	5.55E-06
4000	LD2h	No	0.7548	7.8	0.257	1.38E+05	2.28E+05	2.51E+05	5.28E-06
4000	LD2h	20 Hz	0.7548	8.7	0.294	1.54E+05	2.07E+05	2.28E+05	4.79E-06
4000	LD3h	No	0.7598	7.1	0.261	1.40E+05	2.24E+05	2.46E+05	4.63E-06
4000	LD3h	20 Hz	0.7598	8.3	0.303	1.64E+05	1.93E+05	2.12E+05	3.99E-06
4000	LD4h	No	0.7734	6.2	0.275	1.40E+05	2.20E+05	2.42E+05	3.80E-06
4000	LD4h	20 Hz	0.7734	7.8	0.325	1.76E+05	1.73E+05	1.91E+05	3.00E-06
6000	Base	No	0.7173	11.6	0.093	1.18E+05	2.69E+05	3.02E+05	9.94E-06
6000	Base	20 Hz	0.7173	11.8	0.094	1.20E+05	2.66E+05	2.99E+05	9.83E-06
6000	LD1h	No	0.7518	8.3	0.233	1.33E+05	2.35E+05	2.65E+05	6.19E-06
6000	LD1h	20 Hz	0.7518	9.1	0.266	1.46E+05	2.18E+05	2.45E+05	5.74E-06
6000	LD2h	No	0.7548	7.3	0.237	1.29E+05	2.40E+05	2.70E+05	5.68E-06
6000	LD2h	20 Hz	0.7548	8.3	0.274	1.47E+05	2.16E+05	2.43E+05	5.13E-06
6000	LD3h	No	0.7598	6.7	0.242	1.32E+05	2.35E+05	2.64E+05	4.95E-06
6000	LD3h	20 Hz	0.7598	8	0.282	1.58E+05	2.01E+05	2.26E+05	4.25E-06
6000	LD4h	No	0.7734	5.6	0.245	1.26E+05	2.38E+05	2.67E+05	4.20E-06
6000	LD4h	20 Hz	0.7734	7.4	0.287	1.67E+05	1.85E+05	2.08E+05	3.28E-06

Table 3.8 Concentration polarization and transport mode for $CaCl_2$.

Conc. (ppm)		Mag. Field	δ (m)	β	C_m/C_b	k (m s^{-1})	R	$(C_m-C_b)/\delta$ (mol $L^{-1}m^{-1}$)	Pe_m	Pe_l
2000	Base	No	8.34E-04	10.01	2.60	1.60E-06	0.705	37.07	2.836	2.403
2000	Base	20 Hz	8.32E-04	10.22	2.61	1.60E-06	0.702	37.03	2.647	2.415
2000	LD1h	No	9.85E-04	5.59	2.39	1.35E-06	0.726	27.08	2.078	1.811
2000	LD1h	20 Hz	8.24E-04	4.67	2.24	1.62E-06	0.723	28.95	1.972	1.634
2000	LD2h	No	1.04E-03	5.35	2.36	1.28E-06	0.725	24.99	1.955	1.760
2000	LD2h	20 Hz	8.25E-04	4.32	2.16	1.61E-06	0.717	26.93	1.727	1.552
2000	LD3h	No	1.09E-03	5.12	2.31	1.22E-06	0.720	22.78	1.672	1.712
2000	LD3h	20 Hz	8.03E-04	3.88	2.04	1.66E-06	0.705	24.79	1.406	1.442
2000	LD4h	No	1.17E-03	4.74	2.23	1.13E-06	0.715	19.99	1.334	1.641
2000	LD4h	20 Hz	7.46E-04	3.30	1.85	1.78E-06	0.680	21.83	0.974	1.278
4000	Base	No	7.44E-04	5.96	1.82	1.79E-06	0.573	42.76	0.755	1.911
4000	Base	20 Hz	7.32E-04	5.97	1.81	1.82E-06	0.570	42.99	0.740	1.911
4000	LD1h	No	6.91E-04	3.05	1.60	1.92E-06	0.584	33.23	0.621	1.228
4000	LD1h	20 Hz	5.55E-04	2.60	1.51	2.40E-06	0.578	35.39	0.602	1.066
4000	LD2h	No	7.27E-04	2.95	1.58	1.83E-06	0.582	30.67	0.603	1.185
4000	LD2h	20 Hz	5.38E-04	2.38	1.46	2.47E-06	0.573	33.06	0.571	0.977
4000	LD3h	No	7.73E-04	2.81	1.56	1.72E-06	0.582	27.62	0.580	1.146
4000	LD3h	20 Hz	5.12E-04	2.18	1.41	2.60E-06	0.558	30.23	0.510	0.887
4000	LD4h	No	8.45E-04	2.70	1.54	1.57E-06	0.580	24.22	0.517	1.094
4000	LD4h	20 Hz	4.41E-04	1.82	1.30	3.01E-06	0.543	26.15	0.428	0.719
6000	Base	No	6.87E-04	4.57	1.55	1.94E-06	0.489	46.11	0.474	1.665
6000	Base	20 Hz	6.72E-04	4.53	1.54	1.98E-06	0.486	46.59	0.467	1.655
6000	LD1h	No	5.35E-04	2.22	1.34	2.49E-06	0.493	36.62	0.388	0.927
6000	LD1h	20 Hz	3.91E-04	1.83	1.26	3.40E-06	0.488	38.35	0.378	0.744
6000	LD2h	No	6.07E-04	2.21	1.34	2.19E-06	0.501	32.70	0.394	0.926
6000	LD2h	20 Hz	4.15E-04	1.82	1.26	3.20E-06	0.485	35.49	0.364	0.720
6000	LD3h	No	6.39E-04	2.16	1.33	2.08E-06	0.495	29.76	0.371	0.894
6000	LD3h	20 Hz	3.72E-04	1.63	1.20	3.58E-06	0.472	31.47	0.332	0.621
6000	LD4h	No	7.65E-04	2.16	1.33	1.74E-06	0.500	25.17	0.346	0.894
6000	LD4h	20 Hz	3.43E-04	1.48	1.16	3.88E-06	0.455	26.34	0.280	0.530

Table 3.9 Membrane performances of $MgSO_4$ salt solutions.

Conc. (ppm)		Mag. Field	σ	J_v (L $m^{-2}h^{-1}$)	R_o	ΔP_e (N m^{-2})	$\Delta\pi_{eff}$ (N m^{-2})	$\Delta\pi$ (N m^{-2})	Js (mol m^{-2} s^{-1})
2000	Base	No	0.9531	8.2	0.304	8.31E+04	2.38E+05	3.97E+05	1.05E-06
2000	Base	20 Hz	0.9531	8.3	0.304	8.41E+04	2.37E+05	3.95E+05	1.05E-06
2000	LD1h	No	0.9714	6.7	0.7	1.08E+05	2.09E+05	3.48E+05	6.85E-07
2000	LD1h	20 Hz	0.9714	7.3	0.741	1.17E+05	1.99E+05	3.31E+05	6.53E-07
2000	LD2h	No	0.9728	5.7	0.701	1.01E+05	2.15E+05	3.59E+05	6.38E-07
2000	LD2h	20 Hz	0.9728	6.5	0.752	1.15E+05	2.01E+05	3.35E+05	5.95E-07
2000	LD3h	No	0.9752	4.8	0.705	9.46E+04	2.21E+05	3.69E+05	5.85E-07
2000	LD3h	20 Hz	0.9752	5.9	0.761	1.16E+05	1.99E+05	3.32E+05	5.27E-07
2000	LD4h	No	0.9812	3.8	0.709	8.58E+04	2.29E+05	3.81E+05	5.06E-07
2000	LD4h	20 Hz	0.9812	5.4	0.769	1.22E+05	1.92E+05	3.20E+05	4.25E-07
4000	Base	No	0.9531	7.7	0.283	7.81E+04	2.44E+05	4.13E+05	1.09E-06
4000	Base	20 Hz	0.9531	7.8	0.285	7.91E+04	2.43E+05	4.11E+05	1.09E-06
4000	LD1h	No	0.9714	6.3	0.683	1.01E+05	2.15E+05	3.65E+05	7.19E-07
4000	LD1h	20 Hz	0.9714	7	0.737	1.12E+05	2.04E+05	3.45E+05	6.81E-07
4000	LD2h	No	0.9728	5.3	0.691	9.38E+04	2.23E+05	3.77E+05	6.70E-07
4000	LD2h	20 Hz	0.9728	6.2	0.748	1.10E+05	2.06E+05	3.49E+05	6.21E-07
4000	LD3h	No	0.9752	4.4	0.696	8.67E+04	2.29E+05	3.89E+05	6.17E-07
4000	LD3h	20 Hz	0.9752	5.5	0.757	1.08E+05	2.07E+05	3.51E+05	5.58E-07
4000	LD4h	No	0.9812	3.4	0.702	7.68E+04	2.38E+05	4.03E+05	5.35E-07
4000	LD4h	20 Hz	0.9812	5	0.766	1.13E+05	2.01E+05	3.41E+05	4.53E-07
6000	Base	No	0.9531	7.3	0.265	7.40E+04	2.48E+05	4.20E+05	1.11E-06
6000	Base	20 Hz	0.9531	7.3	0.266	7.40E+04	2.48E+05	4.20E+05	1.11E-06
6000	LD1h	No	0.9714	5.9	0.67	9.47E+04	2.22E+05	3.76E+05	7.41E-07
6000	LD1h	20 Hz	0.9714	6.7	0.73	1.08E+05	2.09E+05	3.54E+05	6.97E-07
6000	LD2h	No	0.9728	4.9	0.675	8.67E+04	2.30E+05	3.90E+05	6.93E-07
6000	LD2h	20 Hz	0.9728	5.8	0.738	1.03E+05	2.13E+05	3.62E+05	6.43E-07
6000	LD3h	No	0.9752	4	0.682	7.88E+04	2.37E+05	4.02E+05	6.39E-07
6000	LD3h	20 Hz	0.9752	5.1	0.747	1.00E+05	2.15E+05	3.65E+05	5.80E-07
6000	LD4h	No	0.9812	3	0.686	6.78E+04	2.47E+05	4.19E+05	5.56E-07
6000	LD4h	20 Hz	0.9812	4.6	0.755	1.04E+05	2.10E+05	3.56E+05	4.74E-07

Table 3.10 Concentration polarization and transport mode of $MgSO_4$.

Conc. (ppm)		Mag. Field	δ (m)	β	C_m/C_b	k ($m\ s^{-1}$)	R	$(C_m-C_b)/\delta$ ($mol\ L^{-1}m^{-1}$)	Pe_m	Pe_l
2000	Base	No	9.95E-04	12.96	5.17	8.64E-07	0.882	74.27	0.459	2.637
2000	Base	20 Hz	9.83E-04	12.96	5.15	8.75E-07	0.881	74.88	0.455	2.635
2000	LD1h	No	8.21E-04	5.55	4.26	1.05E-06	0.937	70.04	0.584	1.777
2000	LD1h	20 Hz	7.10E-04	5.00	4.02	1.21E-06	0.943	75.26	0.671	1.674
2000	LD2h	No	9.81E-04	5.72	4.39	8.77E-07	0.939	60.86	0.568	1.806
2000	LD2h	20 Hz	7.96E-04	5.01	4.07	1.08E-06	0.946	67.83	0.666	1.672
2000	LD3h	No	1.18E-03	5.83	4.49	7.30E-07	0.942	52.26	0.531	1.828
2000	LD3h	20 Hz	8.67E-04	4.90	4.02	9.92E-07	0.947	61.44	0.609	1.652
2000	LD4h	No	1.51E-03	6.03	4.65	5.68E-07	0.944	42.39	0.391	1.857
2000	LD4h	20 Hz	9.20E-04	4.67	3.87	9.34E-07	0.947	55.09	0.421	1.605
4000	Base	No	8.28E-04	7.25	3.03	1.04E-06	0.791	86.74	0.206	2.059
4000	Base	20 Hz	8.14E-04	7.21	3.03	1.06E-06	0.790	87.72	0.205	2.051
4000	LD1h	No	5.69E-04	2.97	2.38	1.51E-06	0.882	85.78	0.250	1.158
4000	LD1h	20 Hz	4.56E-04	2.62	2.22	1.88E-06	0.895	94.45	0.289	1.032
4000	LD2h	No	6.89E-04	3.03	2.44	1.25E-06	0.888	73.99	0.251	1.179
4000	LD2h	20 Hz	5.14E-04	2.60	2.22	1.67E-06	0.900	84.51	0.291	1.029
4000	LD3h	No	8.46E-04	3.11	2.51	1.02E-06	0.893	62.84	0.238	1.203
4000	LD3h	20 Hz	5.75E-04	2.59	2.23	1.49E-06	0.904	75.59	0.273	1.022
4000	LD4h	No	1.12E-03	3.20	2.58	7.67E-07	0.898	49.89	0.184	1.232
4000	LD4h	20 Hz	6.08E-04	2.50	2.17	1.41E-06	0.904	67.82	0.200	0.983
6000	Base	No	7.34E-04	5.16	2.29	1.17E-06	0.716	93.15	0.133	1.730
6000	Base	20 Hz	7.28E-04	5.05	2.27	1.18E-06	0.718	93.40	0.134	1.716
6000	LD1h	No	4.22E-04	2.08	1.74	2.04E-06	0.832	93.20	0.158	0.804
6000	LD1h	20 Hz	3.06E-04	1.81	1.60	2.81E-06	0.850	104.08	0.184	0.663
6000	LD2h	No	5.26E-04	2.14	1.79	1.64E-06	0.839	79.54	0.157	0.832
6000	LD2h	20 Hz	3.60E-04	1.83	1.63	2.39E-06	0.857	91.87	0.183	0.675
6000	LD3h	No	6.62E-04	2.20	1.84	1.30E-06	0.846	66.76	0.150	0.855
6000	LD3h	20 Hz	4.07E-04	1.82	1.62	2.11E-06	0.862	81.33	0.174	0.671
6000	LD4h	No	9.18E-04	2.27	1.90	9.37E-07	0.853	51.54	0.117	0.889
6000	LD4h	20 Hz	4.30E-04	1.77	1.59	2.00E-06	0.863	72.64	0.129	0.639

For almost all the functionalized membranes, improvement in membrane performance correlates with a reduction in concentration polarization in the presence of 20 Hz magnetic field compared to without field. A decreased concentration polarization is demonstrated by enhancements in J_v, R_o, k and ΔP_e accompanying reductions in $\Delta\pi$, C_m/C_b, δ, β and J_s. Although

the base membranes also exhibit the similar trends, they are significantly less compared to the functionalized membranes. This agrees with the expected outcome for the effects of micro-mixing on concentration polarization and related transport properties. As expected, micro-mixing generated by the concerted movement of hydrophilic polymer chains grafted on the membrane surface increases the mobility of the sat ions and decreases the concentration of the rejected salt ions at the membrane-liquid boundary layer. The permeate flux increases due to the increased effective operation pressure resulting from the decreased osmotic pressure difference across the membrane. Presence of micro-mixing also improves NF membrane selectivity due to decreased cross-membrane solute transport under a decreased solute concentration gradient within the NF membrane layer.

Under the same feed concentration, mobility decreases and rejection increases following the order NaCl, $CaCl_2$ and $MgSO_4$[75] due to the increase in molecular weight, ionic valence and ionic hydration free energy.[76] For different salts with the same feed concentration and the same membrane modification condition, a reduced ΔP_e, an enhanced $\Delta\pi$ and a larger C_m/C_b ratio are observed for the lower mobility salts.[4, 26] In the presence of 20 Hz oscillating magnetic field, for the same feed type and feed concentration, membranes with longer polymer chains demonstrate a larger reduction in concentration polarization indicated by an increase in ΔP_e accompanied by a decrease in δ, C_m/C_b and $\Delta\pi$. This is due partly to the increased resistance to cross-membrane water flux for membranes with higher grafting degrees, resulting in the decrease in the rate of salt accumulation within the boundary layer.[26] In addition, longer polymer chains are more effective in inducing the micro-mixing effects. For the same feed, the increased resistance of membrane layer to solvent and solute transport for the membranes

grafted with longer polymer chains is demonstrated by decreased J_v and J_s, respectively. Although increased ATRP time often generates longer polymer chains therefore stronger micro-mixing, this occurs under the sacrifice of permeability due to increased membrane layer resistance. With the increase in feed concentration, an increase in $\Delta\pi$ and a decrease in ΔP_e are expected. A decrease in C_m/C_b is also observed.[28, 37]

The induced micro-mixing by applying a 20 Hz magnetic field can be analyzed by comparing the membrane performance, concentration polarization and ion transport in the presence and absence of magnetic field while keeping the same feed composition and membrane modification condition. Most importantly, the changes in δ, k, β and C_m/C_b, as well as in R, Pe and $(C_m-C_b)/\delta$ help to explain the differences in the cross-membrane transport modes of different types of ions in the presence of a micro-mixer at the membrane-liquid interface.

3.5.1 Membrane Performance

As indicated by earlier membrane performance data, the effects of micro-mixing are mainly demonstrated in the increased rejection for salts with low reflection coefficient, and in the enhanced permeate flux for salts with high reflection coefficient. This results from the differences in the transport mechanisms of different types of salts, which can be primarily explained by variations in ΔP_e and $\Delta\pi$ that are shown in Figures 3.3 and 3.4, respectively. The decreases in $\Delta\pi$ and increases in ΔP_e are both affected more by polymer chain length compared to salt concentration, and percentage changes in both $\Delta\pi$ and ΔP_e always tend to increase as the polymer chain length increases. Improvements in ΔP_e are larger under higher feed salt concentrations. For the same functionalized membrane, decreases in $\Delta\pi$ are always more

evident for salts like NaCl and $CaCl_2$ that are relatively easy to go through the NF membranes compared to $MgSO_4$. Meanwhile, increases in ΔP_e are the greatest for $MgSO_4$, the salt with both the highest rejection coefficient by the NF membranes and the lowest bulk diffusivity among the three investigated salts.

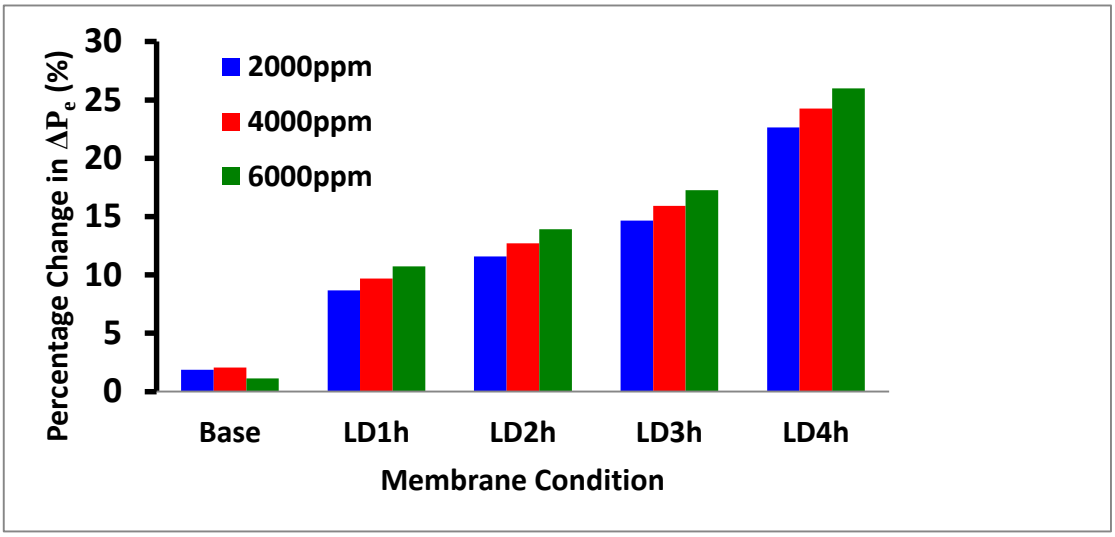

(a) NaCl

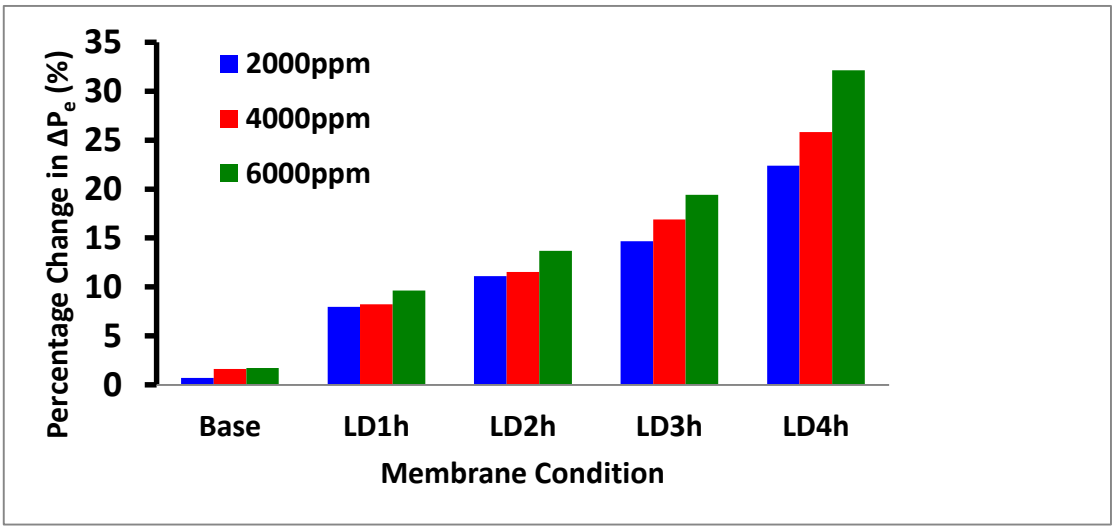

(b) $CaCl_2$

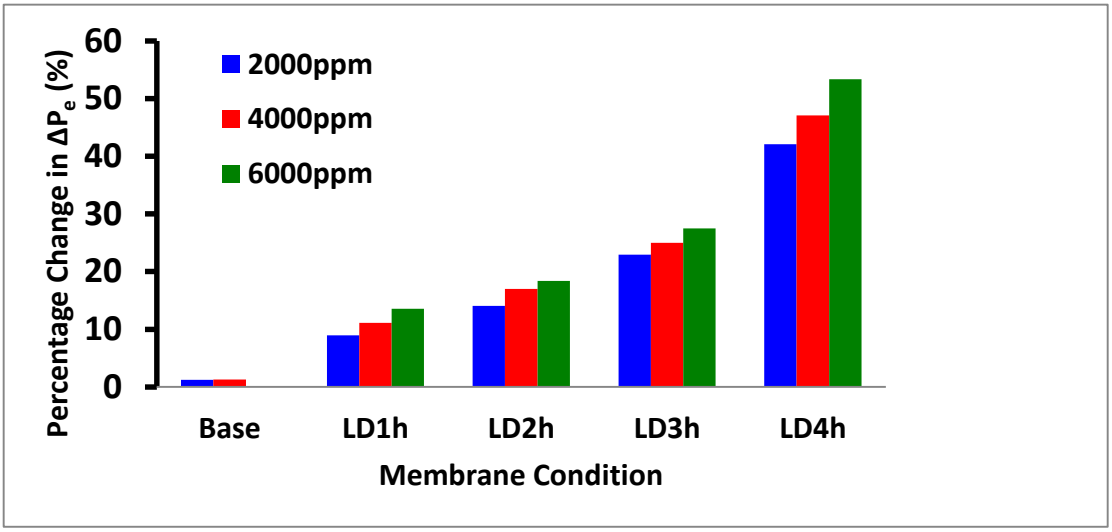

(c) $MgSO_4$

Figure 3.3 Percentage change in ΔP_e for (a) NaCl, (b) $CaCl_2$ and (c) $MgSO_4$ in the presence of a magnetic field compared to the value in the absence of a field.

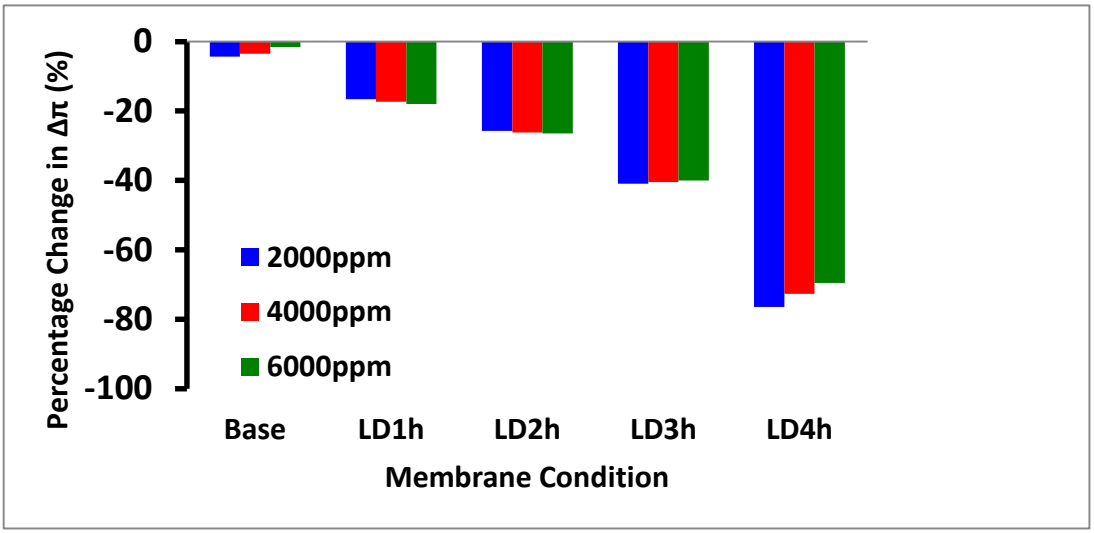

(a) NaCl

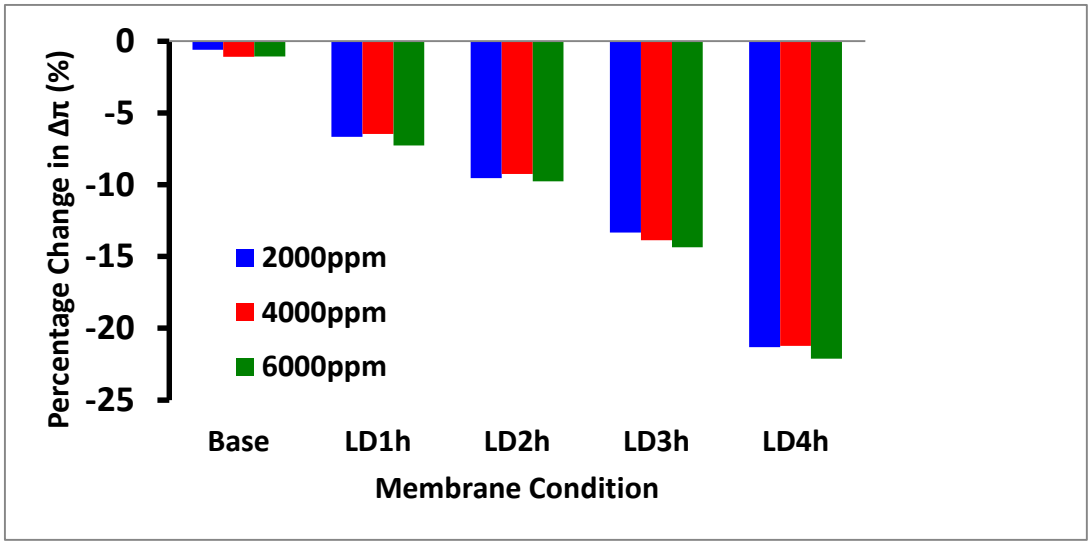

(b) $CaCl_2$

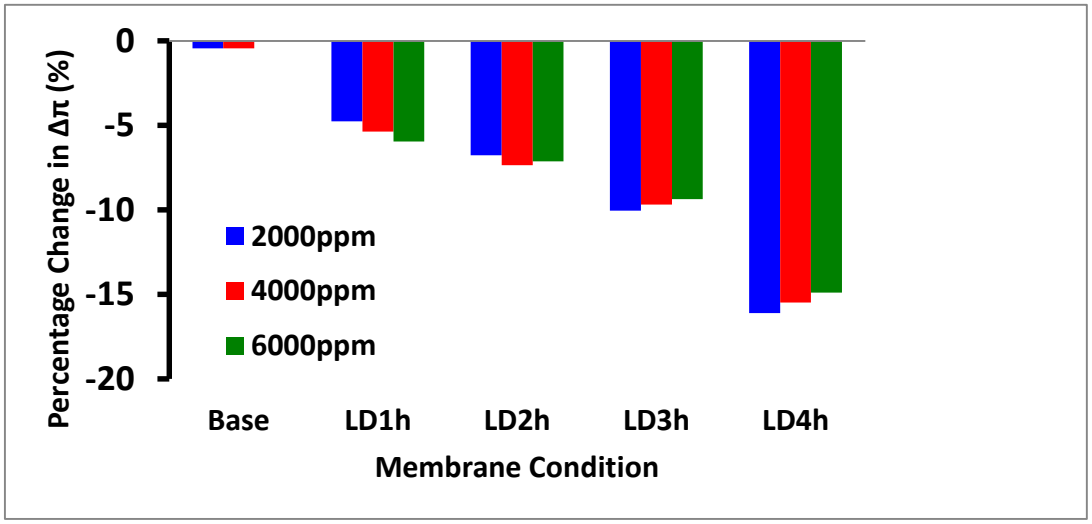

(c) $MgSO_4$

Figure 3.4 Percentage change in Δπ for (a) NaCl, (b) $CaCl_2$ and (c) $MgSO_4$ in the presence of a magnetic field compared to the value in the absence of a field.

Generally, the oscillating magnetic field exerts minor effect on the performances of base NF270 membranes due to their unavailability of micro-mixing. According to Chen et *al.*, the external 15-20 Hz oscillating magnetic field itself could possibly increase the mobility of charged ions and decrease water viscosity to improve membrane performance.[77] However, this is almost negligible during the presence of concentration polarization. For the functionalized NF270 membranes, variations in membrane performance in the presence compared to absence of external field always tend to increase with ATRP time. Without the nanoparticles conjugated onto the chain ends, there is still no theoretical evidence that the low frequency oscillating magnetic field could affect the molecular structures of NF270's polyamide barrier layer or the grafted poly(HEMA) chains and nano layer. In addition to that longer polymer chains generate stronger micro-mixing within the concentration boundary layer to more effectively break concentration polarization, variations in membrane performance in the presence compared to absence of external field are also due to the structural changes of functionalized membrane layer. When an external magnetic field is exerted onto the nanoparticles attached to the polymer chain ends, greater structural changes would take place for the longer polymer chains and thicker surface nano layers that are both formed after longer ATRP time.[78]

3.5.2 Concentration Polarization

Concentration polarization modulus, which is the ratio of surface to bulk concentration, is most important in the quantification of concentration polarization.[4, 18, 37] C_m/C_b indicates the effect of concentration polarization on membrane separation processes. Percentage decrease in C_m/C_b is shown in Figure 3.5. Figure 3.6 and 3.7 both show the relation between percentage

changes in C_m/C_b, ΔP_e and $\Delta\pi$.

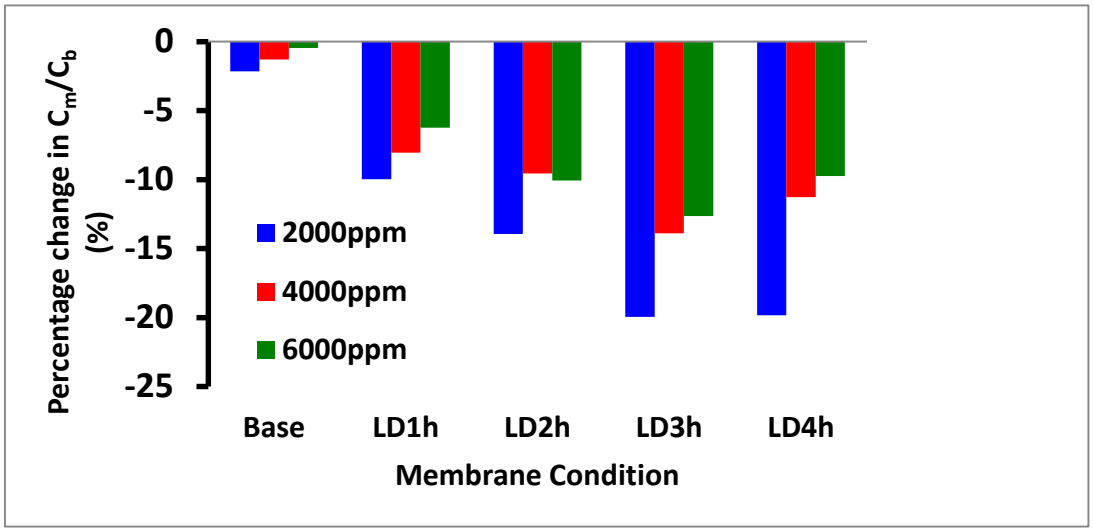

(a) NaCl

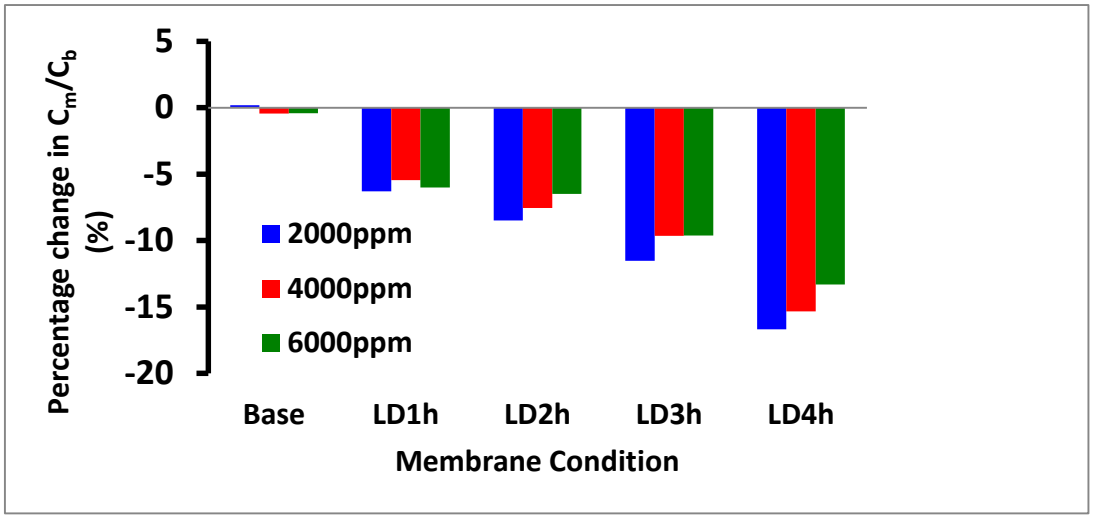

(b) $CaCl_2$

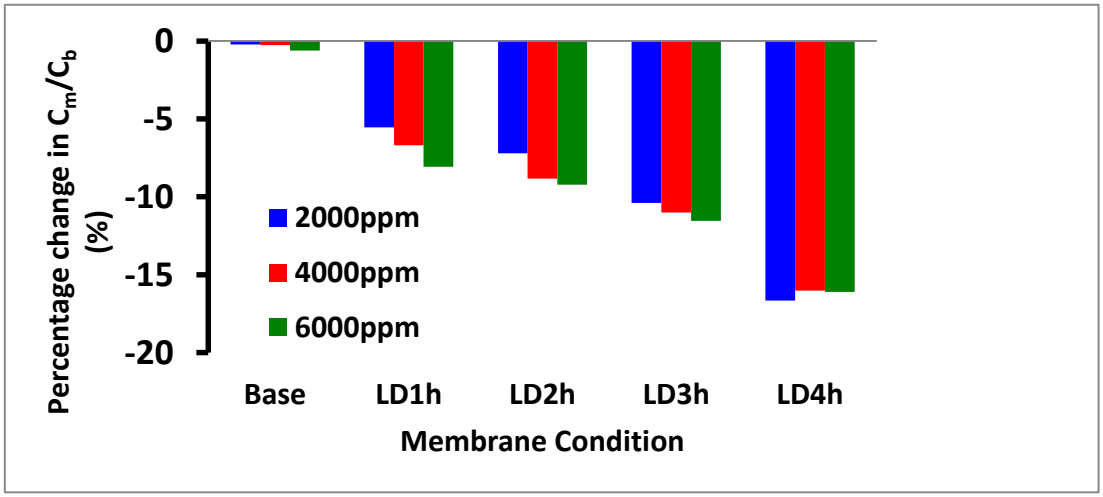

(c) $MgSO_4$

Figure 3.5 Percentage change in C_m/C_b for (a) NaCl, (b) $CaCl_2$ and (c) $MgSO_4$ in the presence of a magnetic field compared to the value in the absence of a field.

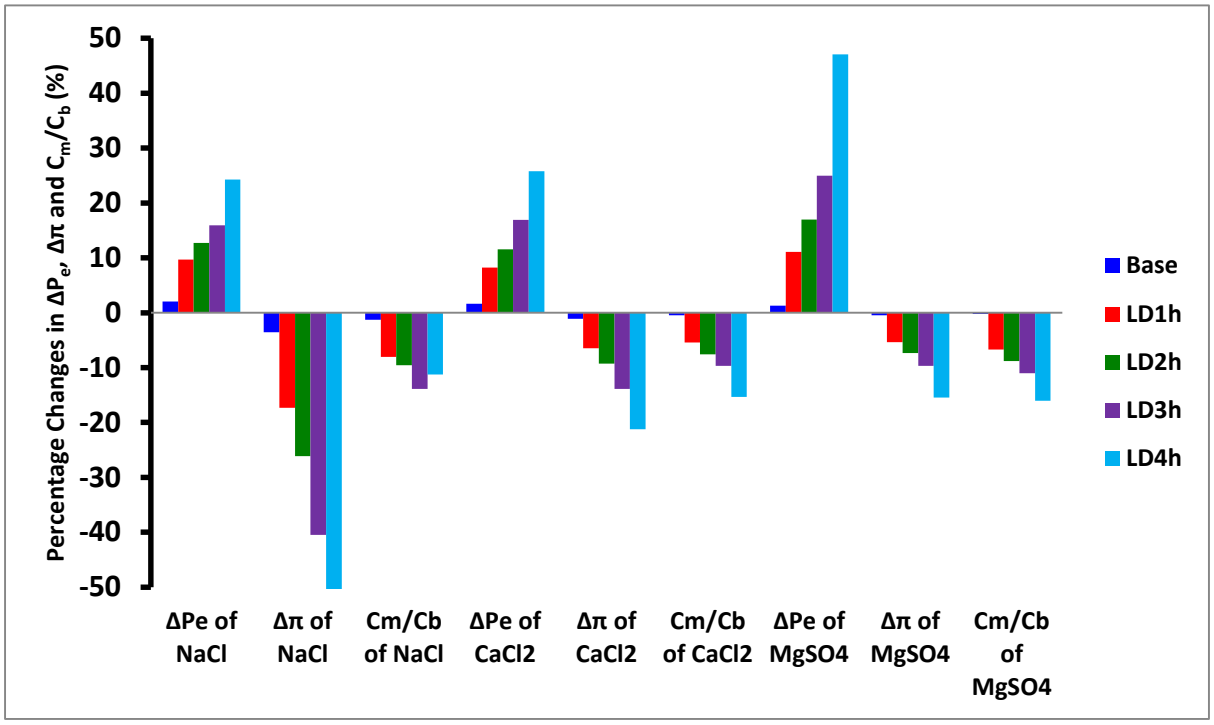

Figure 3.6 Percentage changes in ΔP_e, $\Delta\pi$ and C_m/C_b for the 4000 ppm salt solution in the presence/absence of a 20 Hz magnetic field.

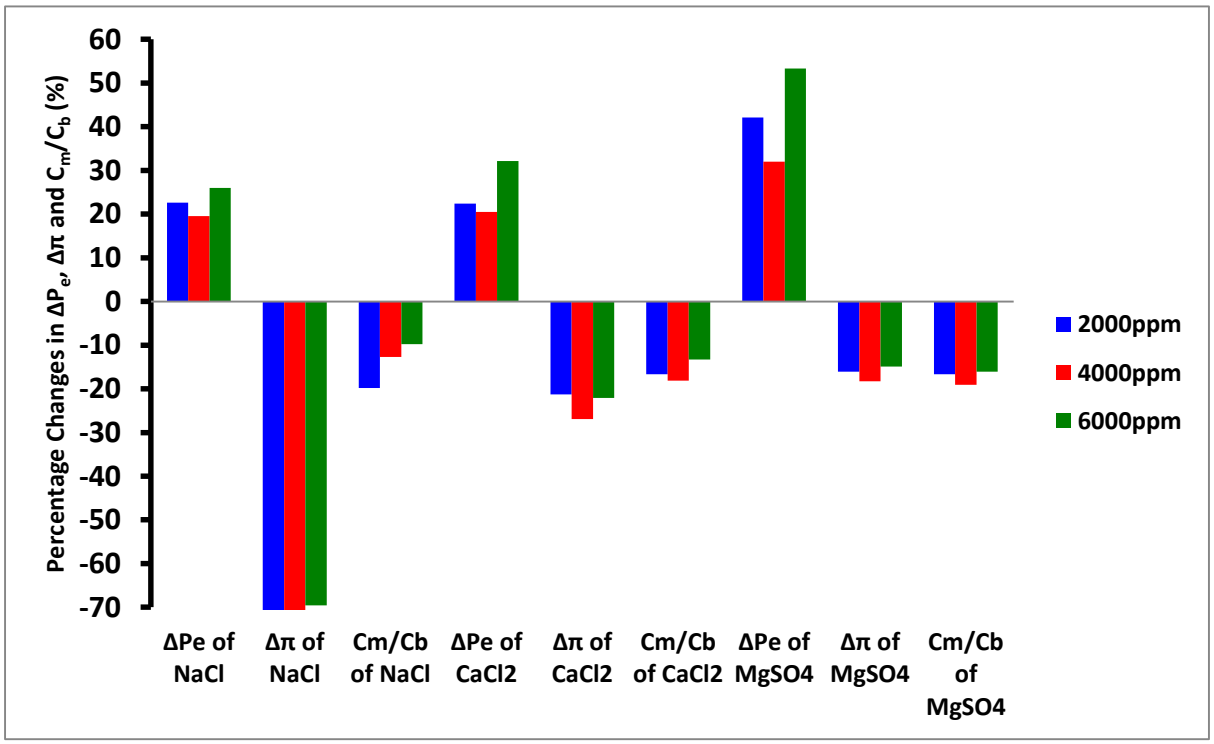

Figure 3.7 Percentage changes in ΔP_e, $\Delta\pi$ and C_m/C_b for the LD4h membrane in the presence/absence of a 20 Hz magnetic field.

Figures 3.6 and 3.7 indicate flux improvements in the presence of micro-mixing for low mobility salt solutions are mainly due to increased effective operation pressure, but those for high mobility salt solutions are mainly brought by decreased osmotic pressure difference under a decreased surface concentration. A decreased value of C_m/C_b in the presence compared to absence of external oscillating field directly indicates that micro-mixing reduces concentration polarization. Figure 3.6 also indicates stronger micro-mixing generated by functionalized NF270 membranes with longer polymer chains would more effectively reduce concentration polarization. In addition, longer polymer chains lead to more significant changes in both ΔP_e and $\Delta\pi$, especially for the reduction of $\Delta\pi$. According to both the Hagen-Poiseuille mechanism and the Darcy's law,[1] cross-membrane solvent flux is always linear versus ΔP_e for the NF membranes.[16] The trends of ΔP_e percentage improvement generally agree with those of flux improvement under the investigated salt concentrations below 10,000 ppm. That is, flux improvements are always larger for lower mobility salts with higher bulk concentrations, and increases with membrane chain length. Meanwhile, the values and trends of C_m/C_b percentage reductions are similar for each salt, and affected mainly by polymer chain length rather than salt concentration.

Together with the C_m/C_b ratio, concentration boundary layer thickness (δ) has been widely used in recent year's NF and RO papers to indicate concentration polarization and salt transport.[4, 26, 28, 79] Presence of the concentration boundary layer is due to a decreased mixing between the bulk flow and the surface area. Concentration boundary layer thickness above the upstream NF or RO membrane surface indicates the accumulation of rejected ions and molecules above the membrane.[4, 26, 28, 79] Concentration boundary layer thickness affects

transport across the membrane since both solvent and solute permeating through the membrane have to cross the concentration boundary layer first. Similar to most recent NF and RO literature, with polymer chain length, salt and magnetic field condition held constant, δ tends to decrease with increase in feed salt concentration.[27, 28, 68] According to Chaabane *et al.*, for the base polyamide membranes, the decreases in δ with increases in feed salt concentration is mainly due to the neutralization of surface charge by the formation of a "screen" layer immediately above the membrane surface, neutralizing surface charge to increase salt transport across the membrane.[28] That is, besides the increased cross-membrane concentration difference, the increased cross-membrane salt transport during the presence of concentration polarization is also due to a reduced dielectric exclusion.[28] However, for the functionalized membranes without surface charge, the decreases in δ with increases in feed salt concentration is mainly due to a slower accumulation of rejected ions under a decreased permeate flux that is brought by an increased Δπ.

Since increases in δ are caused by decreased exchange between the bulk feed and the concentration boundary layer, δ is subject to mixing effect.[79] Functionalized membranes generally demonstrate a decreased δ in the presence compared to absence of an oscillating magnetic field. Percentage decreases in δ are greater for membranes modified with longer ATRP time since longer polymer chains tend to generate stronger micro-mixing effect in the presence of an oscillating magnetic field. In addition, percentage decreases in δ are generally greater under higher feed salt concentrations. Based on Fick's law, increase in bulk feed concentration slows down the diffusion of rejected salt from the membrane surface back into the bulk feed. Therefore, micro-mixing has a stronger effect in reducing concentration

polarization under higher feed salt concentrations. Generally, the trend of percentage reduction of δ for each salt in the presence compared to absence of field is similar to each other, and depends strongly on both polymer chain length and salt concentration. Variations of δ become more evident with increases in either polymer chain length or salt feed concentration, and are slightly more evident for solutes with lower rejection and higher mobility.

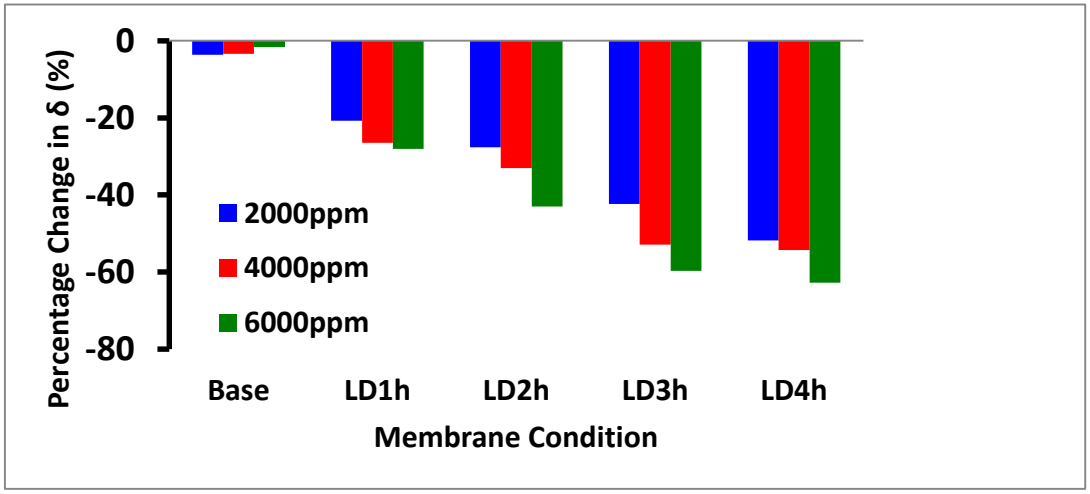

(a) NaCl

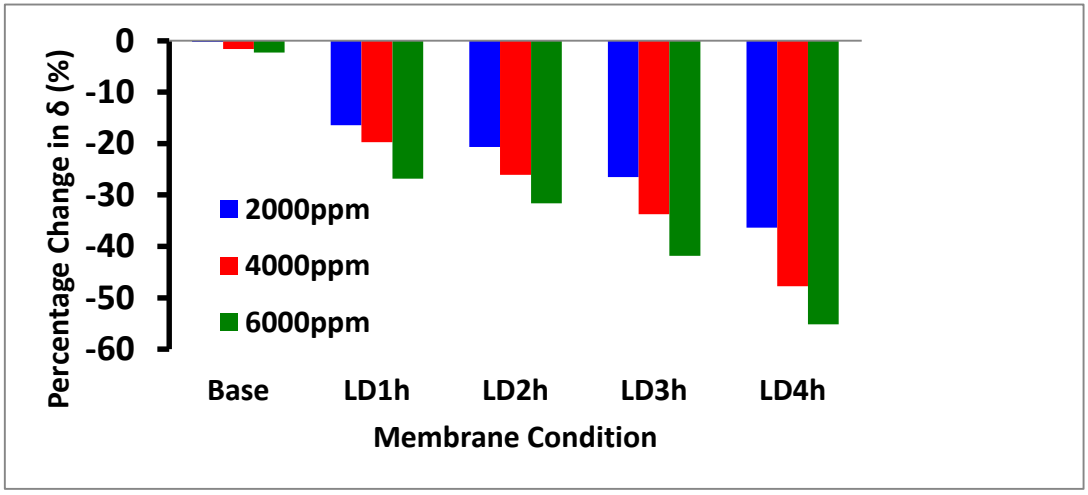

(b) $CaCl_2$

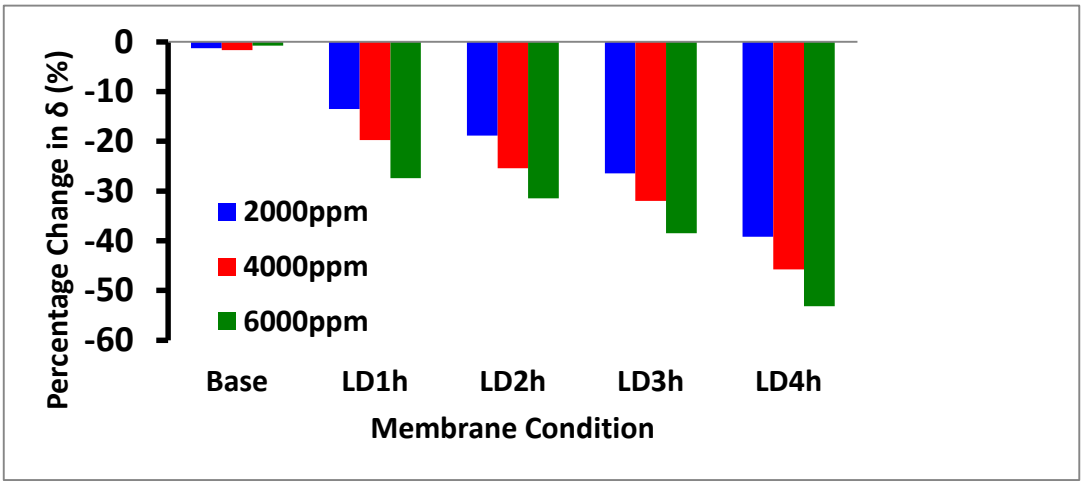

(c) $MgSO_4$

Figure 3.8 Percentage change in concentration polarization boundary layer thickness (δ) for (a) NaCl, (b) $CaCl_2$ and (c) $MgSO_4$ in the presence of a magnetic field compared to the value in the absence of a field.

Besides concentration boundary layer thickness and concentration polarization modulus, concentration polarization factor (β) has also been widely used to indicate and investigate concentration polarization. As theoretically defined, β equals to the solute concentration difference between membrane surface and permeate that is divided by the solute concentration difference between bulk feed and permeate. As indicated by Tables 3.6, 3.8 and 3.10, for the same membrane sample and concentration, β is often the weakest for NaCl and the strongest for $MgSO_4$. In other words, β increases with both the increases in reflection coefficient and the decreases in salt diffusivity. Similar to C_m/C_b, β decreases with increases in membrane ATRP time due to increases in membrane layer resistance to both solute and solvent transport. Decrease in cross-membrane salt transport reduces salt concentration in the permeate, and a decreased cross-membrane water flux reduces the accumulation of rejected salt ions above the upstream membrane surface. Moreover, β decreases with increase in feed salt concentration due to decreases in salt rejection limitation, indicating increased cross-membrane salt transport under a higher salt concentration gradient within NF membrane barrier layer. Percentage changes of β are shown in Figure 3.9. For each salt investigated, the percentage change of β in the presence compared to absence of an external field is dominated by the ATRP time during membrane functionalization. A stronger micro-mixing effect generated by the longer polymer chains on the surface of membranes with longer ATRP time leads to a greater percentage reduction in β. The percentage reduction of β decreases with the increases in rejection and the decreases in salt diffusivity.

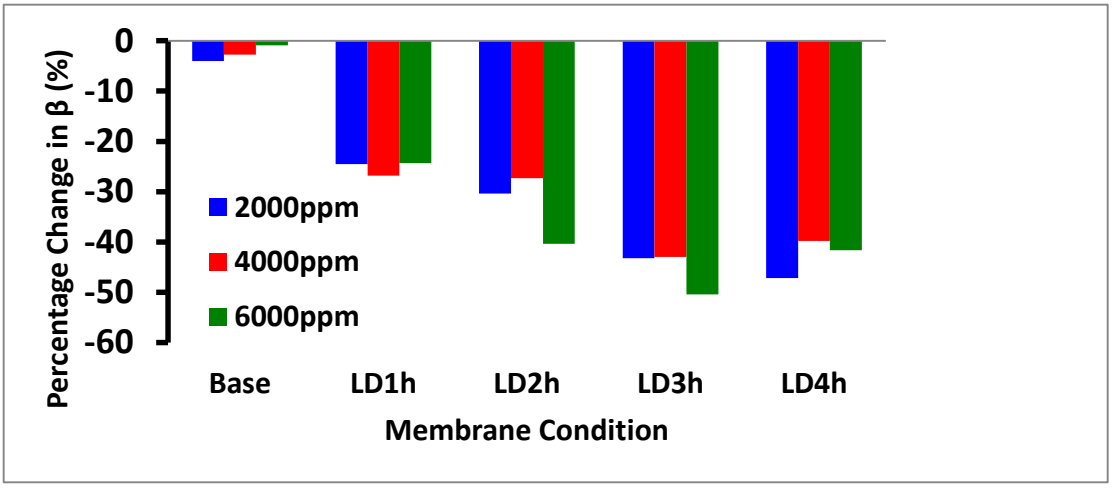

(a) NaCl

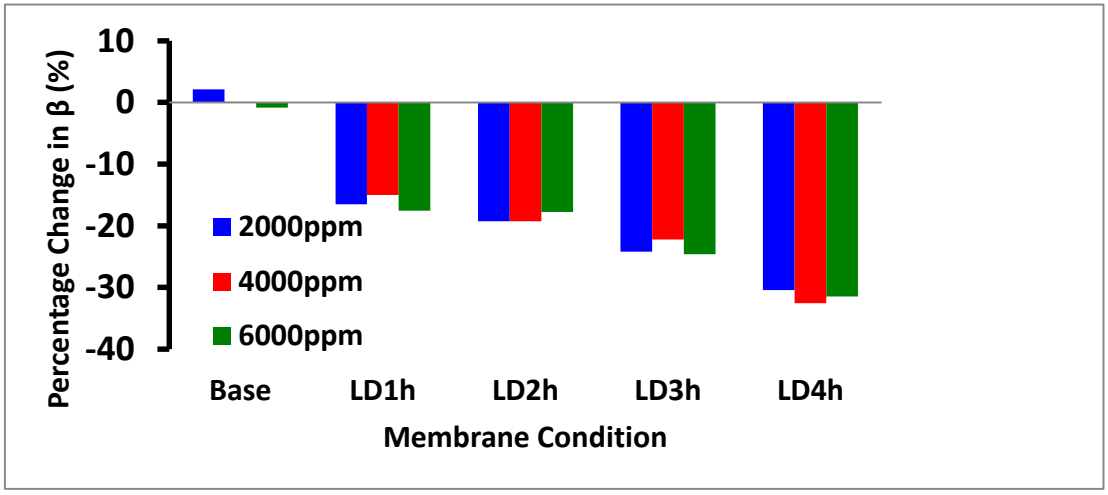

(b) $CaCl_2$

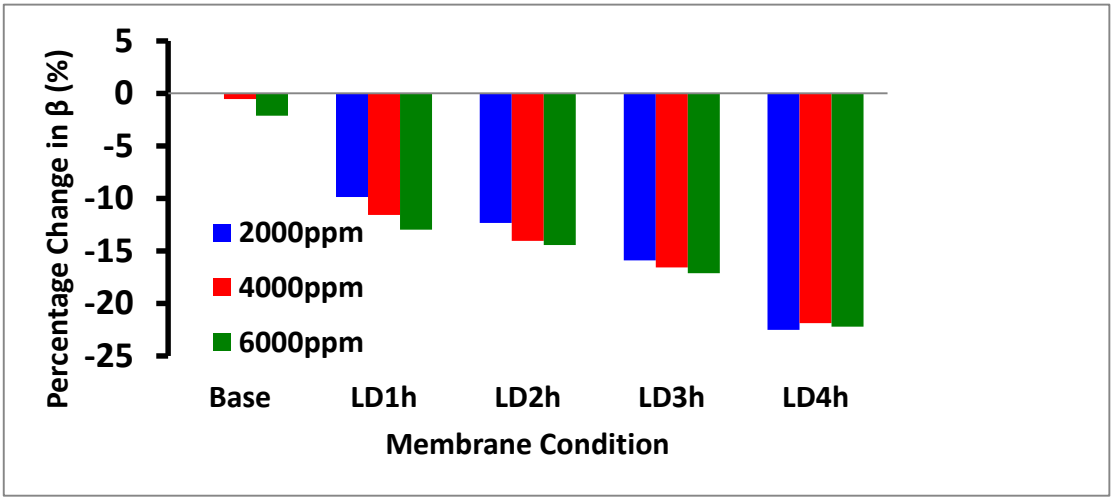

(c) $MgSO_4$

Figure 3.9 Percentage change in concentration polarization factor (β) for (a) NaCl, (b) $CaCl_2$ and (c) $MgSO_4$ in the presence of a magnetic field compared to the value in the absence of a field.

In the Film Theory, the value of solute mass transfer coefficient (k) equals the ratio of bulk diffusivity to concentration boundary layer thickness. The value of k directly indicates solute transport therefore solute accumulation within the concentration boundary layer outside the membrane layer.[18, 80] According to Lee *et al.*, an increased mass transfer coefficient indicates an enhanced transport of the rejected ions and molecules away from the membrane surface. In other words, an increased k value is helpful with decreasing the accumulation of rejected species on the membrane surface.[18] According to Murthy and Gupta, the value of k depends on both the permeate flux across the NF membrane and the hydrodynamic conditions above the membrane's upstream surface.[29] Park and Barnett mentioned a reduced concentration boundary layer thickness therefore an increased mass transfer coefficient under an increased Reynolds number above the NF membrane's feed side surface.[81] Based on the Film Theory, the mass transfer coefficient also depends on the cross-membrane transport and the bulk diffusivity of rejected species.[29]

The values of k are given by Figure 3.10 (1). Under constant polymer chain length, feed concentration and magnetic field condition, k decreases with the decreases in salt bulk diffusivity and the increases in salt reflection coefficient. Within the dead end filtration NF system in this work, k increases with the increases in feed salt concentrations. This indicates a decreased salt accumulation brought by both a decreased permeate flux resulted from an increased osmotic pressure difference and an increased cross-membrane salt transport resulted from an increased concentration gradient within the membrane layer. For $MgSO_4$ with all concentrations and $CaCl_2$ with high concentrations in the absence of field, the value of k increases after the 1st hour of polymerization and then starts to decrease after the 2nd hour of

polymerization. Indicated by the values of J_v and σ in Tables 3.7 and 3.9, increases in membrane layer resistance during the first hour of polymerization are mainly in water transport, decreasing salt accumulation under a significantly decreased permeate flux while a slightly decreased cross-membrane salt transport. During the 2-4th hours of polymerization, the increases in membrane layer resistance are more at salt compared to water transport, increasing salt accumulation under slightly decreased flux. This is evident for the high rejection salts with high feed concentration. While for the low rejection salts with low feed concentration, especially in the presence of magnetic field, k simply increases with ATRP time under the same magnetic field condition. Indicated by the J_v and σ values in Tables 3.5 and 3.7, this is simply due to a decreased salt accumulation under a reduced permeate flux as a result of an increased membrane layer resistance after a longer ATRP time.[30] However, the effect of membrane functionalization on k mainly depends on the effect of micro-mixing generated in the presence of an external oscillating field.

Percentage changes of k are given by Figure 3.10 (2). A stronger micro-mixing effect generated by longer polymer chains generally leads to a greater improvement in k. For $CaCl_2$ and $MgSO_4$ under each concentration, the increases in k for the ATRP=4h membranes are greater than the other membranes. Meanwhile, increases in k are slightly higher for NaCl and similar for $CaCl_2$ and $MgSO_4$ for the same membrane under the same feed concentration, and are affected by both ATRP time and feed concentration. For each salt investigated, more evident increases in k have generally been observed both under higher salt concentrations and for membranes with longer polymer chains (ATRP time). Increases in k are always negligible for the base membranes since they are unable to generate micro-mixing in the presence of an

external oscillating field. For the functionalized membranes, the universal increase in k in the presence compared to absence of an external oscillating field indicates the effect of micro-mixing in decreased concentration polarization due to an increased solute mass transfer coefficient within the concentration boundary layer. This is particularly important in maintaining constant NF membrane performance during the removal of salts under a high feed concentration, improving the rejection for low rejection salts and enhancing the flux for high rejection salts. Despite the increased membrane layer resistance, membranes with increased ATRP time often have longer polymer chains on the membrane surface. The movement of long polymer chains triggered by a 20 Hz magnetic field helps to generate stronger micro-mixing to more evidently decrease concentration polarization by improving solute mass transfer coefficient values.

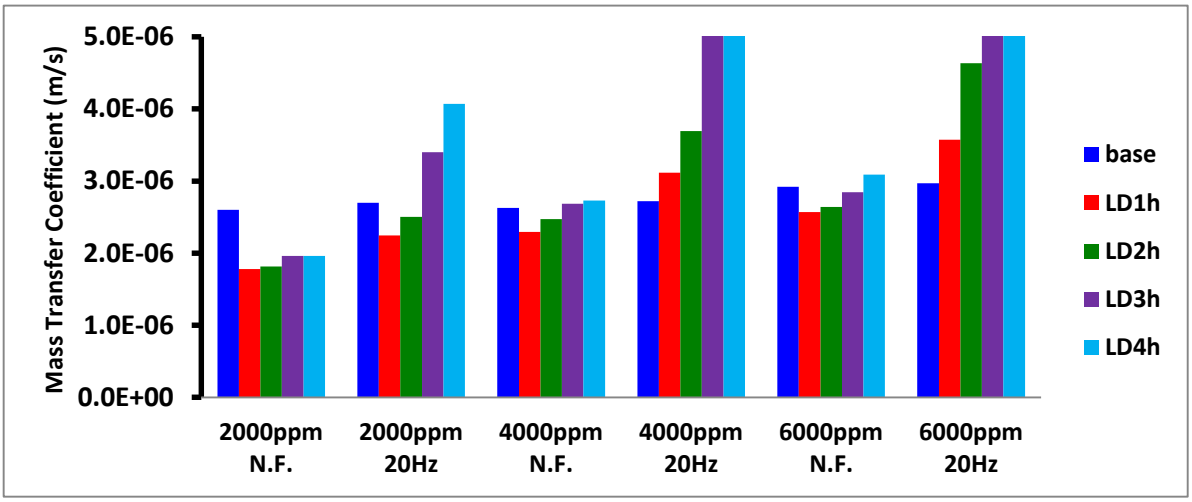

(a) NaCl

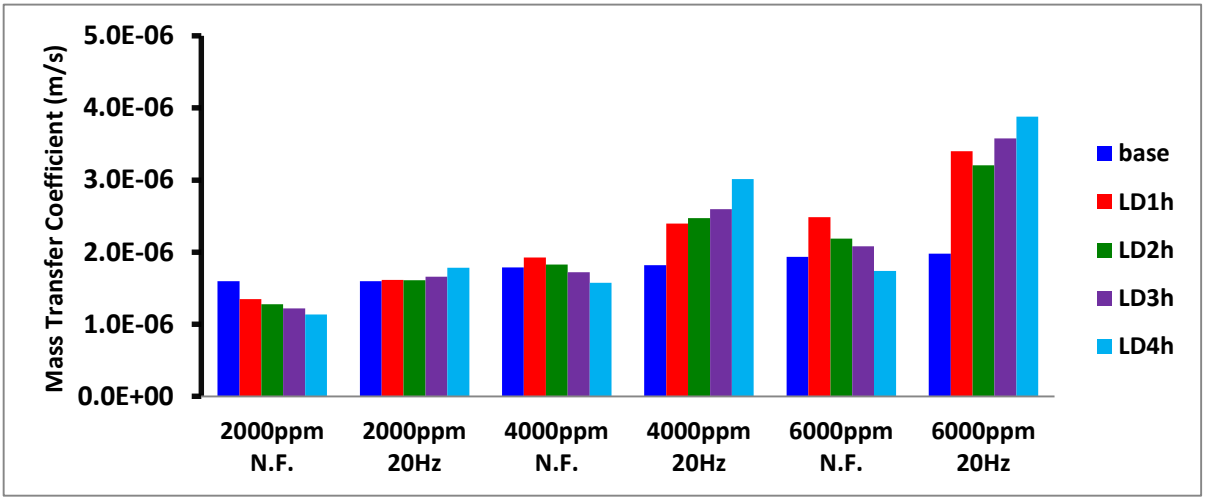

(b) $CaCl_2$

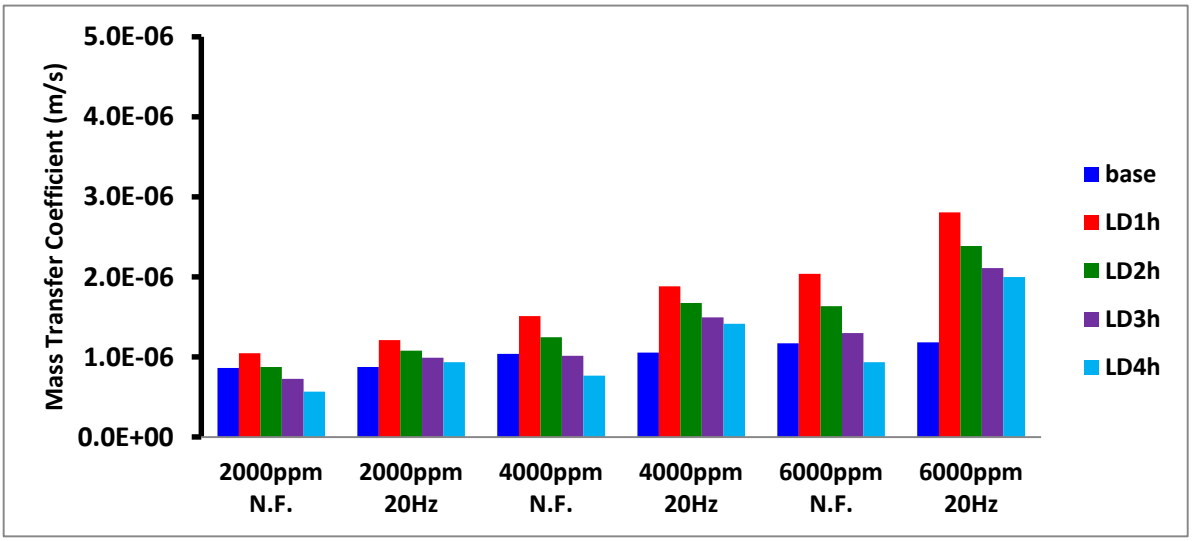

(c) $MgSO_4$

Figure 3.10 (1) Solute mass transfer coefficient (k) values for (a) NaCl, (b) $CaCl_2$ and (c) $MgSO_4$ within the concentration boundary layer.

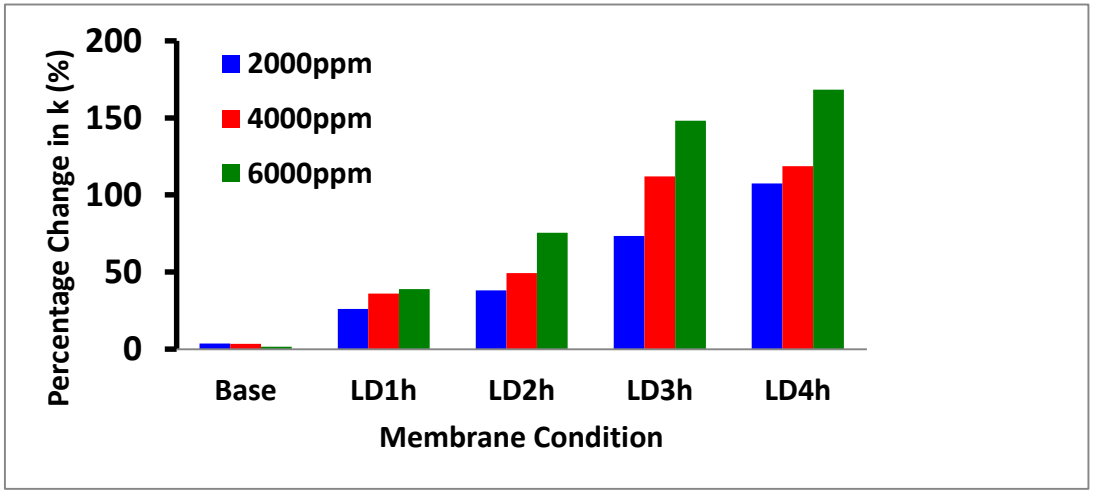

(a) NaCl

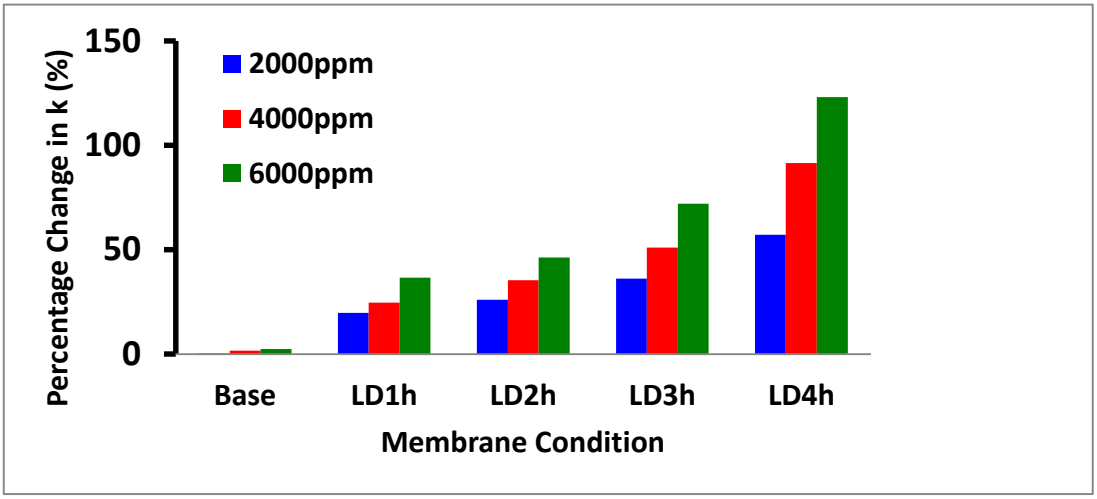

(b) $CaCl_2$

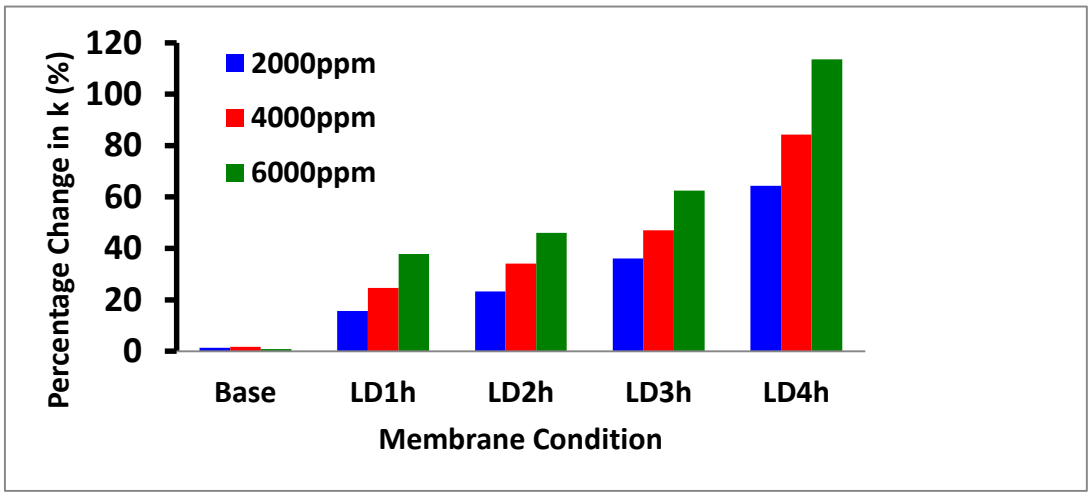

(c) $MgSO_4$

Figure 3.10 (2) Percentage change in the solute mass transfer coefficient (k) for (a) NaCl, (b) $CaCl_2$ and (c) $MgSO_4$ in the presence of a magnetic field compared to the value in the absence of a field.

3.5.3 Salt Transport

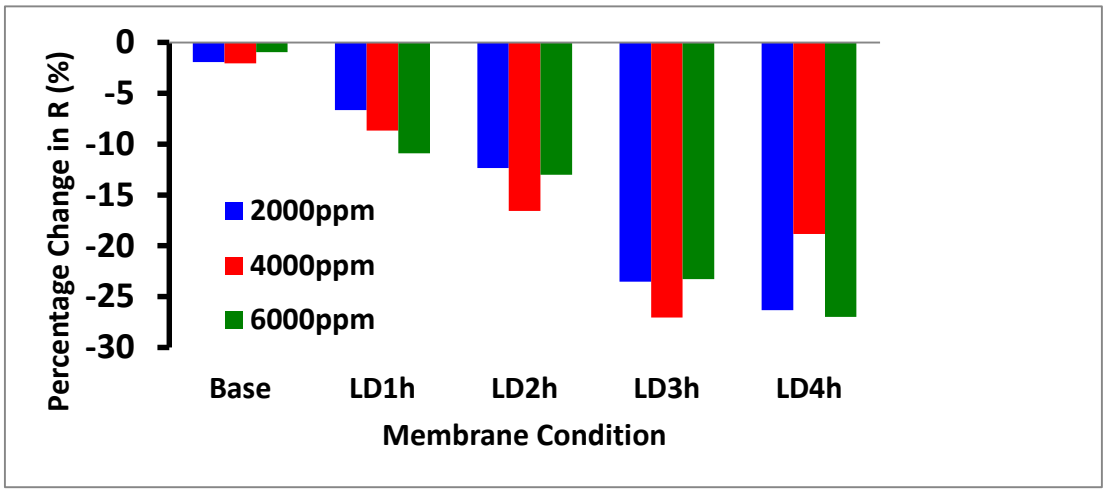

(a) NaCl

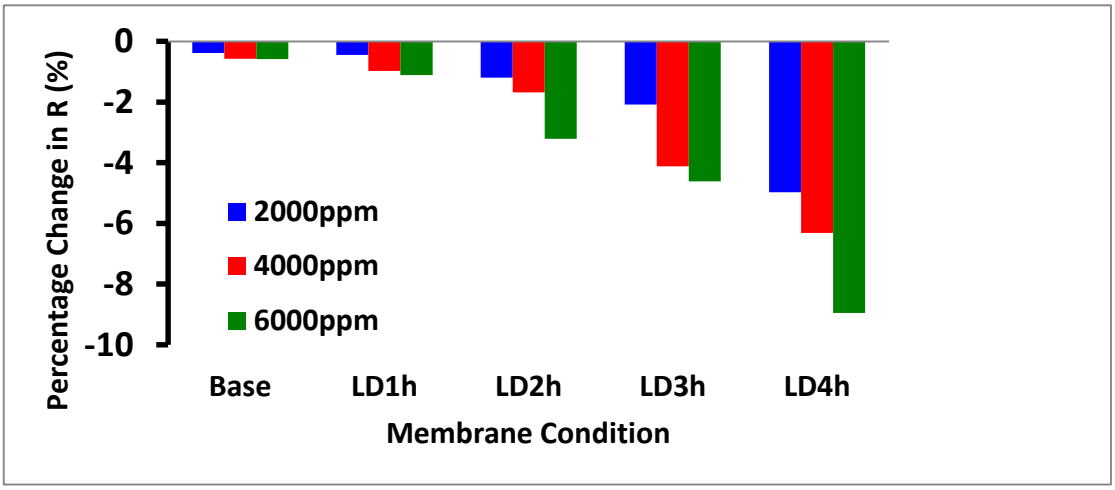

(b) $CaCl_2$

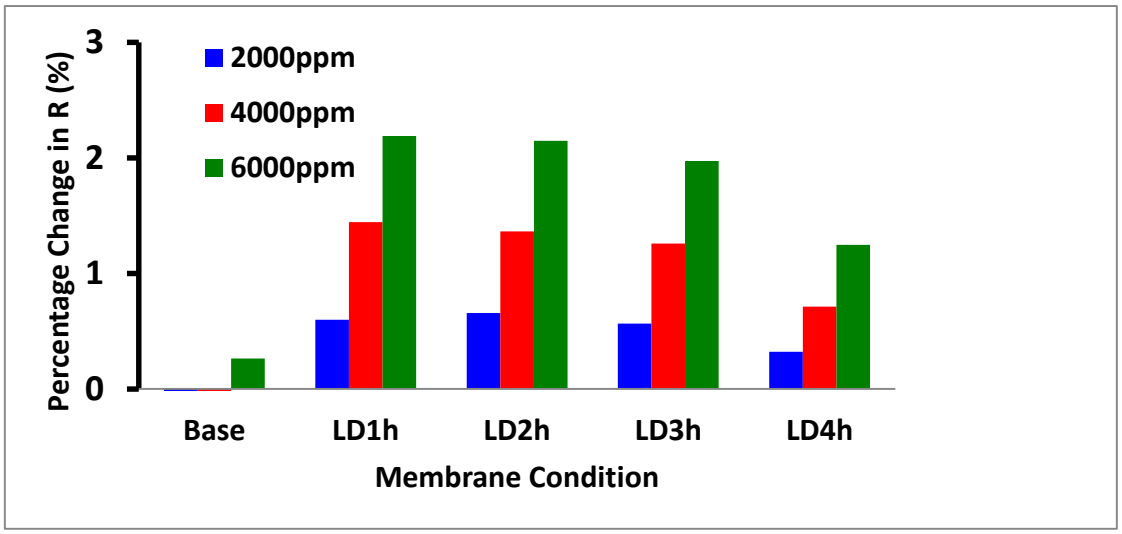

(c) $MgSO_4$

Figure 3.11 Percentage change in intrinsic rejection (R) for (a) NaCl, (b) $CaCl_2$ and (c) $MgSO_4$ in the presence of a magnetic field compared to the value in the absence of a field.

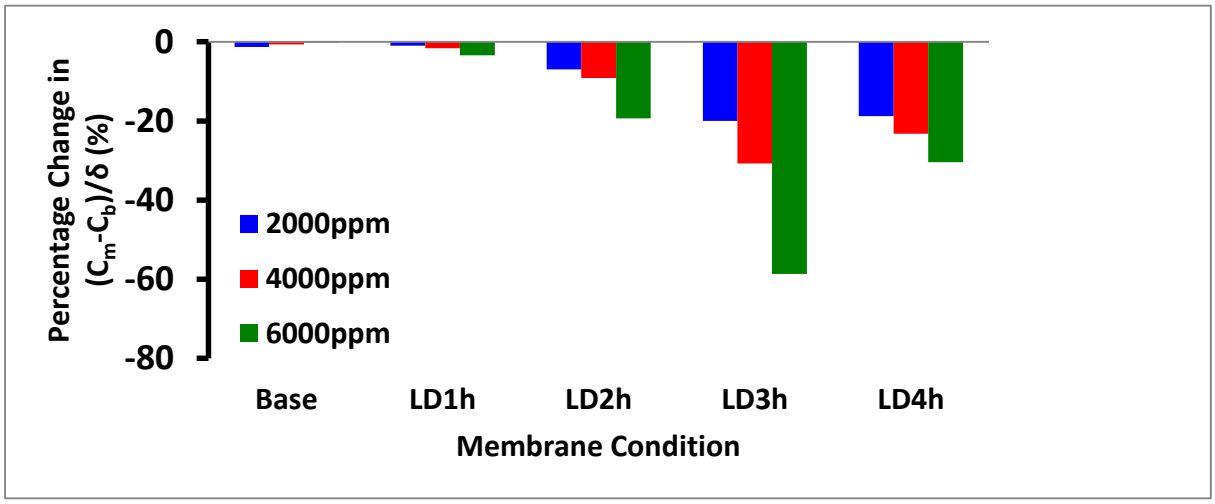

(a) NaCl

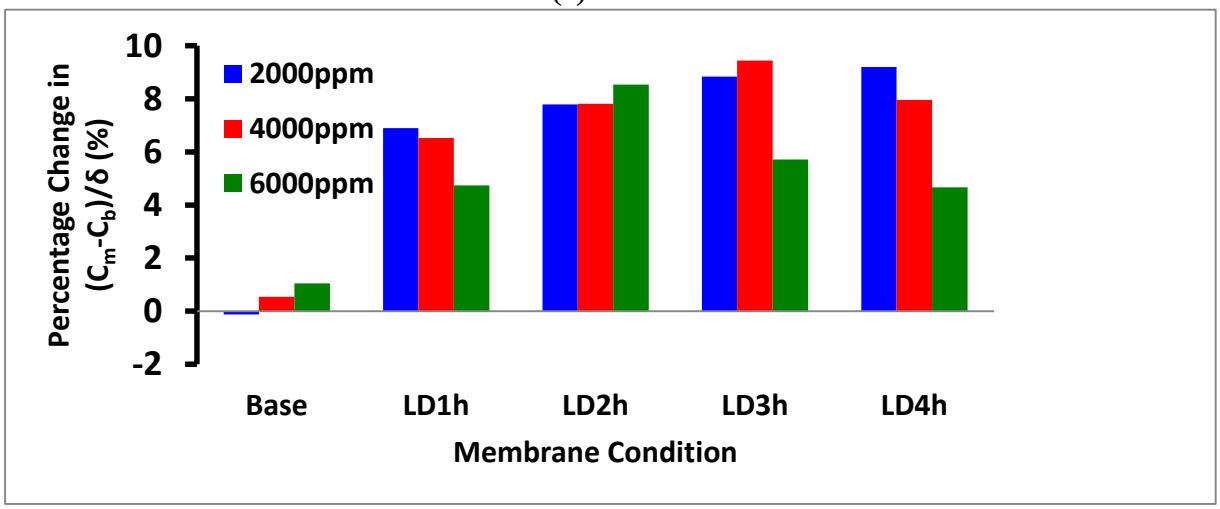

(b) $CaCl_2$

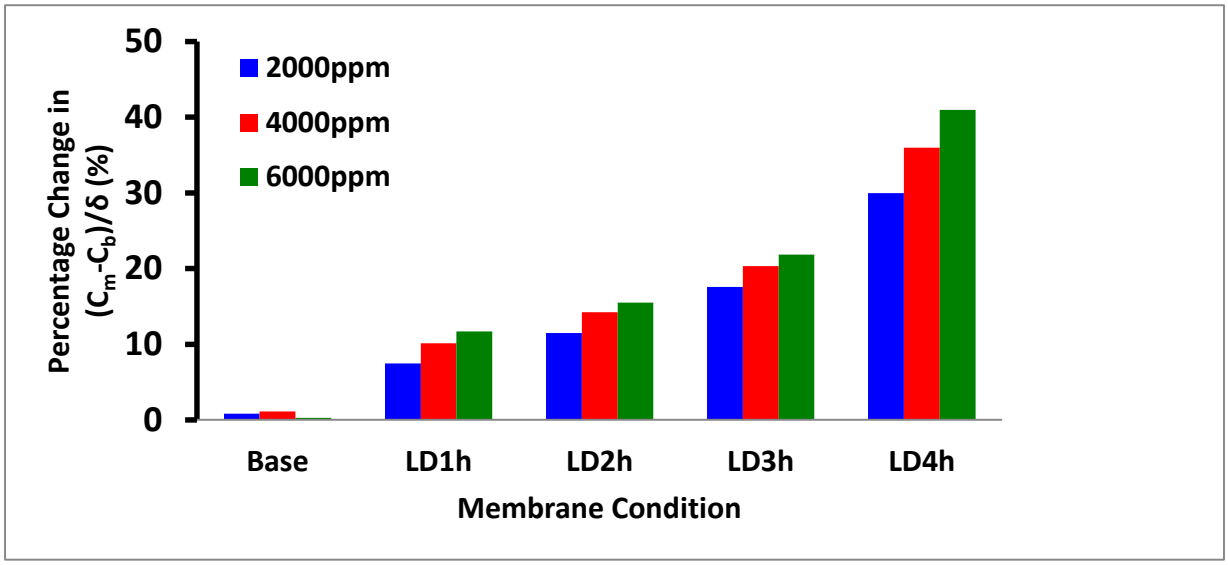

(c) $MgSO_4$

Figure 3.12 Percentage change in $(C_m-C_b)/\delta$ for (a) NaCl, (b) $CaCl_2$ and (c) $MgSO_4$ in the presence of a magnetic field compared to the value in the absence of a field.

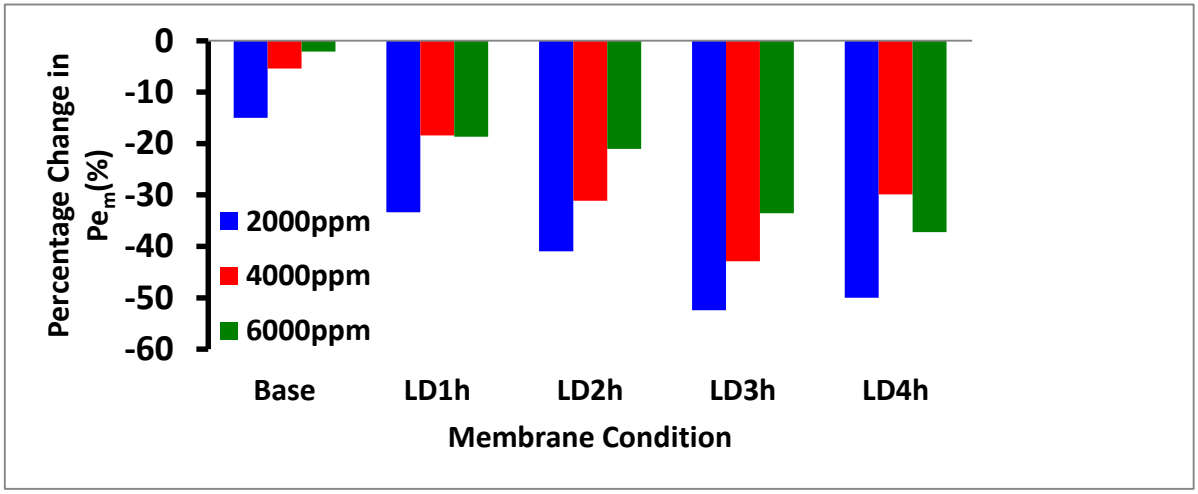

(a) NaCl

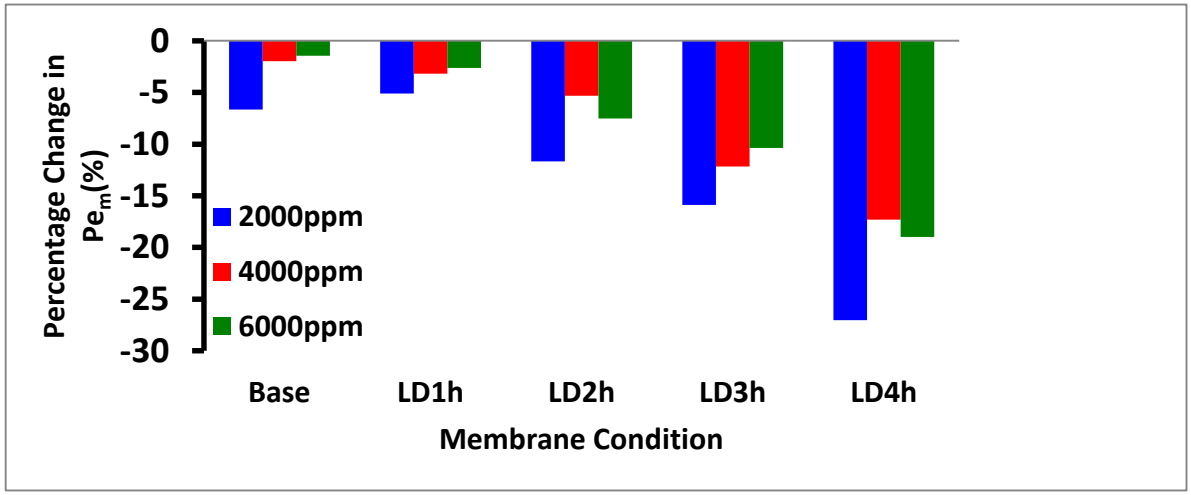

(b) $CaCl_2$

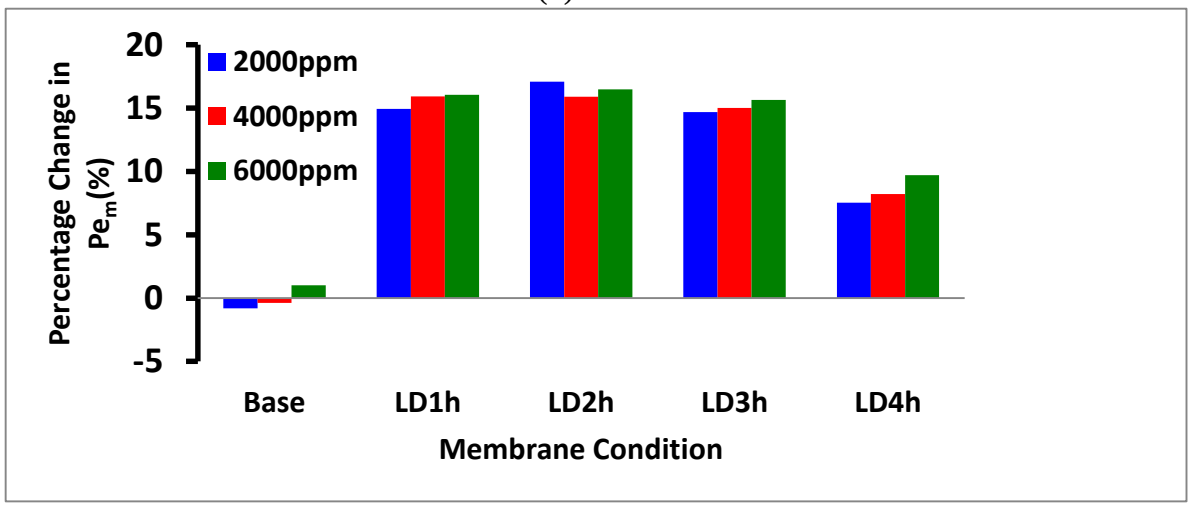

(c) $MgSO_4$

Figure 3.13 (1) Percentage change in the membrane's Peclet number (Pe_m) for (a) NaCl, (b) $CaCl_2$ and (c) $MgSO_4$ in the presence of a magnetic field compared to the value in the absence of a field.

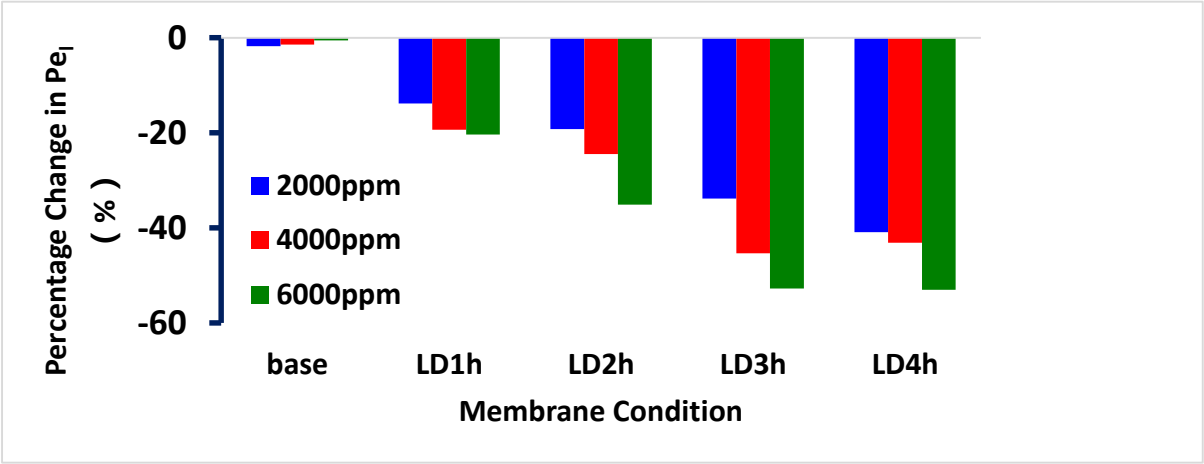

(a) NaCl

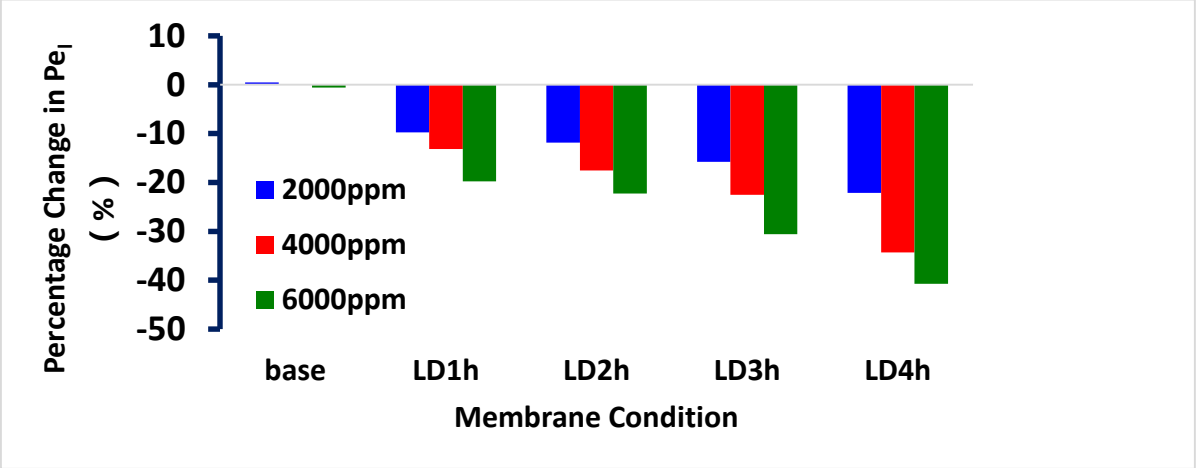

(b) $CaCl_2$

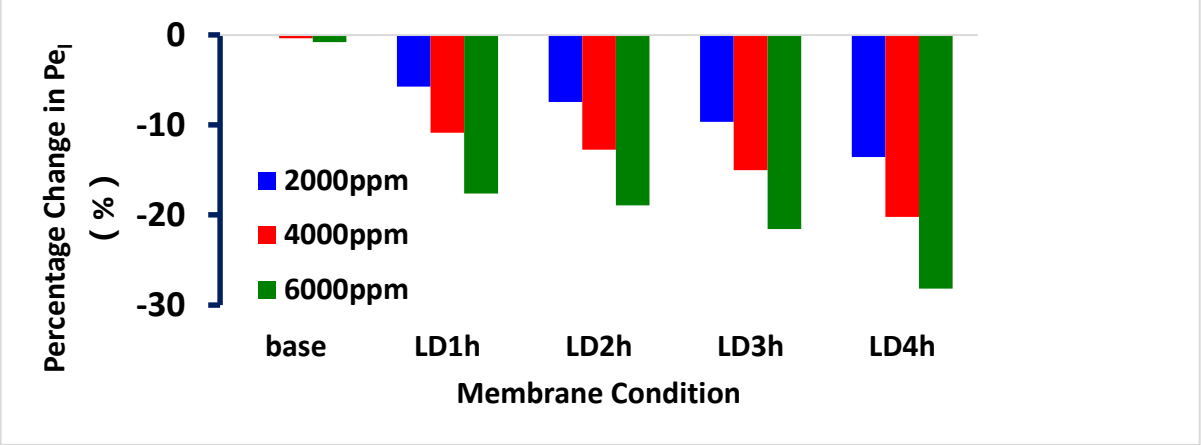

(c) $MgSO_4$

Figure 3.13 (2) Percentage change in the concentration boundary layer Peclet number (Pe_l) for (a) NaCl, (b) $CaCl_2$ and (c) $MgSO_4$ in the presence of a magnetic field compared to the value in the absence of a field.

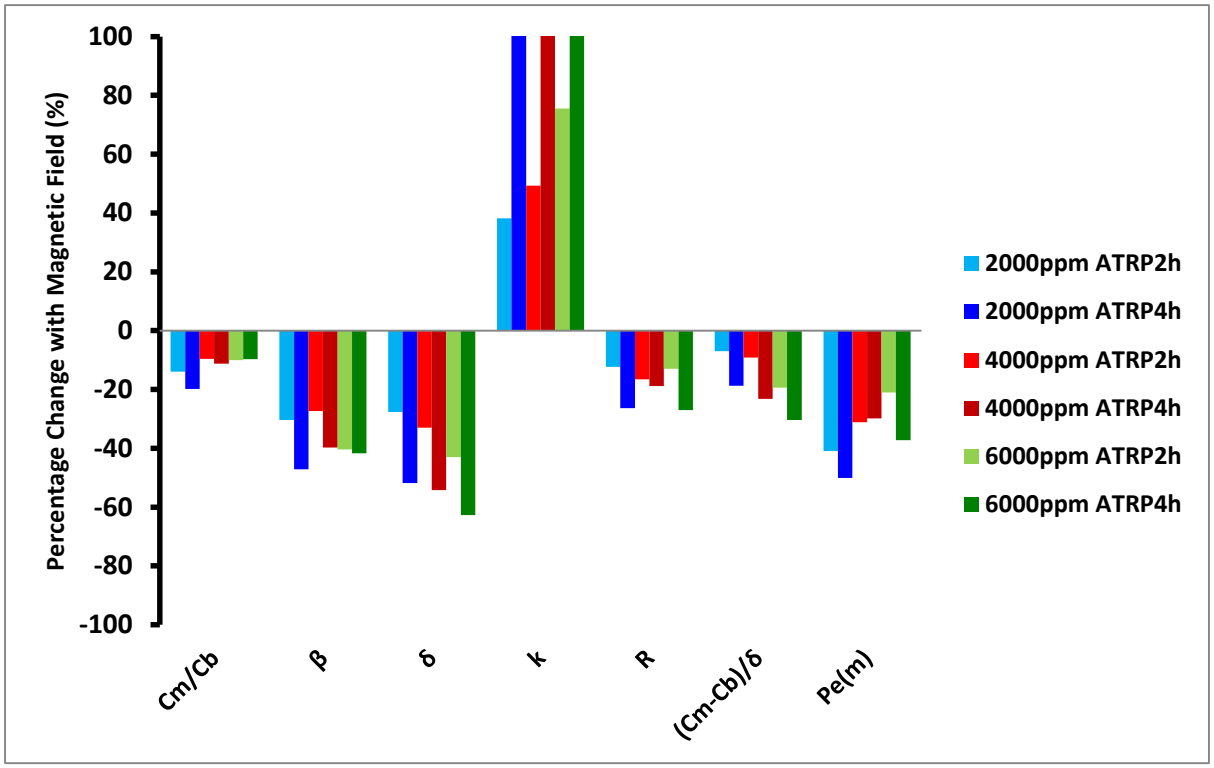

Figure 3.14 Percentage change of different parameters for NaCl in the presence of a magnetic field compared to the values in the absence of a field.

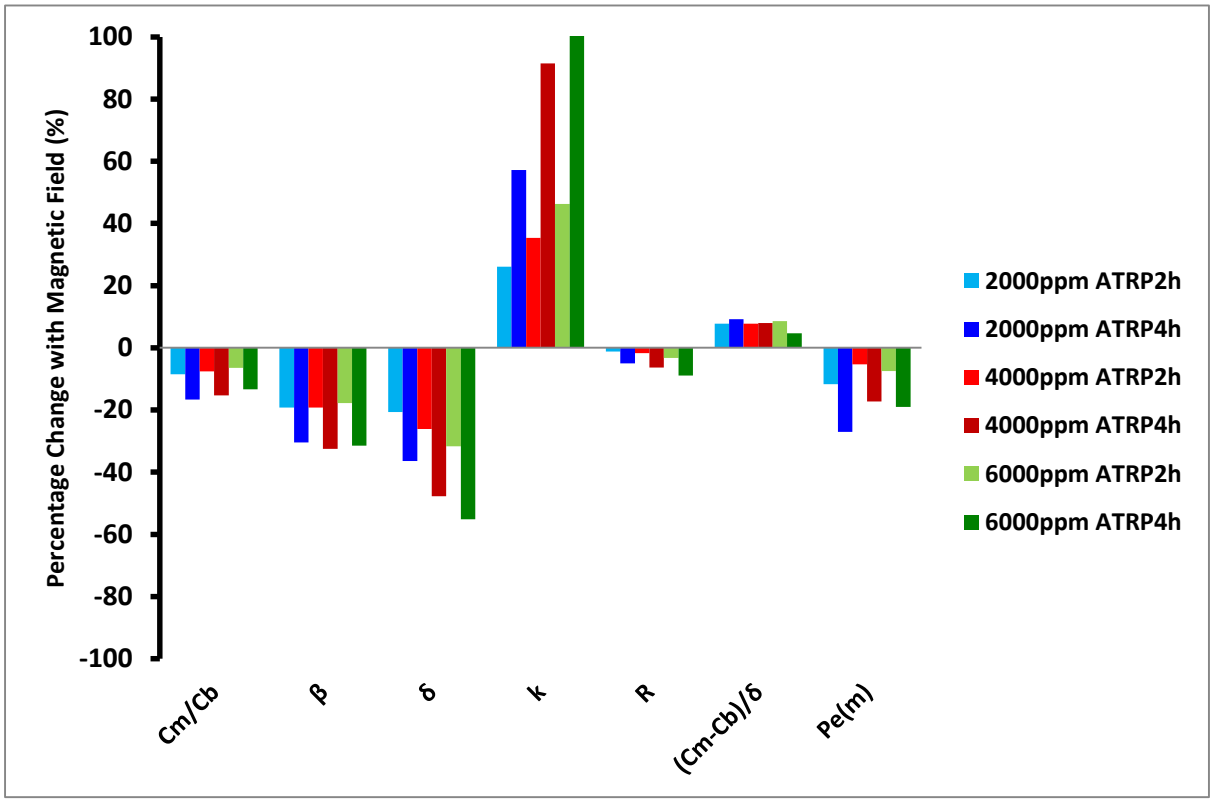

Figure 3.15 Percentage change of different parameters for $CaCl_2$ in the presence of a magnetic field compared to the values in the absence of a field.

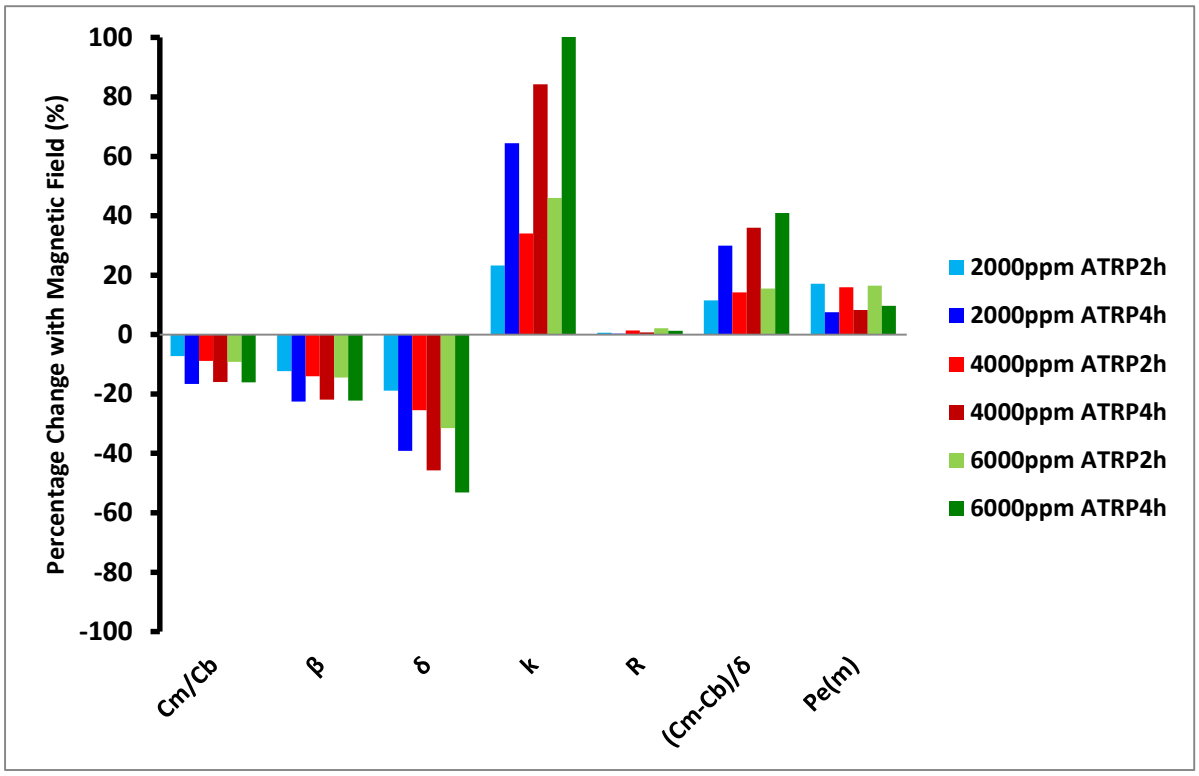

Figure 3.16 Percentage change of different parameters for $MgSO_4$ in the presence of a magnetic field compared to the values in the absence of a field.

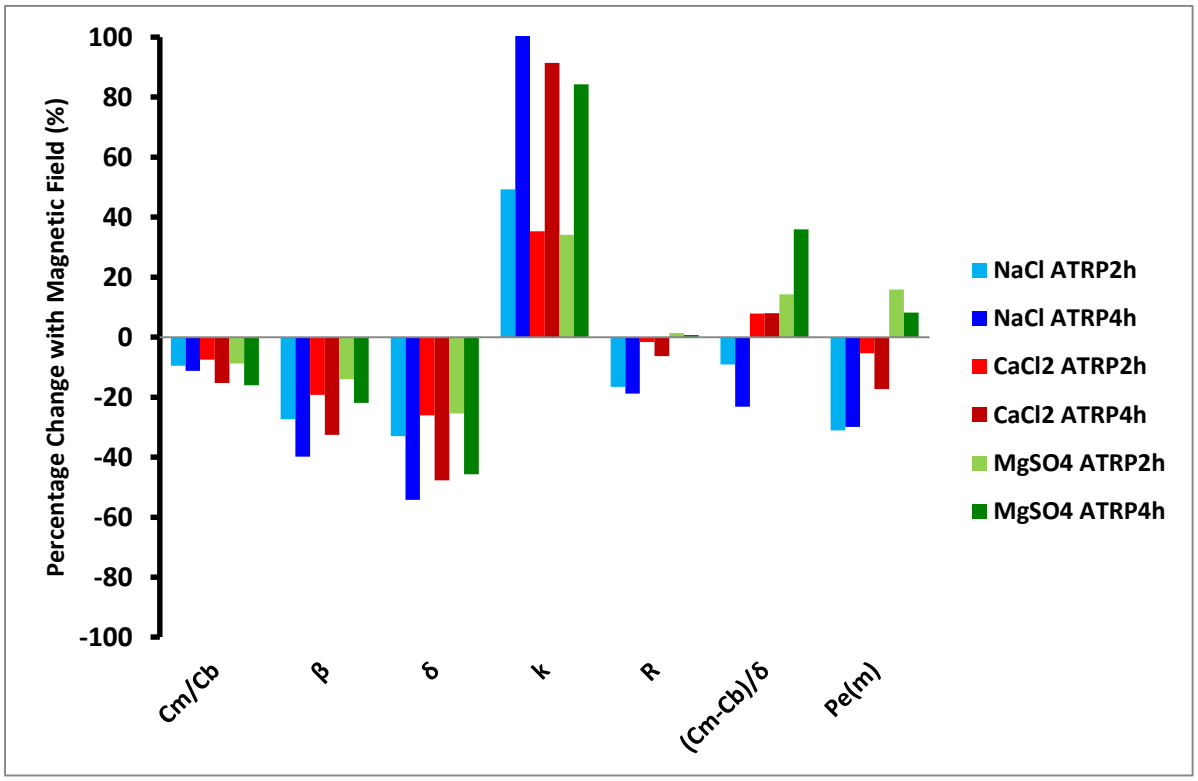

Figure 3.17 Percentage change of different parameters for each 4000 ppm salt solution in the presence of a magnetic field compared to the values in the absence of a field.

The intrinsic rejection (R) depends on the ratio of salt concentration in the permeate to that immediately above the upstream membrane surface. Therefore, R is affected by solute transport within both the concentration boundary layer and the membrane barrier layer. As indicated by Tables 3.6, 3.8 and 3.10, the intrinsic rejection is the highest for $MgSO_4$ and the lowest for NaCl, and decreases with increase in feed salt concentration. Under the same magnetic field condition, the intrinsic rejection slightly increases with increases in ATRP time for $MgSO_4$, but increases during the 1st and decreases during the 2-4th hour of ATRP for both NaCl and $CaCl_2$. Moreover, as shown in Figure 3.11, presence of the oscillating magnetic field decreases the intrinsic rejection of NaCl and $CaCl_2$ but increases that of $MgSO_4$. Therefore, decreases of C_p are more than those of C_m for $MgSO_4$ and vise versa for NaCl in the presence of micro-mixing, with $CaCl_2$ somewhere in between.

Concentration gradient within the concentration boundary layer ($(C_m-C_b)/\delta$) is seldom used for quantifying concentration polarization. However, the concentration gradient helps to better understand concentration polarization when interacting with other variables. Tables 3.6, 3.8 and 3.10 indicate $(C_m-C_b)/\delta$ increases with increases in feed salt concentration but decreases with increases in ATRP time. Variations of $(C_m-C_b)/\delta$ in the presence compared to in the absence of magnetic field are shown in Figure 3.12. Presence of the 20 Hz field reduces $(C_m-C_b)/\delta$ for NaCl but increases that for $CaCl_2$ and $MgSO_4$. Therefore, for the functionalized membranes in the presence compared to absence of an oscillating magnetic field, decreases in concentration polarization for NaCl are mainly due to decreased surface concentration, but those for $CaCl_2$ and $MgSO_4$ are mainly due to decreased concentration boundary layer thickness.

Peclet numbers of the membrane layer (Pe_m) are given in Tables 3.6, 3.8 and 3.10. The transport of 2000 ppm NaCl and 2000 ppm $CaCl_2$ across the base and ATRP=1 and 2 h membranes are mostly convective. Diffusive transport dominates NaCl and $CaCl_2$ with 4000 and 6000 ppm concentrations going across the base and ATRP=1-4 h membranes. As indicated by the Pe_m values in Table 3.10, diffusive transport dominates $MgSO_4$ with all the investigated concentrations going across the base and the functionalized membranes with each ATRP time length. With increases in the membrane's ATRP time, transition from convective to diffusive transport across membranes with thicker and denser barrier layers are same as theoretically expected.[66] In addition, percentage of diffusive transport increases with increases in ion valence therefore decreases in ion mobility due to increases in ionic hydration free energy. Therefore, NF membrane removes almost all trivalent and most divalent but few monovalent ions, and salt rejection under the same magnetic field condition increases with increase in ATRP time.[12, 14, 23] Moreover, Pe_m decreases with increases in feed salt concentration due to an increased diffusive transport under an increased cross-membrane concentration gradient, together with a decreased convective transport under a decreased J_v brought by an increased osmotic pressure difference.[4, 12] Percentage changes of Pe_m in the presence compared to in the absence of external magnetic field are given by Figure 3.13 (1). The oscillating magnetic field exerts less effect on Pe_m for the base compared to functionalized membranes. Presence of the oscillating magnetic field decreases the Pe_m more evidently for NaCl compared to $CaCl_2$, but increases the Pe_m of $MgSO_4$. Therefore, presence of micro-mixing decreases the percentage of dominate transport mechanism for each salt across the membrane barrier layer.

The Peclet number of concentration boundary layer (Pe_l) quantifies the ratio of

convective to diffusive transport rate above the upstream NF membrane surface.[4, 30, 32] As theoretically defined, the value of Pe_l is the ratio of solute mass transfer coefficient to permeate flow velocity.[4, 30, 32] According to Murthy and Chaudhari, there is a balance between the convective solute transport towards the membrane and the diffusive solute transport away from the membrane. In case of a high Pe_l value, the value of C_m/C_b would increase to significantly higher than 1 since convective solute flow towards the membrane could be difficult to be balanced by solute diffusion away from the membrane. On the other hand, C_m/C_b gets closer to 1 with decreases in Pe_l value, indicating a stronger capacity of solute diffusion away from the membrane to balance the convective solute flow towards the membrane.[32] As indicated in Tables 3.6, 3.8 and 3.10, the values of Pe_l are greater than Pe_m under the same condition, indicating a greater role of convective solute flow in the liquid compared to the membrane barrier layer. Due to a decreased convective flow towards the membrane surface under a decreased permeate flux, Pe_l decreases with increases in the membrane's ATRP time and the feed salt concentration.[4, 32] The Pe_l values for different salts are quite similar under the same feed concentration and magnetic field condition, but somehow increases with increases in rejection and decreases in the diffusivity of solute. Therefore, within the concentration boundary layer, convective transport has more influence on the salts with higher rejection and lower diffusivity. Despite an increased permeate flow velocity, Figure 3.13 (2) indicates Pe_l decreases in the presence compared to absence of external oscillating field due to an increased solute movement away from the membrane in the presence of micro-mixing. Polymer chain length and feed salt concentration both dominate the effect of oscillating magnetic field on Pe_l.

Figures 3.14-3.17 indicate micro-mixing generated by the external oscillating field

increases the solute mass transfer coefficient within the concentration boundary layer, therefore decreases C_m/C_b, β and δ. In addition, Figures 3.14-3.17 show the interaction between the decreased concentration polarization and the variations of R, $(C_m-C_b)/\delta$ and Pe_m in the presence compared to in the absence of an external oscillating field. Variations in intrinsic rejection (R), concentration gradient ($(C_m-C_b)/\delta$) and membrane Peclet number (Pe_m) work together to elucidate the effects of both membrane functionalization and external oscillating field on salt transport. Generally, stronger micro-mixing generated by the membranes with longer polymer chains leads to greater percentage changes in concentration polarization and salt transport. The effect of micro-mixing somehow tends to increase with increases in feed salt concentration. However, within the concentration range of 2000-6000 ppm, salt valency coupled by polymer chain length dominate the effect of external field to salt transport and concentration polarization.

As indicated by Figure 3.17, decreases in C_m/C_b, β and δ and increases in k are generally similar among different salts. Decreases in R, $(C_m-C_b)/\delta$ and Pe_m are the most evident for NaCl, while increases in $(C_m-C_b)/\delta$ and Pe_m are the most evident for $MgSO_4$. For $CaCl_2$, there are evident decreases in Pe_m and R but observable increases in $(C_m-C_b)/\delta$. Figure 3.17 indicates the surface concentration of low valence and high mobility salts are more prone to the hydrodynamic conditions above the membrane surface. In the presence of micro-mixing, decreases in δ, $(C_m-C_b)/\delta$ and C_m/C_b for NaCl simultaneously indicate the instantaneous redistribution of the low rejection and high mobility salts in the feed. For $MgSO_4$, increase in $(C_m-C_b)/\delta$ accompanies decrease in δ and C_m/C_b in the presence compared to in the absence of magnegic field. This indicates for the high valency salts with low mobility and high rejection,[82] the dominating effect of micro-mixing is in a decreased δ therefore the increased salt mobility

from membrane surface into bulk feed.

Figure 3.17 also indicates decreases in Pe_m for NaCl in the presence of an external field are mainly brought by a decreased convective transport under a significantly decreased surface concentration while slightly increased permeate flux. A decreased concentration gradient within the membrane layer for the low rejection and high mobility salts plays a significant role in an increased R_o. On the other hand, the slight increases in Pe_m for $MgSO_4$ indicates an increased salt back diffusivity away from membrane surface leading to a decreased C_m/C_b value somehow helps to reduce the diffusive transport in membrane barrier layer.[4] An increased back diffusivity of low mobility and high rejection solutes from upstream membrane surface into the bulk feed plays dominating role in enhancing J_v by decreasing the osmotic pressure difference.

3.5.4 Total Cross-membrane Salt Transport Rate

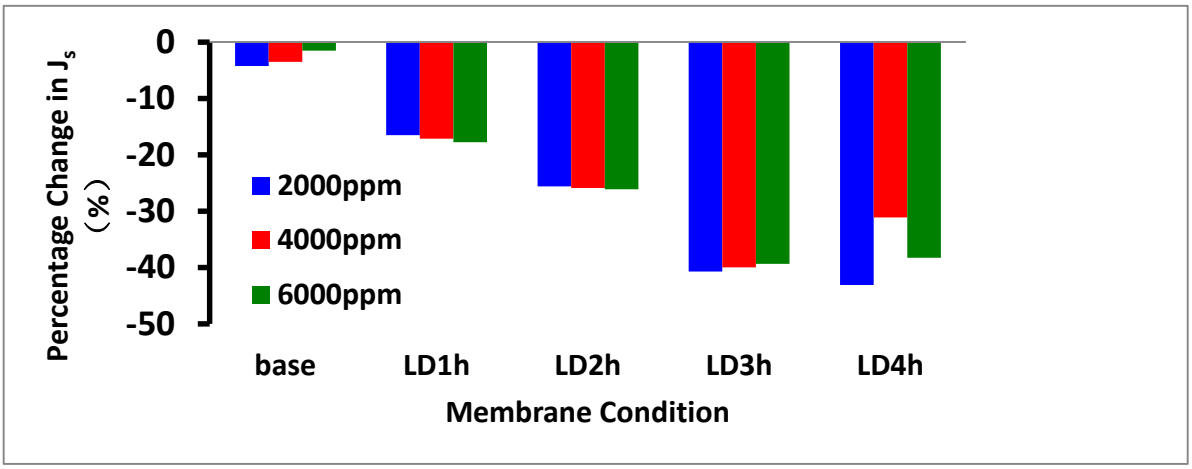

(a) NaCl

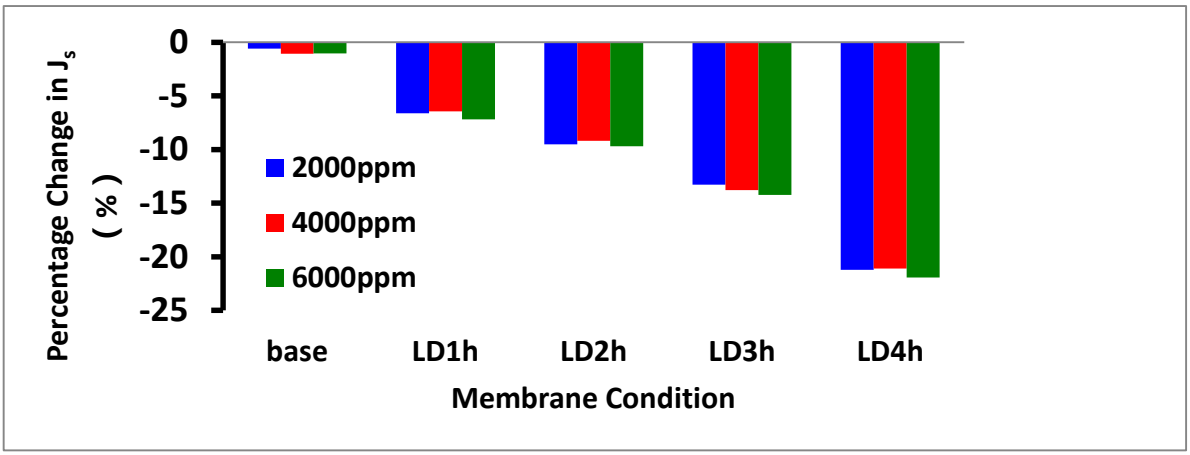

(b) $CaCl_2$

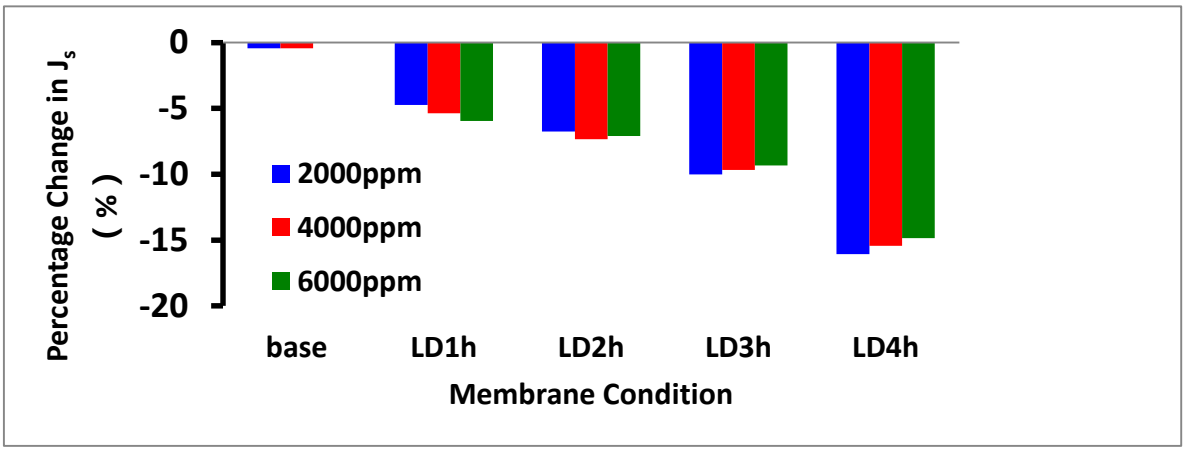

(c) $MgSO_4$

Figure 3.18 Percentage change in the overall cross-membrane salt transport rate (J_s) for (a) NaCl, (b) $CaCl_2$ and (c) $MgSO_4$ in the presence of a magnetic field compared to the value in the absence of a field.

The total salt transport rate across the NF membrane layer (J_s) includes both convective and diffusive transport. As indicated by Tables 3.5, 3.7 and 3.9, J_s decreases with decreases in the diffusivity and increases in the rejection of salt, and J_s decreases with increases in membrane's ATRP time due to increases in membrane layer resistance. In addition, J_s increases with the feed salt concentration due to an increased concentration gradient within the membrane layer.

The percentage changes of J_s in the presence compared to absence of field are given by Figure 3.18. Since the base NF270 membranes are unable to generate micro-mixing, the oscillating field effects on J_s are minor and irregular for the base compared to the functionalized membranes. On the other hand, each functionalized membrane demonstrate universal decreases of J_s in the presence compared to in the absence of an oscillating magnetic field since micro-mixing decreases surface concentration of solute. Compared to salt concentration, the effect of external oscillating field on J_s depends more on polymer chain length and salt diffusivity. Decreases of J_s are the most evident for NaCl, the salt with the highest diffusivity and the lowest reflection coefficient. For each salt investigated, stronger micro-mixing generated by the membranes functionalized with longer polymer chains brings about a greater J_s decreases.

Therefore, as theoretically expected, the effect of external oscillating field on the reduction of cross-membrane salt transport is more evident under a stronger micro-mixing generated by longer polymer chains on the membrane surface. Moreover, the effect of micro-mixing on the percentage decreases of J_s is expected to be more evident for the salts with higher diffusivity and lower rejection. Improvements in the selectivity of functionalized micro-mixing NF membranes in the presence compared to in the absence of an external oscillating field is

indicated by an increased J_v accompanying a decreased J_s.

3.6 Conclusions

Mathematical models have been successfully applied to investigate concentration polarization and ion transport during the self-cleaning micro-mixing NF membrane processes. Several extensively used NF membrane transport models have worked together to quantify concentration polarization and ion transport that are both unavailable from experimental measurements. The modeling was run by correlating membrane performances to the physical properties of membranes and the dynamical characteristics of ions. Through comparison of concentration polarization and ion transport in the presence compared to in the absence of an external oscillating magnetic field, the combined effect of membrane functionalization and micro-mixing has been theoretically investigated.

In the presence compared to absence of an external oscillating magnetic field, decreases of concentration polarization and cross-membrane salt transport are both observed for each salt solution going through LD functionalized membranes with 1-4 hours of ATRP. Due to a stronger micro-mixing generated by the movements of longer polymer chains on the membrane surface, there observes stronger effects of the oscillating magnetic field for membranes functionalized with longer ATRP time. Since the base membranes are unable to generate micro-mixing, the effect of external oscillating field on the base membranes are both minor and irregular compared to the functionalized membranes. Besides polymer chain length, the effect of external oscillating magnetic field on concentration polarization and salt transport also depends on the valence and somehow on the feed concentration of salt.

For the higher valence ions with typically higher hydration free energy, the mode of transport changes from convective to diffusive. The same change in transport mechanism also takes place when the ions are going through thicker and denser membranes with longer polymer chains that are functionalized with a longer ATRP time. Therefore, salt rejection by the NF membranes increases with increases in either the salt's valence or the membrane's ATRP hours.

The dominating effect of micro-mixing for the low rejection and high mobility salts is in the decreased surface concentration due to the instant redistribution of ions in the feed, and that for high rejection and low mobility salt is in an increased effective operation pressure due to the enhanced movement of rejected salt from the membrane surface back into the bulk feed.

For the functionalized membranes, the universal decreases of concentration polarization in the presence compared to absence of micro-mixing is mainly due to an enhanced solute mass transfer coefficient within the concentration boundary layer, facilitating the transport of rejected salts away from the membrane surface. The effect of micro-mixing in the decreases of concentration polarization is helpful with improvements in the productivity and selectivity of NF membranes.

References

1. Fane, A. G. F. I. S. D. W. G., *Nanofiltration: Principles and Applications*. Elsevier Advanced Technology: Australia, 2004.

2. **Mulder, M.**, ***Basic Principle of Membrane Technology***. 2 ed.; **Enschede: Kluwer Academic Publishers**: **Netherlands**, 1996.

3. Deon, S.; Dutournie, P.; Fievet, P.; Limousy, L.; Bourseau, P., Concentration polarization phenomenon during the nanofiltration of multi-ionic solutions: Influence of the filtrated solution and operating conditions. *Water Research* **2013,** *47* (7), 2260-2272.

4. Bhattacharya, S.; Hwang, S. T., Concentration polarization, separation factor, and Peclet number in membrane processes. *Journal of Membrane Science* **1997,** *132* (1), 73-90.

5. Khalaf, T. Y., Effect of feed temperature on concentration polarization and efficiency of reverse osmosis systems. In ***The 1st Regional Conference of Eng. Sci. NUCEJ Spatial ISSUE***, 2008; Vol. 11, pp 145-152.

6. Himstedt, H. H.; Yang, Q.; Dasi, L. P.; Qian, X.; Wickramasinghe, S. R.; Ulbricht, M., Magnetically Activated Micromixers for Separation Membranes. *Langmuir* **2011,** *27* (9), 5574-5581.

7. Yang, Q.; Himstedt, H. H.; Ulbricht, M.; Qian, X.; Wickramasinghe, S. R., Designing magnetic field responsive nanofiltration membranes. *Journal of Membrane Science* **2013,** *430*, 70-78.

8. Cot, S. N. D. A. D. K. D., *Intrinsic properties and performances of NF270 and XLE membranes for water purification*. *Water Science&Technology: Water Supply* **2011,** *11* (2), 186-193.

9. Himstedt, H. H. Novel Fouling Resistant Magnetically-Responsive Membranes for Treatment of Impaired Water. Department of Chemical and Biological Engineering, Colorado State University, Fort Collins, CO, 2012.

10. Bowen, W. R.; Welfoot, J. S., Predictive modeling of nanofiltration: membrane specification and process optimisation. *Desalination* **2002,** *147* (1-3), 197-203.

11. Coronell, O.; Mi, B.; Marinas, B. J.; Cahill, D. G., Modeling the Effect of Charge Density in the Active Layers of Reverse Osmosis and Nanofiltration Membranes on the Rejection of Arsenic(III) and Potassium Iodide. *Environmental Science & Technology* **2013,** *47* (1), 420-428.

12. Kelewou, H.; Lhassani, A.; Merzouki, M.; Drogui, P.; Sellamuthu, B., Salts retention by nanofiltration membranes: Physicochemical and hydrodynamic approaches and modeling. *Desalination* **2011,** *277* (1-3), 106-112.

13. Welfoot, J. S., Predictive modeling of nanofiltration: membrane specification and process optimisation. Bowen, W. R., Ed. Desalination: 2002.

14. Fierro, D.; Boschetti-de-Fierro, A.; Abetz, V., The solution-diffusion with imperfections model as a method to understand organic solvent nanofiltration of multicomponent systems. *Journal of Membrane Science* **2012,** *413*, 91-101.

15. Geens, J.; Van der Bruggen, B.; Vandecasteele, C., Transport model for solvent permeation through nanofiltration membranes. *Separation and Purification Technology* **2006,** *48* (3), 255-263.

16. Otero, J. A.; Mazarrasa, O.; Villasante, J.; Silva, V.; Pradanos, P.; Calvo, J. I.; Hernandez, A., Three independent ways to obtain information on pore size distributions of nanofiltration membranes. *Journal of Membrane Science* **2008,** *309* (1-2), 17-27.

17. Tu, C.-H.; Fang, Y.-Y.; Wang, X.-L., Analysis of transmembrane electrical potential across nanofiltration membranes based on electrostatic and steric-hindrance model. *Desalination and Water Treatment* **2011,** *36* (1-3), 152-163.

18. Lee, S.; Amy, G.; Cho, J., Applicability of Sherwood correlations for natural organic matter (NOM) transport in nanofiltration (NF) membranes. *Journal of Membrane Science* **2004,** *240* (1-2), 49-65.

19. Ho, W. S. W.; Sirkar, K. K., Membrane Handbook. Springler: 1992.

20. Kedem, O.; Leaf, A., RELATION BETWEEN SALT AND IONIC TRANSPORT COEFFICIENTS. *Journal of General Physiology* **1966,** *49* (4), 655-&.

21. Bason, S.; Kedem, O.; Freger, V., Determination of concentration-dependent transport coefficients in nanofiltration: Experimental evaluation of coefficients. *Journal of Membrane Science* **2009,** *326* (1), 197-204.

22. Garba, Y.; Taha, S.; Gondrexon, N.; Dorange, G., Ion transport modeling through nanofiltration membranes. *Journal of Membrane Science* **1999,** *160* (2), 187-200.

23. Fang, J.; Deng, B., Rejection and modeling of arsenate by nanofiltration: Contributions of convection, diffusion and electromigration to arsenic transport. *Journal of Membrane Science* **2014,** *453*, 42-51.

24. Xiao, H.; Hefei, Z.; Ruijin, Y.; Wenbing, Z.; Wei, Z., Coupled model of extended Nernst-Planck equation and film theory in nanofiltration for xylo-oligosaccharide syrup. *Journal of Food Engineering* **2010,** *100* (2), 302-9.

25. Sharma, R. R.; Chellam, S., Temperature and concentration effects on electrolyte transport across porous thin-film composite nanofiltration membranes: Pore transport mechanisms and energetics of permeation. *Journal of Colloid and Interface Science* **2006,** *298* (1), 327-340.

26. Zydney, A. L., Stagnant film model for concentration polarization in membrane systems. *Journal of Membrane Science* **1997,** *130* (1-2), 275-281.

27. Jae-Hong, K.; Hoon, H., A mechanistic study on boron rejection by sea water reverse osmosis membranes. *Journal of Membrane Science* **2006,** *286* (1-2), 269-78.

28. Chaabane, T.; Taha, S.; Ahmed, M. T.; Maachi, R.; Dorange, G., Coupled model of film theory and the Nernst-Planck equation in nanofiltration. *Desalination* **2007,** *206* (1-3), 424-432.

29. Murthy, Z. V. P.; Gupta, S. K., Estimation of mass transfer coefficient using a combined nonlinear membrane transport and film theory model. *Desalination* **1997,** *109* (1), 39-49.

30. Nagy, E.; Kulcsar, E.; Nagy, A., Membrane mass transport by nanofiltration: Coupled effect of the polarization and membrane layers. *Journal of Membrane Science* **2011,** *368* (1-2), 215-22.

31. Murthy, Z. V. P.; Chaudhari, L. B., Rejection behavior of nickel ions from synthetic wastewater containing Na(2)SO(4), NiSO(4), MgCl(2) and CaCl(2) salts by nanofiltration and characterization of the membrane. *Desalination* **2009,** *247* (1-3), 610-622.

32. Murthy, Z. V. R.; Chaudhari, L. B., Application of nanofiltration for the rejection of nickel ions from aqueous solutions and estimation of membrane transport parameters. *Journal of Hazardous Materials* **2008,** *160* (1), 70-77.

33. Gupta, V. K.; Hwang, S.-T.; Krantz, W. B.; Greenberg, A. R., Characterization of nanofiltration and reverse osmosis membrane performance for aqueous salt solutions using irreversible thermodynamics. *Desalination* **2007,** *208* (1-3), 1-18.

34. Mohammad, A. W.; Hilal, N.; Al-Zoubi, H.; Darwish, N. A., Prediction of permeate fluxes and rejections of highly concentrated salts in nanofiltration membranes. *Journal of Membrane Science* **2007,** *289* (1-2), 40-50.

35. Szymczyk, A.; Fievet, P., Investigating transport properties of nanofiltration membranes by means of a steric, electric and dielectric exclusion model. *Journal of Membrane Science* **2005,** *252* (1-2), 77-88.

36. Darvishmanesh, S.; Vanneste, J.; Tocci, E.; Jansen, J.; Tasseli, F.; Degreve, J.; Drioli, E.; Van der Bruggen, B., Physicochemical Characterization of Solute Retention in Solvent Resistant Nanofiltration: the Effect of Solute Size, Polarity, Dipole Moment, and Solubility Parameter. *Journal of Physical Chemistry B* **2011,** *115* (49), 14507-14517.

37. Nam, J.-W.; Park, J.-Y.; Kim, J.-H.; Kwon, S.; Chon, K.; Lee, E.-J.; Kim, H.-S.; Jang, A., The evaluation on concentration polarization for effective monitoring of membrane fouling in seawater reverse osmosis membrane system. *Journal of Industrial and Engineering Chemistry* **2014,** *20* (4), 2354-2358.

38. Bowen, R.; Mohammad, W., Nidal, Characterisation of nanofiltration membranes for predictive purposes - use of salts, uncharged solutes and atomic force microscopy. *Journal of Membrane Science* **1997,** *126* (1), 91-105.

39. Bandini, S.; Vezzani, D., Nanofiltration modeling: the role of dielectric exclusion in membrane characterization. *Chemical Engineering Science* **2003,** *58* (15), 3303-3326.

40. Ghiu, S. M. S.; Carnahan, R. P.; Barger, M., Mass transfer in RO TFC membranes - dependence on the salt physical and thermodynamic parameters. *Desalination* **2003,** *157* (1-3), 385-393; Gupta, V. K. *Experimental and theoretical studies in reverse osmosis and nanofiltration*. University of Cincinnati, Cincinnati, 2003.

41. Partanen, J.; Minkkinen, P., Activity and osmotic coefficients of dilute sodium chloride solutions at 273 K. *Journal of Chemical & Engineering Data* **1991,** *36* (4), 432-435.

42. Staples, B.; Nuttall, R., The activity and osmotic coefficients of aqueous calcium chloride at 298.15 K. *Journal of Physical and Chemical Reference Data* **1977,** *6* (385), 385-407.

43. Archer, D. G.; Rard, J. A., Isopiestic investigation of the osmotic and activity coefficients of aqueous MgSO4 and the solubility of MgSO4 center dot 7H(2)O(cr) at 298.15 K: Thermodynamic properties of the MgSO4+H2O system to 440 K. *Journal of Chemical and Engineering Data* **1998,** *43* (5), 791-806.

44. Hamer, W.; Wu, Y.-C., Osmotic Coefficients and Mean Activity Coefficients of Uni-univalent Electrolytes in Water at 25°C. *Journal of Physical and Chemical Reference Data* **1972,** *1* (4), 1047-1099.

45. Yaroshchuk, A.; Martinez-Llado, X.; Llenas, L.; Rovira, M.; de Pablo, J.; Flores, J.; Rubio, P., Mechanisms of transfer of ionic solutes through composite polymer nano-filtration membranes in view of their high sulfate/chloride selectivities. *Desalination and Water Treatment* **2009,** *6* (1-3), 48-53.

46. Park, N.; Cho, J.; Hong, S.; Lee, S., Ion transport characteristics in nanofiltration membranes: measurements and mechanisms. *Journal of Water Supply Research and Technology-Aqua* **2010,** *59* (2-3), 179-190.

47. Lei, J. Biofouling-resistant polymer hydrogel coating for desalination membranes. Universität Duisburg-Essen, Essen, Germany, 2012.

48. Kongshuang, Z.; Yuhong, L., Dielectric characterization of a nanofiltration membrane in electrolyte solutions: its double-layer structure and ion permeation. *Journal of Physical Chemistry B* **2006,** *110* (6), 2755-63.

49. Yaroshchuk, A. E., Optimal charged membranes for the pressure-driven separations of ions of different mobilities: theoretical analysis. *Journal of Membrane Science* **2000,** *167* (2), 149-161.

50. Hagmeyer, G.; Gimbel, R., Modeling the salt rejection of nanofiltration membranes for ternary ion mixtures and for single salts at different pH values. *Desalination* **1998,** *117* (1-3), 247-256.

51. Lefebvre, X.; Palmeri, J.; David, P., Nanofiltration theory: An analytic approach for single salts. *Journal of Physical Chemistry B* **2004,** *108* (43), 16811-16824.

52. Chang, K.-T.; Weng, C.-I., The effect of an external magnetic field on the structure of liquid water using molecular dynamics simulation. *Journal of Applied Physics* **2006,** *100* (4).

53. Cussler, E. L., *Diffusion, Mass Transfer in Fluid Systems*. 2nd Edition ed.; 1997.

54. Hussain, A. A.; Abashar, M. E. E.; Al-Mutaz, I. S., Influence of ion size on the prediction of nanofiltration membrane systems. *Desalination* **2007,** *214* (1-3), 150-166.

55. Hussain, A. A.; Nataraj, S. K.; Abashar, M. E. E.; Al-Mutazb, I. S.; Aminabhavi, T. M., Prediction of physical properties of nanofiltration membranes using experiment and theoretical models. *Journal of Membrane Science* **2008,** *310* (1-2), 321-336.

56. Chellam, S.; Taylor, J. S., Simplified analysis of contaminant rejection during ground- and surface water nanofiltration under the information collection rule. *Water Research* **2001,** *35* (10), 2460-2474.

57. Seidel, A.; Waypa, J. J.; Elimelech, M., Role of charge (Donnan) exclusion in removal of arsenic from water by a negatively charged porous nanofiltration membrane. *Environmental Engineering Science* **2001,** *18* (2), 105-113.

58. Vezzani, D.; Bandini, S., Donnan equilibrium and dielectric exclusion for characterization of nanofiltration membranes. *Desalination* **2002,** *149* (1-3), 477-483.

59. Ghaee, M. M. Z. S.-N. J. H. S., Mathematical Modeling of Nanofiltration-based Deionization from Aqueous Solutions. *International Journal of Nanoscience and Nanotechnology* **2013,** *9* (3), 163-172.

60. Hilal, N.; Al-Zoubi, H.; Mohammad, A. W.; Darwish, N. A., Nanofiltration of highly concentrated salt solutions up to seawater salinity. *Desalination* **2005,** *184* (1-3), 315-326.

61. Kuyucak, S.; Andersen, O. S.; Chung, S. H., Models of permeation in ion channels. *Reports on Progress in Physics* **2001,** *64* (11), 1427-1472.

62. Kumaran, M.; Bajpai, S., Application of Extended Nernst Planck Model in Nano Filtration Process –A Critical Review. *International Journal of Engineering Research and Reviews* **2015,** *3* (3), 40-49.

63. Ballet, G. T.; Gzara, L.; Hafiane, A.; Dhahbi, M., Transport coefficients cadmium salt rejection in nanofiltration membrane. *Desalination* **2004,** *167* (1-3), 369-376.

64. Koter, S., Determination of the parameters of the Spiegler-Kedem-Katchalsky model for nanofiltration of single electrolyte solutions. *Desalination* **2006,** *198* (1-3), 335-345; Mehiguene, K.; Garba, Y.; Taha, S.; Gondrexon, N.; Dorange, G., Influence of operating conditions on the retention of copper and cadmium in aqueous solutions by nanofiltration: experimental results and modeling. *Separation and Purification Technology* **1999,** *15* (2), 181-187.

65. Junwen, L.; Kai Yu, W.; Tai-Shung, C., Investigation of amphoteric polybenzimidazole (PBI) nanofiltration hollow fiber membrane for both cation and anions removal. *Journal of Membrane Science* **2008,** *310* (1-2), 557-66.

66. Yoon, Y.; Amy, G.; Cho, J. W.; Her, N.; Pellegrino, J., Transport of perchlorate (ClO4-) through NF and UF membranes. *Desalination* **2002,** *147* (1-3), 11-17.

67. Ben Amar, N.; Saidani, H.; Deratani, A.; Palmeri, J., Effect of temperature on the transport of water and neutral solutes across nanofiltration membranes. *Langmuir* **2007,** *23* (6), 2937-2952.

68. Korson, L.; Drosthan.W; Millero, F. J., VISCOSITY OF WATER AT VARIOUS TEMPERATURES. *Journal of Physical Chemistry* **1969,** *73* (1), 34-&.

69. Freger, V., Swelling and morphology of the skin layer of polyamide composite membranes: An atomic force microscopy study. *Environmental Science & Technology* **2004,** *38* (11), 3168-3175.

70. Eren, B.; Ileri, R.; Dogan, E.; Caglar, N.; Koyuncu, I., Development of artificial neural network for prediction of salt recovery by nanofiltration from textile industry wastewaters. *Desalination and Water Treatment* **2012,** *50* (1-3), 317-328.

71. van der Bruggen, B.; Schaep, J.; Wilms, D.; Vandecasteele, C., A comparison of models to describe the maximal retention of organic molecules in nanofiltration. *Separation Science and Technology* **2000,** *35* (2), 169-182.

72. Waniewski, J., Physiological Interpretation of Solute Transport Parameters for Peritoneal Dialysis. *Journal of Theoretical Medicine* **2001,** *3* (3), 177-190.

73. Zhou, C.; Shi, Y.; Sun, C.; Yu, S.; Liu, M.; Gao, C., Thin-film composite membranes formed by interfacial polymerization with natural material sericin and trimesoyl chloride for nanofiltration. *Journal of Membrane Science* **2014,** *471*, 381-391; Diop, S. N.; Diallo, M. A.; Diawara, C. K.; Cot, D., Intrinsic properties and performances of NF270 and XLE membranes for water filtration. *Water Science and Technology-Water Supply* **2011,** *11* (2), 186-193.

74. Coday, B. D.; Luxbacher, T.; Childress, A. E.; Almaraz, N.; Xu, P.; Cath, T. Y., Indirect determination of zeta potential at high ionic strength: Specific application to semipermeable polymeric membranes. *Journal of Membrane Science* **2015,** *478*, 58-64.

75. Ikeda, T.; Boero, M.; Terakura, K., Hydration properties of magnesium and calcium ions

from constrained first principles molecular dynamics. *Journal of Chemical Physics* **2007,** *127* (7).

76. Tansel, B., Significance of thermodynamic and physical characteristics on permeation of ions during membrane separation: Hydrated radius, hydration free energy and viscous effects. *Separation and Purification Technology* **2012,** *86*, 119-126.

77. Chen, L.; Li, N.; Chai, F.; Cheng, S. K., Comparison on Effect of Oscillating and Stationary Magnetic Field on the Conductivity of NaCl Solutions. *Chemical Engineering and Material Properties, Pts 1 and 2* **2012,** *391-392*, 1095-1099.

78. Lukawska, A.; Jagoo, Z.; Kozlowski, G.; Turgut, Z.; Kosai, H.; Sheets, A.; Bixel, T.; Wheatley, A.; Abdulkin, P.; Knappett, B.; Houlding, T.; Degirmenci, V., AC Magnetic Heating of Superparamagnetic Fe and Co Nanoparticles. *Defect and Diffusion Forum* **2013,** *336*, 159-167.

79. Geraldes, V.; Semiao, V.; de Pinho, M. N., Flow and mass transfer modeling of nanofiltration. *Journal of Membrane Science* **2001,** *191* (1-2), 109-128.

80. Hoek, E. M. V.; Elimelech, M., Cake-enhanced concentration polarization: A new fouling mechanism for salt-rejecting membranes. *Environmental Science & Technology* **2003,** *37* (24), 5581-5588.

81. Park, E.; Barnett, S. M., Oil/water separation using nanofiltration membrane technology. *Separation Science and Technology* **2001,** *36* (7), 1527-1542.

82. Richards, L. A.; Schafer, A. I.; Richards, B. S.; Corry, B., Quantifying barriers to monovalent anion transport in narrow non-polar pores. *Physical Chemistry Chemical Physics* **2012,** *14* (33), 11633-11638.

4. Performance and Anti-fouling Properties of the Magnetically Responsive Micro-mixing Nanofiltration Membranes

4.1 Introduction

Microfiltration (MF), ultrafiltration (UF), nanofiltration (NF) and reverse osmosis (RO) are pressure-driven membrane processes widely used for separations in biotechnology and biopharmaceutical areas as well as for wastewater treatment and desalination. NF membranes are always considered loose RO and dense UF membranes at the same time. NF membranes are mainly used for the removal of small organic molecules and divalent or trivalent salt ions from water.[1] The performance and durability of NF membranes are compromised by membrane fouling due significantly to concentration polarization. Concentration polarization refers to the accumulation of the rejected ions and molecules within the concentration boundary layer immediately above the upstream membrane surface, leading to the formation of a concentration gradient that increases towards the membrane. Membrane fouling is the deposition, precipitation or adsorption of undesired species onto the membrane surface or into the membrane layer.[2] Concentration polarization and membrane fouling reduce the effective operation pressure due to increased osmotic pressure difference across the membrane layer. Membrane fouling also potentially reduces the effective operation area of the membranes. If the rejected ions and molecules accumulate continuously within the concentration boundary layer, the concentration immediately above the upstream membrane surface could exceed their solubility and they immediately crystalize onto the membrane surface leading to fouling.[3]

Extending the prior work from our group, the anti-fouling effects of the magnetically responsive micro-mixing NF membranes are investigated and analyzed in this dissertation.[4] At

first, the hydrophilic poly (2-hydroxyethyl methacrylate (HEMA)) chains were grafted from the membrane surface using ATRP. The SPNs were subsequently conjugated onto the ends of the grafted polymer chains. The applied external oscillating magnetic field exerts a force on the nanoparticles to induce the particles to move at the same frequency as the external field, leading to the movement of the conjugated polymer chains. ATRP is a well-controlled polymerization reaction with low polydispersity. The estimated length of the grafted polymer chains on the membrane surface is around 100-150 nm. Furthermore, nanoparticles with 25 nm in diameter are only conjugated to the ends of the grafted polymer chains. Therefore, movement of the chains serves as micro-mixers within the concentration boundary layer. The induced micro-mixing reduces concentration polarization and membrane fouling by enhancing the transport of rejected species from the membrane surface back into the bulk feed.[4-6]

Chapter 2 and Chapter 3 have investigated the effects of micro-mixing at the membrane-liquid boundary layer on concentration polarization and transport properties of various types of salt ions at different concentrations. It can be seen that micro-mixer is effective in suppressing concentration polarization hence improving the performance of the nanofiltration membranes. Moreover, the effects of micro-mixing is salt type and salt concentration dependent. As is known, membrane fouling is a critical issue in membrane based processes. In particular, fouling from organic molecules or biological species is more rampant compared to the inorganic particles or salts. Membrane fouling significantly affects the productivity and selectivity of membrane as well as reduces the quality of permeate. Therefore, extending our earlier work on the magnetically responsive micro-mixing membranes,[5] one of the major objectives of this research is to obtain more fundamental insights and further develop

the micro-mixing anti-fouling NF membranes. Membranes functionalized with active micro-mixers are expected to suppress concentration polarization and prevent the deposition of undesirable species and therefore are anti-fouling. It is expected to retain a constant flux and rejection for a longer period of time.[4, 5, 7] This chapter focuses on the anti-fouling properties of functionalized membranes using feed streams containing organic species.[2]

Violleau *et al*. reported their investigations on the fouling of commercialized polyamide NF55 membranes using hydrophobic as well as hydrophilic natural organic feed streams.[2] Boussu *et al.* reported their research on the mechanisms of surfactant fouling for the NF membranes.[8] However, so far, there are only very few studies on the fouling of NF membranes. Meanwhile, extensive efforts have recently been devoted to develop anti-fouling NF membranes for many different applications. Earlier investigations of NF membrane fouling focused on the investigations of membrane properties by surface characterizations only. In this chapter, we present our results on the anti-fouling properties of the magnetically responsive micro-mixing NF membranes using feed streams with different organic species.

Chapter 2 describes the transport properties of the magnetically responsive micro-mixing NF membranes with feed streams containing one inorganic salt. Chapter 3 analyzed quantitatively the effects of micro-mixing on concentration polarization based on those experimental data. Here membrane performances with additional feed streams including one organic salt solution of $(CH_3)_3N{\cdot}HCl$ were investigated by up to 3 hours of filtration experiments. The effects of micro-mixing on concentration polarization and membrane transport properties were studied. Finally, the antifouling properties of functionalized

membranes using synthetic oily wastewater were investigated. The model wastewater used here is a mixture of inorganic salt ions, organic molecules and oil emulsions.[9]

Mondal and Wickramasinghe reported their work using the base NF270 membrane to treat produced water from the oil and gas industry. They used field emission scanning electron microscopy (FESEM), XPS, ATR-FTIR and water contact angle to determine the fouling mechanisms of base NF270 during the recovery of oily waste water.[10] More recently, it was shown that the membrane fouling properties of synthetic oily waste water containing NaCl, $CaCl_2$, $MgSO_4$, humic acid and soybean oil are similar to those of the real waste water from the oil and gas industry.[11] The composition of the synthetic oily waste water represents the percentage of oil, salt and organic compounds in the produced water. Therefore, it can be used as a substitute of the real oily waste water to study the fouling of NF membranes when treating the produced water.[12] In reality, there will be large variation in the composition of the actual waste water depending on the origin and sampling time and location. Here, the anti-fouling performance of nanoparticle functionalized membrane during the model oily waste water tests was monitored for over 3 or 6 hour period, and both in the presence and in the absence of an external alternating magnetic field.

From the flux and rejection data of functionalized membranes presented in Chapter 2, it is clear that flux decreases and rejection increases for the functionalized NF270 membranes compared to the base membranes due to the enhanced membrane layer resistance to permeation. However, for each functionalized membrane in the presence of an oscillating magnetic field compared to without an external field, significant improvement in flux and rejection is observed due to the presence of micro-mixing at the membrane-liquid boundary layer.

Moreover, the larger the grafting degree, the greater the flux and rejection improvements. The effects of micro-mixing on concentration polarization are also salt type and salt concentration dependent. The rejection has the greatest improvement for the monovalent salt ions and the flux has a greater improvement for the divalent or trivalent salt ions. LD2h and LD4h membranes have been used for the anti-fouling studies in this chapter.

4.2 Experimental Methods

4.2.1 Membrane Functionalization

Membranes were functionalized following the same protocol as before. Humic acid in fine particles was obtained from VWR (Radnor, PA) with analytical purity, and the soybean oil was purchased from a local supermarket. The organic salt of trimethylamino hydrochloride was supplied by Acros Organics (Thermo Fisher Scientific, NJ) with 98% purity. Synthetic oily waste water was prepared by adding the following compounds into 700-800 mL deionized water (DI water) in this order:[13, 14] 1) 2 mL soybean oil; 2) 1 g NaCl; 3) 1 g $CaCl_2$; 4) 1 g $MgSO_4$; 5) 0.05 g humic acid. At least 10 minutes of stirring was conducted before adding the next compound. Additional DI water was added to keep the final volume at 1L.

4.2.2 Membrane Performance Evaluation

All membrane performance tests were done using the Amicon 8050 filtration cell in the dead end filtration mode. Despite more severe concentration polarization and the membranes are therefore more prone to fouling compared to the tangential flow mode, the dead end filtration mode provides an easily controllable environment. Moreover, in order to clearly

investigate concentration polarization and membrane fouling, all membrane performance tests were done without any stirring. Details about flux tests are described in APPENDIX A2.

Organic and inorganic salt rejections were determined using the conductivity method based on ratio of permeate conductivity to the initial feed conductivity, as described in APPENDIX A3. The alternating magnetic field was generated by alternatively activating the two solenoids placed on the opposite sides of membrane cell. Operation of the alternating magnetic field system is described in APPENDIX A5. Based on our earlier work, a 20 Hz oscillating frequency seems to induce the largest micro-mixing effects.[4] Throughout this work, the frequency of the magnetic field was kept at 20 Hz unless otherwise mentioned.

For both the base and functionalized NF270 membranes, preparation procedures mentioned by APPENDIX A4 were followed before membrane performance tests. Cleaning was required after each membrane performance test. Cleaning after each inorganic and organic salt solution test included feed removal from cell, 1-minute rinsing of the inner cell with DI water, 10-minute DI water flux under constant 45 psig, and finally 2-minute DI water rinsing of the membrane disc in a petri dish. After model oily waste water test, the cleaning procedure included feed removal from cell, DI water rinse of the inner cell for 2 minutes, 0.5 M NaOH flow through the membrane under 45 psig for 1 minute, and finally DI water flux through the membrane under 45 psig for 10 minutes.[11]

The operation pressure was kept constant at 45 psig during each test. The initial feed volume was fixed at the maximal amount of 50 mL. In order to minimize feed concentration change during the filtration experiments, less than 5 g of permeate was drawn at the end of the experiments from a total of 50 mL feed.

4.3 Results and Discussion

4.3.1 500 and 2000 ppm $MgSO_4$ Salt Solutions

Anti-fouling properties of the magnetically activated micro-mixing NF membranes were investigated by performing filtration experiments over a period of 3 hours with the 500 ppm and 2000 ppm $MgSO_4$ feed solutions. This is because divalent salt feed solution tends to have more severe concentration polarization developing at the boundary layer compared to monovalent salt feed solutions.

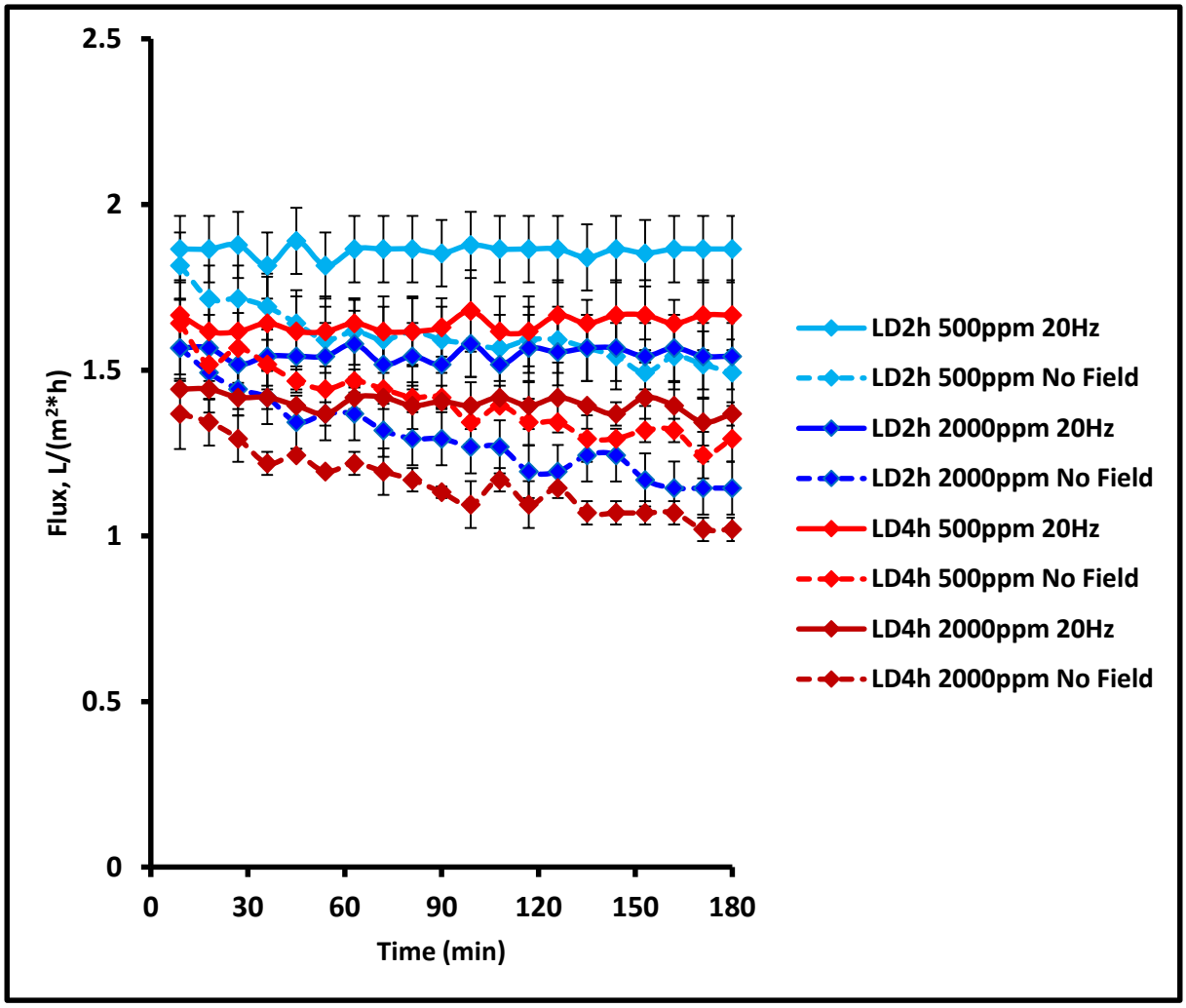

(a) Flux vs. time.

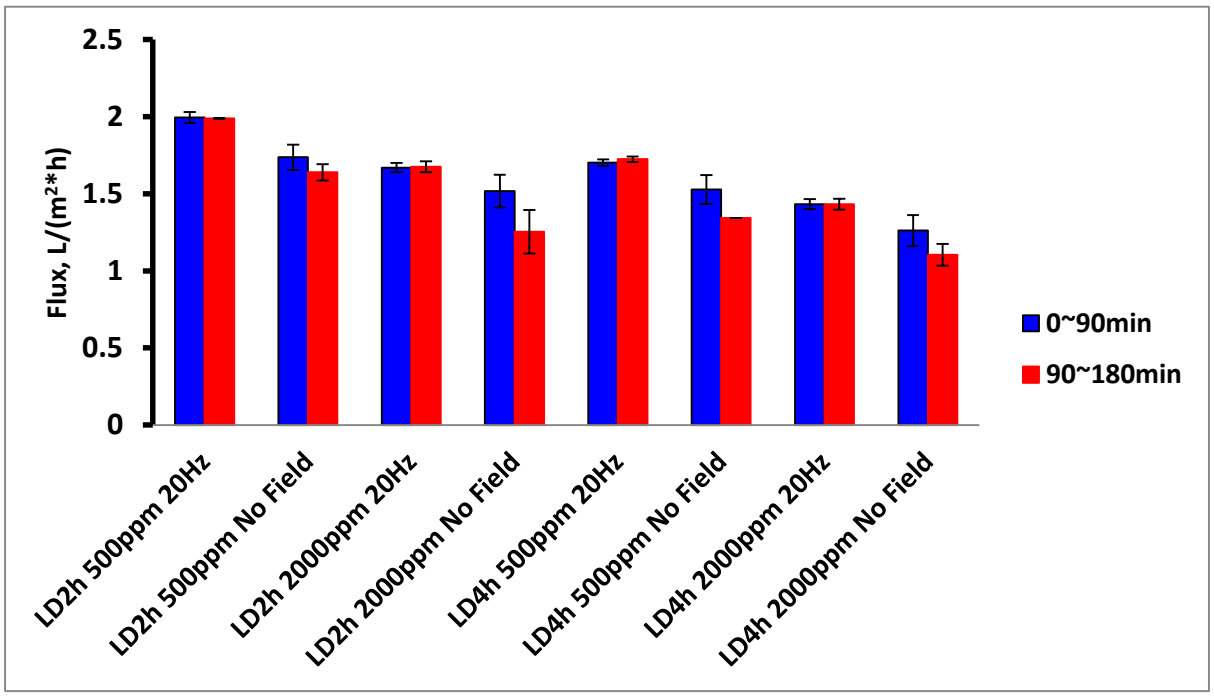

(b) Average fluxes within each 90-minute operation cycle.

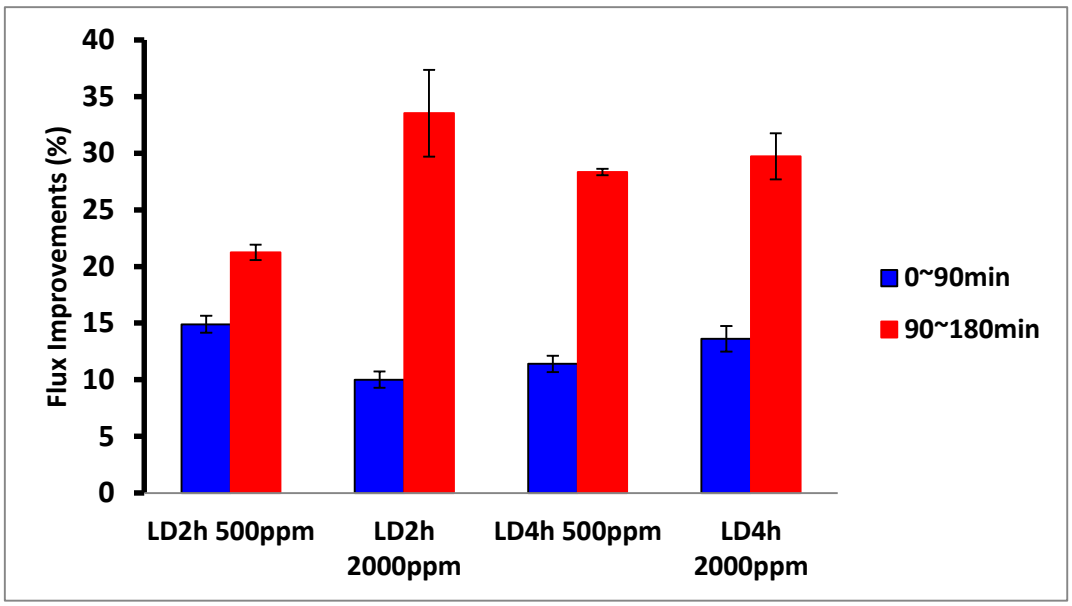

(c) Average flux improvements within each 90-minute operation cycle.

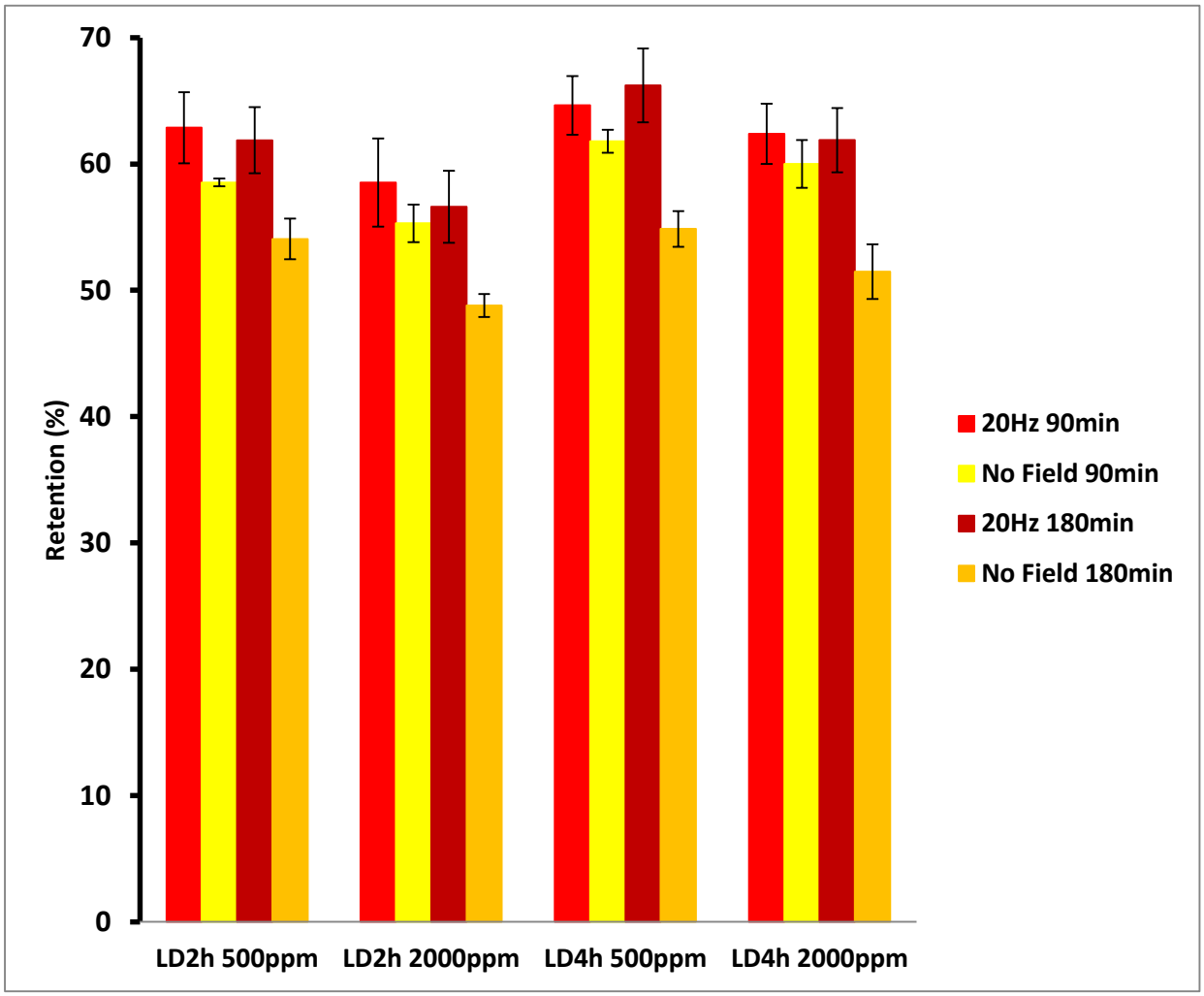

(d) Average rejections within each 90-minute cycle both in the presence and absence of a 20Hz magnetic field.

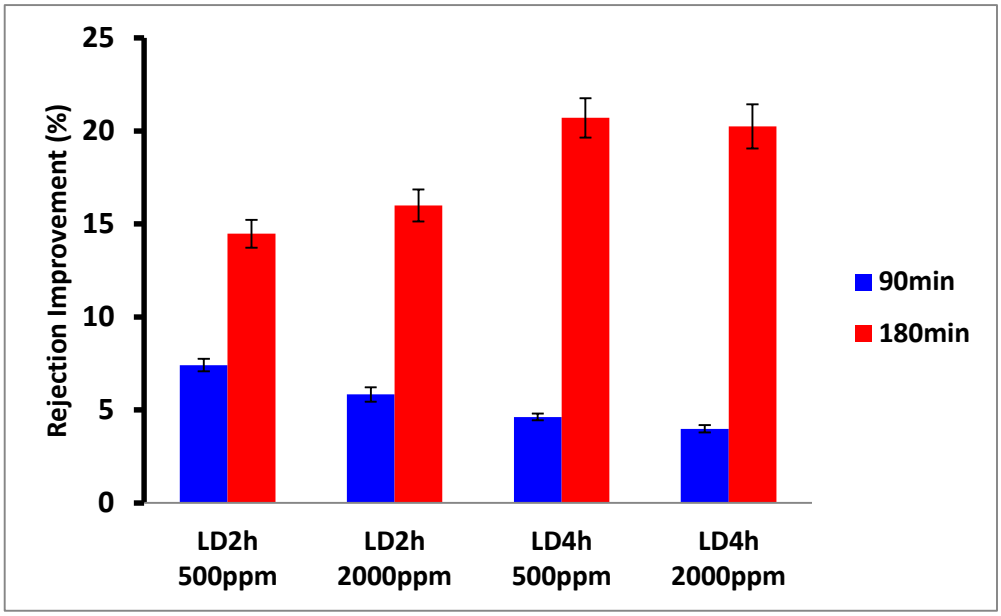

(e) Average rejection improvements within each 90-minute cycle in the presence compared to in the absence of a 20Hz field.

Figure 4.1 Rejection data for LD2h and LD4h functionalized NF270 membrane during 3-hour filtration tests with 500 and 2000 ppm $MgSO_4$ feed solutions in the presence and absence of an external magnetic field.

Figure 4.1 shows the 3 hour flux and rejection measurements for functionalized LD2h and LD4h membranes with 500 and 2000 ppm $MgSO_4$ feed solutions, together with their percentage improvements in the presence and absence of a 20 Hz oscillating magnetic field. Figure 4.1a shows the flux as a function of time during the 3 h test. It can be seen that fluxes remain more or less constant in the presence of 20 Hz magnetic field due to micro-mixing at the membrane-liquid boundary layer that breaks down concentration polarization. However, in the absence of magnetic field, the flux decreases rather quickly at the beginning of each test. A slower flux decline afterwards is observed due to the stabilized diffusion rate of the rejected species back into the bulk feeding liquid mixture. Figure 4.1b shows the average fluxes during the first 90-min and second 90-min test periods. Similarly, the average fluxes are more or less the same in the presence of a field and show decline in the absence of a field. Figure 4.1c plots the average improvement during the two periods for the two membranes at two different feed

concentrations. As concentration polarization tends to degrade membrane performance over time, a larger membrane performance improvement can be seen after a longer filtration time.

Figure 4.1d shows the corresponding data for the 4 filtration experiments during the 3 h period. The rejection data are based on the conductivity measurements of the permeates during the two 90-min periods. It can be seen that rejections for both 500 ppm and 2000 ppm $MgSO_4$ remain more or less the same in the presence of the field. Without the field, the rejections are lower due to the higher salt concentrations at the membrane-liquid boundary layer in the presence of concentration polarization.[2, 15] Although there is a continuous increase of bulk feed concentration during dead end filtration, the total amount of permeate withdrawn from the 50 mL of feed solution is generally less than 5 g after each 90 min test. The increase in feed salt concentration is hence less than 5% during each 90-minute test. Figure 4.1e shows the percentage improvement in rejection during the two testing periods with all four conditions. It can be seen that the improvement in rejection during the first 90-min is only about 5%. However, during the next 90-min period, the improvement reaches 15-20%. Since concentration polarization tends to degrade membrane performance over time, micro-mixing which minimizes concentration polarization will improve the cross-membrane solvent transport property and membrane selectivity more evidently after a longer time of test.

Comparing the LD2h and LD4h membranes, the membrane with higher grafting degree appears to have higher percentage improvement in both flux and rejection over the second 90-min test when concentration polarization becomes more severe. This phenomenon has also been observed in the previous 33 min tests using different single feed salt solutions. Longer polymer chains tend to be more effective as micro-mixers to breakdown concentration

polarization. However, the first-90-min tests performed here do not show a systematic trend. Comparing the 500 and 2000 ppm feed solutions, the improvement in rejection is similar to each other. The improvement in rejection during the first 90-min is only at around 5% and is slightly declining for 2000 ppm compared to 500 ppm salt solution for both LD2h and LD4h membranes. The improvement in rejection during the second half of the test is close to 15-20% for both 500 and 2000 ppm feed streams. During the second half of the test, a similar flux improvement is observed for the LD2h and LD4h with 2000 ppm feed stream, and there shows a similar rejection improvement for the LD4h sample with both 500 and 2000 ppm feed streams.

4.3.2 Organic Trimethylamine Hydrochloride (TMAH) Salt Solutions

Membrane fouling is caused by the attractive interactions between membrane surface and dissolved or suspended species in the feed. For NF membranes, organic fouling is more extensive and severe compared to inorganic fouling.[16] Based on the 3-hour membrane performance investigations using 500 and 2000 ppm $MgSO_4$ feed solutions, effects of micro-mixing at the membrane-liquid boundary layer are investigated for the organic salt $(CH_3)_3N{\cdot}HCl$ (TMAH). Two feed solutions at 500 and 2000 ppm were used for testing LD2h and LD4h membranes. Conductivity measurements were used to determine the rejection. Figure 4.2a gives the average flux within each 9-minute period over the 45-minute test period. Fluxes in Figure 4.2b are the average flux between the 21st and 33rd minute of each test. Rejections in Figure 4.2c are based on the conductivities of the feed and the first 2.8 g of permeate drawn. Figure 4.2d shows the percentage improvements of flux and rejection in the presence compared to the value in the absence of a 20 Hz magmatic field.

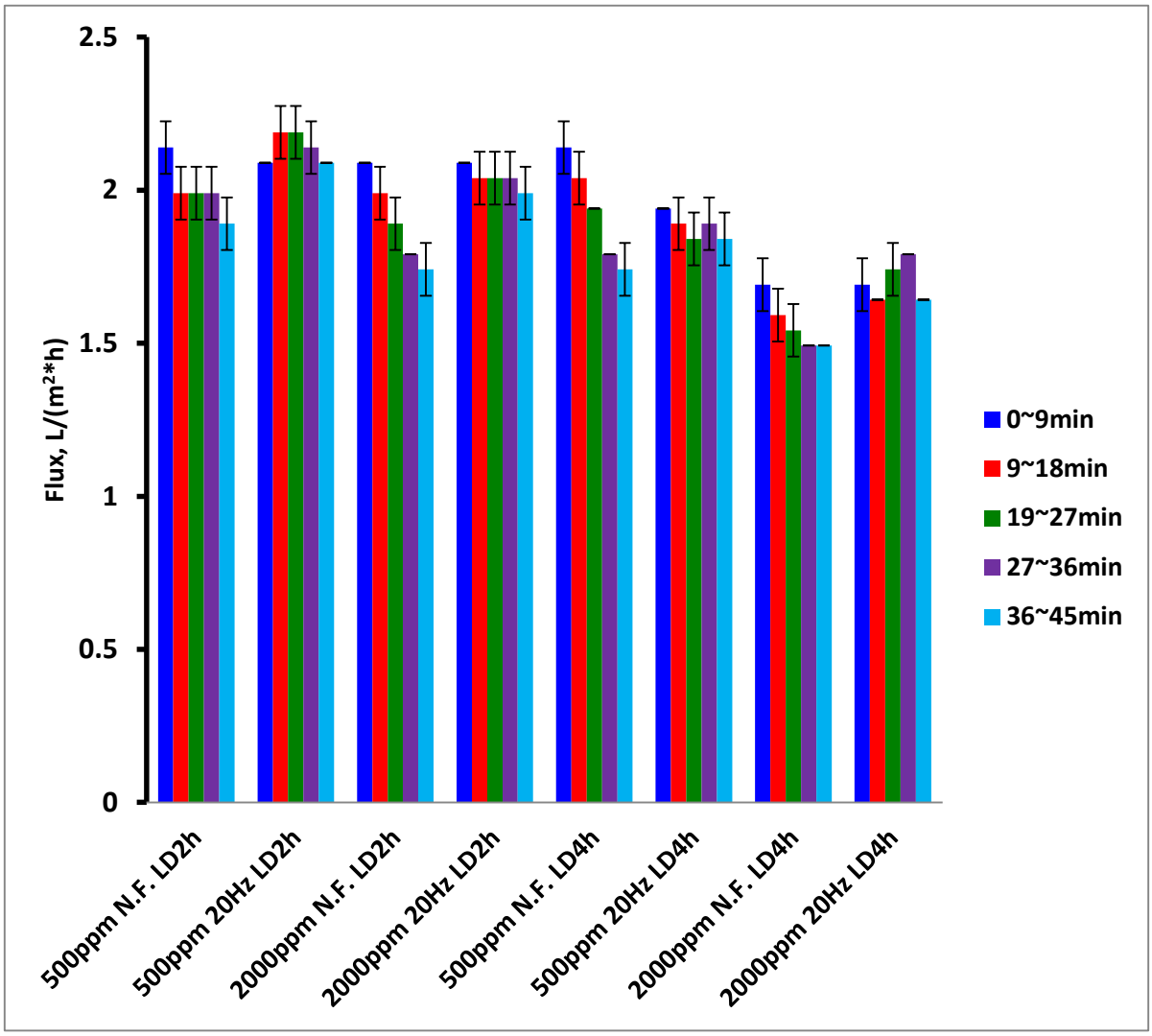

(a) Average fluxes within each 9-minute period over the 45-minute tests, L/(m^2·h).

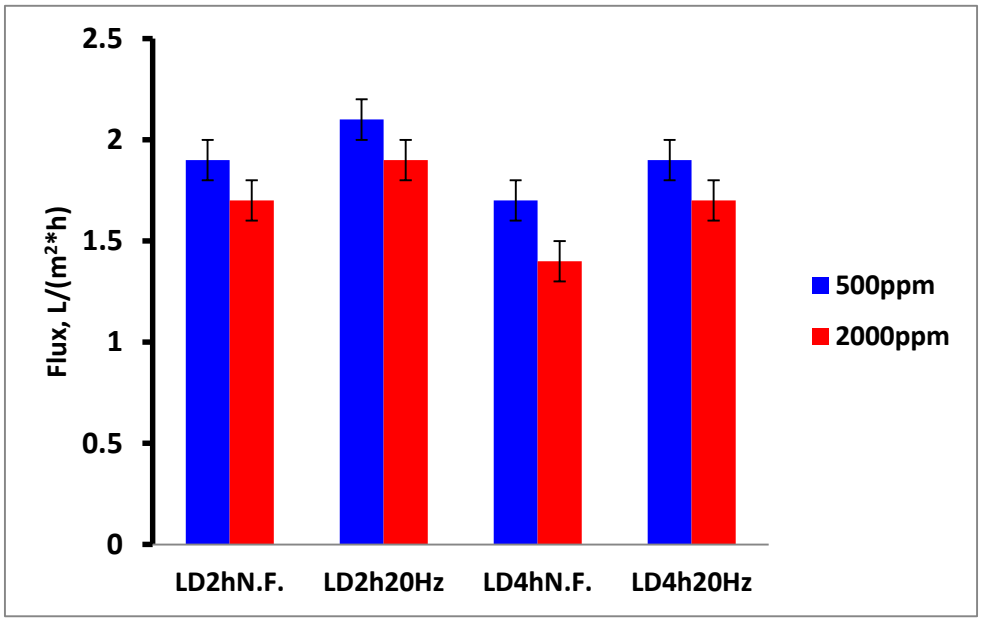

(b) Average fluxes between the 21st and 33rd minute of each 45-minute test, L/(m^2·h).

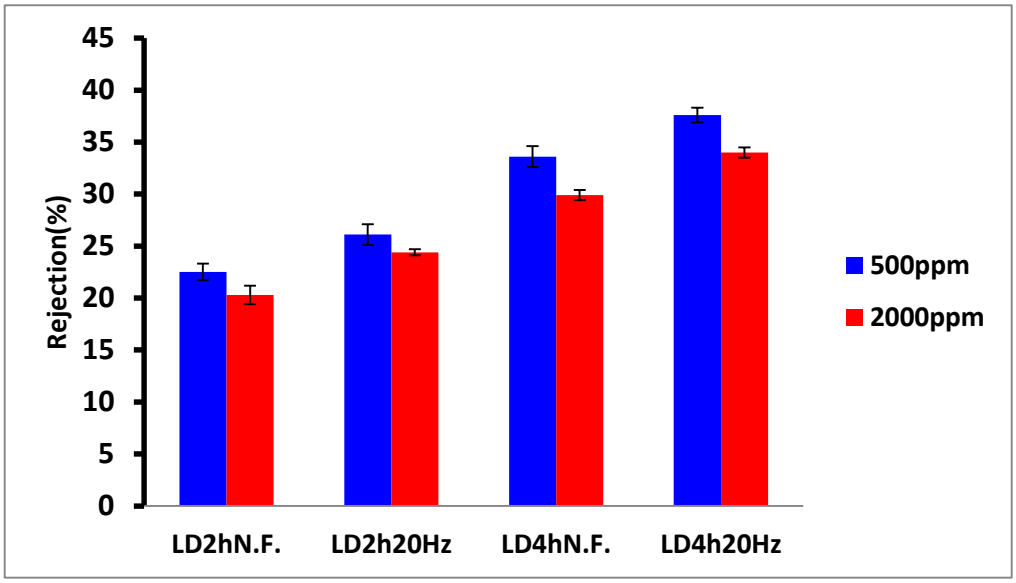

(c) TMAH rejections.

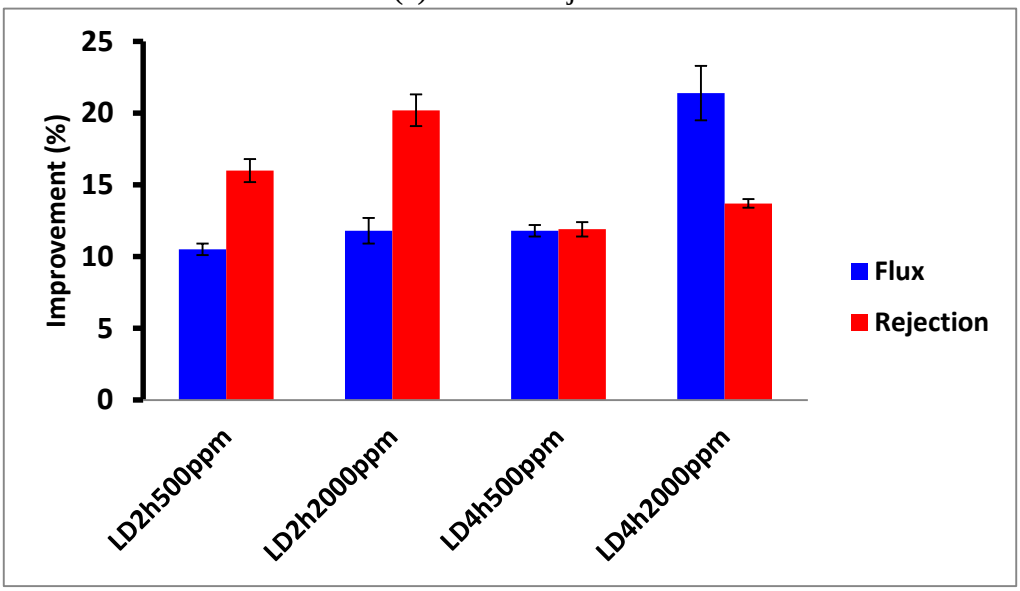

(d) Percentage improvements of flux and rejection in the presence compared to in the absence of a 20 Hz magnetic field.

Figure 4.2 Performances of the LD2h and LD4h functionalized NF270 membranes with the 500 and 2000 ppm TMAH ($Me_3N{\cdot}HCl$) feed solutions. N.F. indicates without an external magnetic field.

After membrane functionalization, the formation of poly(HEMA) nanolayer above upstream membrane surface increases the resistance of NF membrane layer to the transport of both water and TMAH. The membrane layer resistance increases as polymerization time increases from 2 to 4 hours. Therefore, applying the same magnetic field and at the same

TMAH concentration, decrease in flux and increase in rejection are observed for LD4h compared to LD2h membranes. Moreover, increase in the feed concentration reduces permeate flux due to a higher osmotic pressure difference across the membrane. Increase in TMAH concentration also decrease salt retention. However, performances of functionalized membranes in both flux and rejection are improved in the presence of an external oscillating magnetic field compared to the performances without the field.

As can be seen in Figure 4.2a, fluxes decrease continuously in the absence of an external field due to concentration polarization by the accumulation of rejected TMAH above the upstream membrane surface for all the samples. For both 500 and 2000 ppm TMAH feed solutions and both LD2h and LD4h membranes, more stable fluxes accompanying higher TMAH rejections have been observed in the presence of an oscillating magnetic field. Figure 4.2b plots the average flux during filtration experiments from 21 to 33 min. It can be seen that the flux is higher for the LD2h membranes for both 500 and 2000 ppm feed solutions. Flux is also higher for the 500 ppm feed solution for both LD2h and LD4h functionalized membranes. Moreover, there is an apparent improvement in flux for each functionalized membrane in the presence of a 20 Hz magnetic field. These results show that functionalized membranes have similar performance characteristics for both inorganic and organic salt feed solutions. Figure 4.2c shows the rejections for the LD2h and LD4h membranes with 500 and 2000 ppm feed solutions. Similar to inorganic salt feed solutions, rejections increase for LD4h functionalized membrane with both 500 and 2000 ppm TMAH feed solutions. Rejections are lower for the higher concentration feed for both LD2h and LD4h membranes. Moreover, rejections are higher in the presence of an oscillating magnetic field for all the filtration experiments due to

the micro-mixing breaking concentration polarization at the boundary layer. The rejection data are in agreement with the flux results. Again both rejection and flux results demonstrate an improvement in the membrane performance under an external magnetic field for the functionalized membranes.

Figure 4.2d shows flux and rejection improvement for the LD4h membrane, with a higher improvement for the higher salt concentration. It is also clear that rejection improvement is more significant for the LD2h membrane, and there also shows larger flux and rejection improvements for the higher salt concentration. For TMAH, a decreased concentration polarization enhances flux and rejection in the presence of micro-mixing due to a decreased osmotic pressure difference and a decreased cross-membrane concentration difference, respectively. A reduction in the surface concentration of TMAH is also useful in the alleviation of membrane fouling caused by the adsorption of TMAH onto the membrane surface.[2]

4.3.3 Antifouling Properties of Functionalized Membranes using Synthetic Oily Wastewater

Based on slight modifications to the protocol used by Madaeni *et al.*,[13] a synthetic oily waste water containing 2 mL soybean oil, 50 mg humic acid, 1 g NaCl, 1 g $CaCl_2$ and 1 g $MgSO_4$ in 1 L water was used to investigate membrane fouling and the anti-fouling properties of magnetically responsive micro-mixing NF270 membranes.[12, 17] Synthesized to mimic the oil content, TDS and conductivity of actual produced water, earlier studies show that the membrane fouling tendencies using such model waste water are very close to the produced water from the oil and gas industries.[12, 18] Here dead end filtration experiments lasting for

several hours were performed. In order to overcome the feed concentration increases during the tests, the experiments were halted temporarily after each 90-minute period to return all of the collected permeate to the feed reservoir. Permeate conductivity was measured before permeate was returned to the feed. Then filtration experiments continued without cleaning the membrane in order to simulate the continuous filtration processes.

The prior PIV investigation of fluid dynamics under various frequencies of oscillating magnetic field indicated that the strongest micro-mixing occurred under the frequency of 20 Hz magnetic field. However, this optimized frequency was selected based on a short study where heat generation is negligible. However, under much longer filtration studies, the relaxation of superparamagnetic nanoparticles within an oscillating magnetic field would dissipate energies and cause heating. The heat generated is a strong function of the magnetic field frequency applied.

It is well known that flux and/or rejection will be affected by temperature since the viscosity of water is strongly temperature dependent. Moreover, the movement of the polymer chains will be affected by the viscosity and composition of the feed. With the synthetic oily water as the feed stream used here, the movement of the polymer chains induced by the lateral movement of the nanoparticles will probably be somewhat different. Therefore, as shown in Figure 4.3, three different frequencies were used to investigate the effects of polymer chain movements on the flux over a 3 hour time period. The frequencies investigated are 1, 20 and 100 Hz. The LD4h membrane was investigated using the synthetic oily wastewater.

It is important to note that in the presence of an external field, flux remains more or less the same for all three frequencies. In the absence of the magnetic field, flux decreases

continuously due to the worsening in concentration polarization and possibly the accumulation of foulants onto the membrane surface. As mentioned earlier, an increased concentration polarization reduces the effective operation pressure due to an increased osmotic pressure difference, therefore decreases the flux under a constant operation pressure. Membrane fouling also tends to reduce the effective area for separations. The foulants accumulated within the concentration polarization layer typically include humic species, oil emulsion and inorganic scalants.[11] In the absence of mixing, the coexistence of Ca^{2+} ions and humic acid macromolecules accelerates the formation and compaction of cake layer. Cake layer compaction is caused by the attractive interaction between the Ca^{2+} ions and the negatively charged functional groups on humic acid.[19] The humic acid-Ca^{2+} interaction becomes stronger at higher concentrations as within the concentration polarization layer. In the presence of an external alternating field, micro-mixing induced immediately above the upstream membrane surface helps to disrupt the concentration boundary layer. In addition, the presence of micro-mixers reduces the chance for the foulants to precipitate, aggregate or deposit onto the upstream membrane surface, decreasing the rate of direct membrane fouling.

Oil emulsion in the wastewater typically forms a gel layer above the upstream membrane surface since molecules in the oil emulsion are rejected almost completely by NF membranes. Besides decreased concentration polarization and reduced cake layer formation, the observed flux improvement is also due to the accelerated back diffusion of oil emulsion away from the membrane due to micro-mixing at the membrane-liquid boundary layer. Micro-mixing therefore reduces oil gel layer formation in addition to concentration polarization caused by the accumulation of rejected oily molecules on membrane surface.[20] Different

frequencies of magnetic field induces different rates of micro-mixing, resulting in the flux differences at the beginning and the end of the filtration experiments. Our earlier studies demonstrate that the frequency of 20 Hz magnetic field induces the highest fluid dynamics hence leads to the strongest micro-mixing effects at the membrane-liquid boundary layer. However, those studies were conducted with the durations of less than one hour. Indeed, Figure 3 shows that the highest flux during the first hour comes from the test conducted under 20 Hz magnetic field. After longer periods of time, other effects besides micro-mixing may come into play. It is known that the nanoparticles will move laterally in response to the changing field. Relaxation of the magnetic moment within an oscillating magnetic field will cause energy dissipation thus heat generation. The rate of heat generation is dependent on the particle size, external field strength and field frequency. Here different frequencies will have different heating effects. The heat generation is probably more localized since no feed temperature change has been observed even after several hours of operation. Nevertheless, local temperature change could change the viscosity of the water and leads to an enhanced flux. This is probably the reason why the permeate fluxes under 1, 20 and 100 Hz fields all show a significant improvement after 2 hours of test compared to the test without the field. Since micro-mixing and heating are both frequency dependent, the overall improvement of the flux as a function of field frequency becomes more complex. As a result, the improvement does not seem to be systematic.[21]

Table 4.1 gives the conductivity measurement of permeates collected during each 90-minute operation cycle for different field frequencies applied. Permeate conductivity indicates the relative capacity of salt retention by the membrane. The higher the conductivity, the lower

the rejection. As shown in Table 4.1, permeate conductivity is higher for filtration experiment without an external field applied. The permeate conductivity is also higher for the tests under 1 and 100 Hz external field. The differences in permeate conductivity thus rejection is low, within less than 2%. However, the permeate withdrawn from the test under 20 Hz external field is substantially lower than tests under other magnetic field conditions. The reduction in permeate conductivity thus rejection is about 10%. This again indicate that the 20 Hz magnetic field is most effective in inducing micro-mixing at the membrane-liquid boundary layer. Using a complex feed appears to complicate the performance of the functionalized membranes. Besides concentration polarization, the precipitation and aggregation of oil emulsions, humic acid macromolecules and inorganic scalants like $CaSO_4$ always form a mixed cake layer immediately above the upstream membrane surface.[13] The presence of a cake layer typically enhances concentration polarization due to a decreased solute diffusivity within the cake layer, therefore could possibly increase the cross-membrane salt transport due to increased salt concentration gradient within the membrane.[22] Nevertheless, the cake layer exerts resistance to the overall cross-membrane ion transport.[23] The resistance of the cake layer increases after longer filtration time due to increased compaction under a continuous pressure.[24] Besides the effect of operation pressure, the coordination effect between the Ca^{2+} ions and the humic acid molecules also accelerates cake layer compaction in the absence of mixing.[18] Presence of micro-mixing decreases concentration polarization and delays the formation of cake layer. But there is a clear and evident improvement in both flux and rejection when a 20 Hz external field was applied.

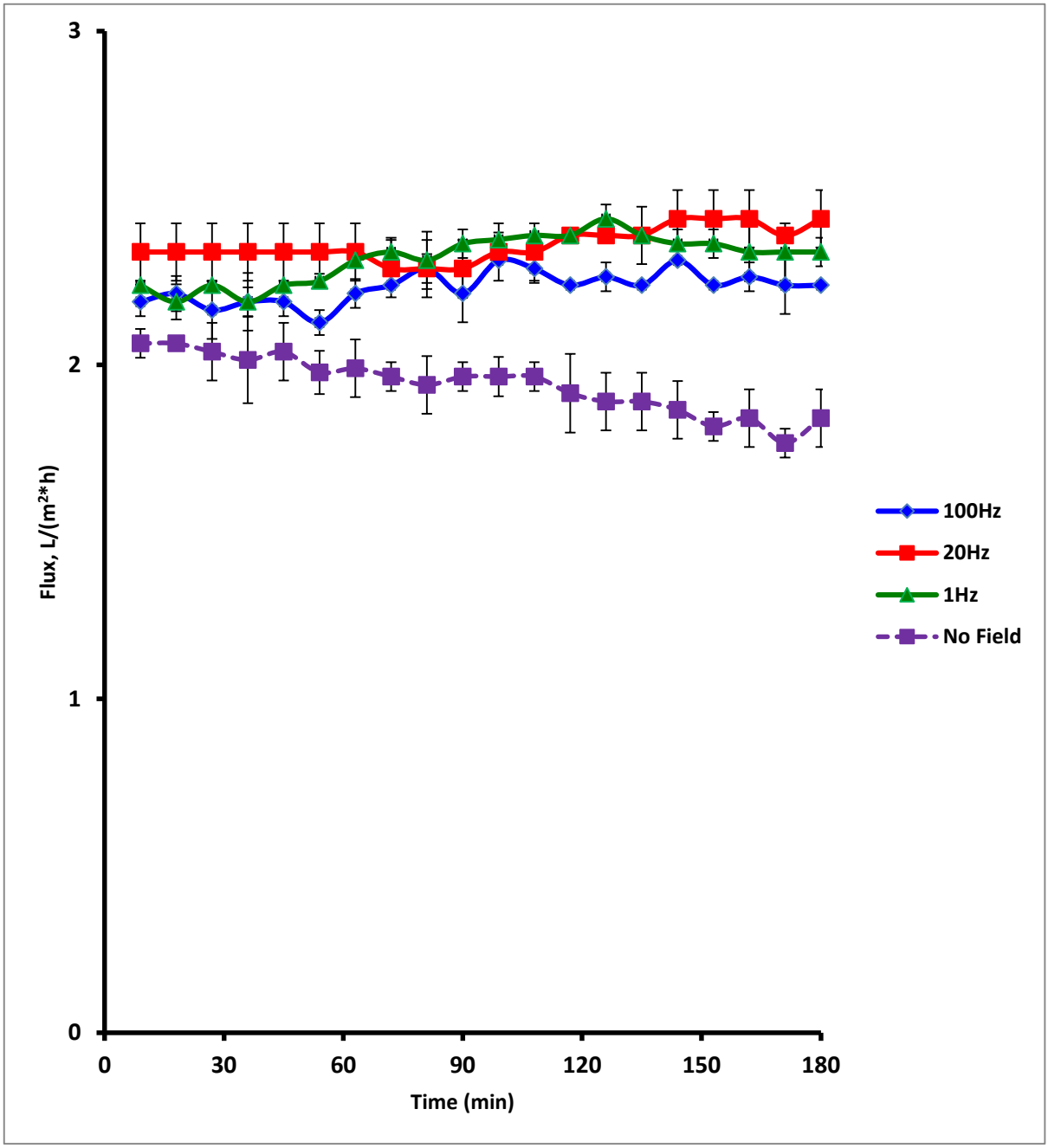

Figure 4.3 Permeate fluxes of the LD4h NF270 membrane under varied magnetic field frequencies during the 3-hour model oily waste water tests.

Table 4.1 Permeate conductivity under several external field conditions with the LD4h membrane during the 3-hour model oily waste water filtration experiments.

Conductivity (µS/cm)	**100 Hz**	**20 Hz**	**1Hz**	**No Field**
90 min	3710±5	3320±5	3710±5	3775±5
180 min	3725±5	3330±5	3725±5	3815±5

Earlier studies on the filtration experiments with the same model oily water as used

here and the similarly poly(HEMA) functionalized membranes show that the functionalized membrane surface properties were quite different compared to the base membrane. ATR-FTIR and FESEM were used to characterize the surfaces of the base and modified membranes both before and after cleaning. The same cleaning protocol was used here. The results indicate that nanoparticle functionalized membranes are much easier to clean compared to base NF270 membranes. Furthermore, the carboxylic acid functionalization does not aggravate membrane fouling. This is probably due to the movement of the grafted polymer chains in the presence of an oscillating magnetic field leading to the reduced compaction or cake layer formation. This in turn helps clean or loosen the foulants deposited on membrane surface.[11]

Finally, in order to investigate the anti-fouling of functionalized membranes after further extended hours of filtration, 6-hour model oily waste water tests were done under constant 45 psig. In order to minimize concentration increases in the dead end filtration feed reservoir, the filtration was paused every 90 minutes. All the collected permeate was then returned to the feed reservoir after measuring permeate conductivity. Filtration experiments recommenced without any cleaning to the membrane surface. Flux variation over time is shown by Figure 4.4. Case 1 shows the flux in the absence of an external magnetic field. Case 2 shows the flux in the presence of a magnetic field in the second and 4^{th} 90-min filtration experiments. The average permeate conductivity measurements based on all of the permeate collected during each 90-minute operation cycle are listed in Table 4.2.

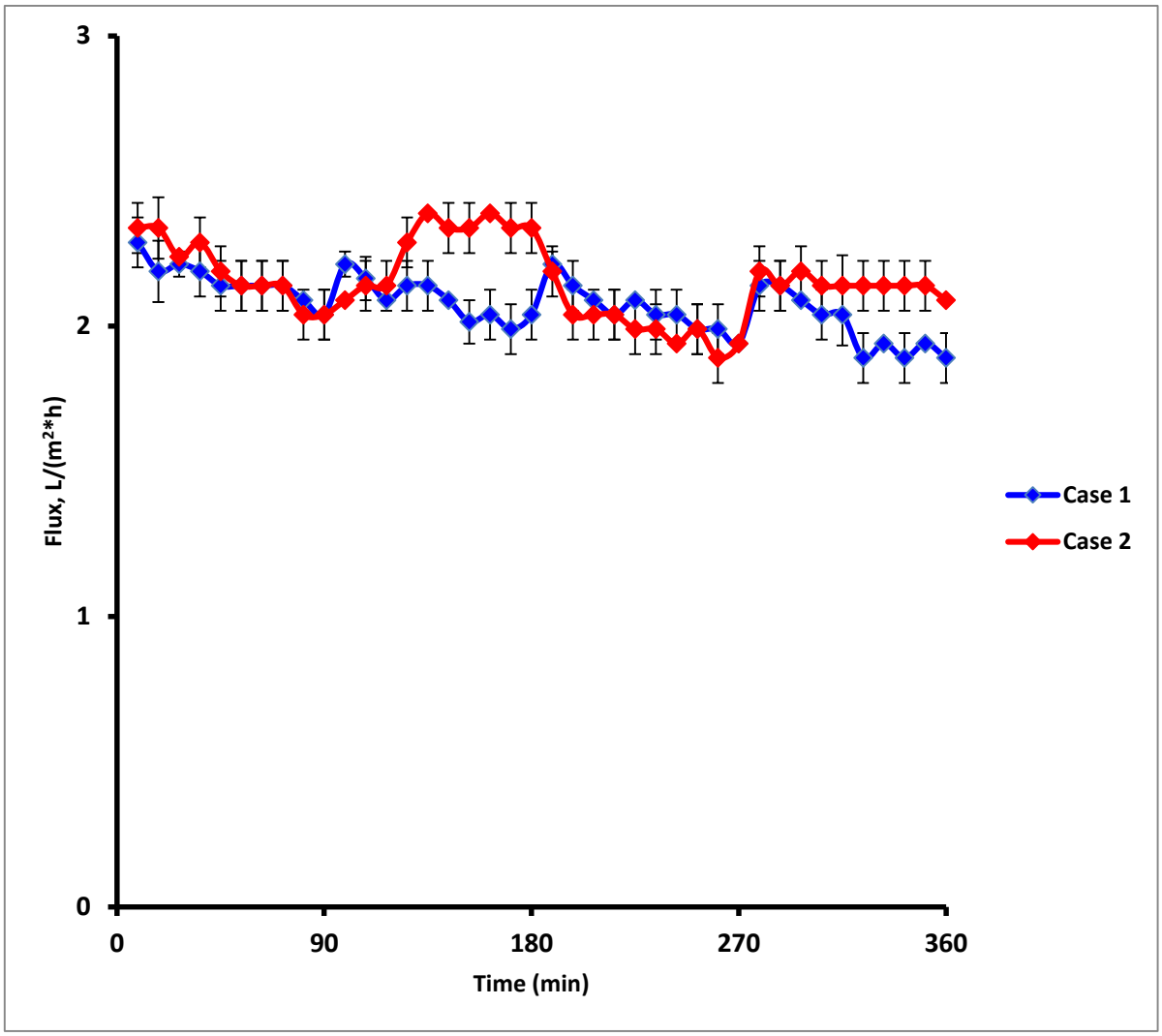

Figure 4.4 Permeate flux for the LD4h membrane during the 6-hour model oily waste water tests. Case 1 was performed without the magnetic field throughout the 6-hour period. Case 2 was conducted in the presence of 20 Hz field during the 2nd and 4th 90-minute operation cycles, but without an external field during the 1st and 3rd 90-minute operation cycles.

Table 4.2 Permeate conductivity during the 6-hour model oily waste water tests using LD4h functionalized membrane (μS/cm).

	90 min	**180 min**	**270 min**	**360 min**
Case 1	3420±10	3520±10	3550±10	3540±10
Case 2	3480±10	3470±10	3560±10	3560±10

Figure 4.4 shows that flux continues to decline during each 90-min test in the absence of an external magnetic field as in case 1. There is a slight increase at the beginning of each 90-min test period due to the return of the collected permeate to the feed leading to a slightly

decreased feed concentration. However, it is evident that concentration polarization or cake layer formation leads to flux decline over time in the absence of an external magnetic field. In case 2, a 20 Hz oscillating magnetic field is applied during the 2nd and 4th 90-min testing periods. It can be seen that flux recovered to the initial level. During the last 90-min period, flux recovery is also quite obvious. However, the recovery during the 4th 90-min period is slightly less compared to the 2nd 90-min period. Applying an external field has evidently improved the performance of functionalized membranes over an extended period of time. Even though membrane fouling is inevitable due to cake layer formation, micro-mixing at the membrane-liquid boundary layer improves the flux and tends to extend the time of operation before cleaning is needed.

Despite the evident flux improvement under external field, no significant improvement in rejection was observed during the model oily waste water test shown in Table 4.3. In case 1, rejection becomes lower after 90-min filtration experiment due to concentration polarization. However, membrane fouling leads to the formation of a cake layer which increases the resistance of cross-membrane ion transport. This additional resistance by cake layer tends to increase the rejection. The two opposing effects appear to stabilize the rejection during the next 3 90-min testing periods. In case 2 where an external field was applied during the 2nd and 4th 90-min testing periods, the decline in rejection was delayed due to the micro-mixing effects at the membrane-liquid boundary layer. The micro-mixing reduces concentration polarization and delays the formation of a cake layer. However, rejection during the 3rd and 4th 90-min periods appears to be reduced due to the inevitable onset of membrane fouling and cake layer formation. Further variation with time is not evident due to the formation of a cake layer that exerts

resistance to cross-membrane ion transport, and the resistance of cake layer increases over time due to the compaction effect under continuous pressure.[24]

Presence of hydrophilic poly (HEMA) chains and nanolayer above functionalized NF270 membranes reduces the attractive interaction between the foulants and membrane surface. An increased surface hydrophilicity is of key importance in decreasing the adsorptive membrane fouling caused by the hydrophobic interactions between oil emulsion and membrane surface.[25] In addition, the reduced surface charge of poly(HEMA) nanolayer compared to the polyamide surface of base NF270 membrane decreases the electrostatic adsorption of humic acids onto membrane surface.[18, 19, 26] As a result, flux recoveries are evident in the presence of micro-mixing during the 2nd and 4th cycles of Case 2 following the absence of micro-mixing during the prior one 90-minute cycle.

Besides the decreased foulant-membrane affinity, flux recoveries are also due to the alleviated fouling based on the reduced theoretical pore sizes within the layer of functionalized compared to base NF270 membranes.[24] A reduced membrane pore size alleviates the chance foulants be trapped within membrane layer during the presence of micro-mixing.[25] Although membrane fouling mainly occurs above the surface of generally non-porous NF membranes, a decreased free volume within the barrier layer of loose NF membranes like NF270 is helpful in decreasing foulant entrapment within the membrane layer.[16] Since micro-mixing is unavailable within the membrane pores, presence of micro-mixers above the surface of generally non-porous NF membranes proves to be useful in NF membrane anti-fouling.

4.4 Conclusions

In the presence of an external alternating magnetic field, functionalized magnetically responsive NF membranes with SPM NPs attached onto the upstream surface via the hydrophilic poly(HEMA) chains generates micro-mixing at the membrane-water interface. The presence of micro-mixing reduces the chance of membrane fouling caused by the accumulation of rejected species onto the upstream membrane surface. Besides decreased solute transport and osmotic pressure difference across the membrane due to reduced concentration polarization, the direct membrane fouling also alleviates since the micro-mixing reduces the chance the undissolvable foulants might stay on the membrane surface.

Surface modification with poly(HEMA) decreases both the attractive foulant-membrane interaction and the membrane's effective pore size, improving the ability of micro-mixing in the recovery of membrane. Micro-mixing generated by the movement of polymer chains gains importance in maintaining a constant NF membrane performance after extended hours of filtration. Despite the decreased flux due to increased membrane layer resistance, extended polymerization time during membrane functionalization leads to an increased average polymer chain length. In the presence of an external oscillating magnetic field, longer polymer chains help to generate more effective micro-mixing at the membrane-liquid boundary layer to better enhance membrane performance and fouling resistance.

Magnetically responsive surface micro-mixers reduce concentration polarization at the membrane-liquid boundary layer and improve the surface anti-fouling property of NF membranes. Magnetically activated NF membranes can be used to improve the performances during water desalination as well as water recovery from produced water. NF270 membranes seem to demonstrate extend lifetime and cleaning cycles after functionalization.

References

1. **Schäfer, A. I.**; Fane, A. G.; Waite, T. D., ***Nanofiltration, Principles and Applications***. Elsevier Advanced Technology: New York, 2005.

2. Violleau, D.; Essis-Tome, H.; Habarou, H.; Croue, J. P.; Pontie, M., Fouling studies of a polyamide nanofiltration membrane by selected natural organic matter: an analytical approach. *Desalination* **2005,** *173* (3), 223-238.

3. Deon, S.; Dutournie, P.; Fievet, P.; Limousy, L.; Bourseau, P., Concentration polarization phenomenon during the nanofiltration of multi-ionic solutions: Influence of the filtrated solution and operating conditions. *Water Research* **2013,** *47* (7), 2260-2272.

4. Himstedt, H. H.; Yang, Q.; Dasi, L. P.; Qian, X.; Wickramasinghe, S. R.; Ulbricht, M., Magnetically Activated Micromixers for Separation Membranes. *Langmuir* **2011,** *27* (9), 5574-5581.

5. Yang, Q.; Himstedt, H. H.; Ulbricht, M.; Qian, X.; Wickramasinghe, S. R., Designing magnetic field responsive nanofiltration membranes. *Journal of Membrane Science* **2013,** *430*, 70-78.

6. Himstedt, H. H.; Yang, Q.; Qian, X.; Wickramasinghe, S. R.; Ulbricht, M., Toward remote-controlled valve functions via magnetically responsive capillary pore membranes. *Journal of Membrane Science* **2012,** *423*, 257-266.

7. Himstedt, H. H.; Marshall, K. M.; Wickramasinghe, S. R., pH-responsive nanofiltration membranes by surface modification. *Journal of Membrane Science* **2011,** *366* (1-2), 373-381.

8. Boussu, K.; Kindts, C.; Vandecasteele, C.; Van der Bruggen, B., Surfactant fouling of nanofiltration membranes: Measurements and mechanisms. *Chemphyschem* **2007,** *8* (12), 1836-1845.

9. James, B. J.; Jing, Y.; Chen, M. D., Membrane fouling during filtration of milk - a microstructural study. *Journal of Food Engineering* **2003,** *60* (4), 431-437.

10. Mondal, S.; Wickramasinghe, S. R., Produced water treatment by nanofiltration and reverse osmosis membranes. *Journal of Membrane Science* **2008,** *322* (1), 162-170.

11. Himstedt, H. H. Novel Fouling Resistant Magnetically-Responsive Membranes for Treatment of Impaired Water. Department of Chemical and Biological Engineering, Colorado State University, Fort Collins, CO, 2012.

12. Wandera, D.; Himstedt, H. H.; Marroquin, M.; Wickramasinghe, S. R.; Husson, S. M., Modification of ultrafiltration membranes with block copolymer nanolayers for produced water treatment: The roles of polymer chain density and polymerization time on performance. *Journal of Membrane Science* **2012,** *403*, 250-260.

13. Madaeni, S. S.; Gheshlaghi, A.; Rekabdar, F., Membrane treatment of oily wastewater from refinery processes. *Asia-Pacific Journal of Chemical Engineering* **2013,** *8* (1), 45-53.

14. Boussu, K.; Zhang, Y.; Cocquyt, J.; Van der Meeren, P.; Volodin, A.; Van Haesendonck, C.; Martens, J. A.; Van der Bruggen, B., Characterization of polymeric nanofiltration membranes for systematic analysis of membrane performance. *Journal of Membrane Science* **2006,** *278* (1-2), 418-427.

15. Li, Q. L.; Elimelech, M., Organic fouling and chemical cleaning of nanofiltration membranes: Measurements and mechanisms. *Environmental Science & Technology* **2004,** *38* (17), 4683-4693.

16. Fane, A. G. F. I. S. D. W. G., *Nanofiltration: Principles and Applications*. Elsevier Advanced Technology: Australia, 2004.

17. Wandera, D.; Wickramasinghe, S. R.; Husson, S. M., Modification and characterization of ultrafiltration membranes for treatment of produced water. *Journal of Membrane Science* **2011,** *373* (1-2), 178-188.

18. Listiarini, K.; Sun, D. D.; Leckie, J. O., Organic fouling of nanofiltration membranes: Evaluating the effects of humic acid, calcium, alum coagulant and their combinations on the specific cake resistance. *Journal of Membrane Science* **2009,** *332* (1-2), 56-62.

19. Tang, C. Y.; Kwon, Y.-N.; Leckie, J. O., Fouling of reverse osmosis and nanofiltration membranes by humic acid - Effects of solution composition and hydrodynamic conditions. *Journal of Membrane Science* **2007,** *290* (1-2), 86-94.

20. Park, E.; Barnett, S. M., Oil/water separation using nanofiltration membrane technology. *Separation Science and Technology* **2001,** *36* (7), 1527-1542.

21. Lukawska, A.; Jagoo, Z.; Kozlowski, G.; Turgut, Z.; Kosai, H.; Sheets, A.; Bixel, T.; Wheatley, A.; Abdulkin, P.; Knappett, B.; Houlding, T.; Degirmenci, V., AC Magnetic Heating of Superparamagnetic Fe and Co Nanoparticles. *Defect and Diffusion Forum* **2013,** *336*, 159-167.

22. Hoek, E. M. V.; Elimelech, M., Cake-enhanced concentration polarization: A new fouling mechanism for salt-rejecting membranes. *Environmental Science & Technology* **2003,** *37* (24), 5581-5588.

23. Lee, S.; Cho, J. W.; Elimelech, M., Combined influence of natural organic matter (NOM) and colloidal particles on nanofiltration membrane fouling. *Journal of Membrane Science* **2005,** *262* (1-2), 27-41.

24. Nghiem, L. D.; Hawkes, S., Effects of membrane fouling on the nanofiltration of pharmaceutically active compounds (PhACs): Mechanisms and role of membrane pore size. *Separation and Purification Technology* **2007,** *57* (1), 176-184.

25. Zuo, G.; Wang, R., Novel membrane surface modification to enhance anti-oil fouling property for membrane distillation application. *Journal of Membrane Science* **2013,** *447,* 26-35.

26. Tang, C. Y. Y.; Kwon, Y. N.; Leckie, J. O., Characterization of humic acid fouled reverse osmosis and nanofiltration membranes by transmission electron microscopy and streaming potential measurements. *Environmental Science & Technology* **2007,** *41* (3), 942-949.

5. Conclusions and Future Directions

5.1 Conclusions

Magnetically responsive NF270 membranes were fabricated by grafting hydrophilic poly(HEMA) chains onto the membrane surface. The polymer chains were subsequently conjugated with the superparamagnetic iron oxide nanoparticles at the chain ends. In the presence of an external oscillating magnetic field, the tethered superparamagnetic nanoparticles move in response to the external field. The well-controlled surface initiated ATRP was used for grafting these polymer chains on membrane surface resulting in uniform growth of the surface nanolayer. The polymer chain density can be controlled by varying initiator concentration as well as initiator immobilization time. The polymer chain length can be controlled by polymerization time. These ATRP grafted polymer chains demonstrate low polydispersity. In an external oscillating magnetic field, the movement of the polymer chains is concerted resulting in fluid effective micro-mixing at the membrane-liquid boundary layer.

Dead-end filtrations were conducted to investigate the effects of an external field on the performance of these functionalized NF270 membranes using various salt feed solutions. Magnetically induced micro-mixing at the membrane-liquid interface leads to a significant flux and rejection improvement due to the reduced concentration polarization at the membrane-liquid interface and the subsequent antifouling effect. Feed solutions investigated include inorganic salt solutions of NaCl, $CaCl_2$, $MgCl_2$, $MgSO_4$ and Na_3PO_4 at concentrations varying from 500 to 2000 ppm. Organic $(CH_3)_3N{\cdot}HCl$ feed solutions at various concentrations were also investigated. The micro-mixing effects leading to the improved membrane performance are found to be salt type and salt concentration dependent. Moreover, membrane performance

is also found to be dependent on polymer chain density and polymer chain length. Quantitative analysis of the solvent and solute transport across the magnetically responsive self-cleaning micro-mixing NF membranes was carried out using phenomenological modeling based on the integration of several well established NF membrane transport models. Concentration polarization under different conditions of membrane functionalization and feed solution has been quantified. A reduced concentration polarization leading to an improved solvent flux and solute rejection due to the micro-mixing effects at the membrane-liquid boundary layer was validated. The effects of grafting degree, in particular, polymer chain length and chain density on micro-mixing leading to the mitigation in concentration polarization for the same feed were analyzed. Moreover, the effects of micro-mixing and subsequent mitigation of concentration polarization with different feed type and feed concentration were also quantified.

Non-stirred dead end filtration experiments with a fixed initial feed volume have been successfully performed to investigate the combined effects of membrane functionalization and external oscillating magnetic field on membrane fouling and concentration polarization during NF processes. The effects of alternating magnetic field on micro-mixing depend on the length and density of poly(HEMA) chains grafted on membrane surface. For the low molecular weight salt solutions with concentrations below 10,000 ppm, flux and rejection improvements become more evident for membranes with longer or denser polymer chains. However, increases in either the length or the density of polymer chains could lead to the loss of membrane permeability.

Under the same membrane modification condition, the effect of micro-mixing on flux and rejection depends on the type and concentration of salt. Micro-mixing induced by an

external magnetic field at the membrane-liquid boundary layer improves the rejection of salt ions that have a higher mobility or permeation through the membrane. On the other hand, micro-mixing improves flux for salt ions that have a lower mobility or permeation through the membrane. In the presence of micro-mixing, surface concentration decreases significantly for the high mobility ions, while ions with lower mobility typically demonstrate a higher percentage improvement of effective operation pressure. In particular, the valence of salt ions and the membrane modification condition appear to play a critical role in concentration polarization and salt transport.

As indicated by the Peclet number, the cross-membrane transport of Na^+ and Cl^- is mainly convective, while diffusive transport dominates Ca^{2+}, Mg^{2+} and SO^{2-} permeation across the membrane barrier. In the presence of an external oscillating magnetic field, Peclet number decreases for NaCl and $CaCl_2$ but increases for $MgSO_4$. Micro-mixing therefore decreases the rate of convective transport in the NaCl and $CaCl_2$ feed solutions and increases the rate of convective transport in the $MgSO_4$ feed solutions.

The induced micro-mixing effects for the magnetically responsive NF membranes lead to their enhanced anti-fouling properties by the reduction of concentration polarization and the decreased foulant deposition onto the upstream membrane surface. In the presence of an external magnetic field, the induced micro-mixing effects lead to improved performance of functionalized membranes over an extended period of time compared to cases with absent field. Together with an increased anti-fouling propensity after modification with hydrophilic poly (HEMA), the presence of active micro-mixers further improves the membrane's self-cleaning capacity. Moreover, the presence of micro-mixing reduces the onset of the cake layer formation

as well as decreases the compaction of cake layer.

5.2 Future Directions

The reaction steps leading to the magnetically responsive micro-mixing membrane functionalization are expected to work on other commercialized polyamide thin film composite membranes, such as NF90 and BW30.

Besides the purification and desalination of water, the application of micro-mixing nanofiltration membranes should be extended to organic solvent purification.

In order to generate an optimal micro-mixing at the membrane-liquid boundary layer, the movement of superparamagnetic nanoparticles should be parallel to the upstream membrane surface and normal to the flow of permeate in the dead end filtration. Moreover, for the magnetically responsive micro-mixing membranes, membrane functionalization should be limited to the upstream membrane surface. Future work could extend magnetically activated micro-mixing to more industrially relevant cross-flow filtration systems.

Appendix A1

Membrane Functionalization Reaction Process

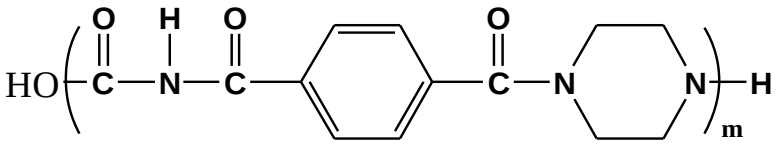

Figure A.1 Molecular structure of NF270 membrane's functional layer.[1]

For the nonporous nanofiltration membrane NF270, the functionalization reactions mainly occur on the feed side surface of the polyamine functional layer. From the molecular structure of the polyamide functional layer that is shown in Figure A.1, there are mainly carboxyl and amide end groups on the membrane's surface.

Before the reaction process, certain preparation procedures were needed for new membranes that were just cut from the original flat sheet, as described below:

1) Rinse with DI water for about 2 minutes to primarily remove the dust and other solid particles attaching on the surface;
2) Remain in 50% ethanol/water (v/v) that is placed on shake bed for 1 hour, to primarily hydrate the membranes;
3) Rinse with DI water on shaker bed for several times to remove the potential protective layers on membrane surface, and totally rinse for 24 hours;
4) Vacuum drying under 37℃ overnight to remove all potential moisture above and within the membrane layers to avoid the disruption of initiator anchoring reaction process by moistures.

Then the membranes were ready for membrane functionalization work or base membrane surface characterization processes except Atomic Force Microscopy (AFM). If base membrane performance tests or surface characterization using AFM needed to be done subsequently, the vacuum-drying step was better to be avoided. Instead, the samples should be generally dried carefully with clean towel paper used for optical instruments, or in air by sandwiching the membranes within clean filter paper layers.

The functionalization reactions have to start from the reactions occurring on the carboxyl or amide functional groups on the membrane surface. The entire reaction process is shown in Figure A.2, and is composed of the following steps that are to be described together with the lab operation process as was developed in earlier studies:[2-4]

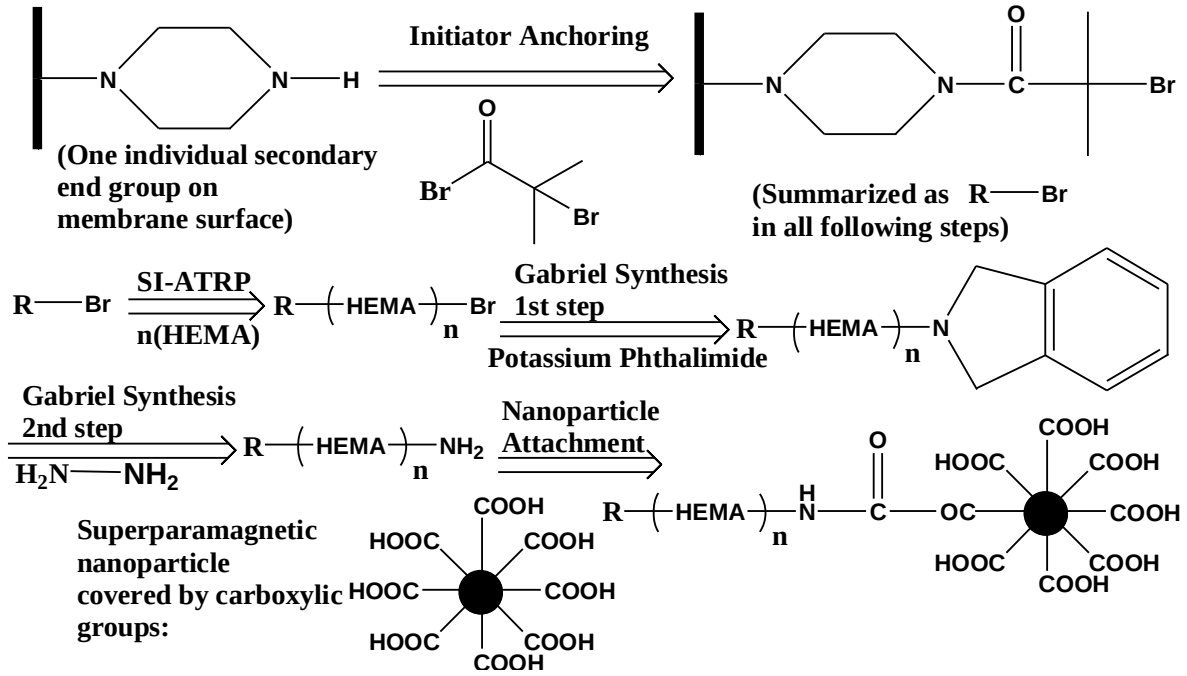

Figure A.2 Chemical modification procedures required to develop magnetically activated NF270 membranes.[2, 3, 5]

(1) Initiator anchoring

The secondary amide end groups on membrane surface react with the initiator, α-bromoisobutyryl bromide to form bromide surface-functionalized membranes. This is done via

condensation reaction to remove HBr, which is then absorbed by triethylamine.[6, 7] 4-(N',N'-dimethylamino) pyridine (DMAP) is required to work as the ligand agent during reaction.

Since the reaction process is sensitive to humidity, the solvent for the reaction was anhydrous acteonitrile. As acetonitrile bought in always contained 1~3% of water, dehydration process was required. This was done by constant pressure distillation under 110℃ by using boric anhydride as the dehydration agent. According to the water absorption capacity of this agent, at least 1 g of solid was required to dry each 20 g of acetonitrile.

1.4 mL of triethylamine and 61.1mg of DMAP were added into each 100 mL of purified acetonitrile. After mixing well, 25 mL of solution was needed for each 44.5 mm membrane sample. Then, after the membranes were completely soaked in the reaction solution, 1mL of α-bromoisobutyryl bromide was added into each 100 mL reaction solution. Then the reaction was done on shaker bed, and the time lengths were 2 or 6 hours to get varied initiator density that leads to varied polymer chain density on membrane.

After reaction, the membranes had to be rinsed at first with anhydrous acetonitrile for one minute, then with 1:1 ethanol/water (v/v) for overnight by replacing the liquid mixture several times. The membranes could then be directly used for ATRP, or vacuum-dried overnight to get the weight for grafting degree determination.

(2) Atom Transfer Radical Polymerization (ATRP)

ATRP is the step leading to the formation of linear polymer chains onto the membrane surface. The monomer used in this work was 2-hydroxyethyl methacrylate (HEMA). Detailed chemistry of ATRP is shown in Figure A.3.[6]

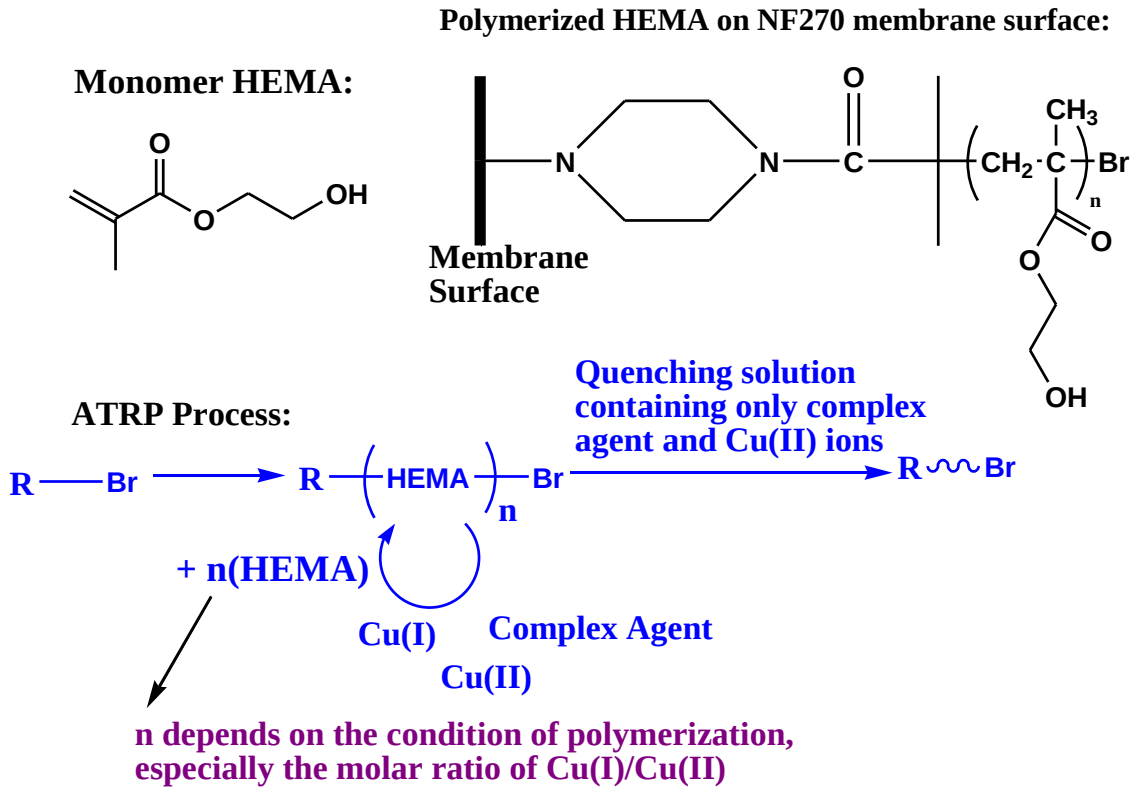

Figure A.3 Atom Transfer Radical Polymerization (ATRP) for grafting poly(HEMA) on membrane surface.[6, 8]

During ATRP processes, copper halides are catalysts for the polymerization reactions. Varying the ratio of Cu(I)/Cu(II) determines the catalytic activity of copper halides. The complex agents such as 2'2'-bipyridine (BPy) and/or N, N, N', N", N"-pentamethyldiethylenetriamine (PMDETA) are required to complex with the Cu ions.[7, 9]

Since earlier studies showed that the chain length and chain density affects the micro-mixing effects, ATRP has the advantage of varying the chain length and chain density independently.[2] Although UV initiated polymerization is relatively easy to operate, ATRP is used here for the following reasons in addition to the independent control of polymer chain length and chain density:[10]

1) Uniform polymer chain growth leads to an extremely narrow distribution of polymer chain

lengths.

2) It is a live and controlled polymerization reaction leading to linear polymer chains that do not cross-link. This is important since it affects the flexibility and movement of the polymer chains.
3) ATRP is a low and reversible reaction. The polymer chain length can be easily controlled by varying the polymerization time.[11]

Since the catalytic Cu(I) ions are extremely sensitive to oxygen in the air, ATRP needs to be done in an atmosphere purged by an inert gas such as argon or nitrogen. Before use, monomer HEMA had to be purified by mixing with aluminum oxide particles for 10 minutes to remove the stabilizing agents. The solvent for ATRP was 1:1 methanol/water (v/v), and the reaction solution was composed of the following components with the corresponding molar ratio. That is, HEMA: CuCl: $CuCl_2$: BPy = 100: 0.5: 0.2: 1.75. HEMA and BPy were both added into the solvent at the beginning. Then, before adding CuCl, mixing accompanied by inert gas purging was done by nitrogen gas bubbling together with stirring for 20 minutes. Subsequently, the same mixing and purging process was required for 20 minutes both before and after adding $CuCl_2$. ATRP reaction solution was ready then. In order to also purge the atmosphere in the reactors, each 100mL flask containing one membrane sample needed to be repeatedly pumped vacuum and then filled with nitrogen for three times. In order to guarantee isolation from oxygen in the air and full immerse of the membranes into the reaction solution, 25 mL of reaction solution needed to be injected into the reactors through the rubber stoppers covering the reactors. ATRP time was varied to adjust the length of polymer chains grafted on membrane.

Termination of ATRP needed to be done by placing the samples into quenching solution that contains 0.5 g of $CuBr_2$ and 1.25 mL of PMEDTA in 100 mL 1:1 methanol/water (v/v). Each sample had to stay in the quenching solution for 10 minutes. After termination, the samples needed to be rinsed in 1:1 methanol/water (v/v) for one minute, then in 1:1 ethanol/water (v/v) for overnight by replacing the liquid mixture several times. At least 10 hours of vacuum drying was required before membrane weight measurement for grafting degree determination. However, ordinary drying with clean towel papers for optical instruments was required if the Gabriel Synthesis would immediately start after membrane rinsing.[2]

(3) Gabriel Synthesis

Gabriel Synthesis is used for converting the halogen end groups at the polymer chains into amine groups that can conjugate with the nanoparticles by forming a peptide bond with the carboxyl groups on the nanoparticle.[12] It is composed of two successive steps: (1) Reaction of the –Br end groups with potassium phthalimide to form phthalimide terminated end groups on polymer chains within a saturated solution of potassium phthalimide; (2) Reaction of the phthalimide terminated end groups with hydrazine hydrate to form amine-terminated end groups under acidic conditions.[13, 14]

Reaction solution for the first step of Gabriel Synthesis was saturated potassium phthalimide solution in anhydrous ethanol, and that for the second step was prepared by adding 7 mL of hydrazine hydrate into each 25 mL of 6 M HCl. 25 mL of reaction solution and 15 mL of 6 M HCl were required for each 44.5 mm NF270 membrane sample during the 1^{st} and 2^{nd} steps of Gabriel Synthesis, respectively. Both steps of Gabriel Synthesis needed to be done

within constant temperature shaker bed under 40℃ and 75/min speed for 6 hours. Rinsing of the membrane samples for 2 minutes in 1:1 ethanol/water (v/v) and then for 2 minutes in anhydrous ethanol was required after the 1st step. Subsequently, the membranes had to be dried in air but sandwiched within filter paper layers overnight, before proceeding to the next step next day since the phthalimide groups tend to depart the end of polymer chains after hydrolysis in water. The cleaning procedure of membrane samples after the 2nd step was only composed of rinsing with 1:1 ethanol/water (v/v) over night. Drying with clean optical instrument towel papers was required after both steps if the membranes needed to be placed into storage.[2, 3]

(4) Nanoparticle Attachment

Catalyzed together by EDC (1-ethyl-3-(3-dimethylaminopropyl)carbodiimide) and NHS (N-hydroxysuccinimide), the amine groups at the polymer chain ends react with the carboxylic groups on the nanoparticles, forming a peptide bond between the chain and the nanoparticle.[14]

EDC forms an active crosslinker between carboxyl and amine groups.[15] At first, EDC reacts with a carboxyl group to form an amine-reactive O-acylisourea intermediate in order to activate this carboxyl group. Then, this intermediate reacts quickly with an amine group, forming an amide bond between the carboxyl and amine groups while releasing an isourea by-product. In aqueous solutions, the O-acylisourea intermediate is very unstable and would undergo hydrolysis quickly in the absence of an amine group. After hydrolysis, the carboxyl group would be regenerated and an N-substituted urea would be released. Presence of NHS helps to stabilize the intermediate by a two-step conjugation procedure.[16] After carboxyl group activation by EDC, NHS replaces EDC to couple onto the carboxyl group to generate an amine-

active ester that is considerably more stable than the O-acylisourea intermediate, increasing the yield of coupling under a nearly neutral pH.[17] Moreover, since the reaction process is sensitive to light, it had to be done in darkness to prevent one nanoparticle from conjugation with multiple polymer chains.[16, 17]

116.1 mg of NHS and 106.8 μL EDC were added into each 30 mL DI water. After short and light stirring to mix well, totally 0.45 mL of superparamagnetic nanoparticles was added in extremely slowly and without stirring. In order to prevent the particles from aggregation, another dribble of nanoparticles was added only after the prior one had completely dispersed into the solution. Then into each 50 mm Petri dish containing one 44.5 mm sample that was already flattened, 5 mL of reaction solution was added to completely cover the functional layer surface of the membrane that was facing above. These Petri dishes were then sealed up and packed with aluminum foil, then placed in dark to react for 4 hours. Overnight DI water rinsing with several DI water replacements was required to clean the membranes after reaction.[2]

Appendix A2

Membrane Flux Test Procedure

As mentioned before, all of the flux tests were done with dead-end filtration, in an Amicon 8010 stirred filtration cell from Millipore without stirring. This cell is 13.4 cm^2 in operation area and 50 mL in feed volume. Each test was done under room temperature, and under constant pressure during each entire test process, at 45 or 55 psig.[2, 3]

Before measuring the flux, each membrane was rinsed with DI water sprayed from a squirt bottle for 30 seconds. Then the membrane was placed into a stirred cell, and the cell was then filled with a 1:1 (v/v) mixture of water and ethanol. Pressurized nitrogen under 30 psig was then used to flux the mixture fluid through the membrane for 20 minutes. Then, the mixture was replaced by DI water, and DI water flux compaction under 55 psig was conducted for 2 hours. During compaction, at least 10 mL of DI water had to be guaranteed in the cell by filling DI water into the cell when required. The flux measurements were then conducted.[2]

Flux test was conducted for varied time lengths and for feed solutions with various compositions. The total amount of permeate was weighted every 3 minutes. Flux in $L/(m^2 \cdot h)$ was determined by the increase of permeate versus time per unit operational area of the Amicon cell (13.4 cm^2). For each membrane sample investigated in this work, at least 10 minutes of DI water flux rinsing followed by at least 2 minutes of DI water rinsing on shaker bed was required after each test in order to remove the salts or small molecules deposited on the membrane.[2, 18] For the flux tests using model oily waste water, additional rinsing with 0.5 M sodium hydroxide

solution was required as described in Chapter 4.

Flux tests with an external alternating magnetic field were done in the Amicon cell surrounded by two stainless-steel core solenoids that were controlled by a software. The system is shown in Figure A.4. According to previous studies[2, 3], in order to generate the strongest magnetic field across the membrane, the two solenoids had to be placed in close proximity to the membrane cell, with their symmetrical axes aligned. The solenoids' symmetrical axes had to be aligned with the membrane's surface functional layer through the center of the membrane disc in the cell. Although a stirred cell had been used, in order to observe the effects of the oscillating magnetic field on membrane performance, stirring of the membrane feed solution had been completely avoided in this work. Then the balance for measuring the total weight of permeate was Mettler Toledo PL 602~S, which was connected to the computer. The data on the balance was automatically recorded using the software of Balance Link after predetermined time intervals. The flux could therefore be determined by total permeate weight vs. time. The setup of the membrane performance testing system is shown in Figure A.4.[2, 3]

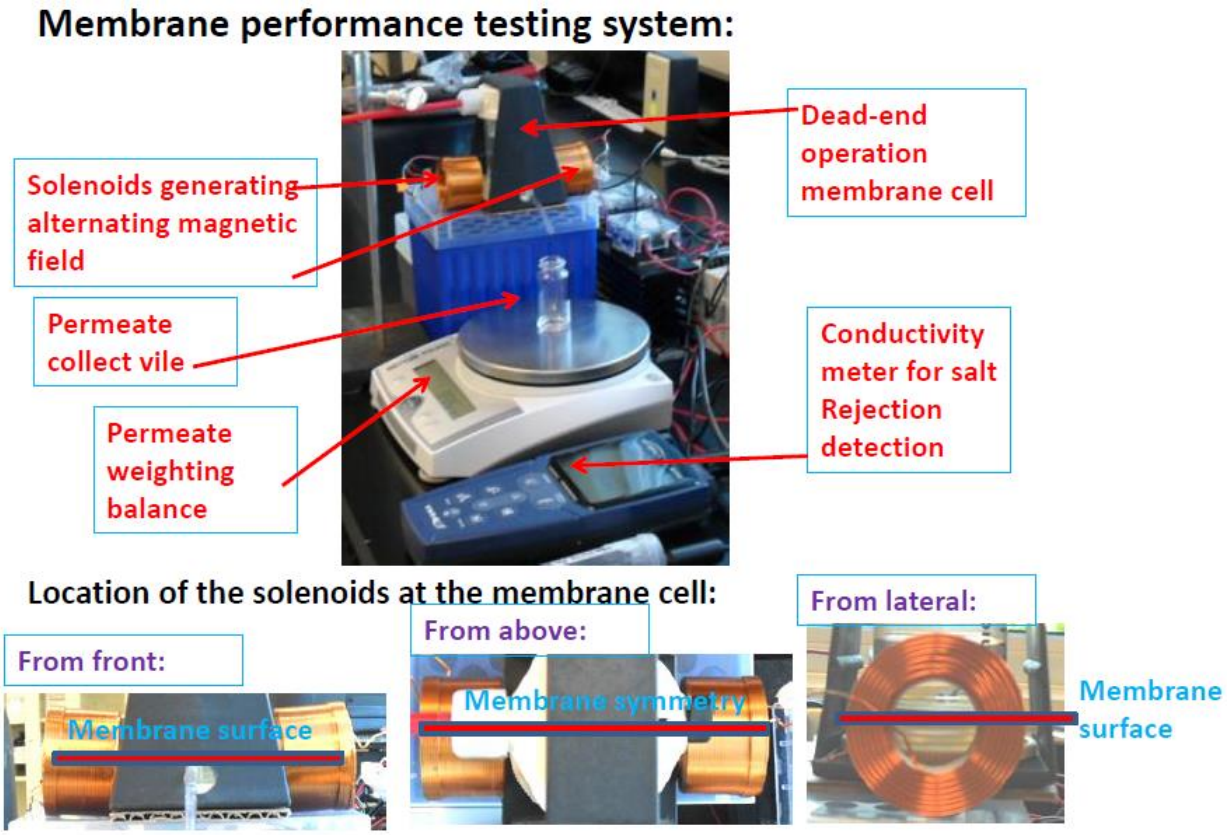

Figure A.4 Membrane performance testing system with oscillating magnetic field.[3]

Dead-end filtration operation mode was used in all the tests. This is because, compared to the widely used tangential flow operation mode, dead-end filtration has the following advantages:[19]

1) Easier to operate and control.
2) Much less membrane area and feeding solution volume are needed.
3) A smaller volume is needed for operation. In this work, the volume of dead end filtration cell was only about 50 mL.
4) Easier to compare the performances of different membranes and feeding solutions under the same operational conditions.

Appendix A3

Salt Rejection Test

For the same type of salt solution under the same operating conditions, the conductivity increase is linear to the salt concentration. Therefore, salt rejections of the membranes were determined using the conductivity method. All conductivities were measured using a VWR SYMPHONY conductivity meter in the unit of μS/cm or mS/cm.[3]

For each membrane performance test, salt rejection was tested immediately after flux measurements were done. Salt rejection was determined by the conductivities of both the feeding salt solution (S_o) and the collected permeate liquid from the membrane (S). Rejection (%)= $(S_o\text{-}S)\times100/S_o$.[2, 3]

Appendix A4

Necessary Preparation Processes for Testing NF270 Membranes

The following procedures were required for an untested membrane, whether base or modified:

1) Pre-condition with flux of 50% ethanol/water (v/v) under 30 psig for 20 minutes.

2) Compact with DI water flux under 55 psig, for at least 2 hours. The flux during compaction needed to be checked and the membrane could be considered ready for testing after the flux had been constant for at least 30 minutes.

Then the membrane was ready for testing.[2]

To note, for new membranes just cut from the sheet, in order to remove the potential protection layer covering the membrane surfaces, 2 minutes of pre-rinse with DI water followed by 1 hour of pre-hydration in 50% (v/v) ethanol/water and then overnight rinsing in DI water was required before conducting the processes mentioned above.[2]

For membrane preservation, it could temporarily be left in DI water if it would be tested within 10 hours. However, 50% ethanol/water (v/v) was a better choice for the membrane to remain hydrated. If the membrane would be tested after less than 7 days, it could be placed in 50% ethanol/water (v/v) to remain hydrated and free of bacteria. If the membrane was not to be tested within 7 days or longer, preservation in 0.5% sodium azide solution was strongly recommended to prevent bacteria growth on the membrane.[2, 20]

After each salt solution test, in order to preserve the membrane integrity, the following

procedures were required:

1) Rinse the inner side of the cell with the membrane disc in it using DI water by shaking for at least 30 seconds, repeating for a total of three times.
2) Then, flux DI water under the same pressure of the prior test for at least 10 minutes.
3) After this, water beads on both sides of the membrane should be removed very carefully using clean optical paper.[2, 3, 5]

Moreover, in order to guarantee precision of the test together with sufficient cleaning of the membrane layer, 2 hours of DI water flux compaction was always required before testing any membrane sample that hadn't been tested during the past 14 hours. Also, compaction effect could be avoided if a continuous test for the same membrane sample is less than 8 hours.

Appendix A5

Operation of the Alternating Magnetic Field

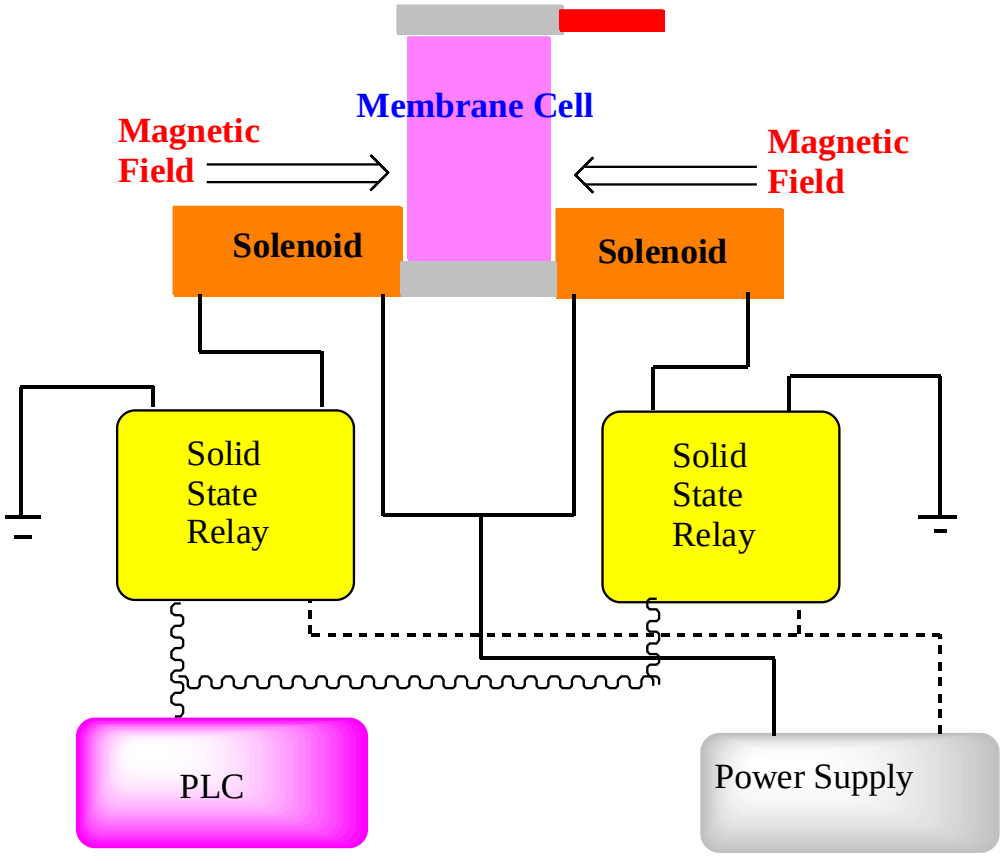

Figure A.5 Controlling system for the alternating magnetic field.[2, 3]

The connection of the controlling system guaranteeing the required frequency and strength of the alternating magnetic field is described by Figure A.5. The magnetic field was operated with the "fixed current and fluctuating voltage" mode, with the current being 1.3±0.5A and the voltage fluctuating between 2.25~5.16V. After all, the strength of electromagnetic field is only related to the magnitude and direction of the current itself. The

magnetic field was generated using Agilent U8000 Series Single Output DC Power Supplies (Santa Clara, CA, USA), and a PLC computer code that controlled the frequency of the alternating magnetic field.[2, 3]

The alternating magnetic field was achieved by alternatively activating the two solenoids, and the rate of on and off for the solenoids was controlled by a computer-operated programmable logic controller (PLC).[2, 3]

Appendix A6

Chemicals

Chemical	Provider	Purity	Remark
ethanol	Alfa Aesar	Brought in completely anhydrous	KOPTEC proof purity
boric anhydride	J. T. Baker, Avantor Chemicals	≥98.0%	Used for acetonitrile dehydration by distillation
acetonitrile	EMD Chemicals	≥99.8%	
triethylamine (TEA)	Alfa Aesar	≥99%	
4-N', N'-dimethylamino-pyridine (DMAP)	Fluka	≥99.0%	
α-bromoisobutyrylbromide	Aldrich	98%	
methanol	EMD Chemicals	≥99.8%	
2-Hydroxyethyl methacrylate (HEMA)	Alfa Aesar	97%, and it contains the stabilizer of ca 500 ppm 4-methoxy phenol	Used as the monomer to form polymer chains during ATRP process, and has to be kept frozen during preservation
Aluminum Oxide	Sigma Aldrich	≥98%	Used for removal of stabilizer from 97% HEMA
2, 2'-bipyridine (Bpy)	Sigma Aldrich	≥99%	Ligand agent for ATRP reaction solution
Cu(I)Cl	Aldrich	≥99.99%	
Cu(II)Cl	Aldrich	≥99.99%	
Cu(II)Br	ACROS Organics	≥99%	

N, N, N', N", N"-pentamethyl diethylenetriamine (PMDETA)	Aldrich	99%	Ligand agent for ATRP quenching solution
potassium phthalimide	Alfa Aesar	≥99%	
12M hydrochloride acid	EMD Chemicals	36.5% water solution	
hydrazine hydrate	Alfa Aesar	≥99%	kept frozen during preservation
1-ethyl-3-(3-dimethyl-aminopropyl) carbodiimide (EDC)	Alfa Aesar	98%	CAS#: 1892-57-5, kept frozen during preservation
N-hydroxysuccinimide (NHS)	ACROS Organics	≥98%	CAS #: 6066-82-6, kept frozen during preservation
NaCl	Avantar Performance Materials	≥99.0%	Macron Chemicals
$CaCl_2$	EMD Chemicals	≥96%	Anhydrous
$MgCl_2$	Alfa Aesar	99%	Anhydrous
$MgSO_4$	J. T. Baker of Avantor	99.5%	
$NaH_2PO_4 \cdot H_2O$	Bought from VWR, and produced by BDH Chemicals	≥98.0%, ACS grade	Used for preparation of sodium phosphate buffer solution
Na_2HPO_4	AMRESCO	Anhydrous and ACS grade	Used for preparation of sodium phosphate buffer solution
Trimethylamino hydrochloride	Acros Organics	98%	Used as the organic salt during membrane tests

References

1. Demas, V.; Lowery, T. J., Magnetic resonance for in vitro medical diagnostics: superparamagnetic nanoparticle-based magnetic relaxation switches. *New Journal of Physics* **2011,** *13*; Zengin, A.; Yildirim, E.; Tamer, U.; Caykara, T., Molecularly imprinted superparamagnetic iron oxide nanoparticles for rapid enrichment and separation of cholesterol. *The Analyst* **2013,** *138* (23), 7238-45.

2. Yang, Q.; Himstedt, H. H.; Ulbricht, M.; Qian, X.; Wickramasinghe, S. R., Designing magnetic field responsive nanofiltration membranes. *Journal of Membrane Science* **2013,** *430*, 70-78.

3. Himstedt, H. H.; Yang, Q.; Dasi, L. P.; Qian, X.; Wickramasinghe, S. R.; Ulbricht, M., Magnetically Activated Micromixers for Separation Membranes. *Langmuir* **2011,** *27* (9), 5574-5581.

4. Himstedt, H. H.; Yang, Q.; Qian, X.; Wickramasinghe, S. R.; Ulbricht, M., Toward remote-controlled valve functions via magnetically responsive capillary pore membranes. *Journal of Membrane Science* **2012,** *423*, 257-266.

5. Himstedt, H. H.; Marshall, K. M.; Wickramasinghe, S. R., pH-responsive nanofiltration membranes by surface modification. *Journal of Membrane Science* **2011,** *366* (1-2), 373-381.

6. Robinson, K. L.; Khan, M. A.; Banez, M. V. D.; Wang, X. S.; Armes, S. P., Controlled polymerization of 2-hydroxyethyl methacrylate by ATRP at ambient temperature. *Macromolecules* **2001,** *34* (10), 3155-3158.

7. Magenau, A. J. D.; Kwak, Y.; Schroeder, K.; Matyjaszewski, K., Highly Active Bipyridine-Based Ligands for Atom Transfer Radical Polymerization. *Acs Macro Letters* **2012,** *1* (4), 508-512.

8. Yang, Q.; Ulbricht, M., Cylindrical Membrane Pores with Well-Defined Grafted Linear and Comblike Glycopolymer Layers for Lectin Binding. *Macromolecules* **2011,** *44* (6), 1303-1310.

9. Kimura, E.; Koike, T.; Kodama, M.; Meyerstein, D., A COPPER(I) N,N,N',N",N"-PENTAMETHYLDIETHYLENETRIAMINE COMPLEX AND ITS CARBON-MONOXIDE ADDUCT IN AQUEOUS-SOLUTIONS. *Inorganic Chemistry* **1989,** *28* (15), 2998-3001.

10. Yagci, Y.; Jockusch, S.; Turro, N. J., Photoinitiated Polymerization: Advances, Challenges, and Opportunities. *Macromolecules* **2010,** *43* (15), 6245-6260.

11. Cheng, C.-J.; Bai, X.-X.; Fan, W.-Q.; Wu, H.-M.; Shen, L.; Huang, Q.-H.; Tu, Y.-M., Synthesis of a photoactive gemini surfactant and its use in AGET ATRP miniemulsion polymerisation and UV curing. *Chemical Papers* **2014,** *68* (1), 136-144.

12. Hauquier, F.; Debou, N.; Palacin, S.; Jousselme, B., Amino functionalized thin films prepared from Gabriel synthesis applied on electrografted diazonium salts. *Journal of Electroanalytical Chemistry* **2012,** *677*, 127-132.

13. Goodman, C. A.; Hamaker, C. G.; Hitchcock, S. R., Synthesis and evaluation of some variants of the Nefkens' reagent. *Tetrahedron Letters* **2013,** *54* (45), 6012-6014.

14. Monge, S.; Giani, O.; Ruiz, E.; Cavalier, M.; Robin, J.-J., A new route for the modification of halogen end groups to amino end-functionalized poly(tert-butyl acrylate)s. *Macromolecular Rapid Communications* **2007,** *28* (23), 2272-2276.

15. Kuo, C.-H.; Liu, Y.-C.; Chang, C.-M. J.; Chen, J.-H.; Chang, C.; Shieh, C.-J., Optimum conditions for lipase immobilization on chitosan-coated Fe3O4 nanoparticles. *Carbohydrate Polymers* **2012,** *87* (4), 2538-2545.

16. Liu, L.; Zhang, X. Q.; Zhang, Y.; Pu, Y. P.; Yin, L. H.; Tang, M.; Liu, H., Optimal Activation of Carboxyl-Superparamagnetic Iron Oxide Nanoparticles Bioconjugated with Antibody Using Orthogonal Array Design. *Journal of Nanoscience and Nanotechnology* **2013,** *13* (12), 8137-8143.

17. Yang, W. R.; Hibbert, D. B.; Zhang, R.; Willett, G. D.; Gooding, J. J., Stepwise synthesis of gly-gly-his on gold surfaces modified with mixed self-assembled monolayers. *Langmuir* **2005,** *21* (1), 260-265.

18. Timmer, J. M. K. Properties of nanofiltration membranes: model development and industrial application. Technische Universiteit Eindhoven, Eindhoven, 2001; Hu, K.; Dickson, J. M., Nanofiltration membrane performance on fluoride removal from water. *Journal of Membrane Science* **2006,** *279* (1-2), 529-538.

19. Kowalska, I., Dead-end and cross-flow ultrafiltration of ionic and non-ionic surfactants. *Desalination and Water Treatment* **2012,** *50* (1-3), 397-410.

20. Cot, S. N. D. A. D. K. D., *Intrinsic properties and performances of NF270 and XLE membranes for water purification*. *Water Science&Technology: Water Supply* **2011,** *11* (2), 186-193.